INCORPORATION OF CYANIDE LIGANDS INTO MODELS OF [FEFE]- AND [NIFE]-HYDROGENASES

BY

BRIAN CHRISTOPHER MANOR

DISSERTATION

Submitted in partial fulfillment of the requirements
for the degree of Doctor of Philosophy in Chemistry
in the Graduate College of the
University of Illinois at Urbana-Champaign, 2014

Urbana, Illinois

Doctoral Committee:

Professor Thomas B. Rauchfuss, Chair
Professor Yi Lu
Professor Kenneth S. Suslick
Professor Gregory S. Girolami

Abstract

Hydrogen is processed in Nature by a class of metalloenzymes called hydrogenases. Hydrogenase enzymes catalyze the reduction of protons into H_2 or oxidized H_2 into protons. The catalytic rates and overpotentials of hydrogenase enzymes are comparable to Pt catalysts. The most prevalent hydrogenase enzymes are bimetallic with FeFe or NiFe active sites. The metals of the active sites are bound to carbonyl and cyanide ligands with the metal centers bridged by thiolates. The use of inexpensive and readily available elements by hydrogenase enzymes has been a driving force for the development of compounds that model both the structure and activity of the enzymes. Though functional models of hydrogenase active sites have been developed, many occur at lower rates and higher overpotentials than the enzymes. The catalytic cycles of these models often differ from the catalytic cycles of hydrogenase. The work presented focuses on the development towards functional hydrogenase models with a biologically accurate coordination spheres particularly the presence of cyanide on the Fe centers. The presence of a biomimetic coordination sphere may develop models that function by more biomimetic catalytic cycles. Chapter 1 highlights the current understanding of the structural features and catalytic cycles of hydrogenase enzymes. An overview of hydrogenase models is presented with a particular focus the structural features of the models that impact production and oxidation of H_2.

Chapter 2 focuses on modeling the hydrogen-bonding environments found in [FeFe]-H_2ase by coordination of triarylboranes to the [FeFe]-H_2ase models $[Fe_2(pdt)(CO)_4(CN)_2]^{2-}$ and $[Fe_2(adt)(CO)_4(CN)_2]^{2-}$. Treatment of two equivalents of borane to $[Fe_2(pdt)(CO)_4(CN)_2]^{2-}$ formed the 2:1 adduct $[Fe_2(pdt)(CO)_4(CNBR_3)_2]^{2-}$. Attempts to model the inequivalent hydrogen bonding environment of [FeFe]-H_2ase with BPh_3 and $B(C_6F_5)_3$ were unsuccessful. The use of the bulky borane $B(C_6F_4\text{-}o\text{-}C_6F_5)_3$ (BAr^F*_3) with $K_2[Fe_2(pdt)(CO)_4(CN)_2]^{2-}$ were found to form the 1:1 adduct $K_2[Fe_2(pdt)(CO)_4(CN)(CNBAr^F*_3]^{2-}$. The 2:1 borane adducts $[Fe_2(pdt)(CO)_4(CNBR_3)_2]^{2-}$ could be readily protonated to form the stable bridging hydrides $[Fe_2(\mu\text{-}H)(pdt)(CO)_4(CNBR_3)_2]^{2-}$. The adducts $[Fe_2(pdt)(CO)_4(CNBR_3)_2]^{2-}$ were found to undergo quasi-reversible oxidation around –0.3 V vs $Fc^{0/+}$ while the hydrides undergo quasi-reversible reductions around –1.7 V vs $Fc^{0/+}$. The coordination of the boranes were found to have a large effect on the electron density of the Fe centers as evidence by higher ν_{CO}, more acidic pK_a's, and more negative oxidation and reduction potentials compared to $[Fe_2(pdt)(CO)_4(CN)_2]^{2-}$. Comparison of certain parameters indicate that PMe_3 is a more basic ligand than $CNBR_3^-$ (ν_{CO}, pK_a) though the presence of $CNBR_3^-$ ligands resulted in

more negative oxidation and reduction potentials than PMe_3. A simplified synthesis of $[Fe_2(pdt)(CO)_4(CN)_2]^{2-}$, $[Fe_2(adt)(CO)_4(CN)_2]^{2-}$, and $[Fe_2(pdt)(CO)_5(CN)]^-$ was developed entailing the reaction of the diiron hexacarbonyl complexes with KCN in MeCN.

With the success of coordination of boranes to $[Fe_2(pdt)(CO)_4(CN)_2]^{2-}$, the coordination of boranes to the Fe-C*N* of the [NiFe]-H_2ase model $[HFe(CO)_3(CN)_2]^-$ was explored in Chapter 3. The compound $[HFe(CO)_3(CN)_2]^-$ is a possible synthon for a one-pot synthesis of [NiFe]-H_2ase models as the Fe center is coordinated by carbonyl, cyanide, and a hydride ligands. Reactions of $[HFe(CO)_3(CN)_2]^-$ with typical Ni reagents for [NiFe]-H_2ase models did not yield any hydride-containing products. In order to allow for facile ligand substitution of $[HFe(CO)_3(CN)_2]^-$ by displacement of CO, two equivalents of boranes were coordinated to $[HFe(CO)_3(CN)_2]^-$ to form the 2:1 adducts $[HFe(CO)_3(CNBR_3)_2]^-$. The coordination of boranes was found to significantly decrease the pK_a of the hydride by at least 13 pK_a units. Treatment of $[HFe(CO)_3(CNBAr^F{}_3)_2]^-$ with Ni(pdt)(dppe) resulted initially in deprotonation to form $[Fe(CO)_3(CNBAr^F{}_3)_2]^{2-}$ before ligand redistribution forms the Fe-H $[HFe(CO)(CNBAr^F{}_3)_2(dppe)]^-$. The treatment of the less acidic $[HFe(CO)_3(CNBPh_3)_2]^-$ with Ni(pdt)(dxpe) results initially in partial deprotonation of the hydride. The use of the diphosphine dppe forms a mix of mono Fe-H $[HFe(CO)(CNBPh_3)_2(dppe)]^-$ and the NiFe hydride $(CO)_2(CNBPh_3)Fe(H)(pdt)Ni(dppe)$ while the diphosphine dcpe forms only $(CO)_2(CNBPh_3)Fe(H)(pdt)Ni(dcpe)$ as the only hydride-containing product.

An alternative route for the synthesis of functional cyanide-containing [NiFe]-H_2ase models are examined in Chapter 4 by decarbonylation the [NiFe]-H_2ase models $(CO)_2(CN)_2Fe(pdt)Ni(dxpe)$. The compound $(CO)_2(CN)_2Fe(pdt)Ni(dppe)$ was present as only the *cis*-CO, *trans*-CN isomer. Using the more basic diphosphine dcpe formed both the *cis*-CO, *trans*-CN isomer and *cis*-CO, *cis*-CN isomers of $(CO)_2(CN)_2Fe(pdt)Ni(dcpe)$. Attempts to decarbonylate the dicarbonyl complexes by photolysis resulted in decomposition to insoluble precipitates. To facilitate decarbonylation, two equivalents of triarylboranes were added to $(CO)_2(CN)_2Fe(pdt)Ni(dxpe)$ forming the 2:1 adducts $(CO)_2(CNBR_3)_2Fe(pdt)Ni(dxpe)$. Irradiation of the adducts resulted in isomerization instead of decarbonylation. Studies of the photoisomerization of the adducts found the isomerization to be slightly inhibited by CO while photolysis under ^{13}CO was found to undergo CO exchange. Both of these results are consistent with the formation of an open coordination site which is thought to occur from CO dissociation.

The formation of NiFe hydrides from hydrogen is highlighted in Chapter 5. Using the models described in Chapter 4, the treatment of the dicarbonyl adducts $(CO)_2(CNBAr^F{}_3)_2Fe(pdt)Ni(dxpe)$ with a decarbonylating agent followed by either BH_4^- or H_2 formed the biomimetic hydrides $[(CO)(CNBAr^F{}_3)_2Fe(H)Ni(dxpe)]^-$. The crystal structure of $[(CO)(CNBAr^F{}_3)_2Fe(H)(pdt)Ni(dppe)]^-$ was found to have asymmetric metal-hydride distances (Fe-H: 1.51Å; Ni-H: 1.71Å). Although bridging hydrides typically have protic character, the hydrides $[(CO)(CNBAr^F{}_3)_2Fe(H)Ni(dxpe)]^-$ were hydric in nature. Treatment of $[(CO)(CNBAr^F{}_3)_2Fe(H)Ni(dxpe)]^-$ with stronger acids (eg. anilinium, HCl) was found to produce H_2. Furthermore, the addition of weak acids (eg. $HNMe_3^+$, pyrollidinium) were found to form a dihydrogen bond with the hydride as indicated by ^1H NMR experiments. Given their hydric nature, the hydrides $[(CO)(CNBAr^F{}_3)_2Fe(H)Ni(dxpe)]^-$ are best described as terminal Fe-H hydrides with a weak Ni-H interaction. The hydrides were oxidized at mild potentials (~0.1 V vs $Fc^{0/+}$) though only a 20 mV difference in oxidation potential was observed between dppe and dcpe ligands, indicative of oxidation at Fe, reverse of [NiFe]-H_2ase. The hydride $[(CO)(CNBAr^F{}_3)_2Fe(H)Ni(dppe)]^-$ was found to serve an electrocatalyst for the oxidation of H_2, a first for [NiFe]-H_2ase models.

Acknowledgements

I have to first thank my advisor Prof. Tom Rauchfuss who everyday approaches chemistry with a high level of enthusiasm. He has challenged me to dig deeper into a result not only when the unexpected occurs but also when things go as planned. There is always more to the problem than what is just at the surface. The more I interact with fellow students the more I understand how rare it is to have an advisor with an open door who is available to their students whenever it is needed. I am forever grateful for being allowed the freedom to take a seemingly simple idea and develop it to the breakthrough it was.

I would not be where I am without the interaction I had with my fellow lab mates. I consider myself lucky to be able to work with a fantastic group of people. I am incredibly grateful for all the advice to transitioning to graduate school and all the hands-on training I was given. I want to thank Bryan Chan for teaching me the importance of a five minute coffee break when I have seemed to hit a wall. I also want to thank David Schilter for regularly putting up with my asking of seemingly dumb questions and providing helpful advice.

I want to also thank my friends, both those in Champaign-Urbana and those further away. You've celebrated with me the good days and encouraged me through the bad. You remind me that I am more than just a "smart" person and there is more to life than just chemistry. I have always enjoyed the sharing the simple pleasures of sitting on a patio with a drink, sitting around a card table laughing, or running up and down a stretch of grass in the heat and humidity of Illinois summers. You have all kept me sane when I otherwise would have been lost.

Finally I want to thank my family for all of their encouragement and support. What I worked on may not have always been easy to understand, but you were always willing to listen when I was elaborating on an exciting result. You have always been so understanding when I seem to drop off the Earth for weeks at a time. I may not have done it often, but coming home has always helped me to place everything back into appropriate priority.

Table of Contents

Terms Used Within This Thesis…….....vii

Chapter 1: Hydrogenase: Role of H_2 in Nature……...1

Chapter 2: Boro-Cyanide Containing Models of [FeFe]-Hydrogenase……31

Chapter 3: Iron Hydride Monomers as Synthons for [NiFe]-Hydrogenase Models…….61

Chapter 4: Synthesis and Characterization of Boro-Cyanide [NiFe]-Hydrogenase Models……83

Chapter 5: Formation of Biomimetic [NiFe]-Hydrogenase Models from H_2…….107

Terms Used Within This Thesis

18-c-6	18-crown-6
adt^{2-}	azadithiolate, $[HN(CH_2S)_2]^{2-}$
$BAr^F{}_3$	tris-(pentafluorophenyl)borane, $B(C_6F_5)_3$
$BAr^{F\#}{}_3$	tris-(2,4,6-trifluorophenyl)borane, $B(2,4,6\text{-}F_3C_6H_2)_3$
$BAr^F{}_3^*$	tris-(2,2´, 2´´-perfluorobiphenyl)borane, $B(C_6F_4\text{-}o\text{-}C_6F_5)_3$
BAr^{F24-}	tetrakis(3,5-bis(trifluoromethyl)phenyl)borate, $[B(C_6H_3\text{-}3,5\text{-}(CF_3)_2)_4]^-$
bda	benzlideneacetone
Bn	benzyl, CH_2Ph
Bu	butyl, C_4H_{10}
Cp^-	cyclopentadienyl, $[C_5H_5]^-$
Cy	cyclohexyl, C_6H_{11}
dcpe	1,2-bis(dicyclohexylphosphino)ethane, $Cy_2PC_2H_4PCy_2$
dppe	1,2-bis(diphenylphosphino)ethane, $Ph_2PC_2H_4PPh_2$
dppv	*cis*-1,2-bis(diphenylphosphino)ethane, *cis*-$Ph_2PC_2H_2PPh_2$
edt^{2-}	1,2-ethanedithiolate, $(S_2C_2H_4)^{2-}$
Et	ethyl, C_2H_5
$Fc^{0/+}$	ferrocene/ferrocenium couple, $[(C_5H_5)_2Fe]^{0/+}$
Me	methyl, CH_3
odt^{2-}	oxadithiolate, $[O(CH_2S)_2]^{2-}$
pdt^{2-}	1,3-propanedithiolate, $(S_2C_3H_6)^{2-}$
Ph	phenyl, C_6H_5
PPN^+	bis(triphenylphosphine)iminium, $Ph_3P{=}N{=}PPh_3^+$

Chapter 1

Hydrogenase: Role of H_2 in Nature

1.1 Introduction

The early atmosphere of Earth was hydrogen rich and highly reducing in nature, requiring early forms of life to relay on hydrogen as a fuel source.[1] The interconversion of H_2, protons, and electrons (i.e. $H_2 \rightleftharpoons 2H^+ + 2e^-$) is mediated in Nature by a class of metalloenzymes known as hydrogenases (H_2ases). Today, H_2ases can be found in a range of archaea and eukarya including bacteria, algae, and fungi.[2] Depending on the oxygen content of the environment, H_2ases serve to either (i) provide energy for organisms by generating electrons from H_2 or (ii) remove reducing equivalents by production of H_2. In anaerobic environments, H_2ase produces H_2 as a result of fermentation of organic material. The resulting H_2 is used as an energy source for lithotrophic organisms such as acetogens (CO_2 to $CH_3CO_2^-$), methanogens (CO_2 to CH_4), sulfate reducers (SO_4^{2-} to H_2S), Fe^{3+} reducers (Fe^{3+} to Fe^{2+}), and denitrifying bacteria (NO_3^- to N_2). Oxidation of H_2 has also been found to occur in aerobic environments by cyanobacteria forming H_2O and generating a proton gradient for use in ATP synthase.

H_2ases are classified by the metals located at the active site. The bimetallic H_2ases have either two Fe centers ([FeFe]-H_2ase) or one Fe center and one Ni center ([NiFe]-H_2ase). Although [FeFe]- and [NiFe]-H_2ase evolved separately, both have similar features. The active sites of both [FeFe]- and [NiFe]-H_2ases feature Fe centers that are ligated by CO and CN^- ligands, first characterized by FTIR spectroscopy.[3,4] The bimetallic centers are bridged by thiolate ligands with a vacant coordination site on at least one metal center that binds substrate (Figure 1.1). Both [FeFe]- and [NiFe]-H_2ase have FeS clusters present that serve as a "molecular wire" to transport electrons to and from the active site. They also feature hydrophobic gas tunnels to transport H_2 to and from the active sites, and networks of water molecules which are proposed to shuttle H^+ to and from the active site.[5]

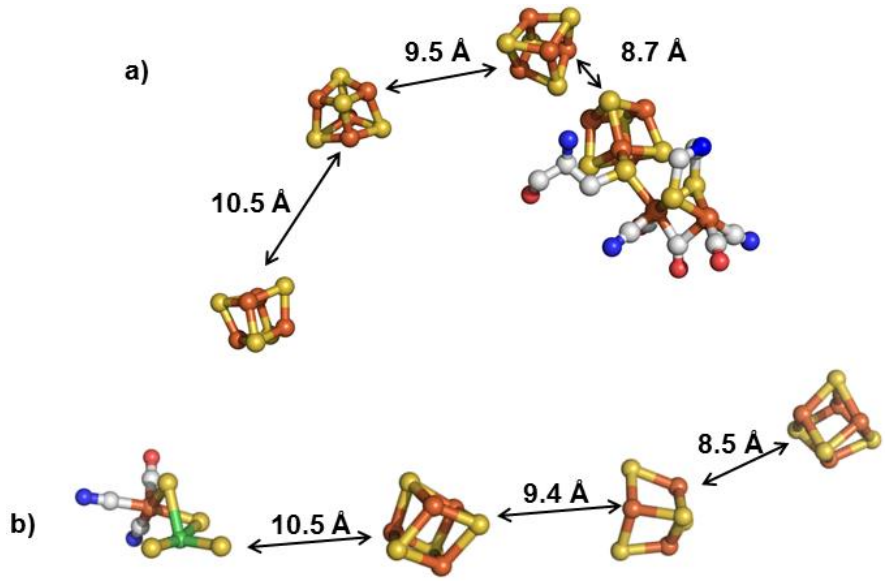


Figure 1.1. a) Structure of [FeFe]-H_2ase active site from *C. pasteurianum* with Fe_4S_4 clusters depicting intermolecular distances (PDB 3C8Y).[6] b) Structure of [NiFe]-H_2ase active site from *A. vinosum* with proximal Fe_4S_4, medial Fe_3S_4, and distal Fe_4S_4 clusters with intermolecular distances (PDB 3MYR).[7]

A range of techniques have been used to probe the structure and mechanism of H_2ase including EPR,[8] FTIR and resonance Raman,[8,9] as well as protein crystallography,[6,7] and a range of voltammetry techniques.[10] These methods are not sensitive for observing the substrates (e.g. H_2, H^-) at the active site. Because hydrogonic ligands are amenable to crystallographic and NMR analysis, structural and functional models allows for better understanding of the structure and mechanism of H_2ases.

The active sites of [FeFe]- and [NiFe]-H_2ase serve as catalysts for the oxidation of H_2 into protons and electrons or the reduction of protons into H_2 at remarkably fast rates (Table 1.1).[5] The enzymes catalyze the reactions at low overpotentials (80 mV) comparable to precious metal catalysts.[11,12] While the enzymes are bidirectional, [FeFe]-H_2ase, the more oxygen sensitive H_2ase, is biased towards H_2 production while [NiFe]-H_2ase, the more oxygen tolerant H_2ase, is biased towards H_2 oxidation.

Table 1.1. Catalytic activity of H_2ases.

	Enzyme	H_2 Production	H_2 Oxidation	ref
[FeFe]-H_2ase	*D. desulfuricans*	8,200	62,200	[13]
[NiFe]-H_2ase	*D. gigas*	440	1,500	[14]

Rate measured as μmol of H_2 per minute per mg of protein at 30 °C.

The desire for carbon-free energy sources has been based on both environmental and political concerns. The production of H_2 on an industrial scale occurs from gasification of coal or steam reforming from natural gas.[15]

Both of these methods of H_2 production would be undesirable as carbon sources are required and CO_2 is formed as a byproduct. The ideal source of H_2 would be water where reduction of protons would form H_2 and oxidation of water to form O_2. The standard catalyst for both the half reactions is platinum,[16] but the high cost and rarity of platinum makes its use as a catalyst undesirable. The presence of cheap and abundant 1st row metals in the active sites of H_2ase has inspired the study of structures and mechanisms of H_2ases.[17]

1.2 [FeFe]-Hydrogenase

1.2.1 Structure of [FeFe]-H_2ase

The active site of [FeFe]-H_2ase, known as the H-cluster, is composed of a Fe_2S_2 cluster that is covalently linked to a Fe_4S_4 cluster (Figure 1.2). The Fe centers of the Fe_2S_2 cluster are both ligated by one CO and one CN^- ligand with one CO ligand bridging the Fe centers. The proximal Fe (Fe_p) is further ligated by a cysteinate residue which is covalently bound to a redox active Fe_4S_4 cluster. The distal Fe (Fe_d) is the site of H_2 coordination and formation and is characterized by a rotated state in which a vacant coordination site is *trans* to the bridging CO ligand. The metal centers are also coordinated by a bridging dithiolate ligand. The bridgehead of the dithiolate ligand is positioned over the vacant site as it serves as a proton relay to and from the coordination site. The identity of the bridgehead ligand of the dithiolate ligand was highly debated as protein crystallography could not distinguish between CH_2 (propanedithiolate, pdt^{2-}), NH (azadithiolate, adt^{2-}), or O (oxadithiolate, odt^{2-}) as the ditholate.[6] Though model complexes and HYSCORE studies of the active site where consistent with adt^{2-} as the dithiolate,[18-20] the presence of adt^{2-} in [FeFe]-H_2ase was confirmed by incorporation of the model complexes $[Fe_2(xdt)(CO)_4(CN)_2]^{2-}$ into the native protein with catalytic activity only found with the adt^{2-} complex.[21]

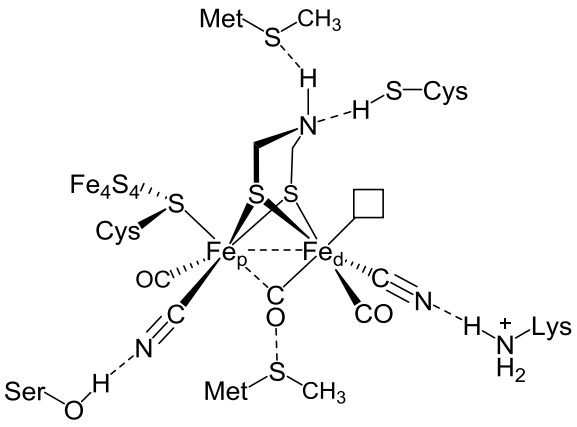


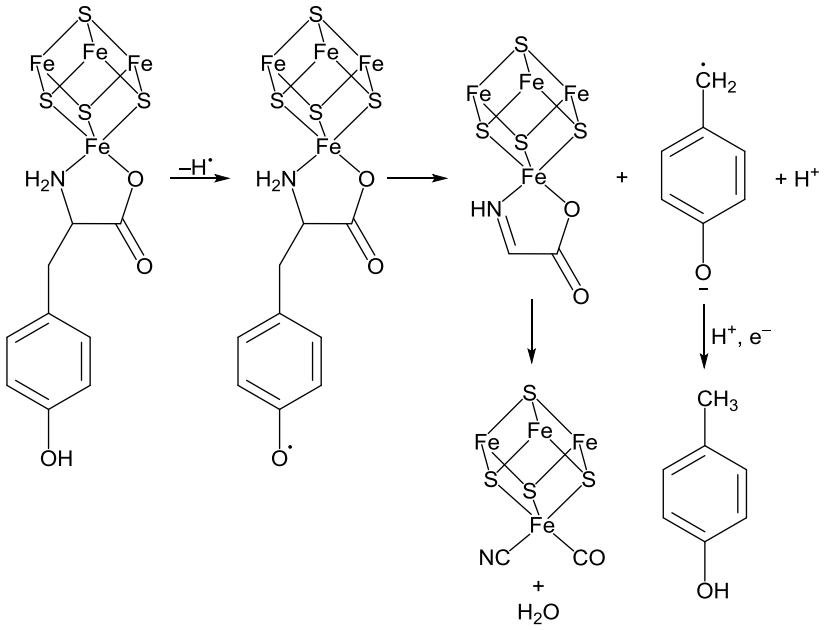
Figure 1.2. Active site of [FeFe]-H_2ase depicting the vacant coordination site on Fe_d (indicated by a square) and the highly conserved interactions between the active site and surrounding protein.

The H-cluster of [FeFe]-H_2ase is weakly attached to the protein, the coordination of Cys to Fe_p being the only covalent bond between the active site and surrounding protein. The active site does display a number of interactions with the surrounding protein as depicted in Figure 1.2. Many of the residues are highly conserved among the [FeFe]-H_2ases and are critical for either H-cluster biosynthesis or catalytic activity.[22] For example, a neighboring Lys forms a strong hydrogen bond to Fe_d-C*N*, an interaction thought to stabilize the rotated structure of Fe_d exposing a vacant site for substrate binding. Further, a nearby Met participates in an electrostatic interaction with the amine of adt^{2-}. The absence of either residue leads to the H-cluster being absent in the protein based on EPR and IR spectroscopy. A Cys side chain is shown to hydrogen bond to the amine of the adt^{2-}. Mutation of the amino acid was found to result in incorporation of the H-cluster, though no catalytically activity was detected. This suggests that Cys shuttles protons to and from the H-cluster. Finally the mutation of the Met that undergoes an electrostatic interaction with the bridging CO was found to shift the catalytic bias of the active site towards H_2 oxidation though no noticeable changes in the EPR or IR spectra were detected.

1.2.2 Maturation of [FeFe]-H_2ase

The stepwise assembly of the Fe_2S_2 moiety in the H-cluster is performed by the assembly proteins HydE, HydF, and HydG. The CO and CN^- ligands are both derived from tyrosine and are attached to a Fe_4S_4 cluster in HydG.[23] The scission of tyrosine occurs by H· abstraction from the *p*-OH of tyrosine to generate a radical intermediate. The radical formation initiates the scission of tyrosine, generating one CO and one CN^- ligand bound to a Fe center along with the formation of H_2O and *p*-cresol as byproducts (Scheme 1.1).[24]

Scheme 1.1. Simplified scheme for the proposed biosynthesis of CN^- and CO in [FeFe]-H_2ase from tyrosine.



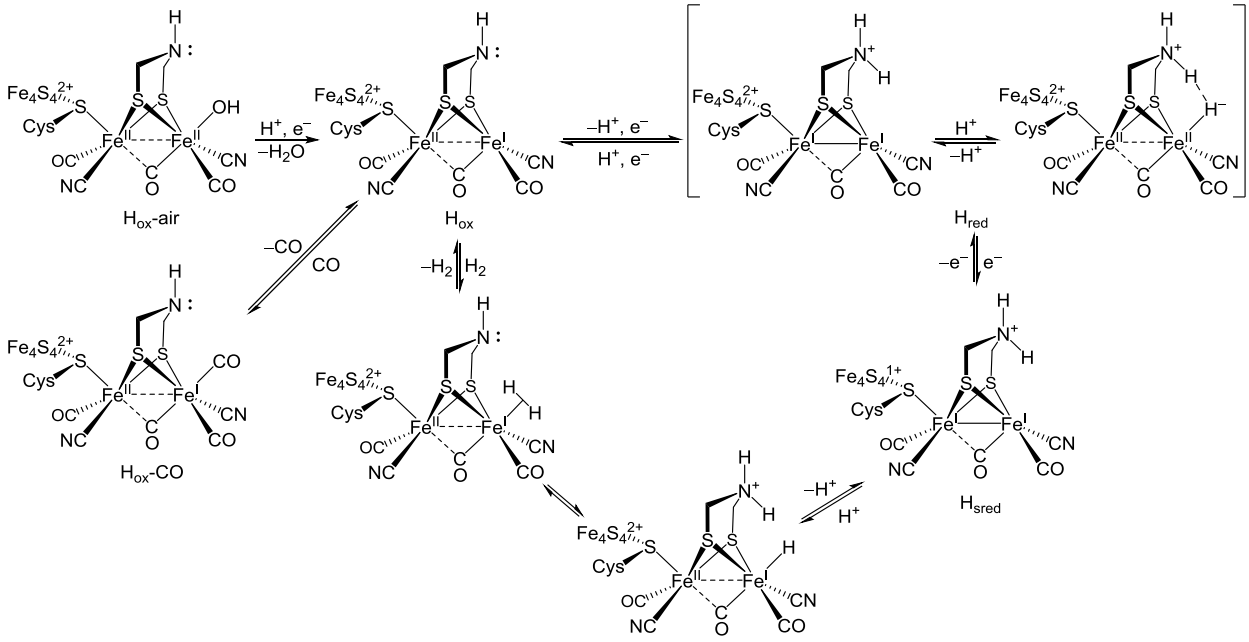
The Fe(CO)(CN) intermediate was found to bind an additional CO ligand to form a $Fe(CO)_2(CN)$-$[Fe_3S_4]$ cluster. The origin of the second CO ligand is not clear. Free CO was only detected later in the maturation processes, suggesting that the second CO was not from external sources and may be derived from another equivalent of tyrosine. Several turnovers would result in a $Fe_2S_2(CO)_4(CN)_2$ species. The formation and installation of the dithiolate cofactor is not well understood. One proposal suggests that the dithiolate is formed by similar methods to CO and CN^- by cleavage of tyrosine in HydG.[25] Another theory states that the ditholate may be formed by HydE after formation of the $Fe_2S_2(CO)_4(CN)_2$ cluster.[26] The presence of HydE has been shown to be necessary for the maturation of [FeFe]-H_2ase,[22] supporting the construction of the dithiolate cofactor occurs at HydE. HydF transports the completed Fe_2S_2 cluster to the apo HydA protein which contains the Fe_4S_4 cluster that binds directly to the Fe_2S_2 cluster forming the final H-cluster.[21]

1.2.3 States of [FeFe]-H_2ase

The catalytic cycle of [FeFe]-H_2ase features two recognized states: H_{ox} and H_{red} (Scheme 1.2).[8] The diiron center of H_{ox} is EPR active, indicative of a Fe(II)Fe(I) mixed state. The Fe_d of H_{ox} has a vacant coordination site *trans* to the bridging CO that can bind H_2 or H^-. H_{ox} can bind CO at the coordination site forming the catalytically inactive H_{ox}-CO state.[27] Binding of H_2 to H_{ox} concomitant with deprotonation and oxidation forms the H_{red} state. The diamagnetic H_{red} state may be Fe(II)Fe(II) with a terminal hydride bound to the Fe_d. An alternative description

of H_{red} could form through deprotonation of the terminal hydride generating a Fe(I)Fe(I) core with a vacant site on the distal Fe. Oxidation of the H_{red} coupled with deprotonation regenerates the H_{ox} state. An additional state has been identified upon the reduction of the covalently bound Fe_4S_4 cluster forms the super-reduced H_{sred} state which may be an intermediate in the catalytic cycle.[28,29] Samples of [FeFe]-H_2ase are isolated in the aerobic inactive state H_{ox}^{air}. Reduction of H_{ox}^{air} forms the active H_{ox} state. [FeFe]-H_2ase is highly air sensitive with exposure of H_{ox} or H_{red} to O_2 irreversibly destroying the active site.[30] The H_{ox}^{air} state was found not to be destroyed by air and could be later activated under anaerobic conditions.[10]

Scheme 1.2. States and proposed catalytic cycle of [FeFe]-H_2ase.

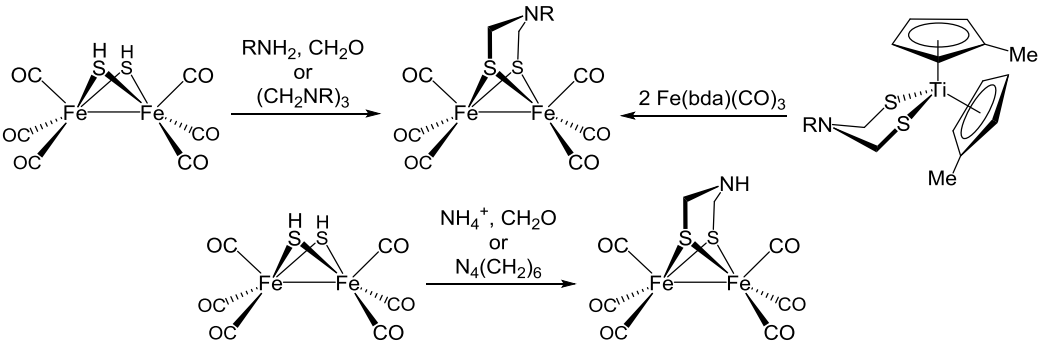


1.2.4 Synthetic Models of [FeFe]-H_2ase

Although the basic structure of [FeFe]-H_2ase was reported after [NiFe]-H_2ase, there has been more development in synthetic models of [FeFe]-H_2ase than for [NiFe]-H_2ase. The plethora of [FeFe]-H_2ase models is due to the fact that the general structure of [FeFe]-H_2ase greatly resembles the readily available $Fe_2(SR)_2(CO)_6$ clusters first reported in the 1920s by the reaction of $Fe(CO)_5$ with thiols.[31] A more versatile route was developed in the 1960s using $Fe_3(CO)_{12}$ with thiols and dithiols.[32] A variety of thiolates, dithiolate, and chalcogenates have been reported in $Fe_2(ER)_2(CO)_6$ clusters.[8,33,34] Azadithiol has yet to be isolated, therefore much work has been devoted towards the development of alternative synthetic routes for the synthesis of [FeFe]-H_2ase models with the biologically relevant adt^{2-}. The first model with an adt^{2-} cofactor was reported from the reaction of $Fe_2(SLi)_2(CO)_6$

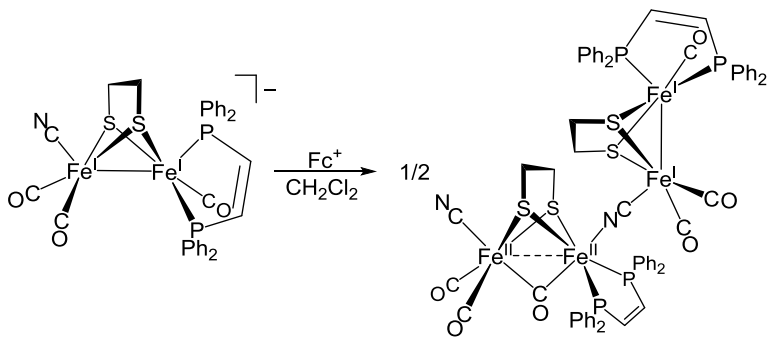
with $(ClCH_2)_2NMe$ to form $Fe_2(Me\text{-}adt)(CO)_6$.[35] A later report showed that the condensation of primary amines with formaldehyde in the presence of $Fe_2(SH)_2(CO)_6$ afforded a range of complexes $Fe_2(R\text{-}adt)(CO)_6$.[36,37] An alternative method has been developed by the transfer of $R\text{-}adt^{2-}$ from $(Cp^{Me})_2Ti(R\text{-}adt)$ to $Fe(bda)(CO)_3$.[38] The instillation of the biologically relevant adt^{2-} can be formed from the reaction of $Fe_2(SH)_2(CO)_6$ with a mixture of NH_4^+ and paraformaldehyde or hexamethylenetetramine. (Scheme 1.3)[36]

Scheme 1.3. Synthetic routes to $Fe_2(R\text{-}adt)(CO)_6$.



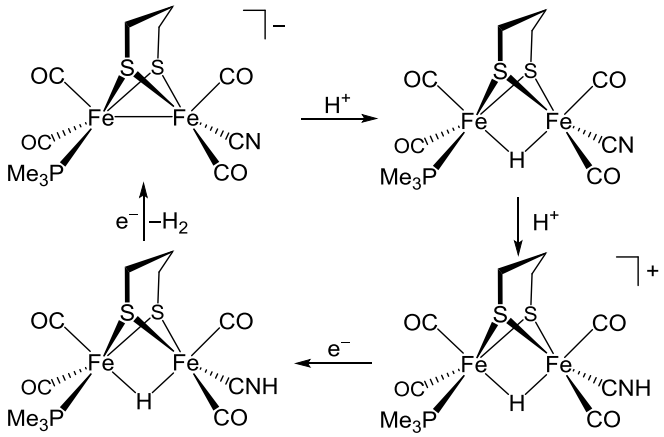
The $Fe_2(SR)_2(CO)_6$ clusters readily undergo ligand substitution with basic ligands, these groups serving as surrogates for the strongly donating cyanide and cysteinate ligands in the H-cluster. The first reported models for [FeFe]-H_2ase was the biomimetic $[Fe_2(pdt)(CO)_4(CN)_2]^{2-}$ formed by the treatment of $Fe_2(pdt)(CO)_6$ with two equivalents of CN^-.[39-41] Though the model greatly resembles the structure and ligand environment of active site, the dicyanide models were unstable towards acid and redox chemistry, both of which are necessary for functional H_2ase models. Protonation of $[Fe_2(pdt)(CO)_4(CN)_2]^{2-}$ forms unstable bridging hydrides that have not been isolated.[42] Oxidation of [FeFe]-H_2ase models with CN^- results in the formation of precipitate, likely formed by Fe-CN-Fe linkages.[33] The one electron oxidation of $[Fe_2(edt)(CO)_3(CN)(dppv)]^-$ resulted in a four Fe compound in which the diiron cores are linked by a bidentate CN^- (Scheme 1.4).[43]

Scheme 1.4. Single electron oxidation of $[Fe_2(edt)(CO)_3(CN)(dppv)]^-$.



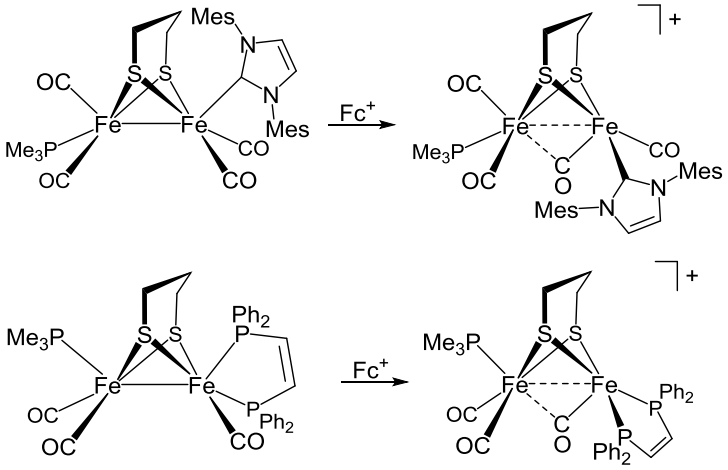
Although the cyanide ligands are not compatible with the functional aspects of H_2ase models, the first reported [FeFe]-H_2ase model to sever as an electrocatalyst in H_2 production was derived from $[Fe_2(pdt)(CO)_4(CN)(PMe_3)]^-$. Protonation of $[Fe_2(pdt)(CO)_4(CN)(PMe_3)]^-$ forms the stable bridging hydride $Fe_2(\mu\text{-}H)(pdt)(CO)_4(CN)(PMe_3)$. Bulk electrolysis of $Fe_2(\mu\text{-}H)(pdt)(CO)_4(CN)(PMe_3)$ at –1.6 V vs $Fc^{0/+}$ in the presence of toluenesulfonic acid to produced six turnovers of H_2 (Scheme 1.5).[44] Given the side reactions arising from the basic nitrogen of CN^- most modeling efforts have focused on the use to neutral σ-donors such as phosphines and N-heterocyclic carbenes.[8,45]

Scheme 1.5. Proposed catalytic cycle for $Fe_2(\mu\text{-}H)(pdt)(CO)_4(CN)(PMe_3)$ as an electrocatalyst for H_2 production.



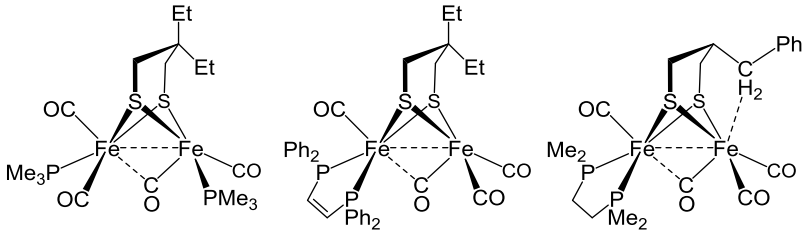
A key structural feature of the [FeFe]-H_2ase active site is the rotated Fe_d center. Rotation of the $Fe(CO)_2L$ center relocates one CO ligand to a semi-bridging position, thereby opening a substrate binding site adjacent to the adt^{2-}. The [FeFe]-H_2ase active site utilizes the surrounding protein scaffold to helps maintain the rotated structure, which poses a serious challenge to the synthesis of active site models. Models of the H_{ox} state with a rotated site have been reported by the one electron oxidation of substituted compounds $Fe_2(pdt)(CO)_{6-x}L_x$ (Scheme 1.6).[46,47]

Scheme 1.6. Rotated structures of H_{ox} [FeFe]-H_2ase models obtained by one electron oxidation of Fe(I)Fe(I) precursors.



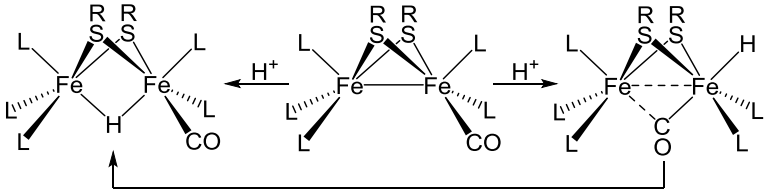
The H_{red} state of [FeFe]-H_2ase is postulated to feature a Fe(I)Fe(I) core with a vacant coordination site. Models of Fe(I)Fe(I) oxidation states with rotated structures have been synthesized using bulky dithiolate ligands, often in combination with asymmetric ligand substitution (Scheme 1.7).[48-50] These rotated models are characterized by the semi-bridging CO ligand is evident by IR spectroscopy with a ν_{CO} ~1800 cm^{-1}.

Scheme 1.7. Rotated structures of Fe(I)Fe(I) models of H_{red}.



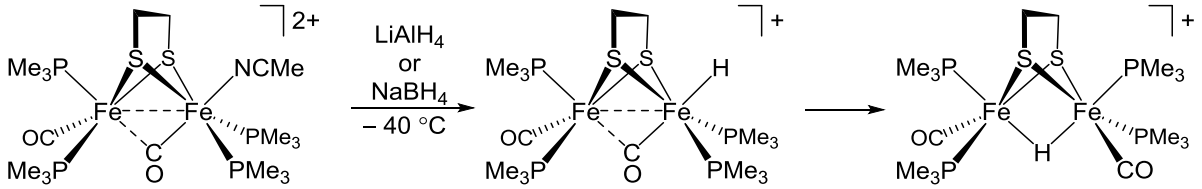
The formation of hydrides by either protonation of a metal center or heterolytic splitting of H_2 is a key step in the catalytic cycle. Protonation of [FeFe]-H_2ase models can form two types of hydride: a bridging hydride, in which the proton spans the two Fe centers, or a terminal hydride, in which the proton is bound to only one iron center together with a bridging or semi-bridging CO between the Fe centers (Scheme 1.8). The synthesis of terminal hydrides has been proven to be quite challenging as they have a relatively short life time at room temperature tending to isomerize to the thermodynamically preferred bridging hydride.[51]

Scheme 1.8. Protonation of $Fe_2(SR)_2L_5(CO)$ forming bridging or terminal hydrides.



The first terminal hydrides in [FeFe]-H_2ase models were generated from hydride transfer from $NaBH_4$ or $LiAlH_4$ to the diferrous species $[Fe_2(edt)(NCMe)(\mu\text{-}CO)(CO)(PMe_3)_4]^{2+}$ at –40 °C (Scheme 1.9). Upon sitting at room temperature the terminal hydride was found to isomerize to the bridging hydride $[Fe_2(\mu\text{-}H)(edt)(CO)_2(PMe_3)_4]^{+}$. Treatment of the terminal hydride with strong acid was found to generate H_2 as identified by ^1H NMR spectroscopy.[52]

Scheme 1.9. Generation of the terminal hydride $[HFe_2(edt)(CO)_2(PMe_3)_4]^{+}$ and subsequent isomerization to the bridging hydride.



The first report of a terminal hydride from protonation involved the treatment of $Fe_2(pdt)(CO)_4(dppe)$ with $HBF_4{\cdot}Et_2O$. The product was only observed at –70 °C before isomerizing to $[Fe_2(\mu\text{-}H)(pdt)(CO)_4(dppe)]^{+}$.[53] The formation of terminal hydrides by low temperature protonation has also been reported with $Fe_2(pdt)(CO)_4(dppv)$, $Fe_2(pdt)(CO)_3(PMe_3)(dppv)$, and $Fe_2(pdt)(CO)_2(dppv)_2$.[51] The increase of electron density of the iron centers was not found to correlate with stability of the terminal hydride. Although the half-life of $[HFe_2(pdt)(CO)_2(dppv)_2]^{+}$ is reported to be ~12 min at room temperature, $[HFe_2(pdt)(CO)_3(PMe_3)(dppv)]^{+}$ is observed only briefly at –90 °C while $[HFe_2(pdt)(CO)_4(dppv)]^{+}$ is stable below –40 °C. The increase in steric bulk of the phosphine ligands likely hinders the isomerization to the bridging hydride.

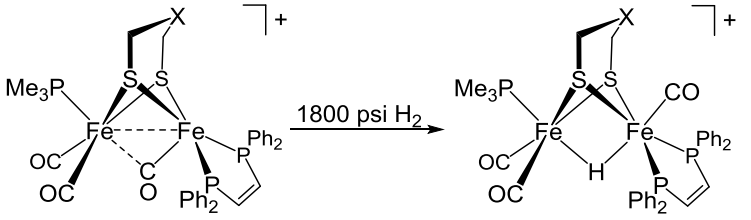
The identity of the dithiolate has a significant effect on the formation of a terminal hydride over a bridging hydride. Protonation of $Fe_2(xdt)(CO)_2(PMe_3)_4$ (xdt^{2-} = pdt^{2-}, edt^{2-}) was found to give a mixture of terminal and bridging hydrides via an intermediate species featuring an S-protonated thiolate. The protonation of $Fe_2(adt)(CO)_2(PMe_3)_4$ affords only the terminal hydride.[54] Treatment of $Fe_2(adt)(CO)_2(dppv)$ with two equivalents of acid forms the H_{red} model $[HFe_2(Hadt)(CO)_2(dppv)]^{2+}$ characterized by both a terminal hydride and an ammonium

cofactor. The crystal structure displayed a close NH···HFe distance of 1.88(7) Å, indicative of the formation of a dihydrogen bond, but spontaneous release of H_2 was not observed.[18]

Terminal hydrides are found to have faster catalytic rates and lower overpotentials for hydrogen evolution than bridging hydrides. The terminal hydride $[HFe_2(adt)(CO)_2(dppv)_2]^+$ catalyzes hydrogen evolution from weak acids at a rate of 5,000 s^{-1} with an overpotential of 0.7 V, while the ammonium hydride $[HFe_2(Hadt)(CO)_2(dppv)_2]^{2+}$ catalyzes for hydrogen evolution from CF_3CO_2H at a faster rate of 58,000 s^{-1} with an overpotential of 0.5 V. The isomeric bridging hydride $[Fe_2(\mu\text{-}H)(Hadt)(CO)_2(dppv)_2]^{2+}$ also serves as catalysts for hydrogen evolution but occurs at a much slower rate (20 s^{-1}) and higher overpotential (0.90 V).[18] Studies have indicated that the bridging hydride serves as a spectator ligand in hydrogen evolution. Treatment of the reduced bridging hydride $Fe_2(\mu\text{-}H)(pdt)(CO)_2(dppv)_2$ with $D(Et_2O)_2BAr^{F24}$ was found to produce D_2 and the diferrous bridging hydride $[Fe_2(\mu\text{-}H)(pdt)(CO)_2(dppv)_2]^+$ with no formation of $[Fe_2(\mu\text{-}D)(pdt)(CO)_2(dppv)_2]^+$.[55]

While there are many reports of [FeFe]-H_2ase models that serve as electrocatalysts for hydrogen evolution, there are relatively few models that split H_2. The first reports of H_2 activation by [FeFe]-H_2ase models occurred under very high pressures of H_2.[20] Treatment of the mixed valent compounds $[Fe_2(xdt)(CO)_3(PMe_3)(dppv)]^+$ with H_2 was found to form the corresponding bridging hydrides (Scheme 1.10). The presence of an amine cofactor at the dithiolate bridgehead was found to form a larger amount of the bridging hydride than when pdt^{2-} or odt^{2-} are present.

Scheme 1.10. H_2 activation by $[Fe_2(xdt)(CO)_3(PMe_3)(dppv)]^+$ at high pressure.

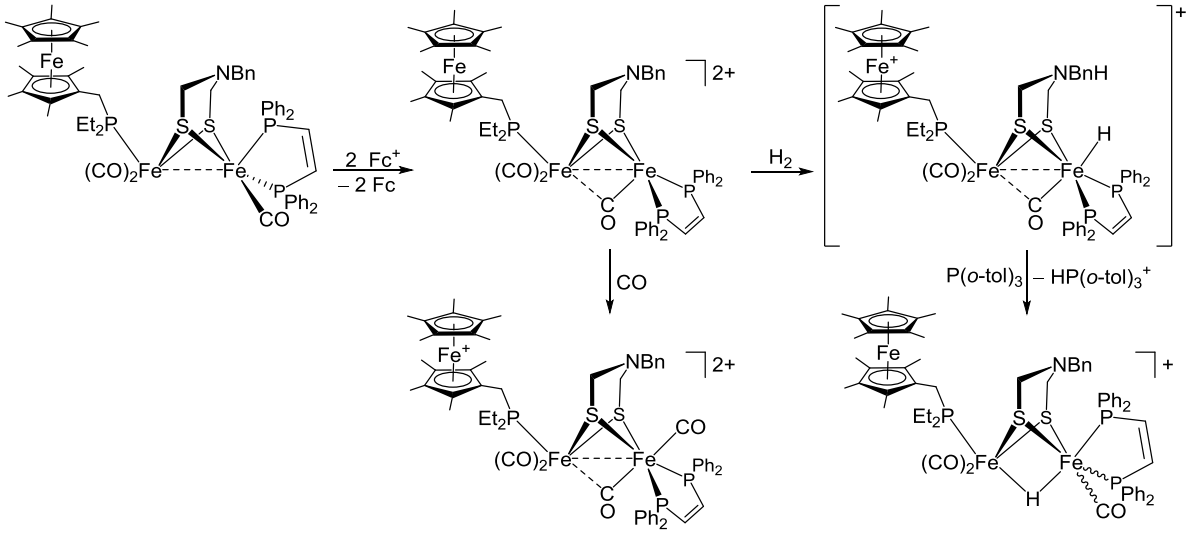


Dithiolate	Hydride Yield
pdt^{2-}	< 5 %
adt^{2-}	~ 30 %
$^{Bn}adt^{2-}$	~ 85 %
odt^{2-}	< 5 %

The use of mild redox agents was found to activate H_2 at much lower pressures.[56] Treatment of $Fe_2(^{Bn}adt)(CO)_3(PMe_3)(dppv)$ with decamethylferrocenium (Fc^{*+}) under 1-2 atm of H_2 formed the bridging hydride $[Fe_2(\mu\text{-}H)(^{Bn}adt)(CO)_3(PMe_3)(dppv)]^+$ over a period of a few hours. The presence of the additional base P(*o*-tol)$_3$ was not found to alter the rate or yield. The rate determining step was suggested to be H_2 binding to the Fe center.

The most synthetically complete [FeFe]-H_2ase model $Fe_2(^{Bn}adt)(CO)_3(dppv)(Fc^*P)$ contains a redox active ferrocenyl phosphine ligand Fc*P ($Cp^*FeC_5Me_4CH_2PEt_2$) which models the covalently bound Fe_4S_4 cluster in the enzyme.[57] Treatment with two equivalents of mild oxidants was found to heterolytically split H_2 to form the diferrous hydride $[Fe_2(\mu\text{-}H)(^{Bn}adt)(CO)_3(dppv)(Fc^*P)]^+$ in the presence of P(*o*-tol)$_3$. Though not observed, the heterolytic splitting of H_2 is proposed to form a terminal hydride that isomerizes to the bridging hydride. Binding of CO formed the CO-inhibited model $[Fe_2(^{Bn}adt)(\mu\text{-}CO)(CO)_3(dppv)(Fc^*P)]^{2+}$ (Scheme 1.11). In the presence of excess amounts of oxidant and base, $[Fe_2(^{Bn}adt)(\mu\text{-}CO)(CO)_3(dppv)(Fc^*P)]^{2+}$ was found to catalytically oxidize H_2 at a rate of 0.4 h^{-1}.

Scheme 1.11. Oxidation of $Fe_2(^{Bn}adt)(CO)_3(dppv)(Fc^*P)$ and binding of CO and activation of H_2.

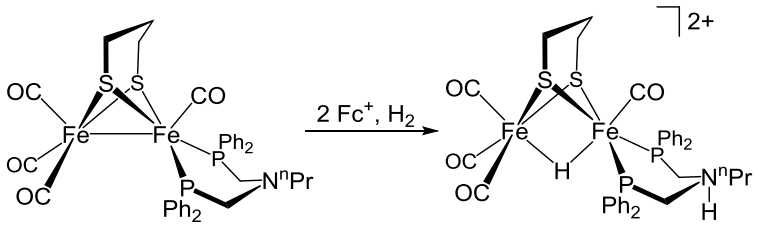


The model $Fe_2(^{Bn}adt)(CO)_3(dppv)(Fc^*P)$ is reported to be the first bidirectional H_2ase model as the model was also found to serve as a hydrogen evolution catalyst. The treatment of $Fe_2(^{Bn}adt)(CO)_3(dppv)(Fc^*P)$ with of excess amounts of $H(Et_2O)_2BAr^{F24}$ was found to produce H_2 without the addition of external reducing agents. The presence of excess amounts of decamethylferrocene (Fc*) and acid formed H_2 catalytically with stronger reducing agents producing H_2 at higher rates. Inactivation of the catalyst over time occurs by formation of the bridging hydride which is catalytically inactive for H_2 production.[58]

While the activation of H_2 by [FeFe]-H_2ase models require a proton relay in the model, proton relays other than the biomimetic adt^{2-} can be used for H_2 activation. Two electron oxidation of the compound $Fe_2(pdt)(CO)_4(PNP)$ (PNP = $(Ph_2PCH_2)_2N^nPr$) in the presence of 1 atm H_2 and P(*o*-tol)$_3$ forms the hydride

ammonium species $[Fe_2(\mu\text{-}H)(pdt)(CO)_4(PNHP)]^+$ (Scheme 1.12).[59] The analogous complex $Fe_2(pdt)(CO)_4(dppp)$ (dppp = $Ph_2P(CH_2)_3PPh_2$) was found not to activate H_2.

Scheme 1.12. H_2 activation by $Fe_2(pdt)(CO)_4(PNP)$ upon oxidation.



1.3 [NiFe]-Hydrogenase

1.3.1 Structure of [NiFe]-H_2ase

The active site of [NiFe]-H_2ase has a Fe center ligated by one CO ligand *trans* to the vacant bridging site and two CN^- ligands in the basal position on Fe. The cyanide ligands undergo hydrogen bonding to the surrounding protein scaffold, however mutation studies on hydrogen bonding to the CN^- ligand has not found to alter the catalytic activity.[60] The Ni center is ligated by four cysteinate ligands with the NiS_4 center in a SF_4-type geometry. Two of the cysteinate ligands are coordinated in a terminal fashion and the other two cysteinate ligands bridge the Ni and Fe centers. An additional bridging site is located between the metal centers. The third bridging site is occupied by a variety of substrates depending on the state of the enzyme within the catalytic cycle (H_2, H_2O, H^-, HO^-, HOO^-) (Figure 1.3).

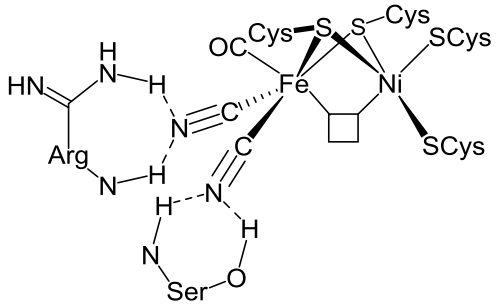


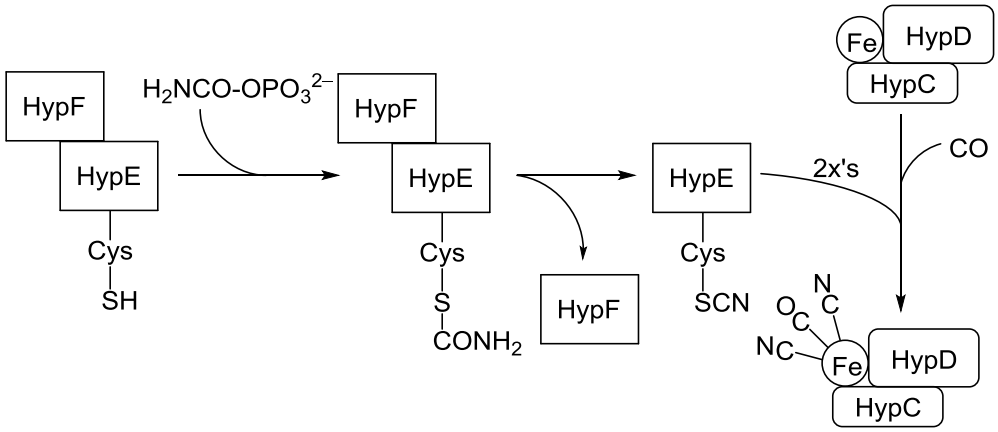
Figure 1.3. Active site of [NiFe]-H_2ase depicting the coordination site between the metal centers by a square and hydrogen bonding interactions with cyanide ligands.

1.3.2 Maturation of [NiFe]-H_2ase

The maturation of [NiFe]-H_2ase can be described by four steps: synthesis of CN^-, synthesis of CO, assembly of $Fe(CN)_2(CO)$, and Ni insertion.[61] The synthesis of CN^- in [NiFe]-H_2ase is different than in [FeFe]-H_2ase. In [NiFe]-H_2ase, CN^- is generated in the accessory proteins HypE and HypF from

carbamoylphosphate. S-carbamoylation with the thiol of cysteine forms a thiocarboxamide which is converted to thiocyanate (Scheme 1.13).[62] The synthesis of CO in [NiFe]-H_2ase occurs independently of CN^-. The origin of CO in the maturation of [NiFe]-H_2ase is not well understood. In *A. vinosum* CO is derived from acetate while in *R. eutropha* CO has been shown to form from glycerol or fructose by ^{13}C labeling studies. The assembly of the $Fe(CN)_2(CO)$ subunit occurs in HypC and HypD.[63] HypE first transfers two CN^- ligands to the Fe center, maintaining a low spin Fe(II) center that is then coordinated by CO. The $Fe(CN)_2(CO)$ subunit is then transferred to the large subunit, which contains the native protein scaffold. The Ni is finally inserted into the active site by the HypA and HypB assembly proteins.

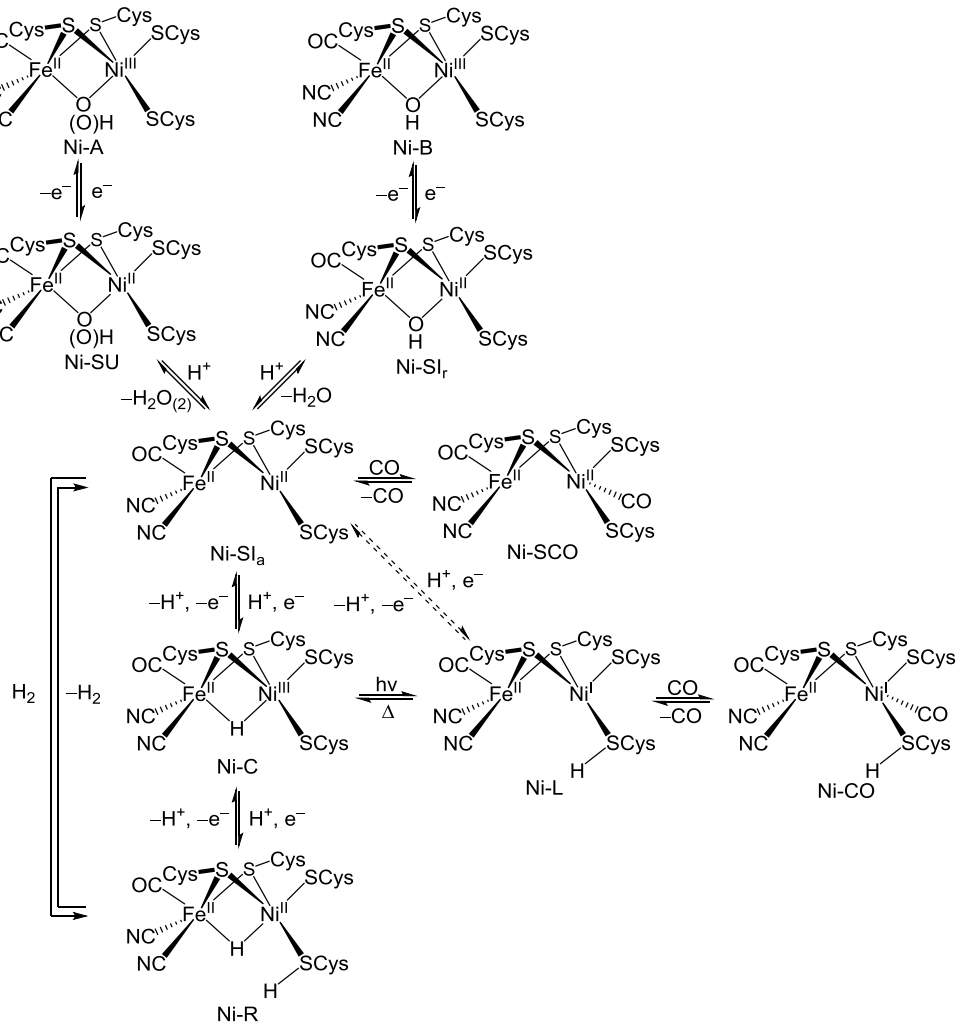
Scheme 1.13. Generation of CN^- and subsequent instillation to form the $Fe(CN)_2(CO)$ subunit in [NiFe]-H_2ase maturation.



1.3.3 States of [NiFe]-H_2ase

Unlike [FeFe]-H_2ase, [NiFe]-H_2ase has many characterized states (Scheme 1.14).[64] The oxidized, inactive states Ni-A and Ni-B form under oxidizing conditions or exposure to O_2. The Ni-A and Ni-B states feature a characteristic EPR-active Ni(III)Fe(II) core. The Ni-B state is bridged by an OH^- ligand while the bridging ligand in Ni-A is thought to be either an OOH^- or OH^- moiety.[65,66] The inactive states can be activated under reducing conditions where activation of Ni-B occurs in seconds while activation of Ni-A is rather slow.[67] Reduction of Ni-A and Ni-B have been detected to produce H_2O and H_2O_2, forming the ready-active Ni-SI_a state.[68] The EPR silent Ni-SI_a is characterized by Ni(II)Fe(II) oxidation states with the bridging site either vacant or occupied by an H_2O molecule.

Scheme 1.14. States and catalytic cycle of [NiFe]-H_2ase with possible conversion between Ni-SI_a and Ni-L.



The catalytic cycle is composed of three or four characterized states. The Ni-SI_a state heterolytically cleaves H_2 to afford the reduced state Ni-R featuring a Ni(II)Fe(II) core in which a hydride ligand bridges the Ni and Fe sites. Furthermore, a protonated terminal cysteinate illustrates the utility of such residues to serve as internal proton relays, similar to the amine in adt^{2-} as found in [FeFe]-H_2ase. Oxidation of Ni and deprotonation of the terminal cysteinate of the Ni-R state forms the EPR-active Ni-C state with Ni(III)Fe(II) oxidation states. The presence of the bridging hydride in Ni-C has been confirmed by ENDOR and HYSCORE studies of *D. vulgaris* Miyazaki F.[69] Although the hydride ligand cannot be identified by protein crystallography, DFT calculations estimate a shorter Ni-H bond (1.61 Å) than Fe-H bond (1.72 Å).[70] Oxidation and deprotonation of Ni-C reforms the Ni-SI_a state. The conversion of Ni-C to Ni-SI_a may occur by a concerted mechanism or via a step-wise mechanism by the light induced state

Ni-L. Irradiation of Ni-C at low temperatures forms the EPR active Ni-L state characterized by Ni(I)Fe(II) oxidation states.[71] The hydride ligand is deprotonated by a terminal cysteinate ligand.[9]

The site of H_2 binding and activation is not apparent in [NiFe]-H_2ase. Molecular catalysts with either Fe or Ni centers have been shown to form H_2 or oxidize H_2.[72,73] Evidence suggests that the Ni center in [NiFe]-H_2ase may be the site of H_2 binding and activation. Placing either the Ni-SI_a state or Ni-L state under a CO atmosphere forms the Ni-SCO or Ni-CO state respectively. The CO-inhibited states are characterized by coordination of the additional CO to Ni.[74] Computational modeling of the activation of H_2 in [NiFe]-H_2ase first proposed Fe to be the site of H_2,[75] however more extensive modeling now suggests that Ni is the site of H_2 binding.[76]

1.3.4 Other [NiFe]-H_2ases

[NiFeSe]-H_2ase is a subclass of [NiFe]-H_2ase where a terminal cysteine bound to the Ni center has been replaced with selenocysteine (SeCys).[77] [NiFeSe]-H_2ase has been identified in *D. baculatum* and *D. vulgaris* Hildenborough. The active site of [NiFeSe]-H_2ase is similar to [NiFe]-H_2ase with the exception of the terminal SeCys. While [NiFe]-H_2ase are biased towards H_2 oxidation, [NiFeSe]-H_2ase is biased towards H_2 production as the terminal SeCys has a lower pK_a than Cys resulting in faster protonation of the hydride in Ni-R.

The exposure of most H_2ases to O_2 either inhibits catalytic activity or irreversibly damages the active site. However, the membrane-bound hydrogease (MBH) class of [NiFe]-H_2ase are catalytically active under aerobic conditions.[78] Exposure of standard [NiFe]-H_2ase (O_2-sensitive) will generate the oxidized Ni-A or Ni-B states that can be reduced back to the active states. The membrane-bound [NiFe]-H_2ases have been shown to undergo catalytic activity in the presence of O_2, termed O_2-tolerant. The active sites of O_2-tolerant and O_2-sensitive [NiFe]-H_2ase show no noticeable differences, suggesting that the origin of O_2 tolerance lies away from the active site.[79] The proximal FeS cluster in O_2-tolerant [NiFe]-H_2ase is coordinated by six cysteine residues forming a Fe_4S_3 cluster compared to the four cysteine residues coordinated to a Fe_4S_4 cluster in O_2-sensitive [NiFe]-H_2ase.[80] The proximal Fe_4S_3 cluster can access three charge states ($3^+/4^+/5^+$). The structure of the super oxidized state of the proximal cluster reveals a deprotonated amide between Cys25 and Cys26 coordinated to a Fe center, breaking a Fe-S bond (Figure 1.4).

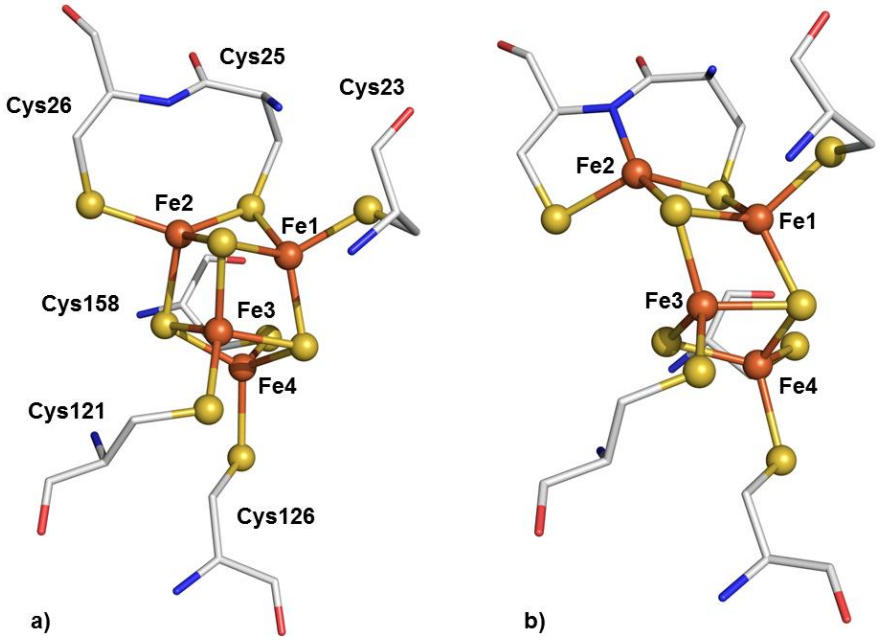


Figure 1.4. Crystal structures of the proximal Fe_4S_3 clusters of *H. marinus* in a) the reduced state (PDB 3AYX) b) the super oxidized state (PDB 3AYY).[80]

1.3.5 Synthetic Models of [NiFe]-H_2ase

There have been extensive efforts in developing molecular models for [NiFe]-H_2ase.[81,82] Early modeling attempts focused on complexes structurally similar to the active site, though very few demonstrated biologically relevant activity.[83] Trimetallic [NiFe]-H_2ase models of the type Ni_2Fe and $NiFe_2$ were first reported to serve as hydrogen evolution catalysts (Figure 1.5).[84-86] Later bimetallic models were also found to function as electrocatalysts for hydrogen production albeit at slow rates (5 h^{-1}) though catalytic intermediates are not well understood.[87]

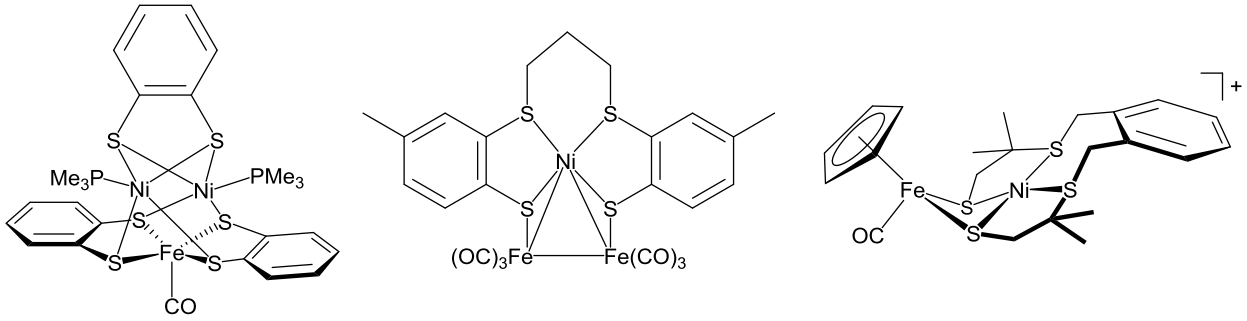


Figure 1.5. Hydrogen evolving catalysts of [NiFe]-H_2ase models.

Metal hydrides are known in the catalytic cycle of [NiFe]-H_2ase and are of great focus in the development of functional [NiFe]-H_2ase models. The first examples of well characterized hydride-containing [NiFe]-H_2ase models are based off of the compound $(CO)_3$Fe(pdt)Ni(dppe) first described by Schröder.[88] The model $(CO)_3$Fe(pdt)Ni(dppe) is diamagnetic with structural and theoretical studies indicating a Ni-Fe bond with a Ni(I)Fe(I) core. The model was first prepared by treating $Fe_2(CO)_9$ with Ni(pdt)(dppe), though a more general synthetic method for $(CO)_3$Fe(xdt)Ni(diphos) was developed later. Treatment of $FeI_2(CO)_4$ with Ni(xdt)(diphos) followed by reduction with cobaltocene gave the desired species.[89] Treatment of $(CO)_3$Fe(xdt)Ni(diphos) with acid produced the first [NiFe]-H_2ase models with a bridging hydride $[(CO)_3Fe(H)(xdt)Ni(diphos)]^+$.[90] The hydride complexes were found to undergo ligand substitution with phosphines to form $[(CO)_2(PR_3)Fe(H)(xdt)Ni(diphos)]^+$ (Scheme 1.15).[90,91] Crystal structures of the NiFe hydrides reveal shorter Fe-H bonds than Ni-H bonds (Table 1.2). IR and Raman measurements of $[(CO)_3Fe(H/D)(pdt)Ni(dppe)]^+$ reveal bands at 1530 and 945 cm^{-1} assigned to ν_{Fe-H} and ν_{Ni-H} respectively, reinforcing the asymmetric coordination of the hydride in solution as well as the solid state.[92]

Scheme 1.15. Protonation and ligand substitution of $(CO)_3$Fe(xdt)Ni(diphos).

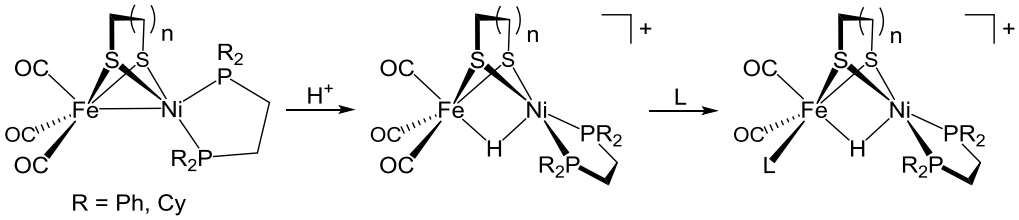
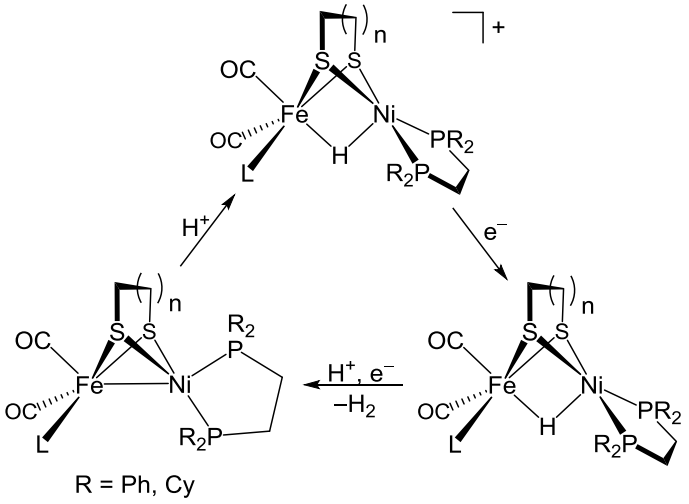


Table 1.2. Fe–H and Ni–H distances in $[(CO)_{3-n}(PR_3)_nFe(H)(SR)_2NiL_2]^+$.

Compound	Fe–H (Å)	Ni–H (Å)	Ref.
$[(CO)_3Fe(H)(pdt)Ni(dppe)]^+$	1.46(6)	1.64(6)	89
$[(CO)_3Fe(H)(edt)Ni(dppe)]^+$	1.58(4)	1.84(3)	88
$[(CO)_2(PPh_3)Fe(H)(pdt)Ni(dppe)]^+$	1.49(3)	1.89(3)	89
$[(CO)_3Fe(H)(pdt)Ni(dcpe)]^+$	1.53(2)	1.90(2)	88
$[(P(OEt)_3)_3Fe(D)Ni(S_2N_2)]^+$	1.577(17)	2.18(4)	95

The hydrides $[(CO)_2LFe(H)(xdt)Ni(diphos)]^+$ were found to serve as electrocatalysts for the production of hydrogen. When treated with carboxylic acids, the catalysts were found to operate at rates varying from 20 to 310 s^{-1} with overpotentials of approximately 0.5-0.65 V. The hydrogen evolution reaction is proposed to proceed via reduction of the cationic hydrides to $[Ni(H)Fe]^0$. Such reduced hydrides would then be susceptible to protonolysis, generating $[NiFe]^+$, which would reduce back to Ni(I)Fe(I) (Scheme 1.16).[89,91]

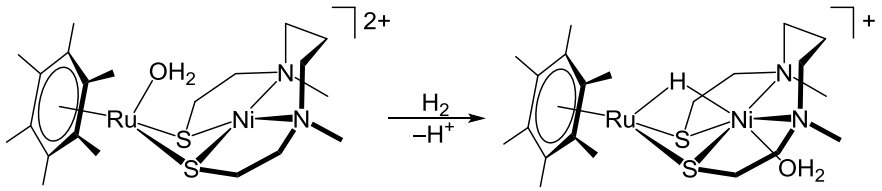
Scheme 1.16. Purposed hydrogen evolution mechanism of $[(CO)_2LFe(H)(xdt)Ni(diphos)]^+$.



Although [NiFe]-H_2ase tends to oxidize H_2 in Nature, there are few reports of [NiFe]-H_2ase models that oxidize H_2. Early models of [NiFe]-H_2ase that activated H_2 had NiRu cores (Scheme 1.17).[93] The treatment of $[(arene)Ru(H_2O)Ni(S_2N_2)]^{2+}$ with H_2 formed $[(arene)Ru(H)Ni(H_2O)(S_2N_2)]^{2+}$ by heterolytic cleavage with the aqueous solvent serving as the proton acceptor. Although the reaction proceeds in aqueous solvent at room temperature, high pressures (0.1 MPa) were required to achieve heterolytic splitting of H_2. The resulting hydride

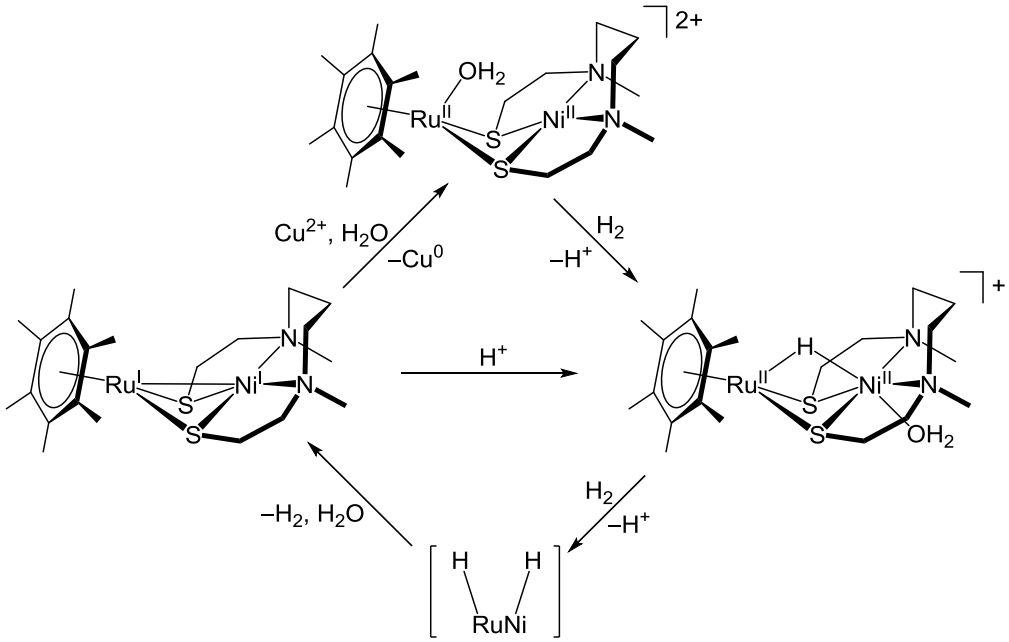
displayed protic character.[94] The addition of strong acid to $[(arene)Ru(H)Ni(H_2O)(S_2N_2)]^+$ was found not to produce H_2 but the hydride was found to undergo H^+/D^+ exchange with D_2O.

Scheme 1.17. Heterolytic splitting of H_2 by $[(arene)Ru(H_2O)Ni(S_2N_2)]^{2+}$.



Catalytic H_2 oxidation was found to occur with $[(arene)Ru(H_2O)Ni(S_2N_2)]^{2+}$ as the catalyst with Cu^{2+} as the sacrificial oxidant.[95] Pressuring D_2O solutions of $[(arene)Ru(H_2O)Ni(S_2N_2)]^{2+}$ and Cu^{2+} with H_2 was found to produce D_2 and traces of HD. One equivalent of D_2 and Cu^0 were produced for the consumption of two equivalents of H_2, leading to the mechanism proposed in Scheme 1.18 where the treatment of $[(arene)Ru(H)Ni(H_2O)(S_2N_2)]^+$ with additional equivalent of H_2 forms a dihydride intermediate that reductively eliminates H_2.

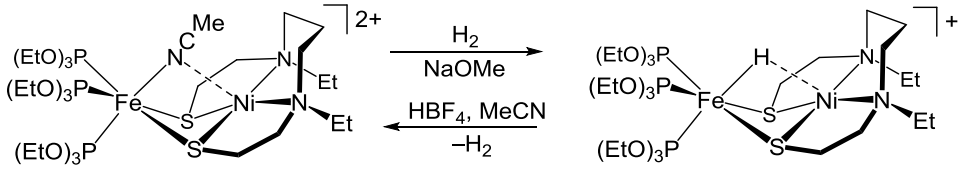
Scheme 1.18. Proposed catalytic cycle for the oxidation of H_2 by $[(arene)Ru(H_2O)Ni(S_2N_2)]^{2+}$.



The model $[(P(OEt)_3)_3Fe(NCMe)Ni(S_2N_2')]^{2+}$ was the first reported model with a NiFe core found to form hydrides from H_2 (Scheme 1.19).[96] The hydride displaces a labile MeCN ligand on Fe though still required high

pressure of H_2 (0.1 – 0.8 MPa). The addition of the NaOMe acts as proton acceptor forming MeOH. The structure determined by neutron diffraction revealed a terminal Fe-H as indicated by a much shorter Fe-H bond (1.577(17) Å) than Ni-H bond (2.18(4) Å). The NiFe hydride demonstrated terminal hydride character. Addition of the strong acid HBF_4 was found to regenerate H_2. Furthermore, the hydride was found to undergo hydride transfer to 10-methylacridinium anion and methylene blue.

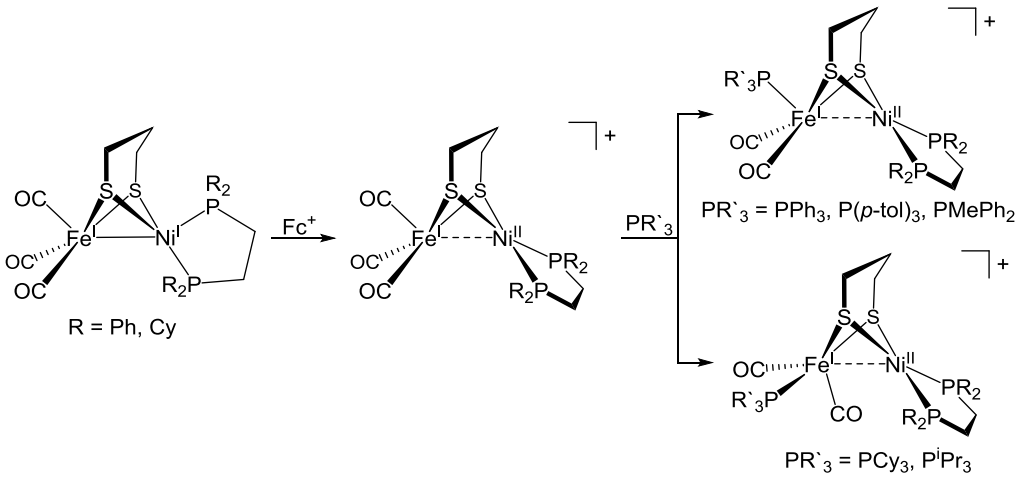
Scheme 1.19. Generation of $[(P(OEt)_3)_3Fe(H)Ni(S_2N_2')]^+$ from H_2 and formation of H_2 upon treatment with strong acid.



The ligand environment on Fe is crucial for H_2 activation. The use of $P(OEt)_3$ keeps the Fe(II) low spin and capable of activating H_2. A related model with tris(pyrazolyl)methane and a labile MeCN bound to Fe was not found to activate H_2 as the tris(pyrazolyl)methane ligand maintains a high spin Fe center.[97] In [NiFe]-H_2ase, Fe is ligated by both carbonyl and cyanide ligands, maintaining a low spin Fe(II) oxidation state.

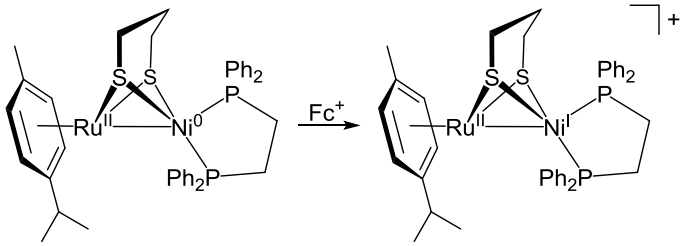
Mixed valent states are prevalent in the catalytic cycle of [NiFe]-H_2ase, but only a few model complexes with mixed valent NiFe centers are reported. No models of Ni-A, Ni-B, or Ni-C have been reported, though a few models of the Ni-L state have been developed. Treatment of $(CO)_3Fe(pdt)Ni(diphos)$ with Fc^+ formed the Ni(II)Fe(I) compounds $[(CO)_3Fe(pdt)Ni(diphos)]^+$, reverse of the oxidation states in Ni-L.[98] Evidence for a Ni(II) oxidation state was present in the X-ray crystal structure of $[(CO)_3Fe(pdt)Ni(diphos)]^+$ as the Ni was found to have a square planar geometry, characteristic of Ni(II). Furthermore, the EPR spectrum of $[(CO)_3Fe(pdt)Ni(diphos)]^+$ was found to have *g*-values consistent with Fe(I). The ^{31}P hyperfine coupling of the EPR signals also indicate Fe(I) as coupling is absent for $[(CO)_3Fe(pdt)Ni(diphos)]^+$ while present for the substituted mixed valent compounds $[(CO)_2PR_3Fe(pdt)Ni(diphos)]^+$.[99] The use of strong σ-donors induced rotation of the $Fe(CO)_2(PR_3)$ subunit, resembling the rotated structure found in [FeFe]-H_2ase (Scheme 1.20).

Scheme 1.20. Oxidation and ligand substitution of $(CO)_3Fe(pdt)Ni(dxpe)$.



The first Ni-L model with Ni(I) oxidation state was developed by use of a NiRu core.[100] Oxidation of the Ni(0)Ru(II) complex (arene)Ru(pdt)Ni(diphos) resulted in the Ni(I)Ru(II) complex $[(arene)Ru(pdt)Ni(diphos)]^+$ (Scheme 1.21). The EPR resonance of $[(arene)Ru(pdt)Ni(diphos)]^+$ displayed *g*-values comparable to those reported for Ni-L. Furthermore the EPR spectrum exhibits ^{31}P coupling from two inequivalent phosphines while the crystal structure of $[(arene)Ru(pdt)Ni(diphos)]^+$ was found to have a distorted tetrahedral geometry at Ni.

Scheme 1.21. Oxidation of (arene)Ru(pdt)Ni(dppe).



1.4 References

(1) Tian, F.; Toon, O. B.; Pavlov, A. A.; De Sterck, H. "A Hydrogen-Rich Early Earth Atmosphere" *Science* **2005**, *308*, 1014.

(2) Vignais, P. M.; Billoud, B. "Occurrence, Classification, and Biological Function of Hydrogenases: An Overview" *Chem. Rev.* **2007**, *107*, 4206.

(3) Pierik, A. J.; Hulstein, M.; Hagen, W. R.; Albracht, S. P. J. "A Low-Spin Iron with CN and CO as Intrinsic Ligands Forms the Core of the Active Site in [Fe]-Hydrogenases" *Eur. J. Biochem.* **1998**, *258*, 572.

(4) Pierik, A. J.; Roseboom, W.; Happe, R. P.; Bagley, K. A.; Albracht, S. P. J. "Carbon Monoxide and Cyanide as Intrinsic Ligands to Iron in the Active Site of [NiFe]-Hydrogenases - $NiFe(CN)_2CO$, Biology's Way to Activate H_2" *J. Biol. Chem.* **1999**, *274*, 3331.

(5) Fontecilla-Camps, J. C.; Volbeda, A.; Cavazza, C.; Nicolet, Y. "Structure/Function Relationships of [NiFe]- and [FeFe]-Hydrogenases" *Chem. Rev.* **2007**, *107*, 4273.

(6) Pandey, A. S.; Harris, T. V.; Giles, L. J.; Peters, J. W.; Szilagyi, R. K. "Dithiomethylether as a Ligand in the Hydrogenase H-Cluster" *J. Am. Chem. Soc.* **2008**, *130*, 4533.

(7) Ogata, H.; Kellers, P.; Lubitz, W. "The Crystal Structure of the NiFe Hydrogenase from the Photosynthetic Bacterium *Allochromatium vinosum*: Characterization of the Oxidized Enzyme (Ni-A State)" *J. Mol. Biol.* **2010**, *402*, 428.

(8) Tard, C.; Pickett, C. J. "Structural and Functional Analogues of the Active Sites of the [Fe]-, [NiFe]-, and [FeFe]-Hydrogenases" *Chem. Rev.* **2009**, *109*, 2245.

(9) Horch, M.; Schoknecht, J.; Mroginski, M. A.; Lenz, O.; Hildebrandt, P.; Zebger, I. "Resonance Raman Spectroscopy on [NiFe] Hydrogenase Provides Structural Insights into Catalytic Intermediates and Reactions" *J. Am. Chem. Soc.* **2014**, *136*, 9870.

(10) Vincent, K. A.; Parkin, A.; Armstrong, F. A. "Investigating and Exploiting the Electrocatalytic Properties of Hydrogenases" *Chem. Rev.* **2007**, *107*, 4366.

(11) Hambourger, M.; Gervaldo, M.; Svedruzic, D.; King, P. W.; Gust, D.; Ghirardi, M.; Moore, A. L.; Moore, T. A. "[FeFe]-Hydrogenase-Catalyzed H_2 Production in a Photoelectrochemical Biofuel Cell" *J. Am. Chem. Soc.* **2008**, *130*, 2015.

(12) Jones, A. K.; Sillery, E.; Albracht, S. P. J.; Armstrong, F. A. "Direct Comparison of the Electrocatalytic Oxidation of Hydrogen by an Enzyme and a Platinum Catalyst" *Chem. Commun.* **2002**, 866.

(13) Hatchikian, E. C.; Forget, N.; Fernandez, V. M.; Williams, R.; Cammack, R. "Further Characterization of the [Fe]-Hydrogenase from *Desulfovibrio desulfuricans* ATCC-7757" *Eur. J. Biochem.* **1992**, *209*, 357.

(14) Fauque, G.; Peck, H. D.; Moura, J. J. G.; Huynh, B. H.; Berlier, Y.; Dervartanian, D. V.; Teixeira, M.; Przybyla, A. E.; Lespinat, P. A.; Moura, I.; Legall, J. "The 3 Classes of Hydrogenases from Sulfate-Reducing Bacteria of the Genus *Desulfovibrio*" *FEMS Microbiol. Lett.* **1988**, *54*, 299.

(15) Häussinger, P.; Lohmüller, R.; Watson, A. M. "Hydrogen, 2. Production" In *Ullmann's Encyclopedia of Industrial Chemistry*; Wiley-VCH: 2000.

(16) Baturina, O. A.; Smirnova, A. E. "Chapter 4 - Catalytic Processes Using Fuel Cells, Catalytic Batteries, and Hydrogen Storage Materials" In *New and Future Developments in Catalysis*; Suib, S. L., Ed.; Elsevier: Amsterdam, 2013, p 69.

(17) Alper, J. ″Water Splitting Goes Au Naturel″ *Science* **2003**, *299*, 1686.

(18) Carroll, M. E.; Barton, B. E.; Rauchfuss, T. B.; Carroll, P. J. ″Synthetic Models for the Active Site of the [FeFe]-Hydrogenase: Catalytic Proton Reduction and the Structure of the Doubly Protonated Intermediate″ *J. Am. Chem. Soc.* **2012**, *134*, 18843.

(19) Silakov, A.; Wenk, B.; Reijerse, E.; Lubitz, W. ″^{14}N HYSCORE Investigation of the H-Cluster of [FeFe] Hydrogenase: Evidence for a Nitrogen in the Dithiol Bridge″ *Phys. Chem. Chem. Phys.* **2009**, *11*, 6592.

(20) Olsen, M. T.; Barton, B. E.; Rauchfuss, T. B. ″Hydrogen Activation by Biomimetic Diiron Dithiolates″ *Inorg. Chem.* **2009**, *48*, 7507.

(21) Berggren, G.; Adamska, A.; Lambertz, C.; Simmons, T. R.; Esselborn, J.; Atta, M.; Gambarelli, S.; Mouesca, J. M.; Reijerse, E.; Lubitz, W.; Happe, T.; Artero, V.; Fontecave, M. ″Biomimetic Assembly and Activation of [FeFe]-Hydrogenases″ *Nature* **2013**, *499*, 66.

(22) Knorzer, P.; Silakov, A.; Foster, C. E.; Armstrong, F. A.; Lubitz, W.; Happe, T. ″Importance of the Protein Framework for Catalytic Activity of [FeFe]-Hydrogenases″ *J. Biol. Chem.* **2012**, *287*, 1489.

(23) Kuchenreuther, J. M.; Myers, W. K.; Suess, D. L. M.; Stich, T. A.; Pelmenschikov, V.; Shiigi, S. A.; Cramer, S. P.; Swartz, J. R.; Britt, R. D.; George, S. J. ″The HydG Enzyme Generates an $Fe(CO)_2(CN)$ Synthon in Assembly of the [FeFe] Hydrogenase H-Cluster″ *Science* **2014**, *343*, 424.

(24) Kuchenreuther, J. M.; Myers, W. K.; Stich, T. A.; George, S. J.; NejatyJahromy, Y.; Swartz, J. R.; Britt, R. D. ″A Radical Intermediate in Tyrosine Scission to the CO and CN^- Ligands of [FeFe] Hydrogenase″ *Science* **2013**, *342*, 472.

(25) Pilet, E.; Nicolet, Y.; Mathevon, C.; Douki, T.; Fontecilla-Camps, J. C.; Fontecave, M. ″The Role of the Maturase HydG in [FeFe]-Hydrogenase Active Site Synthesis and Assembly″ *FEBS Lett.* **2009**, *583*, 506.

(26) Lubitz, W.; Ogata, H.; Rudiger, O.; Reijerse, E. ″Hydrogenases″ *Chem. Rev.* **2014**, *114*, 4081.

(27) Lemon, B. J.; Peters, J. W. ″Binding of Exogenously Added Carbon Monoxide at the Active Site of the Iron-Only Hydrogenase (CpI) from *Clostridium pasteurianum*" *Biochemistry* **1999**, *38*, 12969.

(28) Mulder, D. W.; Ratzloff, M. W.; Shepard, E. M.; Byer, A. S.; Noone, S. M.; Peters, J. W.; Broderick, J. B.; King, P. W. "EPR and FTIR Analysis of the Mechanism of H_2 Activation by [FeFe]-Hydrogenase HydA1 from *Chlamydomonas reinhardtii*" *J. Am. Chem. Soc.* **2013**, *135*, 6921.

(29) Adamska, A.; Silakov, A.; Lambertz, C.; Rudiger, O.; Happe, T.; Reijerse, E.; Lubitz, W. "Identification and Characterization of the "Super-Reduced" State of the H-Cluster in [FeFe] Hydrogenase: A New Building Block for the Catalytic Cycle?" *Angew. Chem. Int. Ed.* **2012**, *51*, 11458.

(30) Lambertz, C.; Leidel, N.; Havelius, K. G. V.; Noth, J.; Chernev, P.; Winkler, M.; Happe, T.; Haumann, M. "O_2 Reactions at the Six-Iron Active Site (H-Cluster) in [FeFe]-Hydrogenase" *J. Biol. Chem.* **2011**, *286*, 40614.

(31) Reihlen, H.; Friedolsheim, A. V.; Oswald, W. "Über Stickoxyd- und Kohlenoxydverbindungen des scheinbar einwertigen Eisens und Nickels." *Justus Liebigs Ann. Chem.* **1928**, *465*, 72.

(32) King, R. B. "Organosulfur Derivatives of Metal Carbonyls .1. Isolation of 2 Isomeric Products in Reaction of Triiron Dodecacarbonyl with Dimethyl Disulfide" *J. Am. Chem. Soc.* **1962**, *84*, 2460.

(33) Gloaguen, F.; Lawrence, J. D.; Schmidt, M.; Wilson, S. R.; Rauchfuss, T. B. "Synthetic and Structural Studies on $[Fe_2(SR)_2(CN)_x(CO)_{6-x}]^{x-}$ as Active Site Models for Fe-Only Hydrogenases" *J. Am. Chem. Soc.* **2001**, *123*, 12518.

(34) Harb, M. K.; Apfel, U. P.; Sakamoto, T.; El-khateeb, M.; Weigand, W. "Diiron Dichalcogenolato (Se and Te) Complexes: Models for the Active Site of [FeFe] Hydrogenase" *Eur. J. Inorg. Chem.* **2011**, 986.

(35) Lawrence, J. D.; Li, H. X.; Rauchfuss, T. B.; Benard, M.; Rohmer, M. M. "Diiron Azadithiolates as Models for the Iron-Only Hydrogenase Active Site: Synthesis, Structure, and Stereoelectronics" *Angew. Chem. Int. Ed.* **2001**, *40*, 1768.

(36) Li, H. X.; Rauchfuss, T. B. "Iron Carbonyl Sulfides, Formaldehyde, and Amines Condense to give the Proposed Azadithiolate Cofactor of the [Fe]-Only Hydrogenases" *J. Am. Chem. Soc.* **2002**, *124*, 726.

(37) Stanley, J. L.; Heiden, Z. M.; Rauchfuss, T. B.; Wilson, S. R.; De Gioia, L.; Zampella, G. "Desymmetrized Diiron Azadithiolato, Carbonyls: A Step Toward Modeling the Iron-Only Hydrogenases" *Organometallics* **2008**, *27*, 119.

(38) Angamuthu, R.; Carroll, M. E.; Ramesh, M.; Rauchfuss, T. B. "A New Route to Azadithiolato Complexes" *Eur. J. Inorg. Chem.* **2011**, 1029.

(39) Schmidt, M.; Contakes, S. M.; Rauchfuss, T. B. "First Generation Analogues of the Binuclear Site in the Fe-Only Hydrogenases: $Fe_2(\mu\text{-}SR)_2(CO)_4(CN)_2^{2-}$" *J. Am. Chem. Soc.* **1999**, *121*, 9736.

(40) Lyon, E. J.; Georgakaki, I. P.; Reibenspies, J. H.; Darensbourg, M. Y. "Carbon Monoxide and Cyanide Ligands in a Classical Organometallic Complex Model for Fe-Only Hydrogenase" *Angew. Chem. Int. Ed.* **1999**, *38*, 3178.

(41) Le Cloirec, A.; Best, S. P.; Borg, S.; Davies, S. C.; Evans, D. J.; Hughes, D. L.; Pickett, C. J. "A Di-Iron Dithiolate Possessing Structural Elements of the Carbonyl/Cyanide Sub-Site of the H-Centre of Fe-Only Hydrogenase" *Chem. Commun.* **1999**, 2285.

(42) Jablonskyte, A.; Wright, J. A.; Pickett, C. J. "Mechanistic Aspects of the Protonation of [FeFe]-Hydrogenase Subsite Analogues" *Dalton Trans.* **2010**, *39*, 3026.

(43) Justice, A. K.; De Gioia, L.; Nilges, M. J.; Rauchfuss, T. B.; Wilson, S. R.; Zampella, G. "Redox and Structural Properties of Mixed-Valence Models for the Active Site of the [FeFe]-Hydrogenase: Progress and Challenges" *Inorg. Chem.* **2008**, *47*, 7405.

(44) Gloaguen, F.; Lawrence, J. D.; Rauchfuss, T. B. "Biomimetic Hydrogen Evolution Catalyzed by an Iron Carbonyl Thiolate" *J. Am. Chem. Soc.* **2001**, *123*, 9476.

(45) Tschierlei, S.; Ott, S.; Lomoth, R. "Spectroscopically Characterized Intermediates of Catalytic H_2 Formation by [FeFe] Hydrogenase Models" *Energ. Environ. Sci.* **2011**, *4*, 2340.

(46) Liu, T. B.; Darensbourg, M. Y. "A Mixed-Valent, Fe(II)Fe(I), Diiron Complex Reproduces the Unique Rotated State of the [FeFe] Hydrogenase Active Site" *J. Am. Chem. Soc.* **2007**, *129*, 7008.

(47) Justice, A. K.; Rauchfuss, T. B.; Wilson, S. R. "Unsaturated, Mixed-Valence Diiron Dithiolate Model for the H_{ox} State of the [FeFe] Hydrogenase" *Angew. Chem. Int. Ed.* **2007**, *46*, 6152.

(48) Hsieh, C. H.; Erdem, O. F.; Harman, S. D.; Singleton, M. L.; Reijerse, E.; Lubitz, W.; Popescu, C. V.; Reibenspies, J. H.; Brothers, S. M.; Hall, M. B.; Darensbourg, M. Y. "Structural and Spectroscopic Features of Mixed Valent $Fe^{II}Fe^{I}$ Complexes and Factors Related to the Rotated Configuration of Diiron Hydrogenase" *J. Am. Chem. Soc.* **2012**, *134*, 13089.

(49) Munery, S.; Capon, J. F.; De Gioia, L.; Elleouet, C.; Greco, C.; Petillon, F. Y.; Schollhammer, P.; Talarmin, J.; Zampella, G. "New $Fe^{I}Fe^{I}$ Complex Featuring a Rotated Conformation Related to the $[2Fe]_H$ Subsite of [Fe-Fe] Hydrogenase" *Chem. Eur. J.* **2013**, *19*, 15458.

(50) Wang, W. G.; Rauchfuss, T. B.; Moore, C. E.; Rheingold, A. L.; De Gioia, L.; Zampella, G. "Crystallographic Characterization of a Fully Rotated, Basic Diiron Dithiolate: Model for the H_{red} State?" *Chem. Eur. J.* **2013**, *19*, 15476.

(51) Barton, B. E.; Zampella, G.; Justice, A. K.; De Gioia, L.; Rauchfuss, T. B.; Wilson, S. R. "Isomerization of the Hydride Complexes $[HFe_2(SR)_2(PR_3)_x(CO)_{6-x}]^+$ (x = 2, 3, 4) Relevant to the Active Site Models for the [FeFe]-Hydrogenases" *Dalton Trans.* **2010**, *39*, 3011.

(52) van der Vlugt, J. I.; Rauchfuss, T. B.; Whaley, C. M.; Wilson, S. R. "Characterization of a Diferrous Terminal Hydride Mechanistically Relevant to the Fe-Only Hydrogenases" *J. Am. Chem. Soc.* **2005**, *127*, 16012.

(53) Ezzaher, S.; Capon, J. F.; Gloaguen, F.; Petillon, F. Y.; Schollhammer, P.; Talarmin, J. "Evidence for the Formation of Terminal Hydrides by Protonation of an Asymmetric Iron Hydrogenase Active Site Mimic" *Inorg. Chem.* **2007**, *46*, 3426.

(54) Zaffaroni, R.; Rauchfuss, T. B.; Gray, D. L.; De Gioia, L.; Zampella, G. "Terminal vs Bridging Hydrides of Diiron Dithiolates: Protonation of Fe_2(dithiolate)$(CO)_2(PMe_3)_4$" *J. Am. Chem. Soc.* **2012**, *134*, 19260.

(55) Wang, W. G.; Nilges, M. J.; Rauchfuss, T. B.; Stein, M. "Isolation of a Mixed Valence Diiron Hydride: Evidence for a Spectator Hydride in Hydrogen Evolution Catalysis" *J. Am. Chem. Soc.* **2013**, *135*, 3633.

(56) Camara, J. M.; Rauchfuss, T. B. "Mild Redox Complementation Enables H_2 Activation by [FeFe]-Hydrogenase Models" *J. Am. Chem. Soc.* **2011**, *133*, 8098.

(57) Camara, J. M.; Rauchfuss, T. B. "Combining Acid-Base, Redox and Substrate Binding Functionalities to Give a Complete Model for the [FeFe]-Hydrogenase" *Nat. Chem.* **2012**, *4*, 26.

(58) Lansing, J. C.; Camara, J. M.; Gray, D. E.; Rauchfuss, T. B. Hydrogen Production Catalyzed by Bidirectional, Biomimetic Models of the [FeFe]-Hydrogenase Active Site. *Organometallics* [Online Early Access]. DOI: 10.1021/om5004013. Published Online: 2014.

(59) Wang, N.; Wang, M.; Wang, Y.; Zheng, D. H.; Han, H. X.; Ahlquist, M. S. G.; Sun, L. C. "Catalytic Activation of H_2 under Mild Conditions by an [FeFe]-Hydrogenase Model via an Active μ-Hydride Species" *J. Am. Chem. Soc.* **2013**, *135*, 13688.

(60) De Lacey, A. L.; Fernandez, V. M.; Rousset, M. "Native and Mutant Nickel-Iron Hydrogenases: Unravelling Structure and Function" *Coord. Chem. Rev.* **2005**, *249*, 1596.

(61) Watanabe, S.; Sasaki, D.; Tominaga, T.; Miki, K. "Structural Basis of [NiFe] Hydrogenase Maturation by Hyp Proteins" *Biol. Chem.* **2012**, *393*, 1089.

(62) Reissmann, S.; Hochleitner, E.; Wang, H. F.; Paschos, A.; Lottspeich, F.; Glass, R. S.; Bock, A. "Taming of a Poison: Biosynthesis of the [NiFe]-Hydrogenase Cyanide Ligands" *Science* **2003**, *299*, 1067.

(63) Stripp, S. T.; Soboh, B.; Lindenstrauss, U.; Braussemann, M.; Herzberg, M.; Nies, D. H.; Sawers, R. G.; Heberle, J. "HypD Is the Scaffold Protein for $Fe(CN)_2CO$ Cofactor Assembly in [NiFe]-Hydrogenase Maturation" *Biochemistry* **2013**, *52*, 3289.

(64) Ogata, H.; Lubitz, W.; Higuchi, Y. "[NiFe] Hydrogenases: Structural and Spectroscopic Studies of the Reaction Mechanism" *Dalton Trans.* **2009**, 7577.

(65) Volbeda, A.; Martin, L.; Cavazza, C.; Matho, M.; Faber, B. W.; Roseboom, W.; Albracht, S. P. J.; Garcin, E.; Rousset, M.; Fontecilla-Camps, J. C. "Structural Differences Between the Ready and Unready Oxidized States of [NiFe]-Hydrogenases" *J. Biol. Inorg. Chem.* **2005**, *10*, 239.

(66) Pandelia, M. E.; Ogata, H.; Lubitz, W. "Intermediates in the Catalytic Cycle of [NiFe] Hydrogenase: Functional Spectroscopy of the Active Site" *ChemPhysChem* **2010**, *11*, 1127.

(67) Kurkin, S.; George, S. J.; Thorneley, R. N. F.; Albracht, S. P. J. "Hydrogen-Induced Activation of the [NiFe]-Hydrogenase from *Allochromatium vinosum* as Studied by Stopped-Flow Infrared Spectroscopy" *Biochemistry* **2004**, *43*, 6820.

(68) Lauterbach, L.; Lenz, O. "Catalytic Production of Hydrogen Peroxide and Water by Oxygen-Tolerant [NiFe]-Hydrogenase During H_2 Cycling in the Presence of O_2" *J. Am. Chem. Soc.* **2013**, *135*, 17897.

(69) Foerster, S.; van Gastel, M.; Brecht, M.; Lubitz, W. "An Orientation-Selected ENDOR and HYSCORE Study of the Ni-C Active State of *Desulfovibrio vulgaris* Miyazaki F Hydrogenase" *J. Biol. Inorg. Chem.* **2005**, *10*, 51.

(70) Stein, M.; Lubitz, W. "The Electronic Structure of the Catalytic Intermediate Ni-C in [NiFe] and [NiFeSe] Hydrogenases" *Phys. Chem. Chem. Phys.* **2001**, *3*, 5115.

(71) Vanderzwaan, J. W.; Albracht, S. P. J.; Fontijn, R. D.; Slater, E. C. "Mono-Valent Nickel in Hydrogenase from *Chromatium vinosum*: Light Sensitivity and Evidence for Direct Interaction with Hydrogen" *FEBS Lett.* **1985**, *179*, 271.

(72) Dubois, M. R.; Dubois, D. L. "Development of Molecular Electrocatalysts for CO_2 Reduction and H_2 Production/Oxidation" *Acc. Chem. Res.* **2009**, *42*, 1974.

(73) Liu, T. B.; DuBois, D. L.; Bullock, R. M. "An Iron Complex with Pendent Amines as a Molecular Electrocatalyst for Oxidation of Hydrogen" *Nat. Chem.* **2013**, *5*, 228.

(74) Ogata, H.; Mizoguchi, Y.; Mizuno, N.; Miki, K.; Adachi, S.; Yasuoka, N.; Yagi, T.; Yamauchi, O.; Hirota, S.; Higuchi, Y. "Structural Studies of the Carbon Monoxide Complex of [NiFe] Hydrogenase from *Desulfovibrio vulgaris* Miyazaki F: Suggestion for the Initial Activation Site for Dihydrogen" *J. Am. Chem. Soc.* **2002**, *124*, 11628.

(75) Niu, S.; Hall, N. B. "Modeling the Active Sites in Metalloenzymes 5. The Heterolytic Bond Cleavage of H_2 in the [NiFe] Hydrogenase of *Desulfovibrio gigas* by a Nucleophilic Addition Mechanism" *Inorg. Chem.* **2001**, *40*, 6201.

(76) Bruschi, M.; Tiberti, M.; Guerra, A.; De Gioia, L. ″Disclosure of Key Stereoelectronic Factors for Efficient H_2 Binding and Cleavage in the Active Site of [NiFe]-Hydrogenases″ *J. Am. Chem. Soc.* **2014**, *136*, 1803.

(77) Baltazar, C. S. A.; Marques, M. C.; Soares, C. M.; DeLacey, A. M.; Pereira, I. A. C.; Matias, P. M. ″Nickel-Iron-Selenium Hydrogenases - An Overview″ *Eur. J. Inorg. Chem.* **2011**, 948.

(78) Fritsch, J.; Lenz, O.; Friedrich, B. ″Structure, Function and Biosynthesis of O_2-Tolerant Hydrogenases″ *Nature Rev. Microbiol.* **2013**, *11*, 106.

(79) Pandelia, M.-E.; Nitschke, W.; Infossi, P.; Giudici-Orticoni, M.-T.; Bill, E.; Lubitz, W. ″Characterization of a Unique [FeS] Cluster in the Electron Transfer Chain of the Oxygen Tolerant [NiFe] Hydrogenase from *Aquifex aeolicus" Proc. Natl. Acad. Sci. U. S. A.* **2011**, *108*, 6097.

(80) Shomura, Y.; Yoon, K.-S.; Nishihara, H.; Higuchi, Y. ″Structural Basis for a [4Fe-3S] Cluster in the Oxygen-Tolerant Membrane-Bound [NiFe]-Hydrogenase″ *Nature* **2011**, *479*, 253.

(81) Ohki, Y.; Tatsumi, K. ″Thiolate-Bridged Iron-Nickel Models for the Active Site of [NiFe] Hydrogenase″ *Eur. J. Inorg. Chem.* **2011**, 973.

(82) Kaur-Ghumaan, S.; Stein, M. ″[NiFe] Hydrogenases: How Close do Structural and Functional Mimics Approach the Active Site?″ *Dalton Trans.* **2014**, *43*, 9392.

(83) Bouwman, E.; Reedijk, J. ″Structural and Functional Models Related to the Nickel Hydrogenases″ *Coord. Chem. Rev.* **2005**, *249*, 1555.

(84) Lauderbach, F.; Prakash, R.; Gotz, A. W.; Munoz, M.; Heinemann, F. W.; Nickel, U.; Hess, B. A.; Sellmann, D. ″Alternative Synthesis, Density Functional Calculations and Proton Reactivity Study of a Trinuclear [NiFe] Hydrogenase Model Compound″ *Eur. J. Inorg. Chem.* **2007**, 3385.

(85) Sellmann, D.; Lauderbach, F.; Geipel, F.; Heinemann, F. W.; Moll, M. ″A Trinuclear NiFe Cluster Exhibiting Structural and Functional Key Features of [NiFe] Hydrogenases″ *Angew. Chem. Int. Ed.* **2004**, *43*, 3141.

(86) Sellmann, D.; Lauderbach, F.; Heinemann, F. W. ″Trinuclear [NiFe] Clusters as Structural Models for [NiFe] Hydrogenase Active Sites″ *Eur. J. Inorg. Chem.* **2005**, 371.

(87) Canaguier, S.; Field, M.; Oudart, Y.; Pecaut, J.; Fontecave, M.; Artero, V. ″A Structural and Functional Mimic of the Active Site of [NiFe] Hydrogenases″ *Chem. Commun.* **2010**, *46*, 5876.

(88) Zhu, W. F.; Marr, A. C.; Wang, Q.; Neese, F.; Spencer, D. J. E.; Blake, A. J.; Cooke, P. A.; Wilson, C.; Schroder, M. ″Modulation of the Electronic Structure and the Ni-Fe Distance in Heterobimetallic Models for the Active Site in [NiFe] Hydrogenase″ *Proc. Natl. Acad. Sci. U. S. A.* **2005**, *102*, 18280.

(89) Carroll, M. E.; Barton, B. E.; Gray, D. L.; Mack, A. E.; Rauchfuss, T. B. "Active-Site Models for the Nickel-Iron Hydrogenases: Effects of Ligands on Reactivity and Catalytic Properties" *Inorg. Chem.* **2011**, *50*, 9554.

(90) Barton, B. E.; Whaley, C. M.; Rauchfuss, T. B.; Gray, D. L. "Nickel-Iron Dithiolato Hydrides Relevant to the [NiFe]-Hydrogenase Active Site" *J. Am. Chem. Soc.* **2009**, *131*, 6942.

(91) Barton, B. E.; Rauchfuss, T. B. "Hydride-Containing Models for the Active Site of the Nickel-Iron Hydrogenases" *J. Am. Chem. Soc.* **2010**, *132*, 14877.

(92) Shafaat, H. S.; Weber, K.; Petrenko, T.; Neese, F.; Lubitz, W. "Key Hydride Vibrational Modes in [NiFe] Hydrogenase Model Compounds Studied by Resonance Raman Spectroscopy and Density Functional Calculations" *Inorg. Chem.* **2012**, *51*, 11787.

(93) Ogo, S.; Kabe, R.; Uehara, K.; Kure, B.; Nishimura, T.; Menon, S. C.; Harada, R.; Fukuzumi, S.; Higuchi, Y.; Ohhara, T.; Tamada, T.; Kuroki, R. "A Dinuclear Ni(μ-H)Ru Complex Derived from H_2" *Science* **2007**, *316*, 585.

(94) Kure, B.; Matsumoto, T.; Ichikawa, K.; Fukuzumi, S.; Higuchi, Y.; Yagi, T.; Ogo, S. "pH-Dependent Isotope Exchange and Hydrogenation Catalysed by Water-Soluble NiRu Complexes as Functional Models for [NiFe] Hydrogenases" *Dalton Trans.* **2008**, 4747.

(95) Matsumoto, T.; Kure, B.; Ogo, S. "Extraction of Electrons from H_2 with a $Ni^{I}Ru^{I}$ Catalyst" *Chem. Lett.* **2008**, *37*, 970.

(96) Ogo, S.; Ichikawa, K.; Kishima, T.; Matsumoto, T.; Nakai, H.; Kusaka, K.; Ohhara, T. "A Functional [NiFe]-Hydrogenase Mimic That Catalyzes Electron and Hydride Transfer from H_2" *Science* **2013**, *339*, 682.

(97) Ichikawa, K.; Matsumoto, T.; Ogo, S. "Critical Aspects of [NiFe] Hydrogenase Ligand Composition" *Dalton Trans.* **2009**, 4304.

(98) Schilter, D.; Nilges, M. J.; Chakrabarti, M.; Lindahl, P. A.; Rauchfuss, T. B.; Stein, M. "Mixed-Valence Nickel-Iron Dithiolate Models of the [NiFe]-Hydrogenase Active Site" *Inorg. Chem.* **2012**, *51*, 2338.

(99) Schilter, D.; Rauchfuss, T. B.; Stein, M. "Connecting [NiFe]- and [FeFe]-Hydrogenases: Mixed-Valence Nickel-Iron Dithiolates with Rotated Structures" *Inorg. Chem.* **2012**, *51*, 8931.

(100) Chambers, G. M.; Mitra, J.; Rauchfuss, T. B.; Stein, M. "Ni^{I}/Ru^{II} Model for the Ni-L State of the [NiFe] Hydrogenases: Synthesis, Spectroscopy, and Reactivity" *Inorg. Chem.* **2014**, *53*, 4243.

Chapter 2

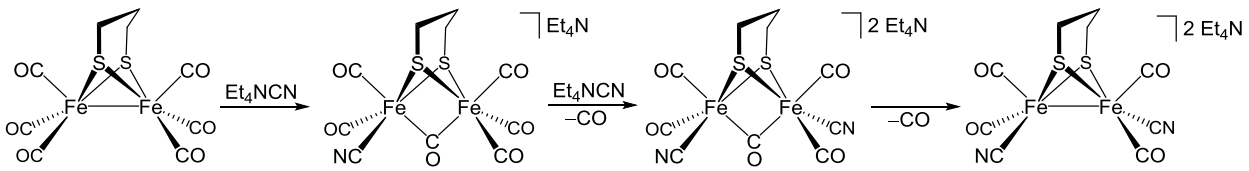
Boro-Cyanide Containing Models of [FeFe]-Hydrogenase

2.1 Introduction

The presence of the diatomic ligands cyanide and carbon monoxide in the active sites of [FeFe]- and [NiFe]-H_2ases was first characterized by FTIR.[1,2] The use of cyanide and carbon monoxide as ligands in biological systems is unusual as they are often associated with inactivation of active sites. For example, the toxicity of cyanide is attributed to inhibiting the binding of O_2 to the active site of cytochrome c oxidase.[3] The role of cyanide in H_2ases is unclear since few models incorporating this cofactor are available for investigation.[4] Cyanide is a powerful σ-donor ligand that in part serves to stabilize ferrous state. The redox inactivity of the $Fe(CN)_2(CO)$ center in the [NiFe]-H_2ases is attributed to the presence of the cyanide ligands, which keep Fe(II) in the low spin state throughout the catalytic cycle.[5] In the [FeFe]-H_2ases each Fe center is ligated by one cyanide, and at least one, and possibly both, of the Fe centers undergoes redox reactions.[6]

The salts of $[Fe_2(pdt)(CO)_4(CN)_2]^{2-}$ were first reported in 1999.[7-9] Treatment of $Fe_2(pdt)(CO)_6$ with two equivalents of Et_4NCN forms $(Et_4N)_2[Fe_2(pdt)(CO)_4(CN)_2]$, $(Et_4N)_2$[**2.1**]. Both CN^- ligands displace CO readily with no observed intermediates. Competition reactions showed that two CN^- ligands substitute faster with $Fe_2(pdt)(CO)_6$ than the substitution of one CN^- ligand in the monocyanide $[Fe_2(pdt)(CO)_5(CN)]^-$ ([**2.2**]$^-$). This result indicated that the second equivalent of CN^- adds faster than the first equivalent and that [**2.2**]$^-$ is not an intermediate in the synthesis of $(Et_4N)_2$[**2.1**]. An unobserved bridging CO intermediate was proposed as an intermediate (Scheme 2.1).[10] A related bridging CO compound has been observed after the addition of two equivalents of CN^- to a [FeFe]-H_2ase model with an tethered thioether ligand.[11]

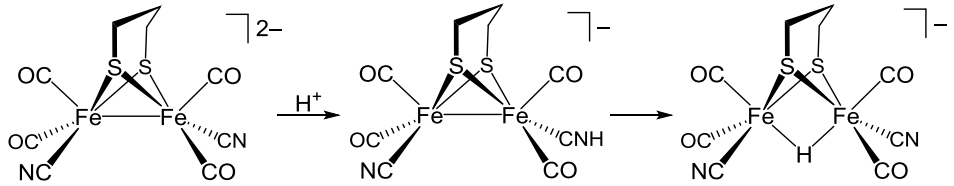
Scheme 2.1. Proposed mechanism for the substitution of two equivalents of Et_4NCN to $Fe_2(pdt)(CO)_6$ via a bridging CO intermediate to form $(Et_4N)_2$[**2.1**].



Few reports of [FeFe]-H_2ase models with cyanide ligands have followed since initially reported as the models are unstable with regard to protonation and oxidation. Protonation of $(Et_4N)_2$[**2.1**] occurs initially at a Fe-C*N* site followed by formation of the bridging hydride $Et_4N[Fe_2(\mu\text{-}H)(pdt)(CO)_4(CN)_2]$, Et_4N[H**2.1**] (Scheme 2.2).[12]

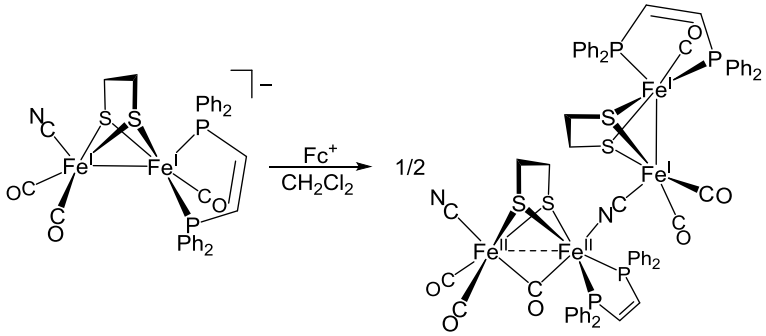
Two major isomers of [H**2.1**]$^-$ have been reported by ^{1}H NMR spectroscopy, but no assignment of the isomers was given.[13] Solutions of [H**2.1**]$^-$ are unstable at room temperature and decomposes over several hours as determined by IR spectroscopy. Attempts to isolate samples of [H**2.1**]$^-$ resulted in an insoluble solid.

Scheme 2.2. Protonation of [**2.1**]$^{2-}$ occurring initially at Fe-C*N* before forming the bridging hydride Et_4N[H**2.1**].



Both chemical and electrochemical studies indicate that oxidized derivatives of [**2.1**]$^{2-}$ are unstable. Studying the redox properties of [**2.1**]$^{2-}$ resulted in the deposition of a blue film on the surface of the working electrode.[10] Chemical oxidation of $[Fe_2(edt)(CO)_3(CN)(dppv)]^-$ results in a four Fe-centered compound consisting of two Fe_2S_2 cores bridged by a bidendate CN^- ligand (Scheme 2.3). As a consequence of problems associated with cyanide-centered reactions, functional models of [FeFe]-H_2ase have focused on using neutral donor ligands such as phosphines.

Scheme 2.3. Single electron oxidation of $[Fe_2(edt)(CO)_3(CN)(dppv)]^-$.



Nature prevents such problems with the ambidentate reactivity of cyanide by encapsulating the active site in globular proteins. The crystal structure of *C. pasteurianum* (Figure 2.1) demonstrates hydrogen bonding between the cyanide ligands and surrounding protein.[14] The distal Fe-C*N* is strongly hydrogen-bonded to Lys358 (N···N distance = 2.74 Å). The lysine group is highly conserved among [FeFe]-H_2ase active sites with the hydrogen-bonding interaction determined to be critical for catalytic activity.[15] The proximal Fe-C*N* is weakly hydrogen-bonded to Ser232 (N···O distance = 2.92 Å) in *C. pasteurianum*.[14] The amino acid hydrogen bonding to

the proximal Fe-C*N* is not highly conserved and has also been found to be substituted with alanine in other [FeFe]-H_2ase enzymes.[15]

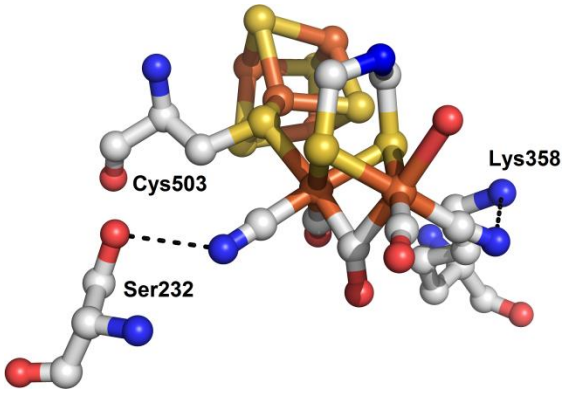


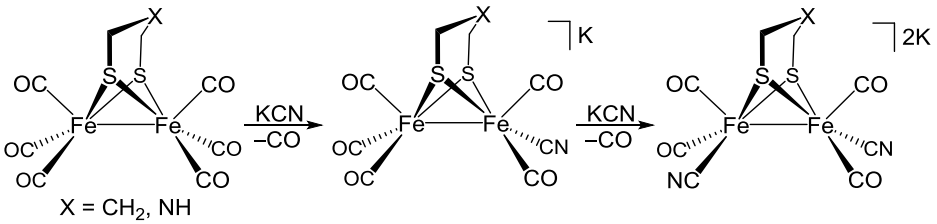
Figure 2.1. Active site of Fe_{ox}^{air} state of [FeFe]-H_2ase from *C. pasteurianum* depicting hydrogen-bonding to cyanide ligands by nearby side chains (PDB: 3C8Y).

In order to tame the ambidenate Nature of the cyanide ligand in [FeFe]-H_2ase models, the coordination of Lewis acids to the Fe-C*N* centers to simulate hydrogen-bonding was explored. The coordination of Lewis acids to metal cyanide complexes is not unprecedented. The ability of triarylboranes to bind to cyanide ligands is well estabilished examples include *trans*-RuH(CNBPh$_3$)(diphos), Ni(diphos)(π-allyl)(CNBPh$_3$), $[M(CNBArF_3)_4]^{2-}$ (M = Ni, Pd) and FeCp(CNBAr$^F_3$)(CO)$_2$.[16-18] Lewis acids are combined with Ni(0) phosphite catalysts to improve selectivity for linear products in the hydrocyanation of alkenes through the formation of $L_nNi(CN{\cdot}LA)R$ intermediates (LA = Lewis acid).[19] The chemistry of boranes has been rapidly developed due to their role in alkene polymerization,[20] and frustrated Lewis base pairs (FLBs),[21] with methods having been developed for evaluating their Lewis acidity.[22]

2.2 New Synthesis of $[Fe_2(xdt)(CO)_4(CN)_2]^{2-}$

A new route to [**2.1**]$^{2-}$ was developed from the reaction of $Fe_2(pdt)(CO)_6$ with excess KCN in refluxing MeCN, to form the potassium salt K_2[**2.1**] (Scheme 2.4). The intermediate [**2.2**]$^-$ was observed while monitoring of the reaction (Figure 2.2). Prolonged reaction times resulted in the formation of precipitate thought to occur from Fe-CN-K-NC-Fe linkages. The intermediate K[**2.2**] could be formed in good yield from the reaction of $Fe_2(pdt)(CO)_6$ with 0.9 equivalents of KCN in refluxing MeCN. Similarly, the treatment of $Fe_2(adt)(CO)_6$ with excess KCN in refluxing MeCN formed $K_2[Fe_2(adt)(CO)_4(CN)_2]$ K_2[**2.3**]. The salts K_2[**2.1**] and K_2[**2.3**] were soluble in MeCN as well as THF and Et_2O in the presence of small amounts of MeCN. Like Et_4N[**2.2**], K[**2.2**] exhibited good solubility in MeCN and THF.

Scheme 2.4. Step-wise substitution of KCN to $Fe_2(xdt)(CO)_6$ forming the intermediate $K[Fe_2(xdt)(CO)_5(CN)]$ and the disubstituted product $K_2[Fe_2(xdt)(CO)_4(CN)_2]$.



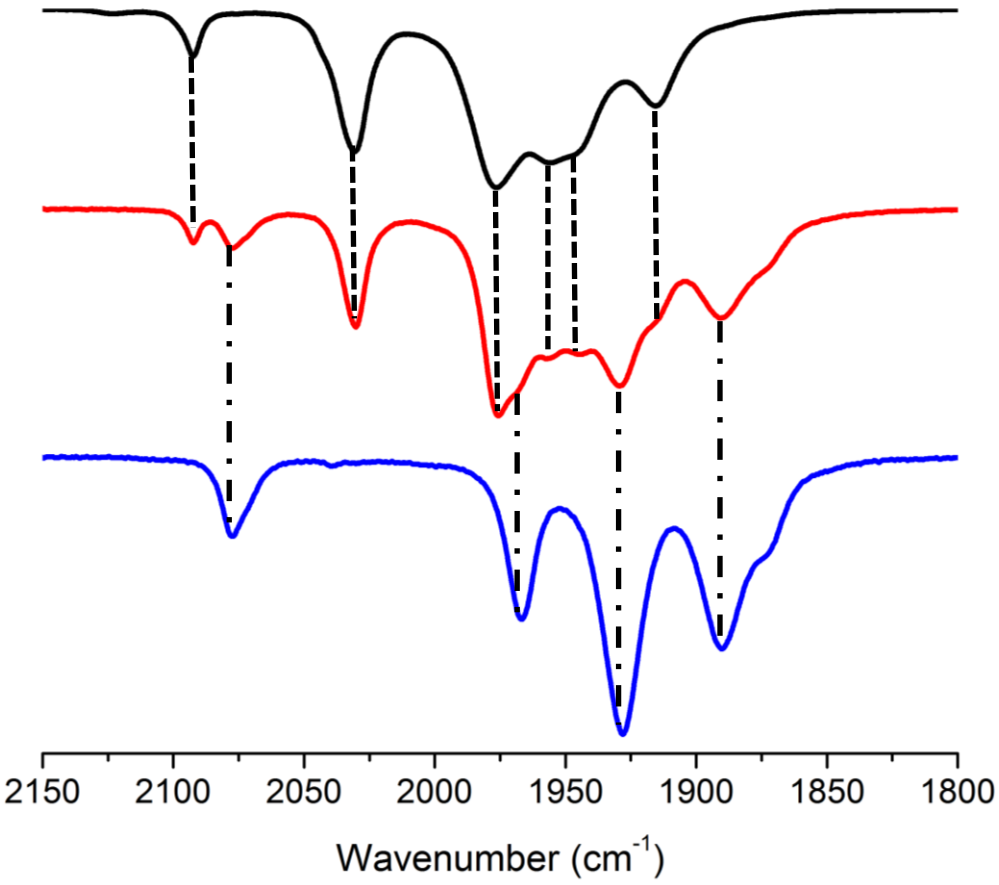


Figure 2.2. IR spectra in MeCN of K[**2.2**] (top), reaction mixture of the synthesis of K_2[**2.1**] (middle), and K_2[**2.1**] (bottom).

The IR spectrum of the potassium salts of $[\mathbf{2.1}]^{2-}$, $[\mathbf{2.2}]^{-}$, and $[\mathbf{2.3}]^{2-}$ were shifted to slightly higher energies from the related Et_4N^+ salts (Table 2.1). The shift in IR frequencies is reasoned to occur from coordination of the K^+ cation to the Fe-C*N*. Coordination of K^+ to Fe-C*N* has been previously observed for the crystal structure of $K[Fe(Cp)(CO)_2(CN)]$.[23] The salt K_2[**2.1**] undergoes cation exchange. Treatment of MeCN solutions of K_2[**2.1**] with Et_4NCl or PPNCl precipitated KCl from solution and formed $(Et_4N)_2$[**2.1**] or $(PPN)_2$[**2.1**] as indicated by IR

spectroscopy.[10,24] The shifting of the ν_{CO} bands to lower energies in the IR spectra is consistent with loss of the Fe-CN-K interaction (Figure 2.3).

Table 2.1. IR bands for Et_4N^+, PPN^+, and K^+ salts of $[\mathbf{2.1}]^{2-}$, $[\mathbf{2.2}]^-$, and $[\mathbf{2.3}]^{2-}$.

Compound	ν_{CN} (cm^{-1})	ν_{CO} (cm^{-1})
$(Et_4N)_2[\mathbf{2.1}]$[a]	2075	1964, 1924, 1885
$(PPN)_2[\mathbf{2.1}]$[a]	2075	1963, 1922, 1884
$K_2[\mathbf{2.1}]$[a]	2077	1967, 1928, 1890
$Et_4N[\mathbf{2.2}]$[b]	2094	2029, 1974, 1955, 1941, 1917
$K[\mathbf{2.2}]$[a]	2092	2031, 1976, 1956, 1946, 1916
$(Et_4N)_2[\mathbf{2.3}]$[a]	2075	1969, 1925, 1892
$K_2[\mathbf{2.3}]$[a]	2078	1969, 1929, 1893

[a]MeCN solution. [b]THF solution, ref [10]

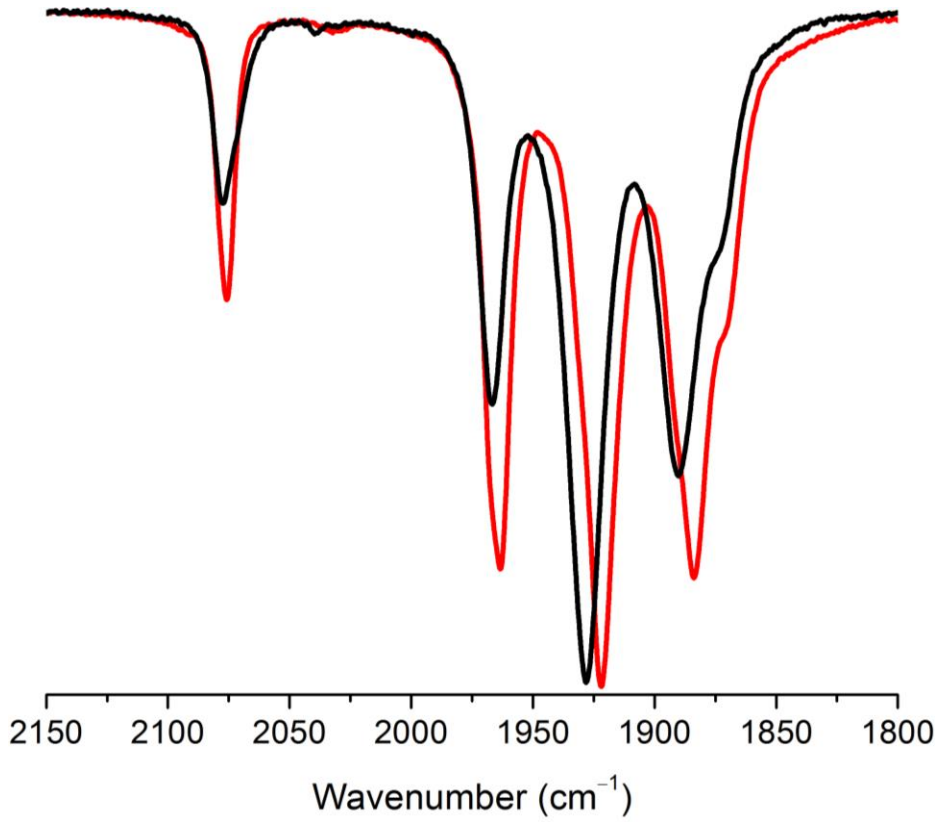


Figure 2.3. IR spectrum of $K_2[\mathbf{2.1}]$ before (black) and after addition of two equivalents of PPNCl (red) in MeCN.

2.3 2:1 Lewis Acid Adducts of $(Et_4N)_2[Fe_2(pdt)(CO)_4(CN)_2]$

Treatment of CH_2Cl_2 solutions of $(Et_4N)_2$[**2.1**] with two equivalents of the Lewis acid $BAr^F{}_3$ forms the 2:1 adduct $(Et_4N)_2$[**2.1**$(BAr^F{}_3)_2$]. The reaction could be monitored by color change from red to orange and by shifts in ν_{CN} and ν_{CO} to higher energies (Table 2.2). The weaker Lewis acids BPh_3 and $B(2,4,6\text{-}C_6F_3H_2)_3$ ($BAr^{F\#}{}_3$) also formed the corresponding 2:1 adducts with $(Et_4N)_2$[**2.1**]. The ν_{CO} energies of the adducts correlate with the relative Lewis acidities of $BAr^F{}_3 > BAr^{F\#}{}_3 > BPh_3$ as established by Child's method,[25-28] computational models,[29] and use as co-catalysts in polymerization studies (Figure 2.4).[30] Compared to the parent compound $(Et_4N)_2$[**2.1**] the adducts exhibit increased solubility in nonpolar solvents. The parent compound $(Et_4N)_2$[**2.1**] is soluble in MeCN and CH_2Cl_2. The adducts are also soluble in THF, and in the case of $(Et_4N)_2$[**2.1**$(BAr^F{}_3)_2$], even in Et_2O.

Table 2.2. IR bands for $(Et_4N)_2$[**2.1**] and related adducts in CH_2Cl_2 solution.

Compound	ν_{CN} **(cm^{-1})**	ν_{CO} **(cm^{-1})**
$(Et_4N)_2$[**2.1**]	2075	1964, 1924, 1885
$(Et_4N)_2$[**2.1**$(BPh_3)_2$]	2137	1984, 1946, 1911
$(Et_4N)_2$[**2.3**$(BPh_3)_2$]	2136	1986, 1949, 1914
$(Et_4N)_2$[**2.1**$(BAr^{F\#}{}_3)_2$]	2147	1986, 1947, 1915
$(Et_4N)_2$[**2.1**$(BAr^F{}_3)_2$]	2136	1990, 1954, 1922

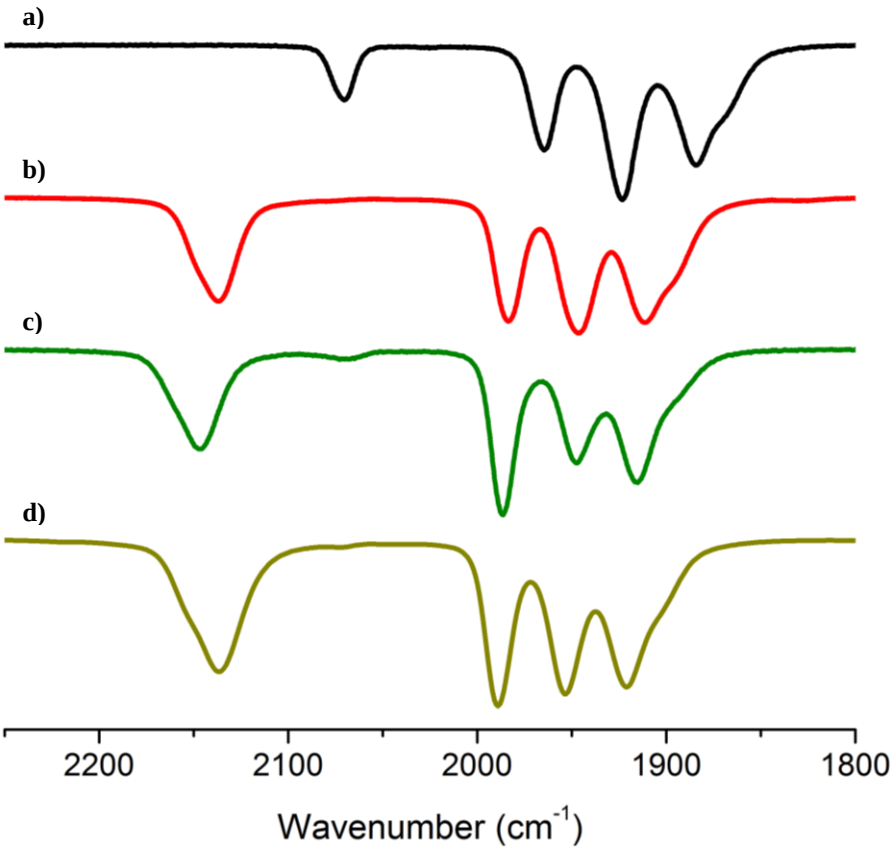


Figure 2.4. IR spectra of a) $(Et_4N)_2$[**2.1**], b) $(Et_4N)_2$[**2.1**$(BPh_3)_2$], c) $(Et_4N)_2$[**2.1**$(BAr^{F\#}{}_3)_2$], and d) $(Et_4N)_2$[**2.1**$(BAr^{F}{}_3)_2$] in CH_2Cl_2.

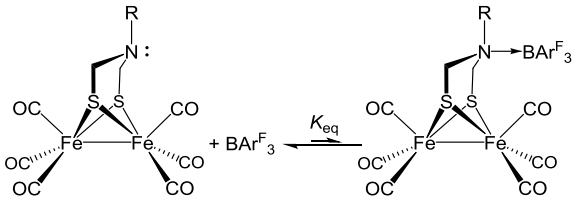
Multiple isomers of [**2.1**]$^{2-}$ are possible with DFT calculations proposing that the major isomer of [**2.1**]$^{2-}$ have the CN^- ligands in an a/b arrangement based on calculations of the IR spectrum.[31,32] A single BR_3 environment was observed in the ^{19}F NMR spectra of $(Et_4N)_2$[**2.1**$(BAr^{F}{}_3)_2$] and $(Et_4N)_2$[**2.1**$(BAr^{F\#}{}_3)_2$] which is not expected for the a/b isomer. Similarly, the ^1H NMR spectra for $(Et_4N)_2$[**2.1**$(BPh_3)_2$] and $(Et_4N)_2$[**2.1**$(BAr^{F\#}{}_3)_2$] also display a BR_3 environment. One explanation for single BR_3 environments by NMR spectroscopy is rapid turnstile rotation of the $Fe(CO)_2(CNBR_3)$ centers. Rapid turnstile rotation of the $Fe(CO)_2(CN)$ centers of $(Et_4N)_2$[**2.1**] has been observed. The ^{13}C NMR spectrum is reported to display a single CN^- and CO environment.[10] The presence of the Fe-$CNBR_3$ linkage was confirmed by ^{11}B NMR spectroscopy. The ^{11}B NMR spectrum of $(Et_4N)_2$[**2.1**$(BAr^{F}{}_3)_2$] featured a broad signal at δ –14, consistent with reported Fe-$CNBAr^{F}{}_3$ linkages in $FeCp(CNBAr^{F}{}_3)(CO)_2$.[18] The alternative Fe-$NCBAr^{F}{}_3$ linkage is expected to exhibit a sharp signal around δ –20. Similarly, the ^{11}B NMR spectrum of $(Et_4N)_2$[**2.1**$(BPh_3)_2$] exhibited a broad signal at δ –4.5, consistent with a M-$CNBPh_3$ linkage.[17] The reverse linkage M-$NCBPh_3$ is expected to display a sharp signal around δ –12. The ^{11}B NMR spectrum of $(Et_4N)_2$[**2.1**$(BAr^{F\#}{}_3)_2$]

displayed a broad signal at δ –15. Although the ^{11}B NMR signal for M-CNBAr$^{F\#}_3$ or the alternative M-NCBAr$^{F\#}_3$ have not been previously reported, the broadness of the signal is consistent with an M-CNBR$_3$ linkage.

2.4 2:1 Lewis Acid Adducts of $[Fe_2(adt)(CO)_4(CN)_2]^{2-}$

Given the presence of adt^{2-} in the active site of [FeFe]-H$_2$ase,[33] the coordination of Lewis acids to $(Et_4N)_2$[**2.3**] was examined. Treatment of $(Et_4N)_2$[**2.3**] with two equivalents of BAr$^F_3$ led to an unstable species that decomposed into an insoluble precipitate. The coordination of BAr$^F_3$ to the additional Lewis basic site of the amine of adt^{2-} may cause the instability of the complex. Coordination of BAr$^F_3$ to the amine of adt^{2-} would leave an uncoordinated Fe-C*N* center. This Fe-C*N* center may coordinate to the Fe center of another molecule, forming a Fe-CN-Fe linkage, resulting in formation of a solid. To test the coordination of BAr$^F_3$ to the amine of adt^{2-}, CH_2Cl_2 solutions of Fe$_2$(R-adt)(CO)$_6$ (R = H, Me, ^{t}Bu, 2,6-diisopropylphenyl) were treated with BAr$^F_3$. The addition of one equivalent of BAr$^F_3$ to Fe$_2$(R-adt)(CO)$_6$ gives a weakly coordinated amine adduct as determined by IR spectroscopy (Scheme 2.5). Coordination of the Lewis acid was confirmed by a shift of ν_{CO} to slightly higher energies ($\Delta\nu_{CO} \approx 25$ cm^{-1}). Protonation of the amine of Fe$_2$(R-adt)(CO)$_6$ is reported to result in similar shifts of ν_{CO} bands.[34]

Scheme 2.5. Partial coordination of BAr$^F_3$ to Fe$_2$(R-adt)(CO)$_6$



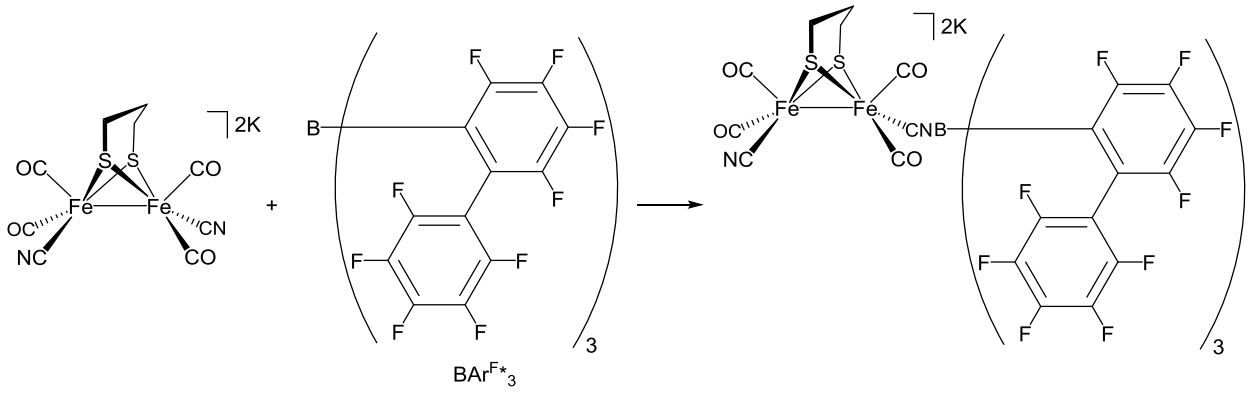
Weaker Lewis acids was found to coordinate to Fe-C*N* of [**2.3**]$^-$ without coordination to the amine of adt^{2-}. Two equivalents of BPh$_3$ coordinate to the Fe-C*N* of $(Et_4N)_2$[**2.3**] to form $(Et_4N)_2$[**2.3**(BPh$_3$)$_2$]. Coordination of BPh$_3$ to only the Fe-C*N* centers of [**2.3**]$^{2-}$ is supported by the IR and NMR spectra of $(Et_4N)_2$[**2.3**(BPh$_3$)$_2$]. The IR spectrum of $(Et_4N)_2$[**2.3**(BPh$_3$)$_2$] was similar to $(Et_4N)_2$[**2.1**(BPh$_3$)$_2$] (Table 2.2). The ^{1}H NMR spectrum of $(Et_4N)_2$[**2.3**(BPh$_3$)$_2$] displayed a single BPh$_3$ environment, consistent with both BPh$_3$ bound to Fe-C*N* centers and rapid rotation of the Fe(CO)$_2$(CNBPh$_3$)$_2$ subunits.

2.5 1:1 Lewis Acid Adducts of $[Fe_2(pdt)(CO)_4(CN)_2]^{2-}$

Treatment of $(Et_4N)_2$[**2.1**] with one equivalent of BPh$_3$ or BAr$^F_3$ produces a mixture of starting material, 2:1 adducts, and an insoluble precipitate. The IR spectrum of the precipitate greatly resembled [**2.1**]$^{2-}$ (ν_{CN} = 2062 cm^{-1}; ν_{CO} = 1968, 1922, 1884 cm^{-1}) suggesting that the diiron center remains intact. The solid precipitate is thought to

form by coordination of Fe-C*N* to another Fe center with displacement of a $CNBAr^{F}{}_{3}^{-}$ or CO ligand. A 1:1 adduct successfully forms by the reaction of the bulky Lewis acid $BAr^{F}*_{3}$ with K_2[**2.1**]. Treatment of K_2[**2.1**] by dropwise addition of one equivalent of the bulky borane $BAr^{F}*_{3}$ gave a homogeneous solution thought to contain the 1:1 adduct K_2[**2.1**($BAr^{F}*_{3}$)] (Scheme 2.6).

Scheme 2.6. Treatment of K_2[**2.1**] with one equivalent of $BAr^{F}*_{3}$ generating K_2[**2.1**($BAr^{F}*_{3}$)].



The IR spectrum of K_2[**2.1**($BAr^{F}*_{3}$)] in CH_2Cl_2 displayed two ν_{CN} at 2126 and 2058 cm^{-1}, consistent with coordination of a single borane (Figure 2.5). Treatment of K_2[**2.1**] with two equivalents of $BAr^{F}*_{3}$ formed the corresponding 2:1 adduct. The identity of the cation for $[\mathbf{2.1}]^{2-}$ was found to be critical in the formation of the 1:1 adduct. Treatment of MeCN solutions of $(Et_4N)_2$[**2.1**] with one equivalent of $BAr^{F}*_{3}$ was found to form precipitate. In contrast, the quick addition of two equivalents of $BAr^{F}*_{3}$ to $(Et_4N)_2$[**2.1**] formed the 2:1 adduct.

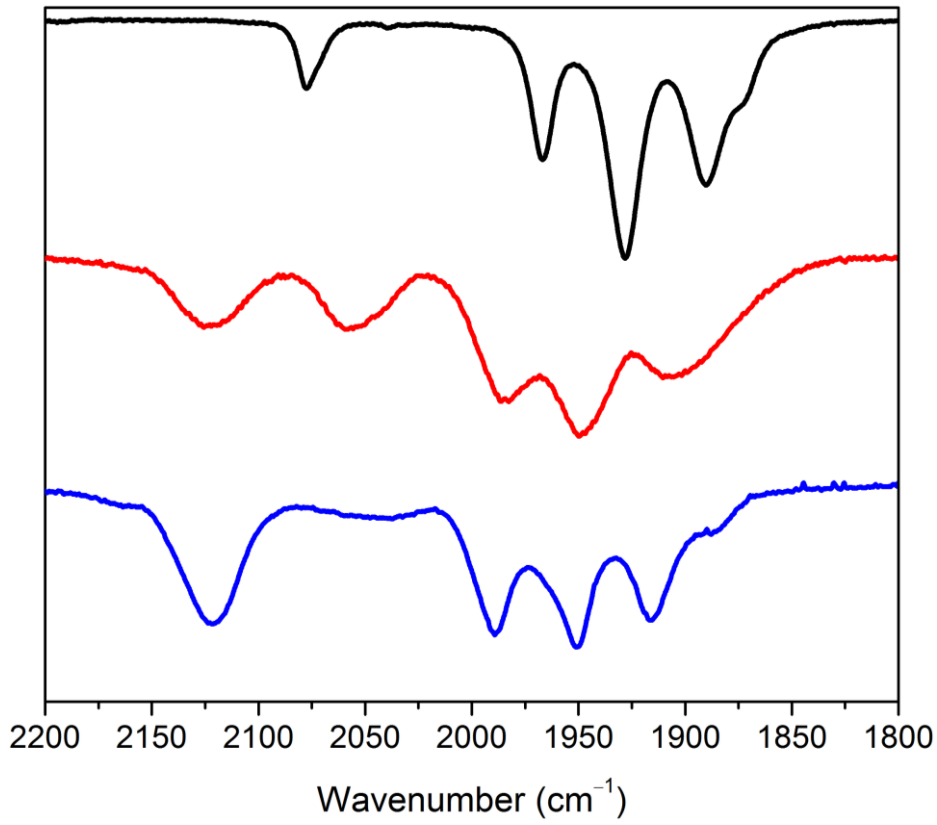


Figure 2.5. IR spectra of K_2[**2.1**] (top), K_2[**2.1**(BAr^F*_3)] (middle), and K_2[**2.1**(BAr^F*_3)$_2$] (bottom) in CH_2Cl_2 solutions.

The choice of solvent greatly affected the IR spectra of the adducts of K_2[**2.1**] and BAr^F*_3. Whereas the IR spectra of K_2[**2.1**(BAr^F*_3)] and K_2[**1**(BAr^F*_3)$_2$] in CH_2Cl_2 displayed three ν_{CO} bands, the IR spectra in MeCN displayed five or six ν_{CO} bands (Table 2.3). The effect was reversible: removal of solvent and redissolving the sample in CH_2Cl_2 produced the initial spectrum.

Table 2.3. Selected IR bands for K_2[**1**] and $(Et_4N)_2$[**1**] in ν_{CN} and ν_{CO} regions and their BAr^F*_3 adducts.

Compound	**Solvent**	**ν_{CN} (cm^{-1})**	**ν_{CO} (cm^{-1})**
$(Et_4N)_2$[**1**]	MeCN	2075	1964, 1924, 1885
K_2[**1**]	MeCN	2077	1967, 1928, 1890
K_2[**1**(BAr^F*_3)]	MeCN	2096, 2081	1990, 1978, 1942, 1931, 1913, 1888
K_2[**1**(BAr^F*_3)]	CH_2Cl_2	2126, 2058	1985, 1950, 1905
K_2[**1**(BAr^F*_3)$_2$]	MeCN	2098	1991, 1959, 1947, 1932, 1910
K_2[**1**(BAr^F*_3)$_2$]	CH_2Cl_2	2119	1989, 1951, 1916
$(Et_4N)_2$[**1**(BAr^F*_3)$_2$]	MeCN	2098	1991, 1932

2.6 Acid/Base Chemistry of Lewis Acid Adducts

Protonation of $(Et_4N)_2$[**2.1**$(BR_3)_2$] was found to be straightforward forming the bridging hydrides $Et_4N[Fe_2(\mu\text{-}H)(pdt)(CO)_4(CNBR_3)_2]$ (Et_4N[H**2.1**$(BR_3)_2$], Scheme 2.7). The increased solubility of $(Et_4N)_2$[**2.1**$(BR_3)_2$] allowed for protonation in Et_2O or THF solutions with $HCl{\cdot}Et_2O$. The reaction is accompanied by lightening of the solution concomitant with precipitation of a white solid, assumed to be Et_4NCl. The ν_{CN} and ν_{CO} bands shifted to higher energies by 45 cm^{-1} and 80-100 cm^{-1} respectively. Similar shifts are reported in the protonation of [**2.1**]$^{2-}$ and are consistent with oxidation of the Fe centers (Table 2.4).[12]

Scheme 2.7. Protonation of [**2.1**$(BR_3)_2$]$^{2-}$ forming the bridging hydride [H**2.1**$(BR_3)_2$]$^-$.

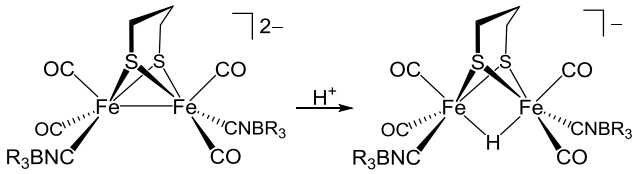


Table 2.4. IR bands in ν_{CN} and ν_{CO} regions for Et_4N[H**2.1**$(BR_3)_2$].

Compound	Solvent	ν_{CN} (cm^{-1})	ν_{CO} (cm^{-1})
Et_4N[H**2.1**]	MeCN	2118, 2112	2045, 2024, 1985
Et_4N[H**2.1**$(BPh_3)_2$]	CH_2Cl_2	2180	2064, 2043, 2009
Et_4N[H**2.1**$(BAr^{F\#}{}_3)_2$]	CH_2Cl_2	2194	2066, 2046, 2012
Et_4N[H**2.1**$(BAr^{F}{}_3)_2$]	CH_2Cl_2	2185	2071, 2051, 2022

The ^{1}H NMR spectra of Et_4N[H**2.1**$(BR_3)_2$] revealed two to three high field signals depending on the Lewis acid. Up to four isomers of [H**2.1**$(BR_3)_2$]$^-$ are expected if flipping of the pdt^{2-} is excluded (Figure 2.6). Of the expected isomers, only the apical/basal isomer (a/b) of [H**2.1**$(BR_3)_2$]$^-$ is expected to have chemically inequivalent $CNBR_3^-$ ligands due to the asymmetry of the isomer. The $CNBR_3^-$ ligands of the other three isomers are symmetry-related.

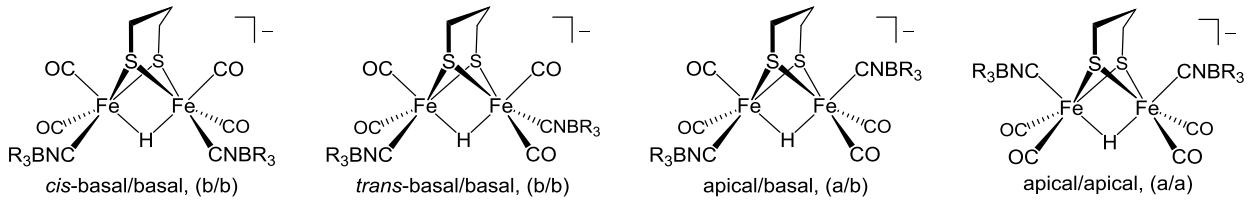


Figure 2.6. Isomers of [H**2.1**$(BR_3)_2$]$^-$.

The ^{1}H NMR spectrum of Et_4N[**2.2**(BAr^{F}_{3})$_2$] display three high field signals at δ –13.7, –16.4, –19.0 in a ratio of 1:11:5. The isomer ratio was found to shift to 1:36:32 over 48 hours. The assignment of the isomers can be partially determined from the ^{19}F NMR spectrum as the *p*-F signals are well resolved. Comparison of the ratio of the hydride signals with the ratio of the *p*-F signals allowed for the assignment of the ^{1}H NMR signal at δ –16.4 to the a/b isomer of Et_4N[H**2.1**(BAr^{F}_{3})$_2$] (Figure 2.7). The remaining hydride signals correspond to symmetrical isomers which are expected to display single ^{19}F NMR signals.

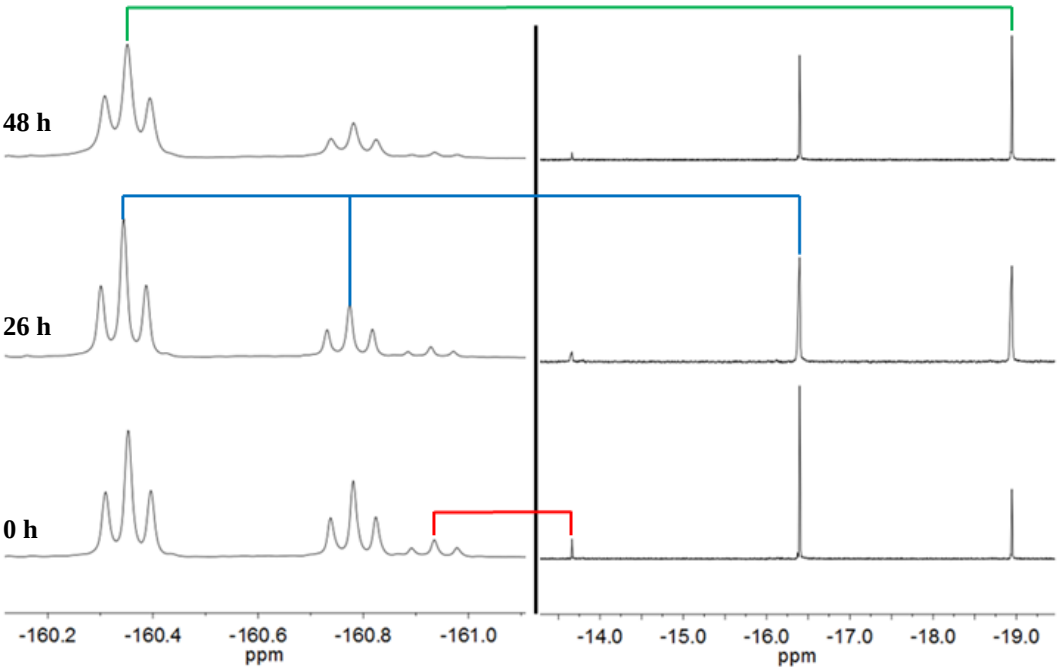


Figure 2.7. Isomerization of Et_4N[H**2.1**(BAr^{F}_{3})$_2$] (CD_2Cl_2 solution) monitored by ^{19}F NMR signals for the *p*-F centers (left) and high field ^{1}H NMR signals (right).

The ^{1}H NMR spectrum of Et_4N[H**2.1**($BAr^{F\#}_{3}$)$_2$] in CD_2Cl_2 displayed two high field signals at δ –16.4, –19.2 in a 3:1 ratio which was found to isomerize to a 1:1.5 ratio over 70 hours. Comparison of the ratio of *o*-F and *p*-F signals in the ^{19}F NMR spectrum with the hydride signals is consistent with one symmetric and one asymmetric isomer (Figure 2.8). The ^{1}H NMR signal at δ –16.4 is assigned as the a/b isomer on the basis of relative integrations of the ^{1}H and ^{19}F NMR signals.

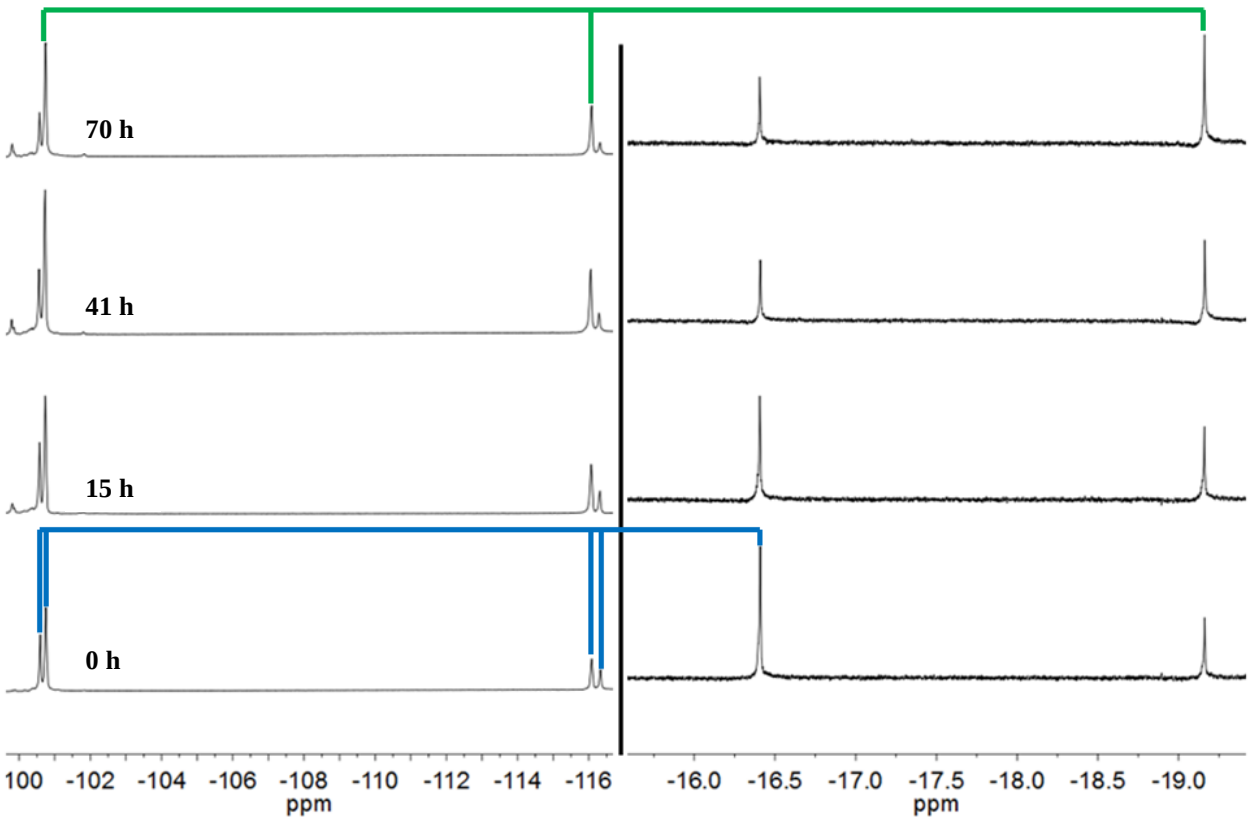


Figure 2.8. Isomerization of $Et_4N[H\mathbf{2.1}(BAr^{F\#}{}_3)_2]$ (CD_2Cl_2 solution) monitored by ^{19}F NMR signals (left) and high field ^1H NMR signals (right).

A solution of $Et_4N[H\mathbf{2.1}(BPh_3)_2]$ in CD_2Cl_2 gave a ^1H NMR spectrum with three high field signals at δ –13.3, –16.1, –19.2 in a ratio of 1.6:4.3:1. The mixture of isomers equilibrated over 47 hours to a ratio of 1:11:11. The low field region of the ^1H NMR spectrum displayed four *o*-H aryl signals for BPh_3, consistent with two symmetric isomers and one asymmetric isomer (Figure 2.9). The hydride signal at δ –16.1 was assigned to the a/b isomer of $Et_4N[H\mathbf{2.1}(BPh_3)_2]$ by the relative intensities of the *o*-H aryl signals to hydride signals.

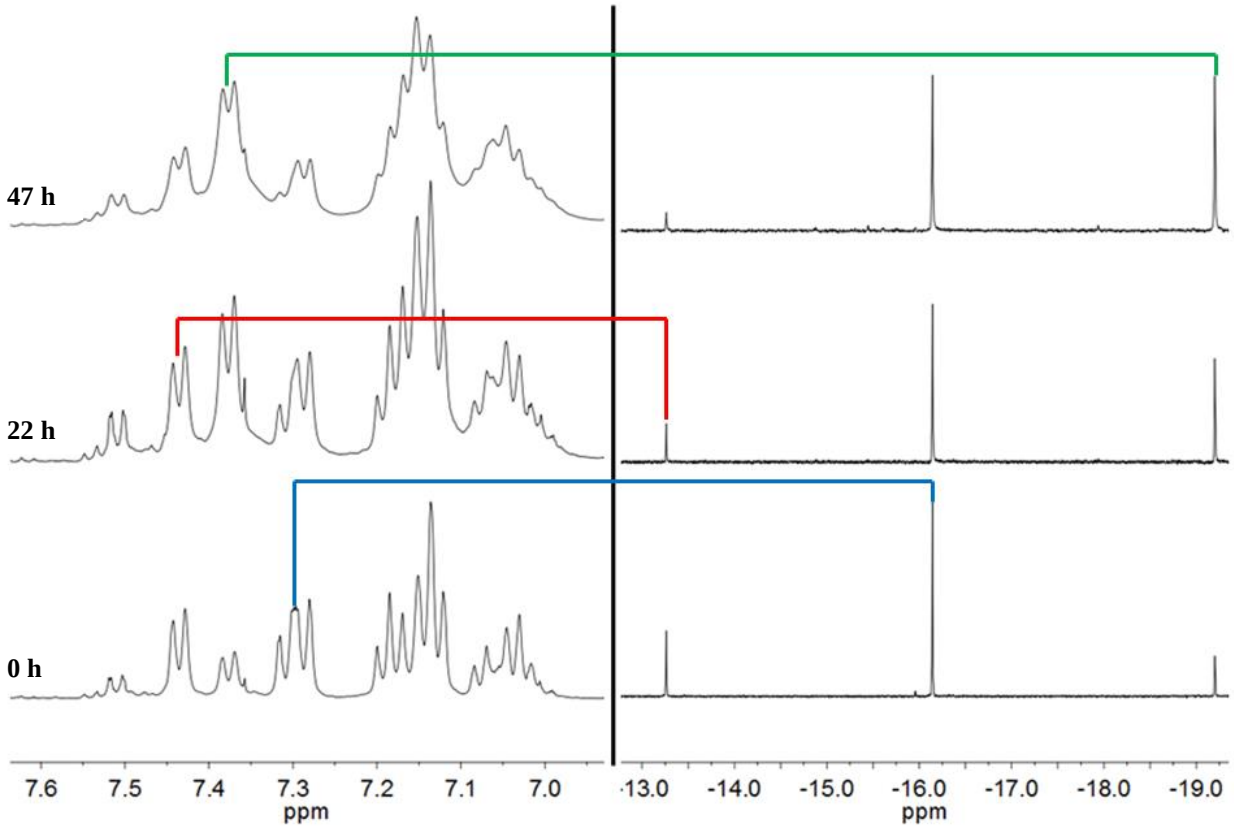


Figure 2.9. Isomerization of $Et_4N[H\mathbf{2.1}(BPh_3)_2]$ (CD_2Cl_2 solutions) monitored by the BPh_3 signals (left) and hydride signals (right) by ^1H NMR spectroscopy.

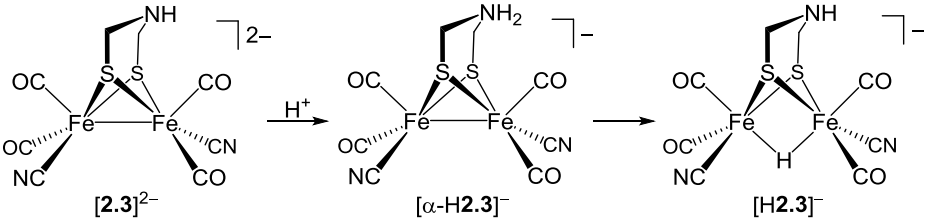
Assignment of the remaining isomers for $Et_4N[H\mathbf{2.1}(BR_3)_2]$ is hindered as the three remaining isomers have symmertrically related $CNBR_3^-$ ligands. The reported structural analogue $[Fe_2(\mu\text{-}H)(pdt)(CO)_4(CN^tBu)_2]^+$ exists as all four possible isomers which have been assigned by ^1H NMR.[35] Given the structural similarity of $Et_4N[H\mathbf{2.1}(BR_3)_2]$ and $[Fe_2(\mu\text{-}H)(pdt)(CO)_4(CN^tBu)_2]^+$, the remaining isomers of $Et_4N[H\mathbf{2.1}(BR_3)_2]$ were assigned as found in $[Fe_2(\mu\text{-}H)(pdt)(CO)_4(CN^tBu)_2]^+$. The lowest field hydride signals of $Et_4N[H\mathbf{2.1}(BR_3)_2]$ around δ –13 are assigned as one of the b/b isomers and the highest field hydride signal around δ –19 is assigned as the a/a isomer.

The coordination of Lewis acids to $(Et_4N)_2[\mathbf{2.1}]$ noticeably affected the basicity of the diiron unit. The pK_a^{MeCN} of $[H\mathbf{2.1}]^-$ is estimated to be ~16 as it is deprotonated by benzylamine (pK_a^{MeCN} = 16.91)[36] and $[\mathbf{2.1}]^{2-}$ is fully protonated by 2,4,6-trimethylpyridinium (pK_a^{MeCN} = 14.98).[36] As observed for $[H\mathbf{2.1}]^-$, both $[H\mathbf{2.1}(BAr^F{}_3)_2]^-$ and $[H\mathbf{2.1}(BAr^{F\#}{}_3)_2]^-$ were reversibly deprotonated. By ^{19}F NMR spectroscopy, the pK_a^{MeCN} of $[H\mathbf{2.1}(BAr^F{}_3)_2]^-$ was calculated to be 10.8±0.2 by monitoring the equilibrium between $[\mathbf{2.1}(BAr^F{}_3)_2]^{2-}$ and anilinium BAr^{F24}

(pK_a^{MeCN} = 10.62).[36] Utilizing similar methods, [H**2.1**($BAr^{F\#}{}_3$)$_2$]$^-$ was calculated to have a pK_a^{MeCN} of 13.5±0.1 using pyridinium BAr^{F24} (pK_a^{MeCN} = 12.53)[36] and [**2.1**($BAr^{F\#}{}_3$)$_2$]$^{2-}$. Deprotonation of [H**2.1**(BPh_3)$_2$]$^-$ did not cleanly produce [**2.1**(BPh_3)$_2$]$^{2-}$, so the pK_a could not be determined. Given the similarity in ν_{CO} frequencies of [H**2.1**(BPh_3)$_2$]$^-$ and [H**2.1**($BAr^{F\#}{}_3$)$_2$]$^-$, their pK_a's are probably similar.

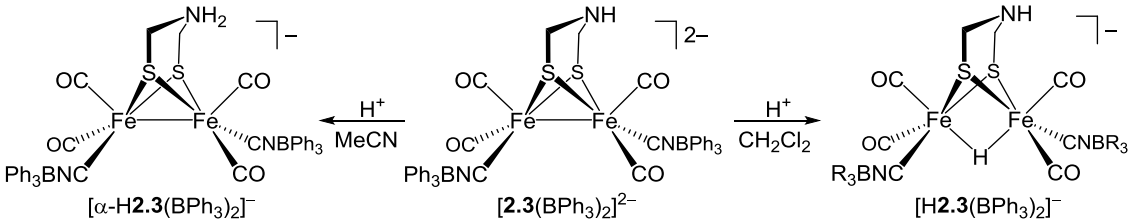
The presence of adt^{2-} in [FeFe]-H_2ase models greatly affects the protonation pathway. The protonation of (Et_4N)$_2$[**2.3**] occurs initially at the amine forming [Fe_2(Hadt)(CO)$_4$(CN)$_2$]$^-$, [α-H**2.3**]$^-$, followed by slow proton transfer over days to form the unstable bridging hydride [Fe_2(μ-H)(adt)(CO)$_4$(CN)$_2$]$^-$, [H**2.3**]$^-$ (Scheme 2.8).[37]

Scheme 2.8. Protonation pathway of [**2.3**]$^{2-}$ initially forming [α-H**2.3**]$^-$ before forming [H**2.3**]$^-$.



The protonation of (Et_4N)$_2$[**2.3**(BPh_3)$_2$] was sensitive to solvent (Scheme 2.9). Treatment of (Et_4N)$_2$[**2.3**(BPh_3)$_2$] with H(Et_2O)$_2$$BAr^{F24}$ in MeCN resulted in a slight shift of the IR frequencies to higher energies ($\Delta\nu_{CN}$ = 2147 cm^{-1}, $\Delta\nu_{CO}$ = 2006, 1970, 1940 cm^{-1}), consistent with protonation at the adt^{2-} to form Et_4N[α-H**2.3**(BPh_3)$_2$]. The compound is unstable, appearing to convert back to [**2.3**(BPh_3)$_2$]$^{2-}$ by IR spectroscopy over the period of hours. The protonation of (Et_4N)$_2$[**2.3**(BPh_3)$_2$] with H(Et_2O)$_2$$BAr^{F24}$ in CH_2Cl_2 produced modest amounts of the bridging hydride Et_4N[H**2.3**(BPh_3)$_2$] and an unstable byproduct that decomposed into a solid precipitate over time (Figure 2.10). The IR spectrum of [H**2.3**(BPh_3)$_2$]$^-$ (ν_{CN} = 2177 cm^{-1}; ν_{CO} = 2064, 2043, 2011 cm^{-1}) was found to match well to the IR spectrum of [H**2.1**(BPh_3)$_2$]$^-$. The ^{1}H NMR spectrum of Et_4N[H**2.3**(BPh_3)$_2$] displayed two high field signals at δ −15.3 and δ −18.4, consistent with a bridging hydride (Figure 2.11).

Scheme 2.9. Solvent-Dependent Pathway for Protonation of [**2.3**(BPh_3)$_2$]$^{2-}$.



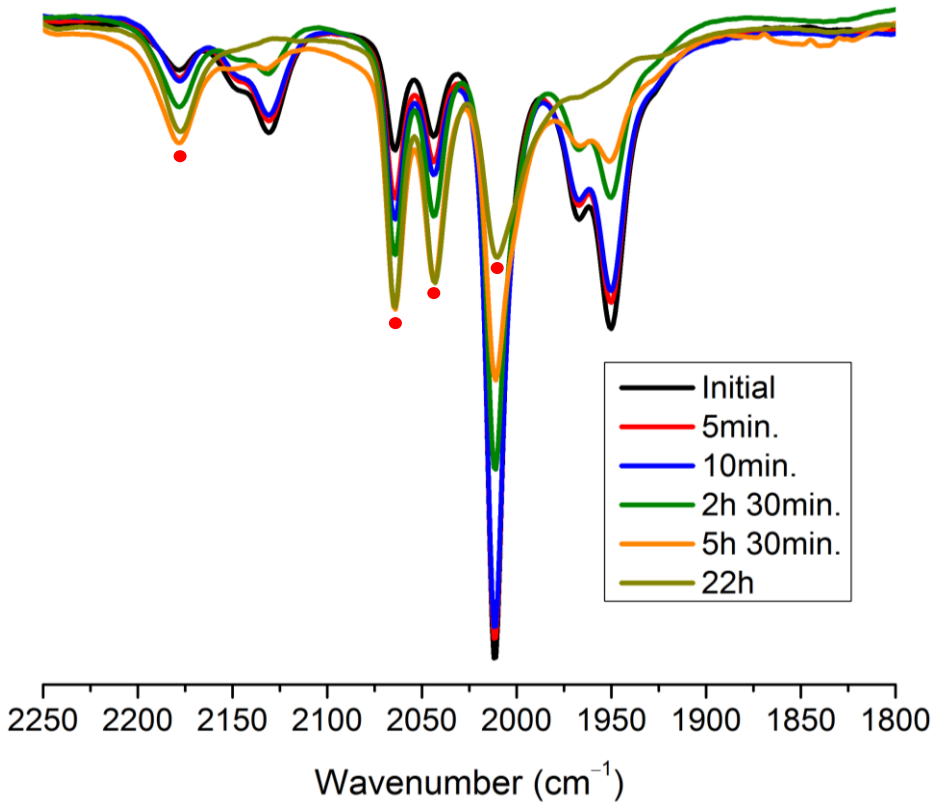


Figure 2.10. IR spectra for stages in the reaction of [**2.3**]$^{2-}$ with one equivalent of $H(Et_2O)_2BAr^{F24}$ in CH_2Cl_2 forming an unstable compound (ν_{CN} = 2146, 2131 cm^{-1}; ν_{CO} = 2011, 1967, 1951 cm^{-1}) and [H**2.3**]$^-$ (●).

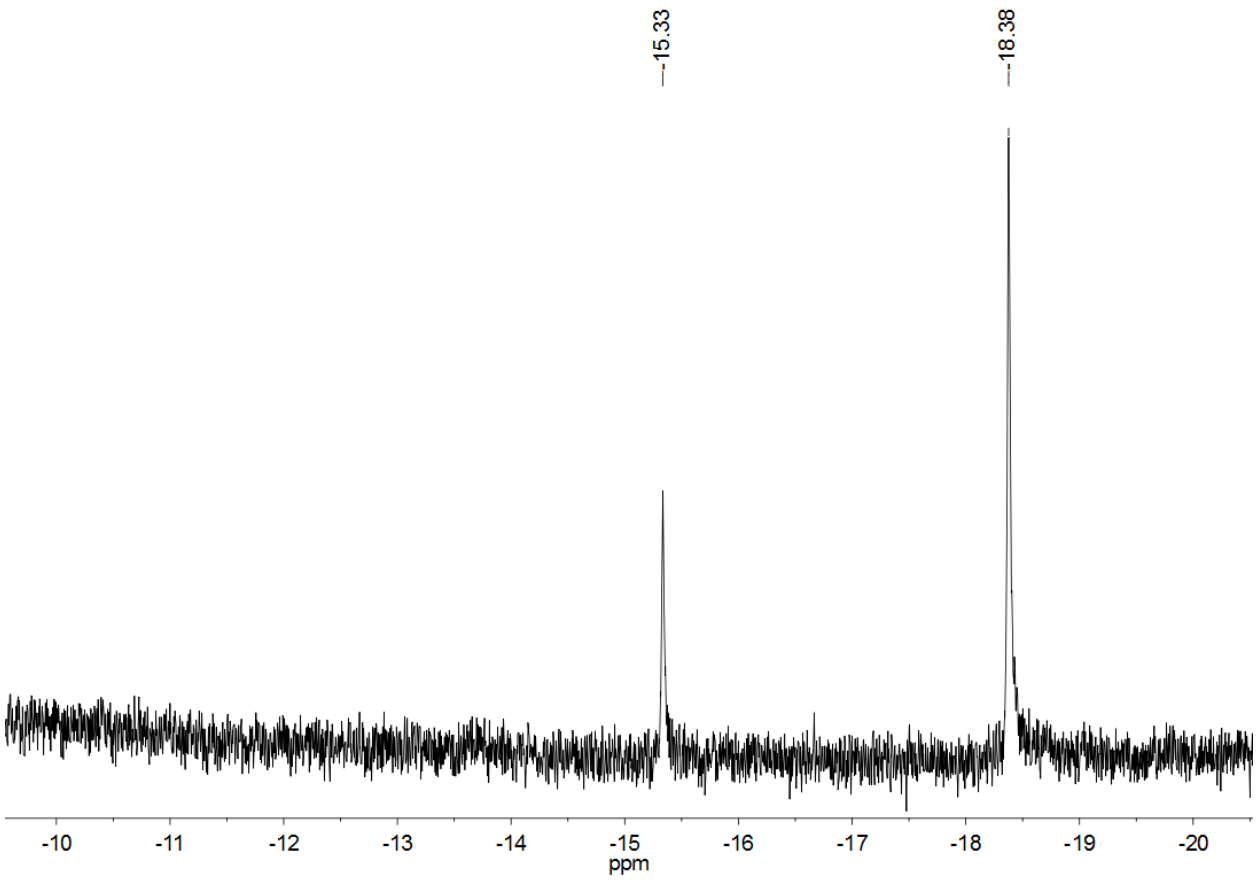


Figure 2.11. High field region of the ^{1}H NMR spectrum of [H**2.3**$(BPh_3)_2]^-$ in CD_2Cl_2.

2.7 Electrochemistry

The cyclic voltammogram of $(Et_4N)_2$[**2.1**] in CH_2Cl_2 revealed an irreversible oxidation event at –0.79 V vs $Fc^{0/+}$. Two more irreversible events at more oxidizing potentials (–0.61, –0.44 V vs $Fc^{0/+}$) were also observed (Figure 2.12). The additional oxidation events are thought to result from decomposition. As described in section 2.1, a film deposited on the surface of the working electrode during electrochemical experiments of $(Et_4N)_2$[**2.1**]. The cyclic voltammogram of $(Et_4N)_2$[**2.1**$(BAr^F{}_3)_2$] in CH_2Cl_2 displayed a quasi-reversible oxidation event at –0.23 V vs $Fc^{0/+}$. The oxidation events of [**2.1**$(BAr^{F\#}{}_3)_2]^{2-}$ and [**2.1**$(BPh_3)_2]^{2-}$ were also quasi-reversible and occurred at similar potentials (–0.34 and –0.36 V vs $Fc^{0/+}$, respectively, Table 2.5). Oxidation of [**2.1**$(BR_3)_2]^{2-}$ occurred without depositing a film on the working electrode.

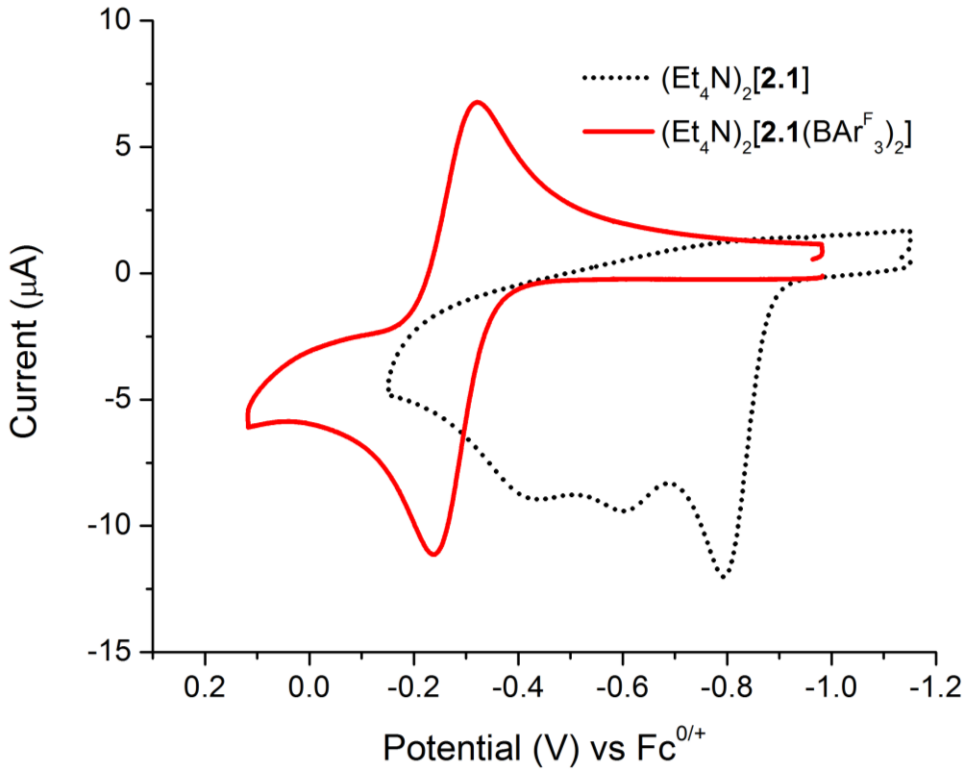


Figure 2.12. Cyclic voltammograms of the oxidation of $(Et_4N)_2$[**2.1**] and $(Et_4N)_2$[**2.1**$(BAr^F{}_3)_2$] in CH_2Cl_2 (1 mM) with Bu_4NPF_6 as electrolyte (100 mM) at 0.1 V/s scan rate.

An irreversible reduction event of [H**2.1**]$^-$ generated in situ occurs at –1.9 V vs $Fc^{0/+}$.[37] The stability of the hydrides [H**2.1**$(BR_3)_2$]$^-$ is noteworthy. Quasi-reversible reduction of [H**2.1**$(BR_3)_2$]$^-$ are observed at potentials from –1.65 to –1.80 V vs $Fc^{0/+}$ (Table 2.5). Reversibility of the reduction events for [H**2.1**$(BAr^{F\#}{}_3)_2$]$^-$ and [H**2.1**$(BPh_3)_2$]$^-$ were only observed at scan rates above 0.5 V/s. As previous FeFe hydrides serve as electrocatalysts for the reduction of protons to form H_2, [H**2.1**$(BAr^F{}_3)_2$]$^-$ was examined for use as an electrocatalyst. The reduction of $HBF_4{\cdot}Et_2O$ in the presence of [H**2.1**$(BAr^F{}_3)_2$]$^-$ resulted in no catalytic activity for H_2 production by cyclic voltammetry.

Table 2.5. Redox potentials (V vs $Fc^{0/+}$) and current ratios of adducts of $[\mathbf{2.1}(BR_3)_2]^{2-}$ and $[H\mathbf{2.1}(BR_3)_2]^{-}$ in CH_2Cl_2.

BR_3	E_{ox} $[\mathbf{1}(BR_3)_2]^{2-/-}$	i_{pa}/i_{pc} (ν = 0.1 V/s)	E_{red} $[H\mathbf{1}(BR_3)_2]^{-/2-}$	i_{pc}/i_{pa} (ν = 0.1 V/s)	i_{pc}/i_{pa} (ν = 1.0 V/s)	E_{ox} $[H\mathbf{1}(BR_3)_2]^{-/0}$	i_{pa}/i_{pc} (ν = 0.1 V/s)
None	–0.79	irrev.					
BPh_3	–0.36	0.16	–1.72	irrev.	0.20		
$BAr^{F\#}{}_3$	–0.34	0.69	–1.76	0.21	0.44	1.11	0.76
$BAr^{F}{}_3$	–0.23	0.82	–1.65	0.28	0.51	1.24	0.57

2.8 Discussion

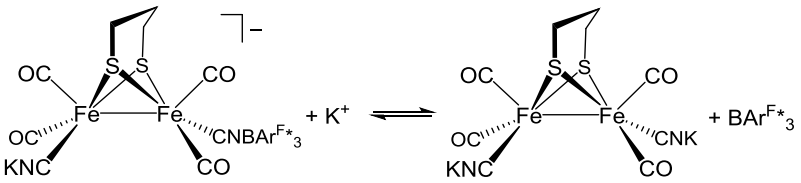
New synthesis of $[Fe_2(xdt)(CO)_5(CN)]^-$ and $[Fe_2(xdt)(CO)_4(CN)_2]^{2-}$ was developed using KCN as a cyanide source. Relative to the quaternary salts of R_4NCN, KCN has several advantages. KCN is much cheaper, more readily available, and safer to handle than ammonium salts of cyanide. Additionally, isotopically labeled forms of cyanide are readily available as the potassium salt. The isolated $K_2[\mathbf{2.1}]$ can undergo cation exchange with the chloride salts of Et_4N^+ and Ph_4P^+. Ligand substitution of $Fe_2(xdt)(CO)_6$ using KCN occurred in a step-wise manner, first forming the mono-substituted $K[Fe_2(xdt)(CO)_5(CN)]$ followed by substitution of a second equivalent of KCN. In contrast in the reaction of Et_4NCN with $Fe_2(xdt)(CO)_6$ the second equivalent of cyanide adds faster than the first.[10] The step-wise addition of KCN is likely due to the low amount of KCN in solution.

The coordination of boranes to the Fe-C*N* sites of $[Fe_2(xdt)(CO)_4(CN)_2]^{2-}$ formed adducts whose acid/base and redox properties could be studied in greater detail than the unprotected cyanides. The adducts $[\mathbf{2.1}(BR_3)_2]^{2-}$ were less electron rich than the parent $[\mathbf{2.1}]^{2-}$ as indicated by higher ν_{CO}, higher pK_a^{MeCN} values, and more positive oxidation and reduction potentials. The "electron-richness" of the Fe centers of $[\mathbf{2.1}(BR_3)_2]^{2-}$ correlated with the reported Lewis acidities of the boranes, with $[\mathbf{2.1}(BPh_3)_2]^{2-}$ being the most electron rich adduct and $[\mathbf{2.1}(BAr^F{}_3)_2]^{2-}$ being the least electron rich adduct.

To model the asymmetric hydrogen-bonding environment of the [FeFe]-H_2ase active site, the 1:1 adduct of $K_2[\mathbf{2.1}(BAr^F{*}_3)]$ was investigated. The use of $K_2[\mathbf{2.1}]$ over $(Et_4N)_2[\mathbf{2.1}]$ was important in the formation of the 1:1 adduct. The K^+ cation is thought to weakly coordinate to Fe-C*N* of $K_2[\mathbf{2.1}(BAr^F{*}_3)]$, stabilizing the 1:1 adduct. The solvent dependence on the IR spectra of $K_2[\mathbf{2.1}(BAr^F{*}_3)]$ and $K_2[\mathbf{2.1}(BAr^F{*}_3)_2]$ is consistent with the interaction of

K^+ with Fe-C*N*. In CH_2Cl_2 solutions, BAr^F*_3 strongly coordinates with Fe-C*N* to give an IR spectrum that resembles $[\mathbf{2.1}(BR_3)_2]^{2-}$. In MeCN solutions, BAr^F*_3 does not strongly coordinate to Fe-C*N* and competes with K^+ for coordination to Fe-C*N*. The competition between BAr^F*_3 and K^+ results in the presence of five or six ν_{CO} bands in the IR spectra of $K_2[\mathbf{2.1}(BAr^F*_3)]$ and $K_2[\mathbf{2.1}(BAr^F*_3)_2]$ in MeCN (Scheme 2.10). The coordination of K^+ in MeCN solutions is supported by the observation that the IR spectrum of $(Et_4N)_2[\mathbf{2.1}(BAr^F*_3)_2]$ is identical in CH_2Cl_2 and MeCN.

Scheme 2.10. Competition of K^+ and BAr^F*_3 for the coordination to Fe-C*N* in MeCN of $K_2[\mathbf{2.1}(BAr^F*_3)_2]$.



Coordination of boranes to Fe-C*N* allowed for more straightforward protonation of $[\mathbf{2.1}(BR_3)_2]^{2-}$ to form the bridging hydrides $[H\mathbf{2.1}(BR_3)_2]^-$. Unlike $[H\mathbf{2.1}]^-$, salts of $[H\mathbf{2.1}(BR_3)_2]^-$ were isolable. Solutions of $[H\mathbf{2.1}(BR_3)_2]^-$ exist as a mix of isomers. The assignment of the asymmetrical isomers of $[H\mathbf{2.1}(BR_3)_2]^-$ was determined based on spectroscopic methods, generally ^{19}F NMR. The assignment of the symmetric isomers of $[H\mathbf{2.1}(BR_3)_2]^-$ was based on their similarities to the previously reported $[Fe_2(\mu\text{-}H)(pdt)(CO)_4(CN^tBu)_2]^+$. The stabilities of $[H\mathbf{2.1}(BAr^F_3)_2]^-$ and $[H\mathbf{2.1}(BAr^{F\#}_3)_2]^-$ allowed for the pK_a^{MeCN} values of the hydrides to be accurately measured.

The effect of solvent on the protonation of $[\mathbf{2.3}(BPh_3)_2]^{2-}$ is not well understood. The protonation of $[\mathbf{2.3}(BPh_3)_2]^{2-}$ in MeCN is proposed to form $[\alpha\text{-}H\mathbf{2.3}(BPh_3)_2]^-$ on the basis of small shifts of ν_{CN} and ν_{CO} bands as previously reported for the generation of $[\alpha\text{-}H\mathbf{2.3}]^-$ ($\Delta\nu_{CN}$ ~ 10 cm^{-1}, $\Delta\nu_{CO}$ ~ 20-30 cm^{-1}). The conversion of $[\alpha\text{-}H\mathbf{2.3}(BPh_3)_2]^-$ to $[H\mathbf{2.3}(BPh_3)_2]^-$ was not observed. The conversion of $[\alpha\text{-}H\mathbf{2.3}]^-$ to $[H\mathbf{2.3}]^-$ in MeCN is reported to occur over days.[37] It is proposed that $[\alpha\text{-}H\mathbf{2.3}(BPh_3)_2]^-$ slowly decomposes as evident by the slow formation of a solid precipitate, deprotonating $[\alpha\text{-}H\mathbf{2.3}(BPh_3)_2]^-$ to reform some $[\mathbf{2.3}(BPh_3)_2]^{2-}$. The protonation of $[\mathbf{2.3}(BPh_3)_2]^{2-}$ in CH_2Cl_2 slowly formed $[H\mathbf{2.3}(BPh_3)_2]^-$ over several hours by means of an protonated, unstable intermediate. The ν_{CN} and ν_{CO} bands of the protonated intermediate are shifted to higher energies than observed for $[\mathbf{2.3}(BPh_3)_2]^{2-}$ though the ν_{CO} are shifted by slightly higher energies than expected for $[\alpha\text{-}H\mathbf{2.3}(BPh_3)_2]^-$ ($\Delta\nu_{CO}$ ~ 20-40 cm^{-1}). The

conversion of the protonated intermediate to $[H\mathbf{2.3}(BPh_3)_2]^-$ is proposed to occur faster in CH_2Cl_2 than the conversion of $[\alpha\text{-}H\mathbf{2.3}(BPh_3)_2]^-$ to $[H\mathbf{2.3}(BPh_3)_2]^-$ in MeCN.

To understand the ligand properties of $CNBR_3^-$, several parameters of $[\mathbf{2.1}(BR_3)_2]^{2-}$ and $[H\mathbf{2.1}(BR_3)_2]^-$ were compared to the related model compounds $Fe_2(pdt)(CO)_4(PMe_3)_2$, **2.4**, and $[Fe_2(\mu\text{-}H)(pdt)(CO)_4(PMe_3)_2]^+$, $[H\mathbf{2.4}]^+$. The ν_{CO} bands of **2.4** (ν_{CO} = 1979, 1942, 1889 cm^{-1}) and $[H\mathbf{2.4}]^+$ (ν_{CO} = 2029, 1989 cm^{-1}) are lower ν_{CO} than $[\mathbf{2.1}(BR_3)_2]^{2-}$ and $[H\mathbf{2.1}(BR_3)_2]^-$.[38] The lower ν_{CO} bands suggest that PMe_3 is a stronger donor ligand than $CNBR_3^-$. Furthermore, the estimated pK_a^{MeCN} of 15 for $[H\mathbf{2.4}]^+$ also suggests PMe_3 is a stronger donor than $CNBR_3^-$.[39] In contrast, electrochemical studies of **2.4** and $[H\mathbf{2.4}]^+$ suggests that $CNBR_3^-$ is a more basic ligand than PMe_3. The oxidation potential of **2.4** in CH_2Cl_2 is reported to be –0.20 V vs $Fc^{0/+}$,[40] similar to the oxidation potential of $[\mathbf{2.1}(BAr^F{}_3)_2]^{2-}$ and less oxidizing than $[\mathbf{2.1}(BAr^{F\#}{}_3)_2]^{2-}$ and $[\mathbf{2.1}(BPh_3)_2]^{2-}$, indicating $CNBR_3^-$ is a stronger donor than PMe_3. Additionally the reduction potentials of $[H\mathbf{2.1}(BR_3)_2]^-$ are much more reducing than $[H\mathbf{2.4}]^+$ (E_{red} = –1.39 V vs $Fc^{0/+}$).[41] The apparent reverse of ligand basicity is attributed to the two charge difference between $CNBR_3^-$ and phosphine-containing models. Though largely overlooked due to the use of neutral donor ligands, the negative charge on [FeFe]-H_2ase models has a noticeable effect on redox potentials.

Table 2.6. Properties of complexes of the type $Fe_2(pdt)(CO)_4L_2$.

L	Avg. ν_{CO} (cm^{-1}) Fe(I)Fe(I)	E_{ox} (V vs $Fc^{0/+}$)	pK_a^{MeCN}	Avg. ν_{CO} (cm^{-1}) HFe(II)Fe(II)	E_{red} (V vs $Fc^{0/+}$)
CN^-	1924	–0.79	~16	2018	–1.9
$CNBPh_3^-$	1947	–0.36	~13.5	2039	–1.72
$CNBAr^{F\#}{}_3^-$	1949	–0.34	13.5±0.1	2041	–1.76
$CNBAr^F{}_3^-$	1955	–0.23	10.8±0.2	2048	–1.65
PMe_3	1937	–0.20	~15	2009	–1.39

2.9 Conclusions

Capping of the Fe-C*N* sites enables the study of acid/base and redox reactions of diiron models with cyanide ligands. The reactivity of the diiron centers could be adjusted by varying the Lewis acidity of the borane. The coordination of amino acid side chains to the cyanide ligands in [FeFe]-H_2ase may serve more than to tether the active site to the protein, but also adjusts the electron density of the Fe centers. For example, the mutation of the methionine side chain coordinated to the bridging carbonyl of the active site changes the catalytic bias from H_2 production to H_2 oxidation.[15] Though the coordination of Lewis acids is a chemical model of hydrogen bonding

between Fe-C*N* and the protein, many challenges remain. Protonation of the capped models were found to form the bridging hydrides in contrast to the biomimetic terminal hydrides. Additionally incorporation of the biologically relevant adt^{2-} cofactor was found not to be compatible with Lewis acids. The use of a protein-like scaffold may enforce a rotated structure and may encourage the formation of terminal hydrides upon protonation.

Though only limited success was found for [FeFe]-H_2ase models with $CNBR_3^-$ ligands, the use of $CNBR_3^-$ ligands may allow for more functional models for [NiFe]-H_2ase. Functional models of [NiFe]-H_2ase release H_2 by protonation of a reduced NiFe hydride, resulting in high overpotentials.[42] This mechanism is in contrast to [NiFe]-H_2ase which release H_2 upon protonation of a Ni(II)Fe(II) hydride with Fe remaining in the ferrous state throughout the catalytic cycle.[5] The presence of cyanide ligands in a functional model of [NiFe]-H_2ase may result in more negative reduction potentials, and therefore result in a [NiFe]-H_2ase mode with a more biomimetic catalytic cycle.

2.10 Experimental Procedures

Standard Schlenk or glovebox techniques were used. Solvents used for syntheses were HPLC grade and further purified by using an alumina filtration system (Glasscontour Co., Irvine, CA) and were deoxygenated by purging prior to use. NMR solvents were purchased from Cambridge Isotope Laboratories and dried with CaH_2 and stored under nitrogen over activated molecular sieves. $(Et_4N)_2[Fe_2(pdt)(CO)_4(CN)_2]$ and $(Et_4N)_2[Fe_2(adt)(CO)_4(CN)_2]$ were prepared as previously described.[43] $BAr^F{}_3$ was purchased from Boulder Scientific and twice sublimed at 90 °C prior to use. BPh_3 was prepared by pyrolysis of $HNMe_3BPh_4$.[44] $BAr^F{}^*{}_3$ and $BAr^{F\#}{}_3$ were made by previously reported methods.[30,45] Infrared spectroscopy was recorded using a Perkin Elmer Spectrum 100 FT-IR spectrometer using a CaF_2 solution cell. Elemental analyses were conducted at the University of Illinois, Microanalytical Laboratory. Cyclic voltammerty was performed under argon at room temperature using a CHI 630D potentiostat with glassy carbon working electrode, Pt wire counter electrode, pseudoreference electrode Ag wire, and with Fc as an internal standard. ^{1}H NMR and ^{19}F NMR spectra were recorded on a 500 MHz Varian Mercury spectrometer. ^{1}H NMR chemical shifts were referenced to the residual protons of deuterated solvents and ^{19}F NMR was referenced to the external standard 1% $CFCl_3$ in $CDCl_3$. ^{11}B-NMR spectra were recorded on a 400 MHz Varian Mercury spectrometer and was referenced to the external standard BF_3•Et_2O.

$K_2[Fe_2(pdt)(CO)_4(CN)_2]$, K_2[2.1]. A two-necked Schlenk flask was charged with $Fe_2(pdt)(CO)_6$ (1.0 g, 2.6 mmol) and KCN (0.51 g, 7.8 mmol) and suspended in MeCN (100 mL). The mixture was heated to reflux for 28

h and was monitored by IR for completion. The mixture was filtered through Celite and the filtrate was dried under vacuum. The resulting solid was washed with Et_2O (50 mL) and hexanes (50 mL) and dried under vacuum. Yield 0.91 g (76%). Anal. Calc. for $C_9H_6Fe_2K_2N_2O_4S_2$•0.33CH_3CN (found): C, 24.49 (24.35); H, 1.49 (1.64); N, 6.81 (6.88). IR (MeCN, cm^{-1}): ν_{CN} = 2077 ; ν_{CO} = 1967, 1928, 1890.

K[Fe_2(pdt)$(CO)_5$(CN)], K[2.2]. A two-necked Schlenk flask was charged with $Fe_2(pdt)(CO)_6$ (0.50 g, 1.30 mmol) and 0.9 equiv of KCN (0.076 g, 1.17 mmol) and suspended in MeCN (50 mL). The mixture was heated to reflux for 6 h and was monitored by IR for completion. The mixture was filtered through Celite and the filtrate was dried under vacuum. The resulting oil was extracted into Et_2O and precipitated upon the addition of pentane. The resulting solid was collected by filtration and washed with pentane (50 mL) and dried under vacuum. Yield 0.42 g (85%). Anal. Calc. for $C_9H_6Fe_2KNO_5S_2$ (found): C, 25.55 (25.62); H, 1.43 (1.71); N, 3.31 (3.17). IR (MeCN, cm^{-1}): ν_{CN} = 2092; ν_{CO} = 2031, 1976, 1956, 1946, 1916.

K_2[Fe_2(adt)$(CO)_4$$(CN)_2$], K_2[2.3]. A two-necked Schlenk flask was charged with $Fe_2(adt)(CO)_6$ (0.1 g, 0.26 mmol) and KCN (0.050 g, 0.78 mmol) and suspended in MeCN (20 mL). The mixture was heated to reflux for 6 h and was monitored by IR for completion. The mixture was filtered through Celite and the filtrate was dried under vacuum. The resulting solid was washed with Et_2O (20 mL) and hexanes (20 mL) and dried under vacuum. Yield 0.090 g (76%). IR (MeCN, cm^{-1}): ν_{CN} = 2078; ν_{CO} = 1969, 1929, 1893.

Ion Exchange of K_2[Fe_2(pdt)$(CO)_4$$(CN)_2$]. An MeCN (5 mL) solution of K_2[**2.1**] (50 mg, 0.11 mmol) was treated with a MeCN solution (5 mL) of PPNCl (125 mg, 0.22 mmol) resulting in the precipitation of a white solid. The mixture was filtered through Celite. The IR spectrum of the filtrate matched the literature values for $(PPN)_2$[**2.1**].[24] The use of Et_4NCl was found to produce a similar result with the IR spectrum of the filtrate matching the literature values of $(Et_4N)_2$[**2.1**].[10]

$(Et_4N)_2$[Fe_2(pdt)$(CO)_4$$(CNBAr^F{}_3)_2$], $(Et_4N)_2$[2.1$(BAr^F{}_3)_2$]. A slurry of $(Et_4N)_2[Fe_2(pdt)(CN)_2(CO)_4]$ (2.40 g, 3.74 mmol) in CH_2Cl_2 (50 mL) was treated with $BAr^F{}_3$ (3.88 g, 7.57 mmol) in CH_2Cl_2 (10 mL). The reaction solution was stirred for 30 minutes and the solvent was evaporated to yield a red oil. The product was triturated with pentane (3 x 10 mL) and crystallized from CH_2Cl_2 (10 mL) layer with Et_2O (10 mL) and pentane (30 mL). Yield 5.25 g (>99%) Anal. Calc. for $C_{61}B_2Fe_2S_2H_{46}O_4N_4F_{30}$ (found): C, 43.97 (43.50); H, 2.78(3.07); N, 3.36 (3.60). IR (CH_2Cl_2, cm^{-1}): ν_{CN} = 2134; ν_{CO} = 1990, 1956, 1925. ^{1}H NMR (CD_2Cl_2): δ 3.10 (16H, m, $(CH_3CH_2)_4N$), 1.73 (4H, t,

SC*H*$_2$CH$_2$C*H*$_2$S), 1.48 (2H, m, SCH$_2$C*H*$_2$CH$_2$), 1.23 (24H, t, (C*H*$_3$CH$_2$)$_4$N). ^{11}B NMR (CD_2Cl_2): δ –14. ^{19}F NMR (CD_2Cl_2): δ –134.3 (d, *o*-F); δ –161.8 (t, *p*-F); δ –166.9 (t, *m*-F).

$(Et_4N)_2$[Fe_2(pdt)(CO)$_4$(CNBAr$^{F\#}_3$)$_2$], $(Et_4N)_2$[2.1(BAr$^{F\#}_3$)$_2$]. A solution of $(Et_4N)_2$[**1**] (0.16 g, 0.25 mmol) in CH_2Cl_2 (10 mL) was treated with a solution of BAr$^{F\#}_3$ (0.20 g, 0.50 mmol) in 10 mL CH_2Cl_2 dropwise. The solvent was evaporated to yield a red oil that was extracted into CH_2Cl_2 (5 mL), layered with pentane (20 mL) and cooled at –30 °C for two days producing a red oil. The filtrate was decanted off and the oil was triturated with pentane (3 x 10 mL) to produce a red solid. Yield 0.34 g (95%). Anal. Calc. for $C_{61}H_{58}B_2F_{18}Fe_2N_4O_4S_2$ (found): C, 50.51 (50.82); H, 4.03 (4.04); N, 3.86 (4.15). IR (CH_2Cl_2, cm^{-1}): ν_{CN} = 2147 cm; ν_{CO} = 1986, 1947, 1915. ^{1}H NMR (CD_2Cl_2): δ 6.41 (12H, t, *m*-Ar*H*); 3.09 (16H, m, (CH$_3$C*H*$_2$)$_4$N); 1.70 (4H, t, SC*H*$_2$CH$_2$C*H*$_2$S); 1.42 (2H, m, SCH$_2$C*H*$_2$CH$_2$); 1.22 (24H, t, (C*H*$_3$CH$_2$)$_4$N). ^{11}B NMR (CD_2Cl_2): δ –15. ^{19}F NMR (CD_2Cl_2): δ –99.9 (s, *o*-F); –117.1 (s, *p*-F).

$(Et_4N)_2$[Fe_2(pdt)(CO)$_4$(CNBPh$_3$)$_2$], $(Et_4N)_2$[2.1(BPh$_3$)$_2$]. A solution of $(Et_4N)_2$[**1**] (0.50 g, 0.78 mmol) in CH_2Cl_2 (20 mL) was treated dropwise with a solution of BPh_3 (0.38 g, 1.6 mmol) in 20 mL CH_2Cl_2. The solvent was evaporated to yield a red oil that was extracted into CH_2Cl_2 (10 mL), layered with pentane (30 mL) and cooled at –30 °C for two days producing a red oil. The filtrate was decanted off and the oil was triturated with pentane (3 x 10 mL) to produce a red solid. Yield 0.83 g (94%). Anal. Calc. for $C_{61}B_2Fe_2S_2H_{76}O_4N_4$ (found): C, 65.03 (65.38); H, 6.80 (7.01); N, 4.97 (5.04). IR (CH_2Cl_2, cm^{-1}): ν_{CN} = 2137; ν_{CO} = 1984, 1946, 1911 cm. ^{1}H NMR (CD_2Cl_2): δ 7.50 (12H, d, *o*-Ar*H*); 7.13 (12H, t, *m*-Ar*H*); 7.01 (6H, t, *p*-Ar*H*); 2.44 (16H, m, (CH$_3$C*H*$_2$)$_4$N); 1.96 (4H, t, SC*H*$_2$CH$_2$C*H*$_2$S); 1.72 (2H, m, SCH$_2$C*H*$_2$CH$_2$); 0.84 (24H, t, (C*H*$_3$CH$_2$)$_4$N). ^{11}B NMR (CD_2Cl_2) δ –4.5.

$(Et_4N)_2$[Fe_2(adt)(CO)$_4$(CNBPh$_3$)$_2$], $(Et_4N)_2$[2.3(BPh$_3$)$_2$]. A solution of $(Et_4N)_2$[**2.3**] (0.050 g, 0.078 mmol) in CH_2Cl_2 (10 mL) was treated dropwise with a solution of BPh_3 (0.038 g, 0.16 mmol) in 10 mL CH_2Cl_2. The mixture was filtered through Celite and the solvent was evaporated to yield a red oil. The oil was triturated with pentane (3 x 10 mL) to produce a red solid. Yield 0.070 g (80%). Anal. Calc. for $C_{60}B_2Fe_2S_2H_{75}O_4N_5$ (found): C, 63.90 (63.75); H, 6.70 (6.85); N, 6.21 (5.85). IR (CH_2Cl_2, cm^{-1}): ν_{CN} = 2136; ν_{CO} = 1986, 1949, 1914.

K_2[Fe_2(pdt)(CO)$_4$(CNBAr^{F}*$_3$)$_2$], K_2[2.1(BAr^{F}*$_3$)$_2$]. A solution of K_2[**1**] (24 mg, 0.052 mmol) in MeCN (5 mL) was treated with BAr^{F}*$_3$ (100 mg, 0.11 mmol) in MeCN (10 mL). The solvent was then removed from the solution under vacuum and the solid was extracted with 5 mL of Et_2O and 20 mL of pentane was added, resulting in

a red oil which was triturated with pentane (3x10 mL) to yield a red solid. Yield 84 mg (68%). IR (MeCN, cm^{-1}): ν_{CN} = 2098; ν_{CO} = 1991, 1959, 1947, 1932, 1909. IR (CH_2Cl_2, cm^{-1}) ν_{CN} = 2119; ν_{CO} = 1989, 1951, 1916.

K_2[Fe_2(pdt)(CO)$_4$(CN)(CNBAr^F*$_3$)], K_2[2.1(BAr^F*$_3$)]. A solution of K_2[**1**] (26 mg, 0.058 mmol) in MeCN (20 mL) was treated dropwise with a MeCN solution (10 mL) of BAr^F*$_3$ (50 mg, 0.052 mmol) over 2 hours. The solvent was then removed from the solution under vacuum and extracted with 5 mL of Et_2O. The mixture was passed through Celite and dried under vacuum to yield a tacky red solid which was triturated with pentane (3x10 mL) to give a red solid. Yield 50 mg (68%). IR (CH_2Cl_2, cm^{-1}) ν_{CN} = 2100; ν_{CO} = 1990, 1927.

Et_4N[Fe_2(μ-H)(pdt)(CO)$_4$(CNBAr^F$_3$)$_2$], Et_4N[H2.1(BAr^F$_3$)$_2$]. A solution of $(Et_4N)_2$[**1**(BAr^F$_3$)$_2$] (0.282 g, 0.169 mmol) in ether (50 mL) was treated with HCl in ether (0.093 mL, 2 M, 0.186 mmol). The reaction solution color became lighter and a colorless precipitate formed upon addition of HCl. The reaction solution was stirred for 30 min and passed through a plug of Celite to remove Et_4NCl. The filtrate was collected and the solvent was evaporated to c.a. 10 mL and pentane (20 mL) was added. The resulting yellow solid was extracted into ether (10 mL) and layered with pentane (30 mL) to yield yellow microcrystals. Yield 107 mg (44%) Anal. Calc. for $C_{53}B_2Fe_2S_2H_{27}O_4N_3F_{30}$ (found): C, 41.41 (41.29); H, 1.77 (1.75); N, 2.73 (2.66). IR (CH_2Cl_2, cm^{-1}): ν_{CN} = 2185; ν_{CO} = 2071, 2051, 2022. ^{1}H NMR (CD_2Cl_2): δ –13.7 (s Fe-*H*); –16.4 (s Fe-*H*); –19.0 (s Fe-*H*). ^{19}F NMR (CD_2Cl_2): δ –134.8 (dd, *o*-F); –134.9 (m, *o*-F); –160.4 (*p*-F); –160.8 (*p*-F); –160.9 (*p*-F); –166.2 (m, *m*-F); –166.5 (td, *m*-F); –166.6 (td, *m*-F). ^{11}B NMR (CD_2Cl_2): δ –15.

Et_4N[Fe_2(μ-H)(pdt)(CO)$_4$(CNBAr$^{F\#}$$_3$)$_2$], Et_4N[H2.1(BAr$^{F\#}$$_3$)$_2$]. A solution of $(Et_4N)_2$[**1**(BAr$^{F\#}$$_3$)$_2$] (100 mg, 0.069 mmol) in THF (1 mL) was treated with a HCl in ether (0.1 mL, 2 M, 0.2 mmol), resulting in the color of the solution lightening and some precipitate forming. The reaction solution was cooled in a –30 °C freezer to precipitate Et_4NCl from solution and was then passed through a plug of Celite. The solution was dried under vacuum and the resulting oil was triturated with pentane (3x10 mL) and left to dry under vacuum overnight, yielding a red solid. Yield 91 mg (99 %). Anal. Calc. for $C_{53}H_{39}B_2F_{18}Fe_2N_3O_4S_2$ (found): C, 48.18 (48.51); H, 2.97 (3.17); N, 3.18 (3.16). IR (CH_2Cl_2, cm^{-1}): ν_{CN} = 2194; ν_{CO} = 2066, 2046, 2012. ^{1}H NMR (CD_2Cl_2): δ –16.41 (s, Fe-*H*); –19.16 (s, Fe-*H*). ^{19}F NMR (CD_2Cl_2): δ –100.6 (*o*-F); –100.8 (*o*-F); –116.1 (*p*-F); –116.3 (*p*-F).

Et_4N[Fe_2(μ-H)(pdt)(CO)$_4$(CNBPh$_3$)$_2$], Et_4N[H2.1(BPh$_3$)$_2$]. A solution of $(Et_4N)_2$[**1**(BPh$_3$)$_2$] (100 mg, 0.089 mmol) in CH_2Cl_2 (3 mL) was treated with HCl in ether (0.087 mL, 2 M, 0.178 mmol) resulting in the color of the solution lightening and some precipitate forming. The reaction solution was cooled in a –30 °C freezer to

precipitate Et_4NCl from solution and was then passed through a plug of Celite. The solution was dried under vacuum and the resulting oil was triturated with pentane (3x10 mL) and left to dry under vacuum overnight, yielding a red solid. Yield 85 mg (96 %). IR (CH_2Cl_2, cm^{-1}): ν_{CN} = 2180; ν_{CO} = 2064, 2043, 2009. ^{1}H NMR (CD_2Cl_2): δ –13.2 (s Fe-*H*); –16.1 (s Fe-*H*); –19.2 (s Fe-*H*).

pK_a Determination Procedure. Solutions of $(Et_4N)_2$[**2.1**$(BAr^F{}_3)_2$] and $Ph_3NHBAr^{F24}\cdot 2Et_2O$ or $(Et_4N)_2$[**2.1**$(BAr^{F\#}{}_3)_2$] and $PyHBAr^{F24}$ were prepared in MeCN with [**2.1**$(BR_3)_2]^{2-}$ to acid approximate ratios of 1:2, 1:1, and 2:1 and monitored by ^{19}F NMR until solutions reached equilibrium after a day at room temperature. The pK_a was then determined using eq 2.1.

$$pK_a^{Fe} = pK_a^{H+} + \log\left(\frac{[B][H\mathbf{2.1}(BR_3)_2^{2-}]}{[HB][\mathbf{2.1}(BR_3)_2^{-}]}\right) \quad (2.1)$$

Where:
pK_a^{Fe} is the calculated pK_a of [**2.1**$(BR_3)_2]^{2-}$ in MeCN
pK_a^{H+} is the known pK_a of acid in MeCN
$[\mathbf{2.1}(BR_3)_2^{2-}]$ is the concentration of [**2.1**$(BR_3)_2]^{2-}$ at equilibrium
$[H\mathbf{2.1}(BR_3)_2^{-}]$ is the concentration of [H**2.1**$(BR_3)_2]^{-}$ at equilibrium
$[HB]$ is the concentration of unreacted acid at equilibrium, $[HB] = [HB]_o - [H\mathbf{2.1}(BR_3)_2]^-$
$[B]$ is the concentration of free base at equilibrium, $[B] = [HB]_0 - [HB]$

Derivation of Equation 2.1.

$$\begin{array}{rr} FeFe + H^+ \leftrightarrow HFeFe & 1/K_a^{Fe} \\ HB \leftrightarrow H^+ + B^- & K_a^{H+} \\ \hline FeFe + HB \leftrightarrow HFeFe + B & K_{eq} \end{array}$$

$$K_{eq} = \frac{K_a^{H+}}{K_a^{Fe}}$$

$$\frac{[HFeFe][B]}{[FeFe][HB]} = \frac{K_a^{H+}}{K_a^{Fe}}$$

$$-\log\frac{[HFeFe][B]}{[FeFe][HB]} = -\log\frac{K_a^{H+}}{K_a^{Fe}}$$

$$-\log\frac{[HFeFe][B]}{[FeFe][HB]} = -\log(K_a^{H+}) + \log(K_a^{Fe})$$

$$-\log\frac{[HFeFe][B]}{[FeFe][HB]} = pK_a^{H+} - pK_a^{Fe}$$

$$pK_a^{Fe} = pK_a^{H+} + \log\frac{[HFeFe][B]}{[FeFe][HB]}$$

Table 2.7. pK_a Determination of $(Et_4N)_2$[**2.1**$(BAr^F{}_3)_2$] with $PhNH_3BAr^{F24}$ in MeCN.

Run	Initial HB	Initial [**2.1**$(BR_3)_2]^{2-}$	Eq [**2.1**$(BR_3)_2]^{2-}$	Eq [H**2.1**$(BR_3)_2]^{-}$	Eq HB	Eq B	pK_a
1	1.07	1	0.40	0.60	0.47	0.60	10.9
2	0.40	1	0.71	0.29	0.11	0.29	10.7
3	1.91	1	0.26	0.74	1.17	0.74	10.9

pK_a^{MeCN} = 10.8±0.2

Table 2.8. pK_a Determination of $(Et_4N)_2$[**2.1**$(BAr^{F\#}{}_3)_2$] with PyHBAr^{F24} in MeCN.

Run	Initial HB	Initial [**2.1**$(BR_3)_2]^{2-}$	Eq [**2.1**$(BR_3)_2]^{2-}$	Eq [H**2.1**$(BR_3)_2]^{-}$	Eq HB	Eq B	pK_a
1	1.33	1	0.16	0.84	0.49	0.84	13.5
2	0.66	1	0.42	0.58	0.08	0.58	13.5
3	2.08	1	0.09	0.91	1.17	0.91	13.4

pK_a^{MeCN} = 13.5±0.1

2.11 References

(1) Pierik, A. J.; Hulstein, M.; Hagen, W. R.; Albracht, S. P. J. "A Low-Spin Iron with CN and CO as Intrinsic Ligands Forms the Core of the Active Site in [Fe]-Hydrogenases" *Eur. J. Biochem.* **1998**, *258*, 572.

(2) Pierik, A. J.; Roseboom, W.; Happe, R. P.; Bagley, K. A.; Albracht, S. P. J. "Carbon Monoxide and Cyanide as Intrinsic Ligands to Iron in the Active Site of [NiFe]-Hydrogenases - $NiFe(CN)_2CO$, Biology's Way to Activate H_2" *J. Biol. Chem.* **1999**, *274*, 3331.

(3) Piantadosi, C. A.; Sylvia, A. L.; Jobsis, F. F. "Cyanide-Induced Cytochrome-A,A3-Oxidation-Reduction Responses in Rat-Brain Invivo" *J. Clin. Invest.* **1983**, *72*, 1224.

(4) Tard, C.; Pickett, C. J. "Structural and Functional Analogues of the Active Sites of the [Fe]-, [NiFe]-, and [FeFe]-Hydrogenases" *Chem. Rev.* **2009**, *109*, 2245.

(5) Ogata, H.; Lubitz, W.; Higuchi, Y. "[NiFe] Hydrogenases: Structural and Spectroscopic Studies of the Reaction Mechanism" *Dalton Trans.* **2009**, 7577.

(6) Mulder, D. W.; Ratzloff, M. W.; Shepard, E. M.; Byer, A. S.; Noone, S. M.; Peters, J. W.; Broderick, J. B.; King, P. W. "EPR and FTIR Analysis of the Mechanism of H_2 Activation by [FeFe]-Hydrogenase HydA1 from *Chlamydomonas reinhardtii*" *J. Am. Chem. Soc.* **2013**, *135*, 6921.

(7) Schmidt, M.; Contakes, S. M.; Rauchfuss, T. B. "First Generation Analogues of the Binuclear Site in the Fe-Only Hydrogenases: $Fe_2(\mu\text{-}SR)_2(CO)_4(CN)_2^{2-}$" *J. Am. Chem. Soc.* **1999**, *121*, 9736.

(8) Le Cloirec, A.; Best, S. P.; Borg, S.; Davies, S. C.; Evans, D. J.; Hughes, D. L.; Pickett, C. J. "A Di-Iron Dithiolate Possessing Structural Elements of the Carbonyl/Cyanide Sub-Site of the H-Centre of Fe-Only Hydrogenase" *Chem. Commun.* **1999**, 2285.

(9) Lyon, E. J.; Georgakaki, I. P.; Reibenspies, J. H.; Darensbourg, M. Y. "Carbon Monoxide and Cyanide Ligands in a Classical Organometallic Complex Model for Fe-Only Hydrogenase" *Angew. Chem. Int. Ed.* **1999**, *38*, 3178.

(10) Gloaguen, F.; Lawrence, J. D.; Schmidt, M.; Wilson, S. R.; Rauchfuss, T. B. "Synthetic and Structural Studies on $[Fe_2(SR)_2(CN)_x(CO)_{6-x}]^{x-}$ as Active Site Models for Fe-Only Hydrogenases" *J. Am. Chem. Soc.* **2001**, *123*, 12518.

(11) George, S. J.; Cui, Z.; Razavet, M.; Pickett, C. J. "The Di-Iron Subsite of All-Iron Hydrogenase: Mechanism of Cyanation of a Synthetic {2Fe3S} - Carbonyl Assembly" *Chem. Eur. J.* **2002**, *8*, 4037.

(12) Jablonskyte, A.; Wright, J. A.; Pickett, C. J. "Mechanistic Aspects of the Protonation of [FeFe]-Hydrogenase Subsite Analogues" *Dalton Trans.* **2010**, *39*, 3026.

(13) Zhao, X.; Georgakaki, I. P.; Miller, M. L.; Yarbrough, J. C.; Darensbourg, M. Y. "H/D Exchange Reaction in Dinuclear Iron Thiolates as Activity Assay Models of [Fe]-H_2ase" *J. Am. Chem. Soc.* **2001**, *123*, 9710.

(14) Pandey, A. S.; Harris, T. V.; Giles, L. J.; Peters, J. W.; Szilagyi, R. K. "Dithiomethylether as a Ligand in the Hydrogenase H-Cluster" *J. Am. Chem. Soc.* **2008**, *130*, 4533.

(15) Knorzer, P.; Silakov, A.; Foster, C. E.; Armstrong, F. A.; Lubitz, W.; Happe, T. "Importance of the Protein Framework for Catalytic Activity of [FeFe]-Hydrogenases" *J. Biol. Chem.* **2012**, *287*, 1489.

(16) Rocchini, E.; Rigo, P.; Mezzetti, A.; Stephan, T.; Morris, R. H.; Lough, A. J.; Forde, C. E.; Fong, T. P.; Drouin, S. D. "Synthesis and Properties of Iron-Group Hydrido-Cyano Complexes *trans*-$[MH(CN)(L)_2$, M = Fe, Ru or Os, L = diphosphine, and Their Hydrogen, Trifluoroboron and Triphenylboron Isocyanide Derivatives of the Type *trans*-$[MH(CNH)(L)_2]O_3SCF_3$, *trans*-$[MH(CNBX_3)(L)_2]$, X = F or Ph, and *trans*-$[M(H_2)(CNBF_3)(dppp)_2]BF_4$ [dppp = $Ph_2P(CH_2)_3PPh_2$]" *J. Chem. Soc., Dalton Trans.* **2000**, 3591.

(17) Brunkan, N. M.; Brestensky, D. M.; Jones, W. D. "Kinetics, Thermodynamics, and Effect of BPh_3 on Competitive C-C and C-H Bond Activation Reactions in the Interconversion of Allyl Cyanide by Ni(dippe)" *J. Am. Chem. Soc.* **2004**, *126*, 3627.

(18) Vei, I. C.; Pascu, S. I.; Green, M. L. H.; Green, J. C.; Schilling, R. E.; Anderson, G. D. W.; Rees, L. H. "Synthesis and Study of New Binuclear Compounds Containing Bridging (μ-CN)$B(C_6F_5)_3$ and (μ-NC)$B(C_6F_5)_3$ Systems" *Dalton Trans.* **2003**, 2550.

(19) Tolman, C. A.; McKinney, R. J.; Seidel, W. C.; Druliner, J. D.; Stevens, W. R. "Homogeneous NIickel-Catalyzed Olefin Hydrocyanation" *Adv. Catal.* **1985**, *33*, 1.

(20) Luo, L.; Marks, T. J. "Ziegler-Natta Catalyst Activation. Thermodynamic and Kinetic Aspects of Metallocenium Ion-Pair Formation, Dissociation, and Structural Reorganization" *Top. Catal.* **1999**, *7*, 97.

(21) Stephan, D. W. "Frustrated Lewis Pairs: A New Strategy to Small Molecule Activation and Hydrogenation Catalysis" *Dalton Trans.* **2009**, 3129.

(22) Sivaev, I. B.; Bregadze, V. I. "Lewis Acidity of Boron Compounds" *Coord. Chem. Rev.* **2014**, *270*, 75.

(23) Darensbourg, D. J.; Reibenspies, J. H.; Lai, C. H.; Lee, W. Z.; Darensbourg, M. Y. "Analysis of an Organometallic Iron Site Model for the Heterodimetallic Unit of [NiFe]-Hydrogenase" *J. Am. Chem. Soc.* **1997**, *119*, 7903.

(24) Boyer, J. L.; Rauchfuss, T. B.; Wilson, S. R. "Nanoscale Ensembles Using Building Blocks Inspired by the [FeFe]-Hydrogenase Active Site" *C. R. Chim.* **2008**, *11*, 922.

(25) Britovsek, G. J. P.; Ugolotti, J.; White, A. J. P. "From $B(C_6F_5)_3$ to $B(OC_6F_5)_3$: Synthesis of $(C_6F_5)_2BOC_6F_5$ and $C_6F_5B(OC_6F_5)_2$ and Their Relative Lewis Acidity" *Organometallics* **2005**, *24*, 1685.

(26) Morrison, D. J.; Piers, W. E. "Weaker Lewis Acid, Better Catalytic Activity: Dual Mechanisms in Perfluoroarylborane-Catalyzed Allylstannation Reactions" *Org. Lett.* **2003**, *5*, 2857.

(27) Welch, G. C.; Cabrera, L.; Chase, P. A.; Hollink, E.; Masuda, J. D.; Wei, P. R.; Stephan, D. W. "Tuning Lewis Acidity Using the Reactivity of "Frustrated Lewis Pairs": Facile Formation of Phosphine-Boranes and Cationic Phosphonium-Boranes" *Dalton Trans.* **2007**, 3407.

(28) Nicasio, J. A.; Steinberg, S.; Inés, B.; Alcarazo, M. ″Tuning the Lewis Acidity of Boranes in Frustrated Lewis Pair Chemistry: Implications for the Hydrogenation of Electron-Poor Alkenes″ *Chem. Eur. J.* **2013**, 11016.

(29) Durfey, B. L.; Gilbert, T. M. ″Computational Studies of Lewis Acidities of Tris(fluorophenyl)-Substituted Boranes: An Additive Relationship between Lewis Acidity and Fluorine Position″ *Inorg. Chem.* **2011**, *50*, 7871.

(30) Chakraborty, D.; Rodriguez, A.; Chen, E. Y. X. ″Catalytic Ring-Opening Polymerization of Propylene Oxide by Organoborane and Aluminum Lewis Acids″ *Macromolecules* **2003**, *36*, 5470.

(31) Zilberman, S.; Stiefel, E. I.; Cohen, M. H.; Car, R. ″Theoretical Studies of [FeFe]-Hydrogenase: Structure and Infrared Spectra of Synthetic Models″ *J. Phys. Chem. B* **2006**, *110*, 7049.

(32) Kaziannis, S.; Wright, J. A.; Candelaresi, M.; Kania, R.; Greetham, G. M.; Parker, A. W.; Pickett, C. J.; Hunt, N. T. ″The Role of CN and CO Ligands in the Vibrational Relaxation Dynamics of Model Compounds of the [FeFe]-Hydrogenase Enzyme″ *Phys. Chem. Chem. Phys.* **2011**, *13*, 10295.

(33) Berggren, G.; Adamska, A.; Lambertz, C.; Simmons, T. R.; Esselborn, J.; Atta, M.; Gambarelli, S.; Mouesca, J. M.; Reijerse, E.; Lubitz, W.; Happe, T.; Artero, V.; Fontecave, M. ″Biomimetic Assembly and Activation of [FeFe]-Hydrogenases″ *Nature* **2013**, *499*, 66.

(34) Stanley, J. L.; Heiden, Z. M.; Rauchfuss, T. B.; Wilson, S. R.; De Gioia, L.; Zampella, G. ″Desymmetrized Diiron Azadithiolato, Carbonyls: A Step Toward Modeling the Iron-Only Hydrogenases″ *Organometallics* **2008**, *27*, 119.

(35) Nehring, J. L.; Heinekey, D. M. ″Dinuclear Iron Isonitrile Complexes: Models for the Iron Hydrogenase Active Site″ *Inorg. Chem.* **2003**, *42*, 4288.

(36) Kaljurand, I.; Kutt, A.; Soovali, L.; Rodima, T.; Maemets, V.; Leito, I.; Koppel, I. A. ″Extension of the Self-Consistent Spectrophotometric Basicity Scale in Acetonitrile to a Full Span of 28 pK_a units: Unification of Different Basicity Scales″ *J. Org. Chem.* **2005**, *70*, 1019.

(37) Boyke, C. A. *Ph.D. Thesis, University of Illinois at Urbana-Champaign*, **2006**.

(38) Zhao, X.; Georgakaki, I. P.; Miller, M. L.; Mejia-Rodriguez, R.; Chiang, C. Y.; Darensbourg, M. Y. ″Catalysis of H_2/D_2 Scrambling and other H/D Exchange Processes by [Fe]-Hydrogenase Model Complexes″ *Inorg. Chem.* **2002**, *41*, 3917.

(39) Eilers, G.; Schwartz, L.; Stein, M.; Zampella, G.; de Gioia, L.; Ott, S.; Lomoth, R. ″Ligand Versus Metal Protonation of an Iron Hydrogenase Active Site Mimic″ *Chem. Eur. J.* **2007**, *13*, 7075.

(40) Zaffaroni, R.; Rauchfuss, T. B.; Gray, D. L.; De Gioia, L.; Zampella, G. ″Terminal vs Bridging Hydrides of Diiron Dithiolates: Protonation of Fe_2(dithiolate)$(CO)_2(PMe_3)_4$″ *J. Am. Chem. Soc.* **2012**, *134*, 19260.

(41) Jablonskyte, A.; Wright, J. A.; Fairhurst, S. A.; Peck, J. N. T.; Ibrahim, S. K.; Oganesyan, V. S.; Pickett, C. J. ″Paramagnetic Bridging Hydrides of Relevance to Catalytic Hydrogen Evolution at Metallosulfur Centers″ *J. Am. Chem. Soc.* **2011**, *133*, 18606.

(42) Carroll, M. E.; Barton, B. E.; Gray, D. L.; Mack, A. E.; Rauchfuss, T. B. ″Active-Site Models for the Nickel-Iron Hydrogenases: Effects of Ligands on Reactivity and Catalytic Properties″ *Inorg. Chem.* **2011**, *50*, 9554.

(43) Mack, A. E.; Rauchfuss, T. B. ″(1,3-Propanedithiolato)-Hexacarbonyldiiron and Cyanide Derivatives″ *Inorg. Synth.* **2010**, *35*, 143.

(44) Reynard, K. E.; Sherman, R. E.; Smith, H. D.; Hohnstedt, L. F.; Gassenheimer, G.; Wartik, T. ″Trimethylammonium Tetraphenylborate: (A Ready Source of Triphenylborane)″ *Inorg. Synth.* **2007**, 52.

(45) Travis, A. L.; Binding, S. C.; Zaher, H.; Arnold, T. A. Q.; Buffet, J. C.; O'Hare, D. ″Small Molecule Activation by Frustrated Lewis Pairs″ *Dalton Trans.* **2013**, *42*, 2431.

Chapter 3

Iron Hydride Monomers as Synthons for [NiFe]-Hydrogenase Models

3.1 Introduction

Motivated both by the novelty of the active site as well as by possible practical applications, much effort has been invested into the structural and functional models of the [NiFe]-H_2ase active site.[1,2] The [NiFe]-H_2ase models $[(CO)_2(L)Fe(H)(xdt)Ni(diphos)]^+$ (L = CO, PR_3) serve as electrocatalysts for H_2 production, but occur at both low rates (20 – 310 s^{-1}) and high overpotentials (0.5 – 0.6 V).[3,4] The catalytic cycle is proposed to occur by reduction of Ni(II)(H)Fe(II) followed by protonation of the reduced hydride to produce H_2. This is in contrast to the catalytic cycle of [NiFe]-H_2ase which forms H_2 by direct protonation of a Ni(II)(H)Fe(II) center (Figure 3.1).[5] The requirement to reduce $[(CO)_2(L)Fe(H)(xdt)Ni(diphos)]^+$ in order to undergo protonolysis may be relevant to the high overpotentials of the catalysis.

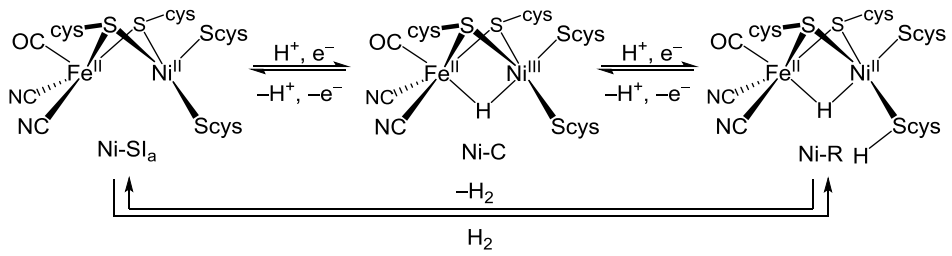


Figure 3.1. Proposed catalytic cycle for [NiFe]-H_2ase.

A more biologically relevant catalytic cycle could be developed by utilizing models that more closely resembling the active site of [NiFe]-H_2ase. The active site is expected to be anionic because six ligands, two cyanide and four thiolates, are anionic. One approach for models with a more accurate coordination sphere is to introduce cyanide ligands on the Fe center. Few models for [NiFe]-H_2ase contain cyanide ligands. The models of [NiFe]-H_2ase with cyanide ligands can be divided into two categories. The monomeric $L_nFe(CO)_x(CN)_y$ compounds with either dithiolates,[6,7] Cp^-,[8] or hydrides.[9,10] In bimetallic NiFe models, the Fe center is coordinatively saturated, generally by two carbonyl and two cyanide ligands (Figure 3.2).[11-13] Models of [NiFe]-H_2ase with cyanide are generally nonfuctional, and are only used in spectroscopic studies.[14,15]

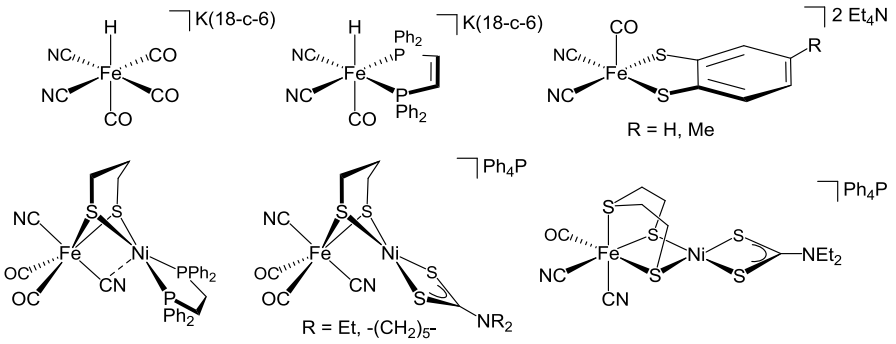


Figure 3.2. Models of [NiFe]-H_2ase with cyanide ligands.

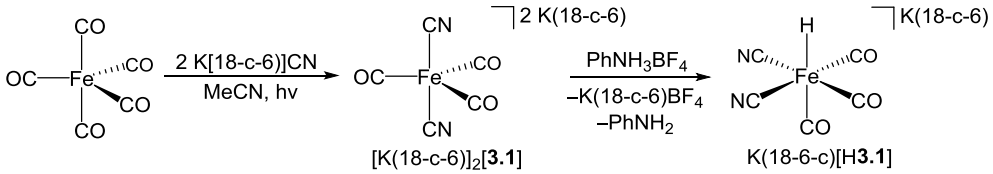
Attempts to form functional cyanide-containing models were first explored by ligand substitution of already functional H_2ase models. Ligand substitution of cyanide with [NiFe]-H_2ase models did not produce favorable results. The model $[(CO)_3Fe(H)(pdt)Ni(dppe)]^+$ undergoes ligand substitution with phosphines.[3] In contrast, treatment of $[(CO)_3Fe(H)(pdt)Ni(dppe)]^+$ with CN^- results in deprotonation of the hydride and formation of HCN. The mixed valent species $[(CO)_3Fe(pdt)Ni(dppe)]^+$ also undergoes ligand substitution with phosphines, but addition of CN^- results in reduction of the NiFe compound to $(CO)_3Fe(pdt)Ni(dppe)$.[16]

Another method for developing functional models is by treatment of a Fe precursor containing cyanide ligands with a Ni precursor. The [NiFe]-H_2ase models $(CO)_2(CN)_2Fe(pdt)NiL_2$ are formed by the treatment of the saturated Fe monomer $[(CO)_2(CN)_2Fe(pdt)]^{2-}$ with Ni monomers.[11-13] As a result of the coordinatively saturated Fe center, no reactivity has been reported. The use of a Fe monomer possessing a hydride ligand may serve as a useful synthon for the development of a biomimetic [NiFe]-H_2ase model. The compound K(18-c-6)$[HFe(CO)_3(CN)_2]$, K(18-c-6)[H**3.1**], is an intriguing synthon for [NiFe]-H_2ase models as it contains the desired cyanide, carbonyl, and hydride ligands in the correct ratio.[9] Although [H**3.1**]$^-$ undergoes ligand substitution with phosphines and cyanide,[10] the reaction of [H**3.1**]$^-$ with Ni(pdt)(dxpe) does not result in products with hydride ligands. The lack of hydride-containing products is thought to result from poor displacement of the CO ligands of [H**3.1**]$^-$. Making the carbonyl ligands more labile would improve the ligand substitution of [H**3.1**]$^-$. A method for making the Fe-CO bonds more labile would be the coordination of Lewis acids the cyanide ligands. The treatment of Lewis acids with metal cyanide compounds results in the coordination of the Lewis acid to the basic M-C*N*.[17] Compounds with CO ligand are reported to have a shift of the bands ν_{CO} to higher energy upon coordination of the Lewis acid.[18] This shift of ν_{CO} bands is indicative weaker M-CO bonds which may be prone to ligand substitution.

3.2 Improved Synthesis of $[K(18\text{-c-}6)]_2[Fe(CO)_3(CN)_2]$ and $[K(18\text{-c-}6)][HFe(CO)_3(CN)_2]$

The salts $[K(18\text{-c-}6)]_2[Fe(CO)_3(CN)_2]$, $[K(18\text{-c-}6)]_2$[**3.1**], and its protonated derivative K(18-c-6)[H**3.1**] have been prepared previously in low yield.[10] Simple modifications of the experimental procedures greatly improved yield and purity. The use of an intense light source (20,000 mW/cm^2) to irradiate a solution of $Fe(CO)_5$ in the presence of two equivalents of K(18-c-6)CN formed $[K(18\text{-c-}6)]_2$[**3.1**] in good yields (Scheme 3.1). The synthesis results in samples of K(18-c-6)[H**3.1**] contaminated with other $[K(18\text{-c-}6)]^+$ salts that are not readily separated. Protonation of $[K(18\text{-c-}6)]_2$[**3.1**] with $H(Et_2O)_2BAr^{F24}$ has been reported to form pure samples of K(18-c-6)[H**3.1**] as the Et_2O soluble $K(18\text{-c-}6)BAr^{F24}$ salt that could be easily removed. The use of $H(Et_2O)_2BAr^{F24}$ as a reagent is not preferred for larger scale reactions because it is difficult to synthesize.[19] Treatment of $[K(18\text{-c-}6)]_2$[**3.1**] with $PhNH_3BF_4$ produced K(18-c-6)[H**3.1**] in good yield without contamination with K(18-c-6)BF_4.

Scheme 3.1. Synthesis of $[K(18\text{-c-}6)]_2$[**3.1**] and K(18-c-6)[H**3.1**].



3.3 Lewis Acid Adducts of $[Fe(CO)_3(CN)_2]^{2-}$

Treatment of $[K(18\text{-c-}6)]_2$[**3.1**] with two equivalents of the boranes BPh_3 or $BAr^F{}_3$ formed the 2:1 adducts $[K(18\text{-c-}6)]_2$[**3.1**$(BR_3)_2$] (eq. 3.1). The IR spectra of [**3.1**$(BR_3)_2]^{2-}$ contains ν_{CN} and ν_{CO} bands shift to higher energies than [**3.1**]$^{2-}$ (Table 3.1). The stronger Lewis acid $BAr^F{}_3$ shifted the ν_{CN} and ν_{CO} bands more than BPh_3.

$$\underset{[K(18\text{-c-}6)]_2[Fe(CO)_3(CN)_2]}{} + 2\ BR_3 \rightarrow \underset{[K(18\text{-c-}6)]_2[\mathbf{3.1}]}{} \quad \underset{[K(18\text{-c-}6)]_2[\mathbf{3.1}(BR_3)_2]}{} \qquad (3.1)$$

Table 3.1. Selected IR bands in ν_{CN} and ν_{CO} regions for [**3.1**]$^{2-}$ and the 2:1 adducts.

Compound	Solvent	ν_{CN} (cm^{-1})	ν_{CO} (cm^{-1})
[**3.1**]$^{2-}$	MeCN	2059	1844
[**3.1**$(BPh_3)_2]^{2-}$	MeCN	2132	1888
[**3.1**$(BAr^F{}_3)_2]^{2-}$	MeCN	2130	1903

The compounds [**3.1**$(BR_3)_2]^{2-}$ interacted with solvents differently than [**3.1**]$^{2-}$. The addition of CH_2Cl_2 to solid samples of [**3.1**]$^{2-}$ resulted in the oxidative addition of CH_2Cl_2, forming $[Fe(CH_2Cl)(CO)_3(CN)_2]^-$ ([CH_2Cl**3.1**]$^-$) as confirmed by ESI-MS (m/z = 241). The IR spectrum of [CH_2Cl**3.1**]$^-$ (ν_{CN} = 2133, 2114 cm^{-1};

ν_{CO} = 2088, 2035 cm^{-1}) resembled the IR spectrum [H**3.1**]$^-$ consistent with oxidation to Fe(II). In contrast, the adduct [**3.1**(BAr^F_3)$_2$]$^{2-}$ was found to be stable in CH_2Cl_2 for days.

3.4 Lewis Acid Adducts of $[HFe(CO)_3(CN)_2]^-$

Treatment of K(18-c-6)[H**3.1**] with two equivalents of the triarylboranes BAr^F_3, BPh_3, or $B(OPh)_3$ formed the 2:1 adducts [K(18-c-6)][$HFe(CO)_3(CNBR_3)_2$] (K(18-c-6)[H**3.1**(BR_3)$_2$]) (eq 3.2). The formation of the adducts could be monitored by IR spectroscopy (Figure 3.3). The ν_{CO} of the adducts correlate to Lewis acidity of the boranes (Table 3.1).[20]

$$\underset{\text{K(18-c-6)[H\mathbf{3.1}]}}{[K(18\text{-c-6})][HFe(CO)_3(CN)_2]} + 2\ BR_3 \rightarrow \underset{\text{K(18-c-6)[H\mathbf{3.1}}(BR_3)_2]}{[K(18\text{-c-6})][HFe(CO)_3(CNBR_3)_2]} \qquad (3.2)$$

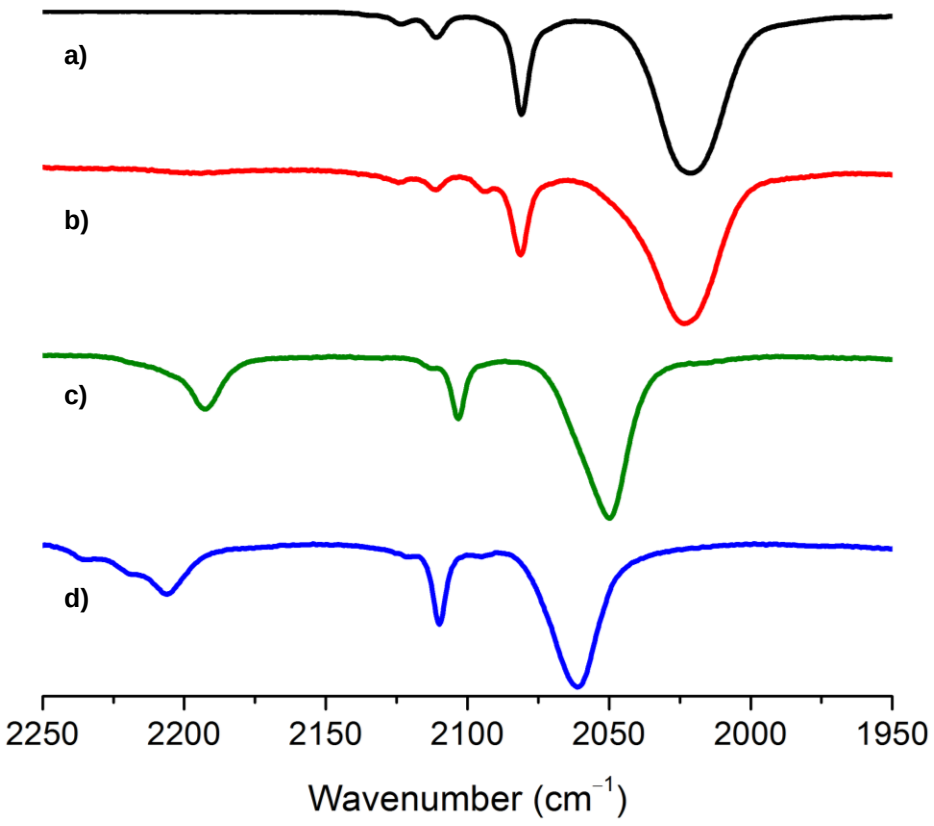


Figure 3.3. IR spectra of a) [H**3.1**]$^-$, b) [H**3.1**($B(OPh)_3$)$_2$]$^-$, c) [H**3.1**(BPh_3)$_2$]$^-$, and d) [H**3.1**(BAr^F_3)$_2$]$^-$ in CH_2Cl_2.

Table 3.2. IR frequencies of $[\mathbf{3.1}]^{2-}$ and $[H\mathbf{3.1}]^{-}$ and 2:1 adducts with boranes.

Compound	Solvent	ν_{CN} (cm^{-1})	ν_{CO} (cm^{-1})
$[H\mathbf{3.1}]^{-}$	CH_2Cl_2	2124, 2112	2081, 2021
$[H\mathbf{3.1}(B(OPh)_3)_2]^{-}$	CH_2Cl_2	2124, 2111	2081, 2023
$[H\mathbf{3.1}(BPh_3)_2]^{-}$	CH_2Cl_2	2215, 2193	2103, 2050
$[H\mathbf{3.1}(BAr^F{}_3)_2]^{-}$	CH_2Cl_2	2218, 2205	2109, 2061

As observed for $[\mathbf{3.1}(BR_3)_2]^{2-}$, the adducts of $[H\mathbf{3.1}(BR_3)_2]^{-}$ interacted differently with solvents than $[H\mathbf{3.1}]^{-}$. Dissolution of $[H\mathbf{3.1}(BAr^F{}_3)_2]^{-}$ in MeCN resulted in deprotonation of the hydride to form $[\mathbf{3.1}(BAr^F{}_3)_2]^{2-}$ as confirmed by IR spectroscopy. The parent compound $[H\mathbf{3.1}]^{-}$ is generated in MeCN and is stable for an indefinite length of time in the absence of air.

The ^{1}H NMR spectrum of $[H\mathbf{3.1}]^{-}$ is characterized by three high field signals at δ –7.90, δ –8.33, and δ –11.2 in a 10:6:1 ratio corresponding to the three possible isomers of $[H\mathbf{3.1}]^{-}$.[9] The ^{1}H NMR spectrum of $[H\mathbf{3.1}(BR_3)_2]^{-}$ also features three high field signals corresponding to the three possible isomers of $[H\mathbf{3.1}(BR_3)_2]^{-}$ (Figure 3.4). High field ^{1}H NMR of $[H\mathbf{3.1}(BAr^F{}_3)_2]^{-}$ displayed three signals at δ –7.87, –8.13, and –10.19 in a 10:10:1 ratio. The ^{1}H NMR spectrum of $[H\mathbf{3.1}(BPh_3)_2]^{-}$ contained three high field signals at δ –7.37, –7.71, and –10.28 in a 10:19:1 ratio. The high field ^{1}H NMR of $[H\mathbf{3.1}(B(OPh)_3)_2]^{-}$ displayed three signals at δ –7.85, –8.03, and –10.79 in a 18:10:1 ratio.

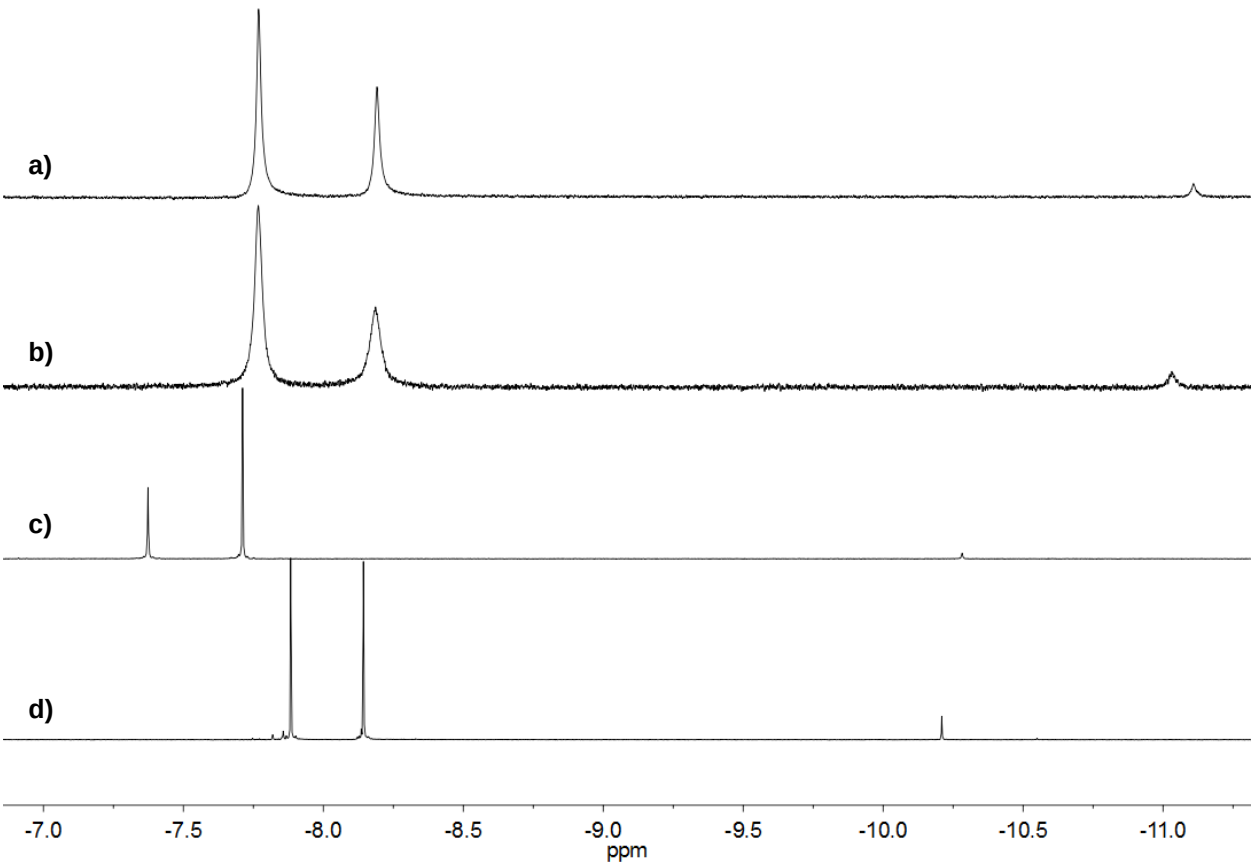


Figure 3.4. ^{1}H NMR spectra of the high-field signals of a) [H**3.1**]$^{-}$, b) [H**3.1**(B(OPh)$_3$)$_2$]$^{-}$, c) [H**3.1**(BPh$_3$)$_2$]$^{-}$, and d) [H**3.1**(BAr$^{F}{}_3$)$_2$]$^{-}$ in CD_2Cl_2.

No assignment of the isomers of [H**3.1**]$^{-}$ is reported.[9] Two isomers of [H**3.1**(BR$_3$)$_2$]$^{-}$ are expected to contain chemically equivalent CNBR$_3^{-}$ ligands. The third isomer is expected to have chemically inequivalent CNBR$_3^{-}$ ligands (Figure 3.5). One isomer of [H**3.1**(BAr$^{F}{}_3$)$_2$]$^{-}$ was assigned by comparison of the integrations of the high field ^{1}H NMR signals and the *p*-F and *m*-F ^{19}F NMR signals. The ^{19}F NMR spectrum of [H**3.1**(BAr$^{F}{}_3$)$_2$]$^{-}$ features two major *p*-F and *m*-F signals of equal intensity. This observation is consistent with the ^{1}H NMR signals at δ –7.87 and –8.13 correlating to the isomer of [H**3.1**(BAr$^{F}{}_3$)$_2$]$^{-}$ with equivalent CNBAr$^{F}{}_3^{-}$ groups. Therefore, the ^{1}H NMR signal at δ –10.19 was assigned to as the isomer with the hydride *trans* to a CNBAr$^{F}{}_3^{-}$ ligand (Figure 3.6). While the isomer with the hydride *trans* to the CNBAr$^{F}{}_3^{-}$ ligand is expected to have two inequivalent CNBAr$^{F}{}_3^{-}$ signals, the integration of the *p*-F and *m*-F signals suggest that the additional set of CNBAr$^{F}{}_3^{-}$ signals are hidden under other signals.

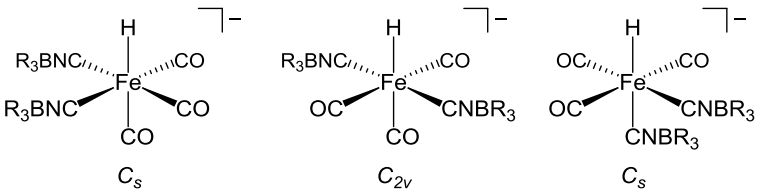


Figure 3.5. Isomers of [H**3.1**$(BR_3)_2$]$^-$ with point groups.

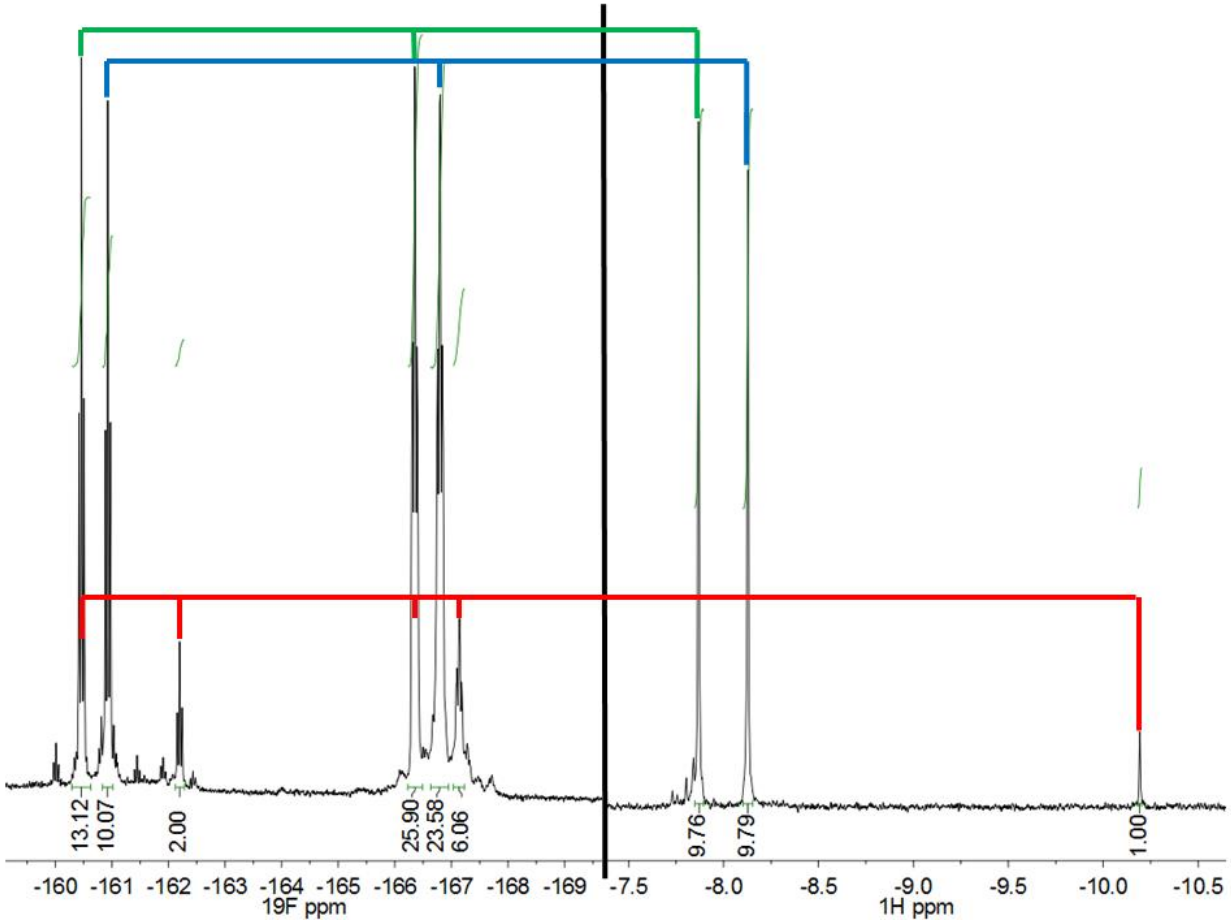


Figure 3.6. ^{19}F NMR spectrum of *p*-F and *m*-F signals of [H**3.1**$(BAr^F{}_3)_2$]$^-$ (left) and ^{1}H NMR high field region of [H**3.1**$(BAr^F{}_3)_2$]$^-$ (right) in CD_2Cl_2.

3.5 Reactions of [$HFe(CO)_3(CNBR_3)_2$]$^-$ with Ni(pdt)(dxpe)

Reactions of [H**3.1**]$^-$ with Ni(pdt)(dppe) did not produce any hydride products. The nonreaction reflects the low lability of the CO ligands of [H**3.1**]$^-$. Treatment of [H**3.1**$(BAr^F{}_3)_2$]$^-$ with Ni(pdt)(dppe) initially resulted in deprotonation of the hydride, forming [**3.1**$(BAr^F{}_3)_2$]$^{2-}$ as determined by IR spectroscopy (Figure 3.7).

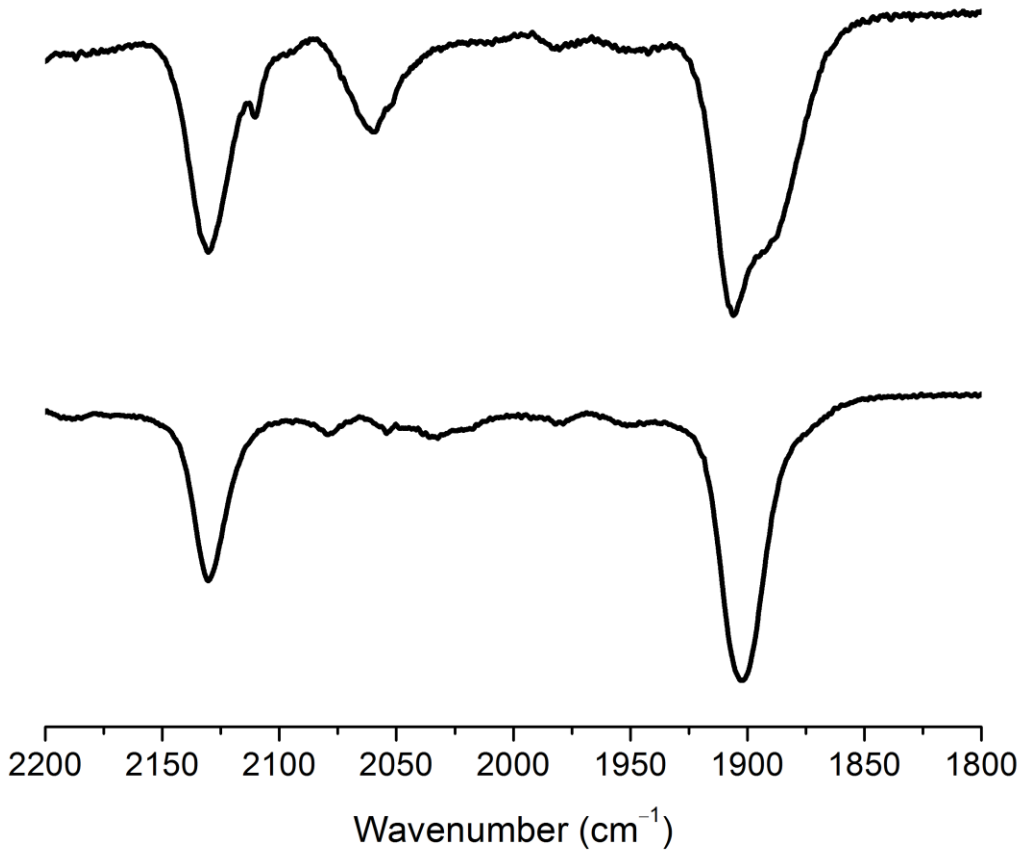


Figure 3.7. IR spectra of the mixture of [H**3.1**$(BAr^F{}_3)_2]^-$ and Ni(pdt)(dppe) (top), and [**3.1**$(BAr^F{}_3)_2]^{2-}$ (bottom) in CH_2Cl_2.

The product displayed two high field ^{1}H NMR signals with large coupling constants (δ –8.80, –8.90 AB quart, $^2J_{HP}$ = 46 Hz; δ –11.50 t, $^2J_{HP}$ = 48 Hz). The $^2J_{HP}$ coupling constant for the hydride signals was not consistent the previously reported NiFe hydrides $[(CO)_2(L)Fe(H)(pdt)Ni(dppe)]^+$ ($^2J_{HP}$ = 6 Hz).[3,4,21] The large coupling constant is consistent with the hydride and diphosphine on a single Fe center as reported in $[HFe(CO)(CN)_2(dppv)]^-$ ($^2J_{HP}$ = 58 Hz).[10] Given the similarities in coupling constant of the ^{1}H NMR hydride signals, the reaction between [H**3.1**$(BAr^F{}_3)_2]^-$ and Ni(pdt)(dppe) is proposed to form $[HFe(CO)(CNBAr^F{}_3)_2(dppe)]^-$ ([H**3.2**$(BAr^F{}_3)_2]^-$). The assignment of [H**3.2**$(BAr^F{}_3)_2]^-$ was confirmed by the independent synthesis of [H**3.2**$(BAr^F{}_3)_2]^-$. The reaction of $[HFe(CO)(CN)_2(dppe)]^-$, [H**3.2**]$^-$, with two equivalents of $BAr^F{}_3$ produced a complex mixture, characterized by several multiplets in the high field region of the ^{1}H NMR spectrum with large coupling constants ($^2J_{HP} \approx 50$ Hz). The high field ^{1}H NMR multiplets observed in the reaction of [H**3.1**$(BAr^F{}_3)_2]^-$ and Ni(pdt)(dppe) were also observed in samples of [H**3.2**$(BAr^F{}_3)_2]^-$ (Figure 3.8).

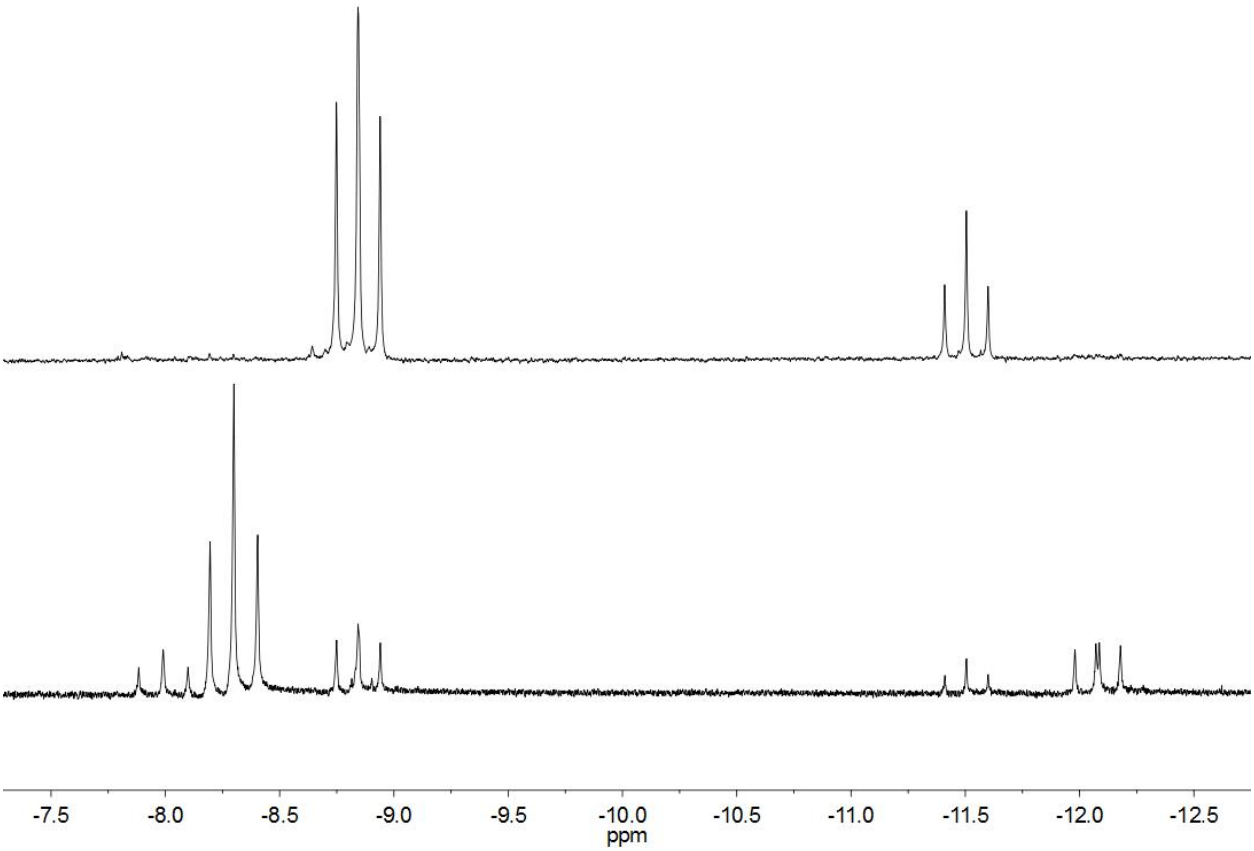


Figure 3.8. High field ^{1}H NMR signals of the reaction of [H**3.1**$(BAr^{F}{}_{3})_{2}]^{-}$ and Ni(pdt)(dppe) (top) and independently synthesized sample of [H**3.2**$(BAr^{F}{}_{3})_{2}]^{-}$ in CD_2Cl_2. The AB quartet at δ –8.80, –8.90 and triplet at –11.50 is observed in both spectra.

Given the highly acidic nature of [H**3.1**$(BAr^{F}{}_{3})_{2}]^{-}$, reaction of Ni(pdt)(dppe) with the less acidic hydride [H**3.1**$(BPh_3)_2]^{-}$ was examined. The treatment of Ni(pdt)(dppe) with [H**3.1**$(BPh_3)_2]^{-}$ resulted in partial deprotonation to form a mixture of [**3.1**$(BPh_3)_2]^{2-}$ and [H**3.1**$(BPh_3)_2]^{-}$ as identified by IR spectroscopy (Figure 3.9). The ^{1}H NMR spectrum of the resulting product displayed two high field signals at δ –6.72 (t, $^{2}J_{HP}$ = 5.5 Hz), –12.08, –12.18 (AB q, $^{2}J_{HP}$ = 47 Hz) (Figure 3.10).

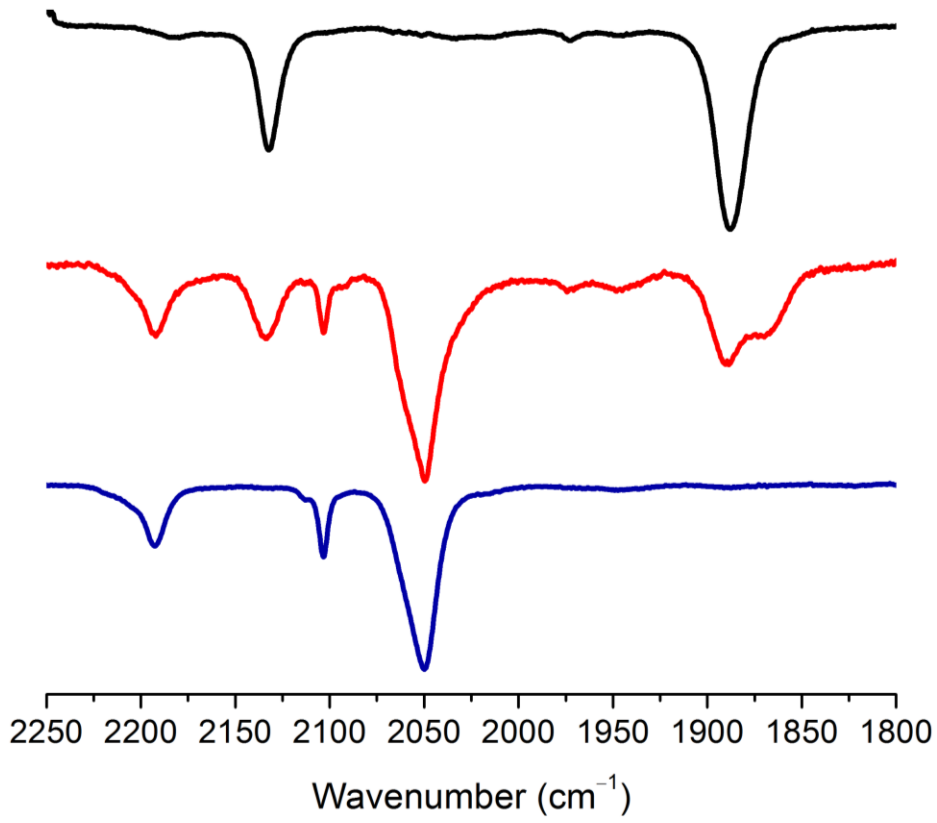


Figure 3.9. IR spectra of [**3.1**$(BPh_3)_2]^{2-}$ (top), reaction mixture of [H**3.1**$(BPh_3)_2]^-$ and Ni(pdt)(dppe) (middle), and [H**3.1**$(BPh_3)_2]^-$ (bottom) in CH_2Cl_2.

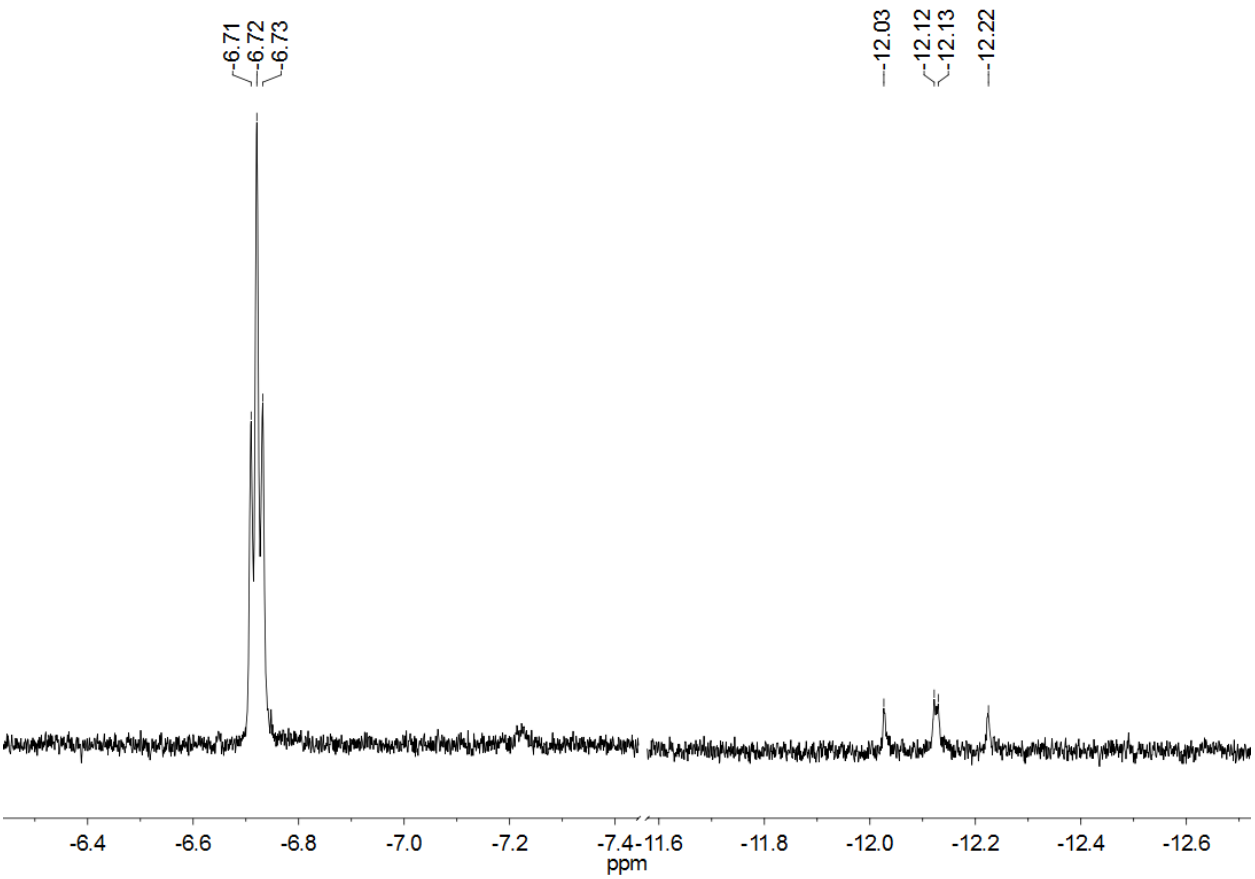


Figure 3.10. High field ^{1}H NMR signals of the reaction mixture of K(18-c-6)[H**3.1**$(BPh_3)_2$] and Ni(pdt)(dppe) in CD_2Cl_2.

On the basis of the large coupling constant the high field AB quartet at δ –12.08, –12.18 was assigned to the monomeric Fe hydride [H**3.2**$(BPh_3)_2]^-$. The 5.5 Hz coupling constant observed for the triplet at δ –6.72 is typical for the NiFe hydrides such as $[(CO)_2(L)Fe(H)(pdt)Ni(dppe)]^+$ (L = CO, PR_3).[3,4,21] Upon purification by column chromatography, the product corresponding to the ^{1}H NMR triplet at δ –6.72 displayed one ν_{CN} band (2167 cm^{-1}) and two ν_{CO} bands (2026, 1973 cm^{-1}) in the IR spectrum. The two ν_{CO} bands of the product were of similar energies to the NiFe hydrides $[(CO)_2(PR_3)Fe(H)(pdt)Ni(dppe)]^+$ (Table 3.2).[3] On the basis of the coupling constant and the IR spectrum, the ^{1}H NMR signal at δ –6.72 was assigned to the NiFe hydride $(CO)_2(CNBPh_3)Fe(H)(pdt)Ni(dppe)$ (**3.3**).

Table 3.3. IR frequencies of $(CO)_2LFeH(pdt)Ni(dxpe)$ in CH_2Cl_2.

Compound	ν_{CN} (cm^{-1})	ν_{CO} (cm^{-1})	ref
$(CO)_2(CNBPh_3)FeH(pdt)Ni(dppe)$, **3.3**	2167	2026, 1973	
$(CO)_2(CNBPh_3)FeH(pdt)Ni(dcpe)$, **3.4**	2167	2019, 1965	
$[(CO)_2(PPh_3)FeH(pdt)Ni(dppe)]^+$		2016, 1964	[3]
$[(CO)_2(PPh_2Py)FeH(pdt)Ni(dppe)]^+$		2022, 1971	[3]
$[(CO)_2(P(OPh)_3)FeH(pdt)Ni(dppe)]^+$		2031, 1981	[3]

The reaction of $[H\mathbf{3.1}(BPh_3)_2]^-$ with Ni(pdt)(dcpe) also resulted in partial deprotonation of $[H\mathbf{3.1}(BPh_3)_2]^-$. Unlike the reaction with Ni(pdt)(dppe), the ^1H NMR spectrum of the reaction mixture of $[H\mathbf{3.1}(BPh_3)_2]^-$ and Ni(pdt)(dcpe) showed formation of one high field triplet (δ –6.28, $^2J_{HP}$ = 3.3 Hz). After purification, the IR spectrum of the hydride product resembled **3.3** (ν_{CN} = 2167 cm^{-1}, ν_{CO} = 2019, 1965 cm^{-1}) leading to the assignment of $(CO)_2(CNBPh_3)Fe(H)(pdt)Ni(dcpe)$ (**3.4**) (Figure 3.11).

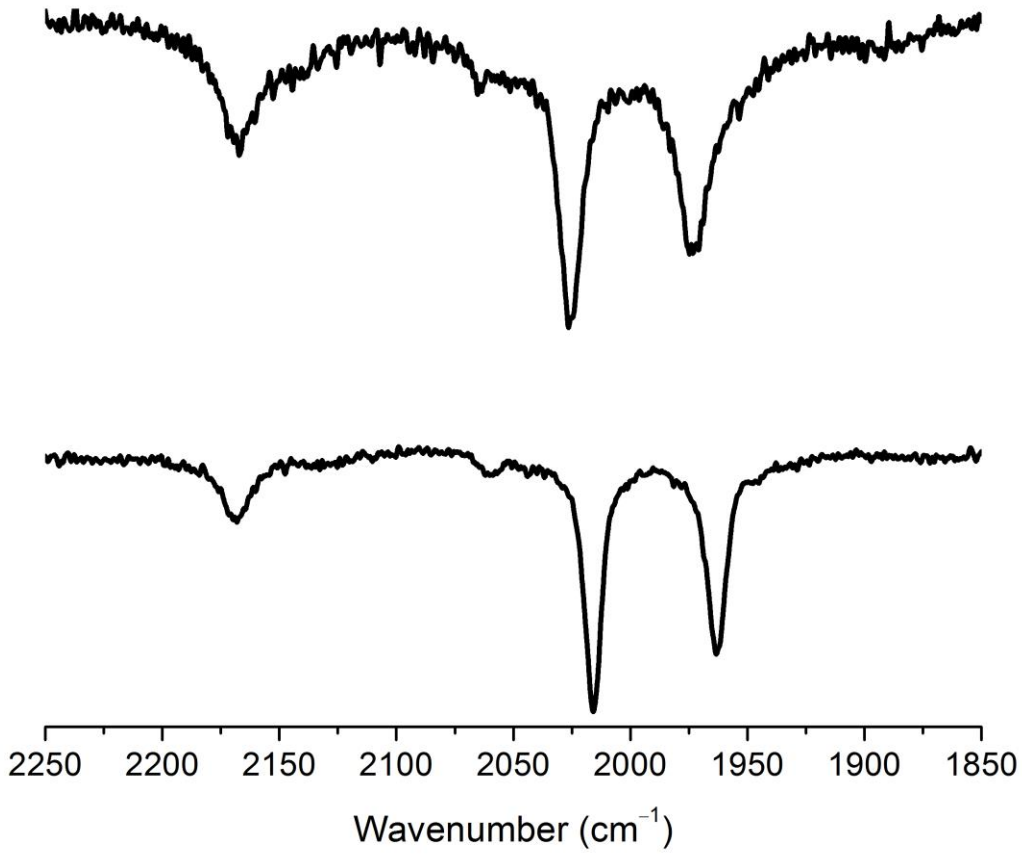


Figure 3.11. IR spectra of **3.3** (top) and **3.4** (bottom) in CH_2Cl_2.

Monitoring the reaction of [H**3.1**$(BPh_3)_2]^-$ and Ni(pdt)(dcpe) by IR spectroscopy over short reaction time revealed the intensity of the ν_{CN} and ν_{CO} bands of [**3.1**$(BPh_3)_2]^{2-}$ changed very little. The IR bands of [H**3.1**$(BPh_3)_2]^-$ decreased in intensity at the expense of the growth of the IR bands of **3.4** (Figure 3.12). The use of longer reaction times of over 48 hours resulted in a loss of [**3.1**$(BPh_3)_2]^{2-}$ and formation of **3.4**. The generation of **3.4** from [H**3.1**$(BPh_3)_2]^-$ would result in the loss of a $CNBPh_3^-$ ligand. No free $CNBPh_3^-$ was observed by IR spectroscopy however the ν_{CN} of $CNBPh_3^-$ is reported at 2167 cm^{-1} and is likely hidden by the ν_{CN} band of **3.4**.[22]

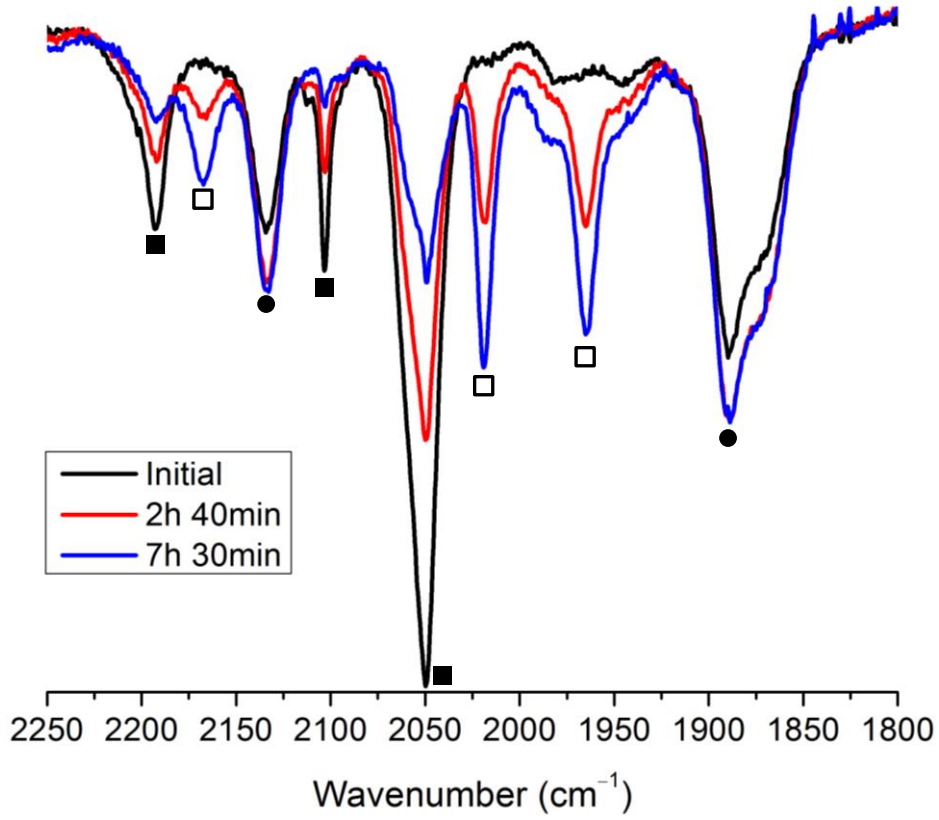


Figure 3.12. IR spectra of the reaction of [H**3.1**$(BPh_3)_2]^-$ and Ni(pdt)(dcpe) over time. ■ [H**3.1**$(BPh_3)_2]^-$, ● [**3.1**$(BPh_3)_2]^{2-}$. □ **3.4**.

To prevent the deprotonation of [H**3.1**$(BR_3)_2]^-$ upon addition of Ni(pdt)(dxpe), the reaction with [H**3.1**$(B(OPh)_3)_2]^-$ and Ni(pdt)(dppe) was explored. As the $B(OPh)_3$ is a much weaker Lewis acid than $BAr^F{}_3$ and BPh_3, the adduct [H**3.1**$(B(OPh)_3)_2]^-$ is not expected to be deprotonated by Ni(pdt)(dxpe). Treatment of [H**3.1**$(B(OPh)_3)_2]^-$ with Ni(pdt)(dppe) did not result in initial deprotonation of the hydride though [H**3.1**$(B(OPh)_3)_2]^-$ was be slowly consumed overtime. The ^{1}H NMR spectrum of the resulting solid gave no evidence for hydride species.

3.6 Discussion

The synthesis of [**3.1**]$^{2-}$ proceeds by stepwise substitution of $Fe(CO)_5$ with two equivalents of CN^-. The addition of the second equivalent of CN^- to $[Fe(CO)_4(CN)]^-$ is slow resulting in $[Fe(CO)_4(CN)]^-$ contaminating samples of [**3.1**]$^{2-}$.[10] The slow addition of the second equivalent of CN^- is caused by self-extinction as [**3.1**]$^{2-}$ has an intense absorption at 230 nm ($\varepsilon = 2 \times 10^5$ cm^{-1} M^{-1}) that overlaps with the absorption band of $[Fe(CO)_4(CN)]^-$ ($\varepsilon = 8 \times 10^3$ cm^{-1} M^{-1}).[10] To increase the rate of addition of CN^- an intense light source was used. By using an

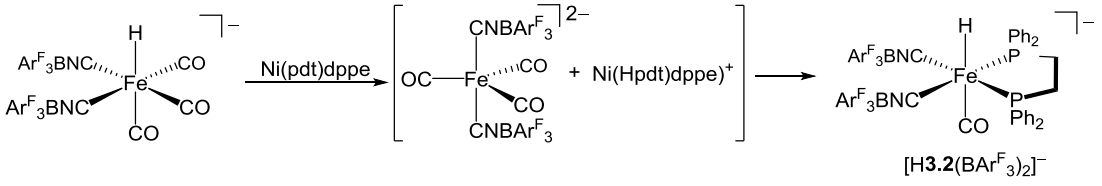
intense light source, the reaction mixtures of $[\mathbf{3.1}]^{2-}$ did not contain $[Fe(CO)_4(CN)]^-$ as determined by IR spectroscopy. As a result, $[\mathbf{3.1}]^{2-}$ could be formed in good yield.

The addition of two equivalents of boranes with different levels of Lewis acidity to $[\mathbf{3.1}]^{2-}$ and $[H\mathbf{3.1}]^-$ readily formed the 2:1 adducts $[\mathbf{3.1}(BR_3)_2]^{2-}$ and $[H\mathbf{3.1}(BR_3)_2]^-$.[23] The relative Lewis acidic strengths of the Lewis acids is demonstrated by the ν_{CO} stretches for $[\mathbf{3.1}(BR_3)_2]^{2-}$ and $[H\mathbf{3.1}(BR_3)_2]^-$. As expected, the largest shift of the ν_{CO} bands in $[\mathbf{3.1}(BR_3)_2]^{2-}$ and $[H\mathbf{3.1}(BR_3)_2]^-$ occurred for $BAr^F{}_3$. The relatively weak Lewis acid $B(OPh)_3$ also coordinated to $[H\mathbf{3.1}]^-$ although no shift in the IR bands was observed. The coordination of boranes with a wide range of Lewis acidities may be attributed to the overall negative charges of $[\mathbf{3.1}]^{2-}$ and $[H\mathbf{3.1}]^-$.

The ν_{CO} shift of $[\mathbf{3.1}(BR_3)_2]^{2-}$ and $[H\mathbf{3.1}(BR_3)_2]^-$ correlate to a decrease in the electron density of the Fe center. This change in electron density upon coordination of the boranes is further demonstrated by the reactivity of $[\mathbf{3.1}]^{2-}$ and $[\mathbf{3.1}(BR_3)_2]^{2-}$ with CH_2Cl_2. The electron rich Fe center of $[\mathbf{3.1}]^{2-}$ reacted with CH_2Cl_2 via oxidative addition forming $[CH_2Cl\mathbf{3.1}]^-$. In contrast, $[\mathbf{3.1}(BAr^F{}_3)_2]^{2-}$ is stable in CH_2Cl_2 for days. Similarly, large differences in the electron density of the Fe center in $[H\mathbf{3.1}]^-$ and $[H\mathbf{3.1}(BR_3)_2]^-$ was observed with MeCN. While $[H\mathbf{3.1}]^-$ is stable in MeCN, dissolving of $[H\mathbf{3.1}(BAr^F{}_3)_2]^-$ in MeCN resulted in deprotonation. The reported pK_a range in MeCN is from –8 to 33,[24] though determining of the p$K_a{}^{MeCN}$ of very strong acids is difficult given the ability of MeCN to serve as a proton acceptor.[25] The p$K_a{}^{MeCN}$ of acids has been accurately measured from 3.8 to 32.0 units,[26,27] indicating that $[H\mathbf{3.1}(BAr^F{}_3)_2]^-$ has a p$K_a{}^{MeCN}$ less than 3.8. The p$K_a{}^{MeCN}$ of the parent compound $[H\mathbf{3.1}]^-$ is reported to be approximately 17,[10] indicating a decrease in the pK_a of the hydride by at least 13 units upon coordination of $BAr^F{}_3$.

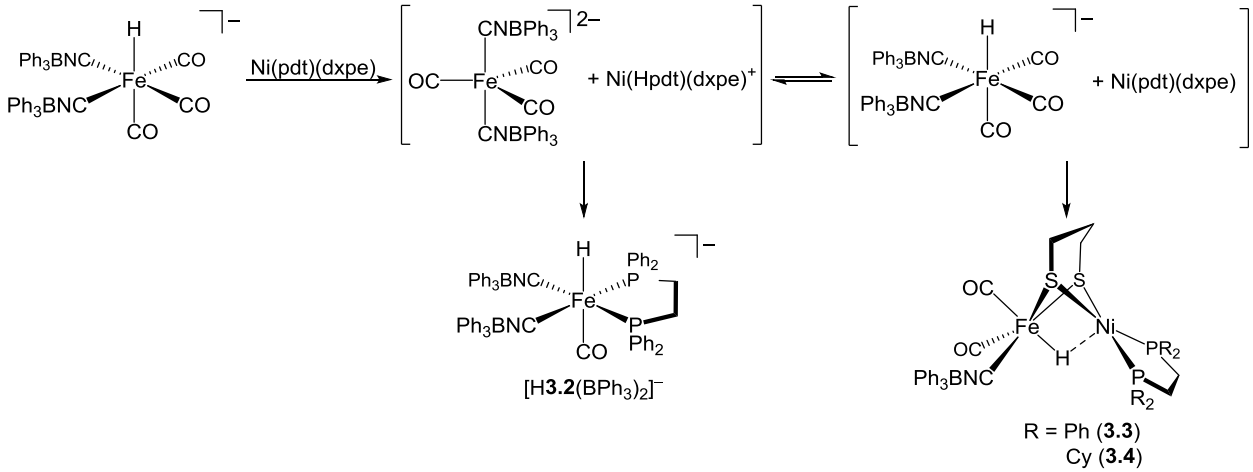
The reactions of $[H\mathbf{3.1}(BR_3)_2]^-$ with Ni(pdt)(dxpe) were not straightforward. The triarylborane in $[H\mathbf{3.1}(BR_3)_2]^-$ and diphosphine of Ni(pdt)(dxpe) influenced the range of products. As $[H\mathbf{3.1}(BAr^F{}_3)_2]^-$ is highly acidic, the treatment of $[H\mathbf{3.1}(BAr^F{}_3)_2]^-$ with Ni(pdt)(dppe) initially formed $[\mathbf{3.1}(BAr^F{}_3)_2]^{2-}$ with Ni(pdt)(dppe) believed to serve as the proton acceptor (Scheme 3.2). Redistribution of the diphosphine and reprotonation of the Fe center is thought to form $[\mathbf{3.2}(BAr^F{}_3)_2]^-$.

Scheme 3.2. Reaction of $[H\mathbf{3.1}(BAr^F{}_3)_2]^-$ with Ni(pdt)(dppe) to form $[H\mathbf{3.2}(BAr^F{}_3)_2]^-$.



The reactions of [H**3.1**$(BPh_3)_2$]$^-$ with Ni(pdt)(dxpe) formed a mixture of [**3.1**$(BPh_3)_2$]$^{2-}$ and [H**3.1**$(BPh_3)_2$]$^-$. Overtime the ^{1}H NMR spectra of the reaction mixtures of [H**3.1**$(BPh_3)_2$]$^-$ and Ni(pdt)(dppe) formed [**3.2**$(BPh_3)_2$]$^-$ and **3.3**. In contrast, the use of Ni(pdt)(dcpe) resulted in **3.4** as the only hydride product (Scheme 3.3). Monitoring of the reaction of [H**3.1**$(BPh_3)_2$]$^-$ and Ni(pdt)(dcpe) by IR spectroscopy indicated **3.4** is formed from [H**3.1**(BPh_3)]$^-$. Long reaction times (50 hours) were found to generate **3.4** from [**3.1**$(BPh_3)_2$]$^{2-}$. The selective formation of **3.4** over monomeric Fe hydrides with Ni(pdt)(dcpe) is attributed to the increased basicity of dcpe over dppe.[28] The strong donor ligand dcpe binds more strongly to Ni than dppe. As a result, mixtures of [**3.1**$(BPh_3)_2$]$^{2-}$ with protonated Ni(pdt)(dcpe) form **3.4**. Mixtures of [**3.1**$(BPh_3)_2$]$^{2-}$ and protonated Ni(pdt)(dppe) undergo ligand redistribution of the diphosphine to the Fe center generating [H**3.2**$(BPh_3)_2$]$^-$.

Scheme 3.3. Proposed pathway for the formation of [H**3.2**$(BPh_3)_2$]$^-$, **3.3**, and **3.4** from the reaction of [H**3.1**$(BPh_3)_2$]$^-$ with Ni(pdt)(dxpe).



3.7 Conclusion

Treatment of [**3.1**]$^{2-}$ or [H**3.1**]$^-$ with two equivalents of triarylboranes of varying Lewis acidity readily formed the 2:1 adducts [**3.1**$(BR_3)_2$]$^{2-}$ or [H**3.1**$(BR_3)_2$]$^-$. The coordination of Lewis acids greatly affected the electron density of the Fe centers and weaken the Fe-CO bond. The reaction of [H**3.1**$(BPh_3)_2$]$^-$ with Ni(pdt)(dxpe) formed NiFe hydrides by a one-pot method with the resulting the bimetallic hydrides **3.3** and **3.4** which have one $CNBR_3^-$ ligand. This is contrast to the active site of [NiFe]-H_2ase where the Fe is ligated by two cyanide ligands. Although the coordination of boranes to [H**3.1**]$^-$ made the Fe-CO bond more labile, the Fe-$CNBR_3$ bond was also prone to displacement. The development of a functional [NiFe]-H_2ase model with two cyanide ligands will require an alternative synthetic route. One method for developing a [NiFe]-H_2ase model with two cyanide ligands would be the

coordination of a borane to [H**3.1**]$^-$ with a Lewis acidity between BPh_3 and $B(OPh)_3$ such as $BPh_2(OPh)$ or $BPh(OPh)_2$.[29] This route may still result in the loss of a $CNBR_3^-$ ligand, forming $(CO)_2(CNBR_3)Fe(H)(pdt)Ni(dxpe)$. Another method for developing functional biomimetic models of [NiFe]-H_2ase is by decarbonylation of the coordinatively saturated models $(CO)_2(CN)_2Fe(pdt)NiL_2$.[11,12]

3.8 Experimental Procedures

All procedures were carried out in a nitrogen-filled MBraun glovebox or using standard Schlenk techniques. All solvents were degassed by sparging with nitrogen and dried by passage through activated alumina. IR spectra were recorded on a Perkin-Elmer Spectrum 100. NMR spectra were recorded on a Varian Unity 500 MHz NMR spectrometer. Signals for ^{19}F and ^{31}P NMR spectra were referenced using external standards of 1% $CFCl_3$ in $CDCl_3$ and 85% H_3PO_4, respectively. ^1H NMR spectra were referenced to internal solvent signals. CD_2Cl_2 (Cambridge Isotope Laboratories) was dried over CaH_2 before being vacuum distilled onto activated 4 Å molecular sieves. $B(C_6F_5)_3$ (Boulder Scientific) was sublimed under vacuum at 90°C. Ni(pdt)(dppe) and Ni(pdt)(dcpe) were prepared by literature methods.[4,21] BPh_3 was synthesized by the pyrolysis of $HNMe_3BPh_4$ followed by sublimation under vacuum at 90 °C.[30] $B(OPh)_3$ (Sigma Aldrich) was used as received.

$[K(18\text{-crown-6})]_2[Fe(CO)_3(CN)_2]$, $[K(18\text{-c-6})]_2$[3.1]. A three-necked flask was charged with KCN (1.1 g, 17 mmol) and 18-crown-6 (4.8 g, 18 mmol) and suspended in CH_3CN (200 mL). The resulting slurry was sonicated (1 hour), until all the solids had dissolved. The $Fe(CO)_5$ (1.1 mL, 8.4 mmol) was added via syringe, and the solution color changed to light yellow. The reaction solution was photolyzed for 36 hours using a Novacure 2100 lamp with no cutoff filter, forming a light green solution. The solution was passed through Celite and concentrated to 20 mL. The final product was precipitated upon addition of ethyl acetate (100 mL). The solid collected via filtration, washed with Et_2O (30 mL) and pentane (30 mL), and dried under vacuum. Yield 4.8 g (72%). IR spectrum matched literature values.

$K(18\text{-crown-6})[HFe(CO)_3(CN)_2]$, K(18-c-6)[H3.1]. A solution of $[K(18\text{-c-6})]_2$[**3.1**] (500 mg, 0.62 mmol) in MeCN (20 mL) was treated with a solution of anilinum BF_4 (110 mg, 0.62 mmol) in MeCN (20 mL) and the solution was stirred for 1 hour. The mixture was treated with Et_2O (120 mL) placed in a –30 °C freezer overnight. The resulting solid was isolated by filtration and extracted into CH_2Cl_2 (15 mL) and the mixture was filtered through Celite. The final product was precipitated from the filtrate upon addition of pentane (150 mL) and isolated by

filtration. Yield 180 mg (59%). Anal. Calc. for $C_{17}H_{25}O_9N_2KFe$ (Found): C, 41.14 (40.74); H, 5.08 (4.90); N, 5.64 (5.71). IR and ^{1}H NMR spectra matched literature values.

[K(18-crown-6)]$_2$[Fe(CO)$_3$(CNBAr$^F_3$)$_2$], [K(18-c-6)]$_2$[3.1(BAr$^F_3$)$_2$]. A solution of [K(18-c-6)]$_2$[**3.1**] (200 mg, 0.25 mmol) in MeCN (20 mL) was treated dropwise with a solution of BAr^F_3 (260 mg, 0.50 mmol) in MeCN. The resulting solution was stirred for 30 minutes. The solvent was removed under vacuum resulting in a yellow oil, which was extracted into Et_2O (20 mL) and the solution was passed through Celite. The solvent was removed under vacuum and the resulting oil was triturated with pentane (3 x 20 mL). The resulting solid was dissolved in CH_2Cl_2 (3 mL) and the solution was layered with Et_2O (3 mL) and pentane (12 mL) and cooled to –30 ºC for 3 days. The resulting solid was isolated and dried. Yield 230 mg (51 %). Anal. Calc. for $C_{65}H_{48}B_2F_{30}FeK_2N_2O_{15}$ (Found): C, 42.83 (42.59); H, 2.65 (2.69); N, 1.54 (1.82). IR (MeCN, cm^{-1}): ν_{CN} = 2130; ν_{CO} = 1903.

[K(18-crown-6)]$_2$[Fe(CO)$_3$(CNBPh$_3$)$_2$], [K(18-c-6)]$_2$[3.1(BPh$_3$)$_2$]. The synthesis of [K(18-c-6)]$_2$[**3.1**(BPh$_3$)$_2$] was performed by similar methods for [K(18-c-6)]$_2$[**3.1**(BAr$^F_3$)$_2$] with 50 mg of [K(18-c-6)]$_2$[**3.1**] (0.063 mmol) and 30 mg of BPh_3 (0.13 mmol) to give 68 mg of product (85 % yield). IR (MeCN, cm^{-1}): ν_{CN} = 2132; ν_{CO} = 1888.

K(18-crown-6)[HFe(CO)$_3$(CNBAr$^F_3$)$_2$], K(18-c-6)[H3.1(BAr$^F_3$)$_2$]. A solution of K(18-c-6)[H**3.1**] (460 mg, 0.928 mmol) in CH_2Cl_2 (20 mL) was treated dropwise with a solution of BAr^F_3 (940 mg, 1.80 mmol) in CH_2Cl_2 (10 mL), and the reaction solution was stirred for 1 hour. Evaporation of the solvent resulted in a light yellow oil, which was extracted into Et_2O (20 mL) the solution was passed through a small plug of Celite. The solvent was evaporated to yield a light yellow solid which was washed with pentane (20 mL) and dried at reduced pressure overnight. The solid product can be crystallized by extraction into CH_2Cl_2 (10 mL) and layering with Et_2O (10 mL) and hexanes (20 mL) and cooling to –30 ºC for 3 days. Yield 1.27 g (83%). Anal. Calc. for $C_{53}B_2FeH_{25}O_9N_2KF_{30}$ (Found): C, 46.18 (46.16); H, 1.83 (1.81); N, 2.04 (2.17). IR (CH_2Cl_2, cm^{-1}): ν_{CN} = 2218, 2205; ν_{CO} = 2109, 2061. ^{1}H NMR (CD_2Cl_2): δ –7.85 (s Fe-*H*); –8.11 (s Fe-*H*); –10.2 (s Fe-*H*).

K(18-crown-6)[HFe(CO)$_3$(CNBPh$_3$)$_2$], K(18-c-6)[H3.1(BPh$_3$)$_2$]. The synthesis of K(18-c-6)[H**3.1**(BPh$_3$)$_2$] was performed by similar methods for K(18-c-6)[H**3.1**(BAr$^F_3$)$_2$] with 50 mg of K(18-c-6)[H**3.1**] (0.10 mmol) and 49 mg of BPh_3 (0.20 mmol) to give 83 mg of product (84 % yield). IR (CH_2Cl_2, cm^{-1}): ν_{CN} = 2215, 2193; ν_{CO} = 2103, 2050. ^{1}H NMR (CD_2Cl_2): δ –7.37 (Fe-H); –7.71 (Fe-H); –10.28 (Fe-H).

K(18-crown-6)[HFe(CO)$_3$(CNB(OPh)$_3$)$_2$], K(18-c-6)[H3.1(B(OPh$_3$)$_2$]. The synthesis of K(18-c-6)[H**3.1**(B(OPh$_3$)$_2$] was performed by similar methods for K(18-c-6)[H**3.1**(BAr$^F{}_3$)$_2$] with 50 mg of K(18-c-6)[H**3.1**] (0.10 mmol) and 59 mg of B(OPh)$_3$ (0.20 mmol) to give 97 mg of product (87 % yield). IR (CH_2Cl_2, cm^{-1}): ν_{CN} = 2124, 2111; ν_{CO} = 2081, 2023. ^{1}H NMR (CD_2Cl_2): δ –7.77 (Fe-H); –8.19 (Fe-H); –11.03 (Fe-H).

Reaction of K(18-c-6)[H3.1(BAr$^F{}_3$)$_2$] with Ni(pdt)(dppe). A solution of K(18-c-6)[H**3.1**(BAr$^F{}_3$)$_2$] (50 mg, 0.033 mmol) in 10 mL of CH_2Cl_2 was added to a solution of Ni(pdt)(dppe) (19 mg, 0.033 mmol) in CH_2Cl_2 (5 mL). The initial IR spectrum showed the formation of [K(18-c-6)]$_2$[**3.1**(BAr$^F{}_3$)$_2$]. The reaction was allowed to stir for 5 hours at which point the solvent was removed. ^{1}H NMR (CD_2Cl_2): δ –8.80, –8.90 (AB quart, $^2J_{HP}$ = 46 Hz); –11.50 (t, $^2J_{HP}$ = 48 Hz).

Reaction of K(18-c-6)[H3.1(BPh$_3$)$_2$] with Ni(pdt)(dppe). A solution of K(18-c-6)[H**3.1**(BPh$_3$)$_2$] (20 mg, 0.020 mmol) in 3 mL of CH_2Cl_2 was treated with a solution of Ni(pdt)(dppe) (11.5 mg, 0.020 mmol) in 1 mL of CH_2Cl_2. After stirring for 5 hours, the solvent was removed under vacuum. The resulting solid was extracted with THF and the mixture was filtered through Celite. The filtrate was concentrated and loaded onto a column of neutral alumina (Brockmann Level IV) and eluted with THF. The first fraction was collected and dried under vacuum and washed with Et_2O yielding a crude sample of (CO)$_2$(CNBPh$_3$)Fe(H)Ni(dppe). IR (CH_2Cl_2, cm^{-1}): ν_{CN} = 2167; ν_{CO} = 2026, 1973. ^{1}H NMR (CD_2Cl_2): δ –6.72 (t, $^2J_{HP}$ = 5.5 Hz). ^{31}P NMR (CD_2Cl_2): δ 68.5 (s).

Reaction of K(18-c-6)[H3.1(BPh$_3$)$_2$] with Ni(pdt)(dcpe). A CH_2Cl_2 solution (3 mL) of K(18-c-6)[H**3.1**(BPh$_3$)$_2$] (30 mg, 0.030 mmol) was treated with Ni(pdt)(dcpe) (18 mg, 0.030 mmol) dissolved in CH_2Cl_2 (1 mL). The mixture was allowed to stir for 8 hours at which point the solvent was removed under vacuum. The solid was extracted with THF, filtered through Celite, and the filtrate was concentrated and loaded onto a neutral alumina column (Brockmann Level IV). The column was eluted with THF and the first band was collected and dried to give a crude sample of (CO)$_2$(CNBPh$_3$)Fe(H)Ni(dcpe). IR (CH_2Cl_2, cm^{-1}): ν_{CN} = 2167; ν_{CO} = 2019, 1965. ^{1}H NMR (CD_2Cl_2): δ –6.28 (t, $^2J_{HP}$ = 3.3 Hz). ^{31}P NMR (CD_2Cl_2): δ 86.1 (s).

[K(18-c-6)][HFe(CO)(CNBAr$^F{}_3$)$_2$(dppe)], [K(18-c-6)][H3.2(BAr$^F{}_3$)$_2$]. A MeCN solution (5 mL) of [K(18-c-6)][H**3.1**] (50 mg, 0.10 mmol) was treated with dppe (40 mg, 0.10 mmol) resulting in a yellow solution. The solvent was removed under vacuum. The solid was extracted into CH_2Cl_2, and the mixture was layered with

pentane, and placed in a –30 °C freezer. This procedure yielded a yellow solid (31 mg, 37%). IR (CH_2Cl_2, cm^{-1}): ν_{CN} = 2091, 2079; ν_{CO} = 1927.

Samples of [K(18-c-6)][H**3.2**] (10 mg, 0.012 mmol) and $BAr^F{}_3$ (12 mg, 0.024 mmol) were dissolved in 1 mL CD_2Cl_2. ^{1}H NMR (CD_2Cl_2): δ –7.99 (t, $^2J_{HP}$ = 54 Hz); –8.30 (t, $^2J_{HP}$ = 54 Hz); –8.80, –8.90 (AB quart, $^2J_{HP}$ = 46 Hz); –11.50 (t, $^2J_{HP}$ = 48 Hz); –12.02, –12.14 (AB quart, $^2J_{HP}$ = 46 Hz).

3.9 References

(1) Ohki, Y.; Tatsumi, K. "Thiolate-Bridged Iron-Nickel Models for the Active Site of [NiFe] Hydrogenase" *Eur. J. Inorg. Chem.* **2011**, 973.

(2) Kaur-Ghumaan, S.; Stein, M. "[NiFe] Hydrogenases: How Close do Structural and Functional Mimics Approach the Active Site?" *Dalton Trans.* **2014**, *43*, 9392.

(3) Barton, B. E.; Rauchfuss, T. B. "Hydride-Containing Models for the Active Site of the Nickel-Iron Hydrogenases" *J. Am. Chem. Soc.* **2010**, *132*, 14877.

(4) Carroll, M. E.; Barton, B. E.; Gray, D. L.; Mack, A. E.; Rauchfuss, T. B. "Active-Site Models for the Nickel-Iron Hydrogenases: Effects of Ligands on Reactivity and Catalytic Properties" *Inorg. Chem.* **2011**, *50*, 9554.

(5) Ogata, H.; Lubitz, W.; Higuchi, Y. "[NiFe] Hydrogenases: Structural and Spectroscopic Studies of the Reaction Mechanism" *Dalton Trans.* **2009**, 7577.

(6) Rauchfuss, T. B.; Contakes, S. M.; Hsu, S. C. N.; Reynolds, M. A.; Wilson, S. R. "The Influence of Cyanide on the Carbonylation of Iron(II): Synthesis of Fe-SR-CN-CO Centers Related to the Hydrogenase Active Sites" *J. Am. Chem. Soc.* **2001**, *123*, 6933.

(7) Liaw, W. F.; Lee, J. H.; Gau, H. B.; Chen, C. H.; Jung, S. J.; Hung, C. H.; Chen, W. Y.; Hu, C. H.; Lee, G. H. "Six-Coordinate and Five-Coordinate $Fe^{II}(CN)_2(CO)_x$ Thiolate Complexes (x=1, 2): Synthetic Advances for Iron Sites of [NiFe]-Hydrogenases" *J. Am. Chem. Soc.* **2002**, *124*, 1680.

(8) Coffey, C. E. "Synthesis and Alkylation of $[Fe(CN)_2(C_5H_5)(CO)]^-$, $[Mo(CN)_2(C_5H_5)(CO)]^{2-}$, $[W(CN)_2(C_2H_5)(CO)]^{2-}$ and $[W(CN)(C_5H_5)(CO)_3]^-$" *J. Inorg. Nucl. Chem.* **1963**, *25*, 179.

(9) Kayal, A.; Rauchfuss, T. B. "Protonation Studies of the New Iron Carbonyl Cyanide *trans*-$[Fe(CO)_3(CN)_2]^{2-}$: Implications with Respect to Hydrogenases" *Inorg. Chem.* **2003**, *42*, 5046.

(10) Whaley, C. M.; Rauchfuss, T. B.; Wilson, S. R. "Coordination Chemistry of $[HFe(CN)_2(CO)_3]^-$ and Its Derivatives: Toward a Model for the Iron Subsite of the [NiFe]-Hydrogenases" *Inorg. Chem.* **2009**, *48*, 4462.

(11) Li, Z. L.; Ohki, Y.; Tatsumi, K. "Dithlolato-Bridged Dinuclear Iron-Nickel complexes $[Fe(CO)_2(CN)_2(\mu\text{-}SCH_2CH_2CH_2S)Ni(S_2CNR_2)]^-$ - Modeling the Active Site of [NiFe]- Hydrogenase" *J. Am. Chem. Soc.* **2005**, *127*, 8950.

(12) Jiang, J.; Maruani, M.; Solaimanzadeh, J.; Lo, W.; Koch, S. A.; Millar, M. "Synthesis and Structure of Analogues for the Ni-Fe Site in Hydrogenase Enzymes" *Inorg. Chem.* **2009**, *48*, 6359.

(13) Tanino, S.; Li, Z. L.; Ohki, Y.; Tatsumi, K. "A Dithiolate-Bridged $(CN)_2(CO)$Fe-Ni Complex Reproducing the IR Bands of [NiFe]-Hydrogenase" *Inorg. Chem.* **2009**, *48*, 2358.

(14) Darensbourg, D. J.; Reibenspies, J. H.; Lai, C. H.; Lee, W. Z.; Darensbourg, M. Y. "Analysis of an Organometallic Iron Site Model for the Heterodimetallic Unit of [NiFe]-Hydrogenase" *J. Am. Chem. Soc.* **1997**, *119*, 7903.

(15) Kamali, S.; Wang, H. X.; Mitra, D.; Ogata, H.; Lubitz, W.; Manor, B. C.; Rauchfuss, T. B.; Byrne, D.; Bonnefoy, V.; Jenney, F. E.; Adams, M. W. W.; Yoda, Y.; Alp, E.; Zhao, J. Y.; Cramer, S. P. "Observation of the Fe-CN and Fe-CO Vibrations in the Active Site of [NiFe]-Hydrogenase by Nuclear Resonance Vibrational Spectroscopy" *Angew. Chem. Int. Ed.* **2013**, *52*, 724.

(16) Schilter, D.; Nilges, M. J.; Chakrabarti, M.; Lindahl, P. A.; Rauchfuss, T. B.; Stein, M. "Mixed-Valence Nickel-Iron Dithiolate Models of the [NiFe]-Hydrogenase Active Site" *Inorg. Chem.* **2012**, *51*, 2338.

(17) Shriver, D. F.; Posner, J. "Bridge Addition Compounds .3. Influence of Boron-Containing Lewis Acids on Electronic Spectra Vibrational Spectra and Oxidation Potentials of Some Iron-Cynanide Complexes" *J. Am. Chem. Soc.* **1966**, *88*, 1672.

(18) Kristoff, J. S.; Shriver, D. F. "Metal-Complexes as Probes of Donor-Acceptor Interaction - Vibrational-Spectra of $(\pi\text{-}C_5H_5)Fe(CO)_2(CNMX_3)$ (M=B, X=H, F, Cl, Br, OR CH_3; M=Al OR Ga, X=Cl or CH_3)" *Inorg. Chem.* **1973**, *12*, 1788.

(19) Brookhart, M.; Grant, B.; Volpe, A. F. "$[(3,5\text{-}(CF_3)_2C_6H_3)_4B]^-[H(OEt_2)_2]^+$: A Convenient Reagent for Generation and Stabilization of Cationic, Highly Electrophilic Organometallic Complexes" *Organometallics* **1992**, *11*, 3920.

(20) Sivaev, I. B.; Bregadze, V. I. "Lewis Acidity of Boron Compounds" *Coord. Chem. Rev.* **2014**, *270*, 75.

(21) Barton, B. E.; Whaley, C. M.; Rauchfuss, T. B.; Gray, D. L. "Nickel-Iron Dithiolato Hydrides Relevant to the [NiFe]-Hydrogenase Active Site" *J. Am. Chem. Soc.* **2009**, *131*, 6942.

(22) Giandomenico, C. M.; Dewan, J. C.; Lippard, S. J. "Synthesis, Structure, and Reactions of $[Mo(SnCl_3)(CN\text{-}t\text{-}Bu)_6][(Ph_3B)_2CN]$, Containing a Potentially Useful New Anioin for Crystallizations" *J. Am. Chem. Soc.* **1981**, *103*, 1407.

(23) Britovsek, G. J. P.; Ugolotti, J.; White, A. J. P. ″From $B(C_6F_5)_3$ to $B(OC_6F_5)_3$: Synthesis of $(C_6F_5)_2BOC_6F_5$ and $C_6F_5B(OC_6F_5)_2$ and Their Relative Lewis Acidity″ *Organometallics* **2005**, *24*, 1685.

(24) Izutsu, K. "Acid–Base Reactions in Nonaqueous Solvents" In *Electrochemistry in Nonaqueous Solutions*; Wiley-VCH: 2009, p 63.

(25) Kutt, A.; Rodima, T.; Saame, J.; Raamat, E.; Maemets, V.; Kaljurand, I.; Koppel, I. A.; Garlyauskayte, R. Y.; Yagupolskii, Y. L.; Yagupolskii, L. M.; Bernhardt, E.; Willner, H.; Leito, I. ″Equilibrium Acidities of Superacids″ *J. Org. Chem.* **2011**, *76*, 391.

(26) Kaljurand, I.; Kutt, A.; Soovali, L.; Rodima, T.; Maemets, V.; Leito, I.; Koppel, I. A. ″Extension of the Self-Consistent Spectrophotometric Basicity Scale in Acetonitrile to a Full Span of 28 pK_a units: Unification of Different Basicity Scales″ *J. Org. Chem.* **2005**, *70*, 1019.

(27) Kutt, A.; Leito, I.; Kaljurand, I.; Soovali, L.; Vlasov, V. M.; Yagupolskii, L. M.; Koppel, I. A. ″A Comprehensive Self-Consistent Spectrophotometric Acidity Scale of Neutral Bronsted Acids in Acetonitrile″ *J. Org. Chem.* **2006**, *71*, 2829.

(28) Sowa, J. R.; Zanotti, V.; Facchin, G.; Angelici, R. J. ″Calorimetric Studies of the Heats of Protonation of the Metal in $Fe(CO)_3$(Bidentate Phosphine, Arsine) Complexes - Effects of Chelate Ligands on Metal Basicity″ *J. Am. Chem. Soc.* **1992**, *114*, 160.

(29) Abel, E. W.; Gerrard, W.; Lappert, M. F. ″Preparation of Esters of Diphenylboronous Acid″ *J. Chem. Soc.* **1957**, 112.

(30) Reynard, K. E.; Sherman, R. E.; Smith, H. D.; Hohnstedt, L. F.; Gassenheimer, G.; Wartik, T. ″Trimethylammonium Tetraphenylborate: (A Ready Source of Triphenylborane)″ *Inorg. Synth.* **2007**, 52.

Chapter 4

Synthesis and Characterization of Boro-Cyanide [NiFe]-Hydrogenase Models

4.1 Introduction

As discussed in Chapter 3, attempts to form functional [NiFe]-H_2ase models with two cyanide ligands from Lewis acid adducts of $[HFe(CO)_3(CN)_2]^-$ resulted in NiFe hydrides containing one $CNBR_3^-$ ligand. Another route for the formation of functional dicyanide [NiFe]-H_2ase models could be derived from the modification of reported bimetallic [NiFe]-H_2ase models. A series of biomimetic models developed by Jiang and Tatsumi are characterized by a Fe center coordinated by both CO and CN^- ligands as well as a bridging Ni dithiolate (Figure 4.1).[1,2]

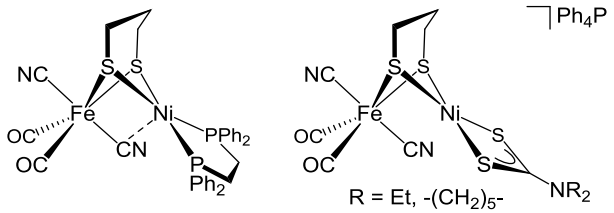


Figure 4.1. Select models of bimetallic [NiFe]-H_2ase models with cyanide ligands.

The Ni and Fe centers of both models are in the biologically relevant 2+ oxidation state with biologically relevant ligands on Fe. The models are coordinatively saturated resembling the CO-inhibited state as the Fe centers are ligated by two CO and two CN^- ligands.[3] As a result of these coordinatively saturated Fe sites, neither model possesses biologically relevant reactivity. Removal of a carbonyl ligand may lead to biomimetic reactivity.

A method of forming more labile Fe-CO bonds may be found in the structure of the [NiFe]-H_2ase active site. The active site of [NiFe]-H_2ase contains hydrogen bonding from surrounding amino acids to the cyanide ligands (Figure 4.2).[4] In active site in *D. fructosovorans*, cyanide forms hydrogen-bonds with Ser499 (N···N, N···O = 2.98, 2.88 Å respectively) and Arg476 (N···N = 2.87, 3.25 Å). Mutations of these amino acids did not alter the catalytic activity,[5] suggesting the cyanide cofactors could be modified in [NiFe]-H_2ase models.

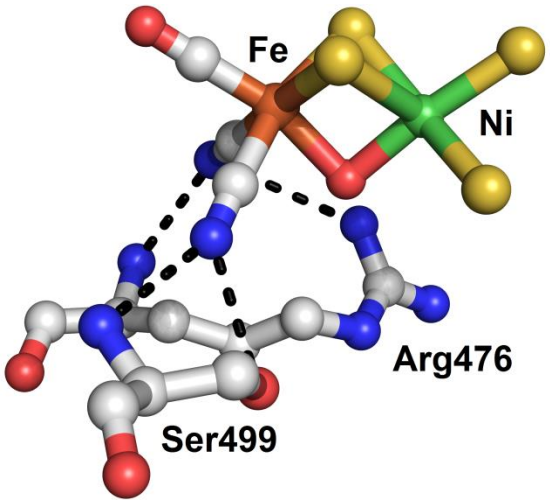


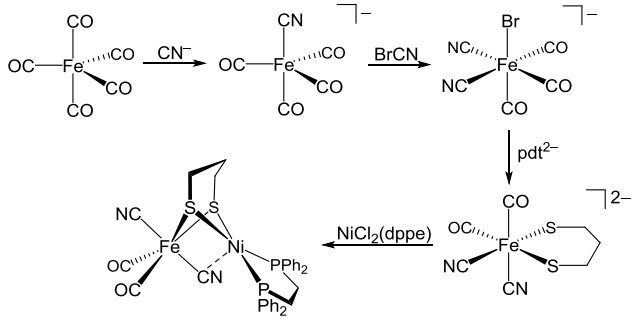
Figure 4.2. Crystal structure of the Ni-B state of [NiFe]-H_2ase from *D. fructosovorans* with hydrogen-bonding interactions (PDB: 1YRQ).[4]

Modeling of the hydrogen bonding environment for H_2ase models has been successful for the coordination of triarylboranes to the cyanides of the [FeFe]-H_2ase model $[Fe_2(pdt)(CO)_4(CN)_2]^{2-}$.[6] Coordination of boranes blocked undesired reactivity at the Lewis basic nitrogen of cyanide. Additionally the coordination of the boranes shifted the ν_{CO} bands for $[Fe_2(pdt)(CO)_4(CN)_2]^{2-}$ to higher energies. This suggests the carbonyl ligands may become more labile upon coordination of boranes, forming an unsaturated Fe center.

4.2 Synthesis and Reactivity of $(CO)_2(CN)_2$Fe(pdt)Ni(dxpe)

Given the thermal stability, attempts to form a more reactive [NiFe]-H_2ase model were explored using $(CO)_2(CN)_2$Fe(pdt)Ni(dppe) (**4.1**). The compound **4.1** has been previously synthesized by the reaction of $[IFe(CO)_3(CN)_2]^-$ and pdt^{2-} to form $[Fe(pdt)(CO)_2(CN)_2]^{2-}$. Treatment of $[Fe(pdt)(CO)_2(CN)_2]^{2-}$ with $NiCl_2$(dppe) formed **4.1**.[1] A new route was developed using the more readily obtained $[BrFe(CO)_3(CN)_2]^-$ in place of $[IFe(CO)_3(CN)_2]^-$ (Scheme 4.1). The synthesis of $[IFe(CO)_3(CN)_2]^-$ is reported form the addition of two equivalents of CN^- to the light-sensitive compound $[I_3Fe(CO)_3]^-$.[7] Treatment of $[Fe(CO)_4(CN)]^-$ with BrCN readily formed $[BrFe(CO)_3(CN)_2]^-$.[8]

Scheme 4.1. Synthesis of $(CO)_2(CN)_2Fe(pdt)Ni(dppe)$, **4.1**.



Only the *cis*-CO/*trans*-CN isomer of **4.1** is observed in with IR signals of ν_{CN} = 2110, 2081 cm^{-1} and ν_{CO} = 2053, 2005 cm^{-1} consistent with previous reports.[1] The geometry is further confirmed by the observation of a singlet in the ^{31}P NMR spectrum at δ 56.9 indicating the phosphines of dppe are symmetry related.

The high energy ν_{CO} of **4.1** suggested that a carbonyl ligand may be subject to decarbonylation, although attempts were unsuccessful. Treatment of **4.1** with the decarbonylating agent Me_3NO resulted in no reaction. An alternative method for decarbonylation was attempted by irradiation with UV light. Irradiation of THF solutions of **4.1** with UV light resulted in the loss of starting material as indicated by IR spectroscopy (Figure 4.3). An insoluble precipitate formed over time. Decomposition of **4.1** is thought to occur by formation of Fe-CN-M (M = Fe, Ni) linkages.

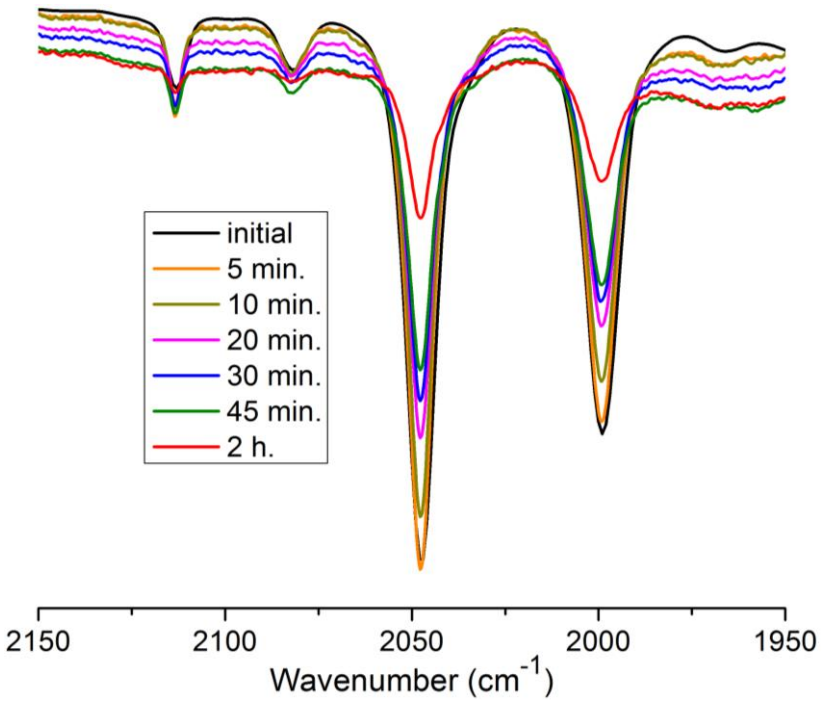
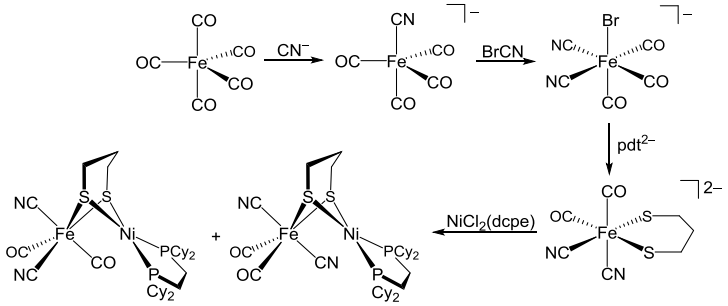


Figure 4.3. IR spectra of the irradiation of THF solutions of *cis*-CO/*trans*-CN **4.1**$(BAr^F{}_3)_2$ by UV light overtime.

In order to probe the effects of ligands on Ni, the related species $(CO)_2(CN)_2Fe(pdt)Ni(dcpe)$ (**4.2**) was synthesized by the reaction of $[BrFe(CO)_2(CN)_2]^-$ with pdt^{2-} followed by the addition of $NiCl_2(dcpe)$. Unlike **4.1** where only the *cis*-CO/*trans*-CN isomer is observed, both the *cis*-CO/*trans*-CN and *cis*-CO/*cis*-CN isomers of **4.2** were present in solution as identified by IR and ^{31}P spectroscopy (Scheme 4.2).

Scheme 4.2. Synthesis of $(CO)_2(CN)_2Fe(pdt)Ni(dcpe)$, **4.2**.



The *cis*-CO/*trans*-CN isomer of **4.2** has a similar IR pattern as the *cis*-CO/*trans*-CN isomer of **4.1** but with lower ν_{CO} bands (ν_{CN} = 2113, 2090 cm^{-1} and ν_{CO} = 2045, 1995 cm^{-1}). The *cis*-CO/*cis*-CN isomer of **4.2** was also observed by

IR with ν_{CN} = 2120 cm^{-1} and ν_{CO} = 2033, 1982 cm^{-1} (Figure 4.4). A second ν_{CN} for the *cis*-CO/*cis*-CN isomer is expected but is likely masked by the ν_{CN} bands of the *cis*-CO/*trans*-CN isomer.

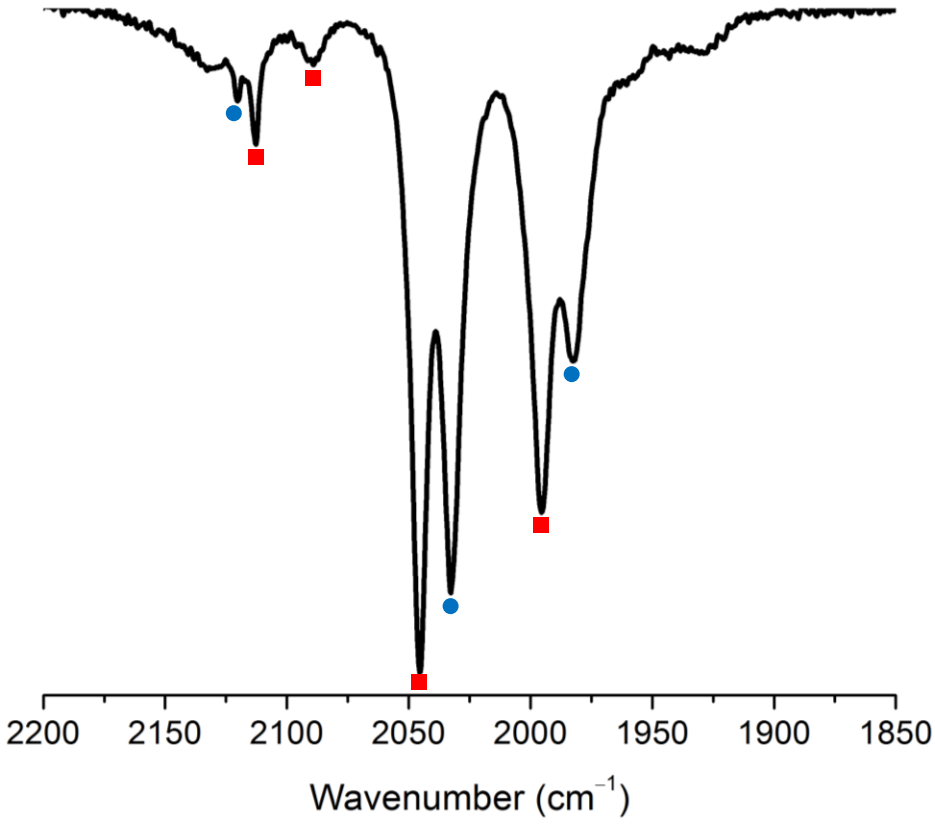


Figure 4.4. IR spectrum of the *cis*-CO/*trans*-CN (■) and *cis*-CO/*cis*-CN isomers (●) of **4.2** in CH_2Cl_2.

The presence of both isomers of **4.2** is confirmed by ^{31}P NMR. The *cis*-CO/*trans*-CN isomer was assigned to a singlet at δ 66.3. The asymmetry of the *cis*-CO/*cis*-CN isomer of **4.2** was identified by an AB quartet at δ 67.8, δ 66.5 ($^2J_{PP}$ = 33 Hz) (Figure 4.5). As with **4.1**, attempts to decarbonylate **4.2** were not successfully. Treatment of **4.2** with Me_3NO produced no change. Exposure of **4.2** to ambient light was found to decompose to Ni(pdt)(dcpe) as determined by ^{31}P NMR spectroscopy.

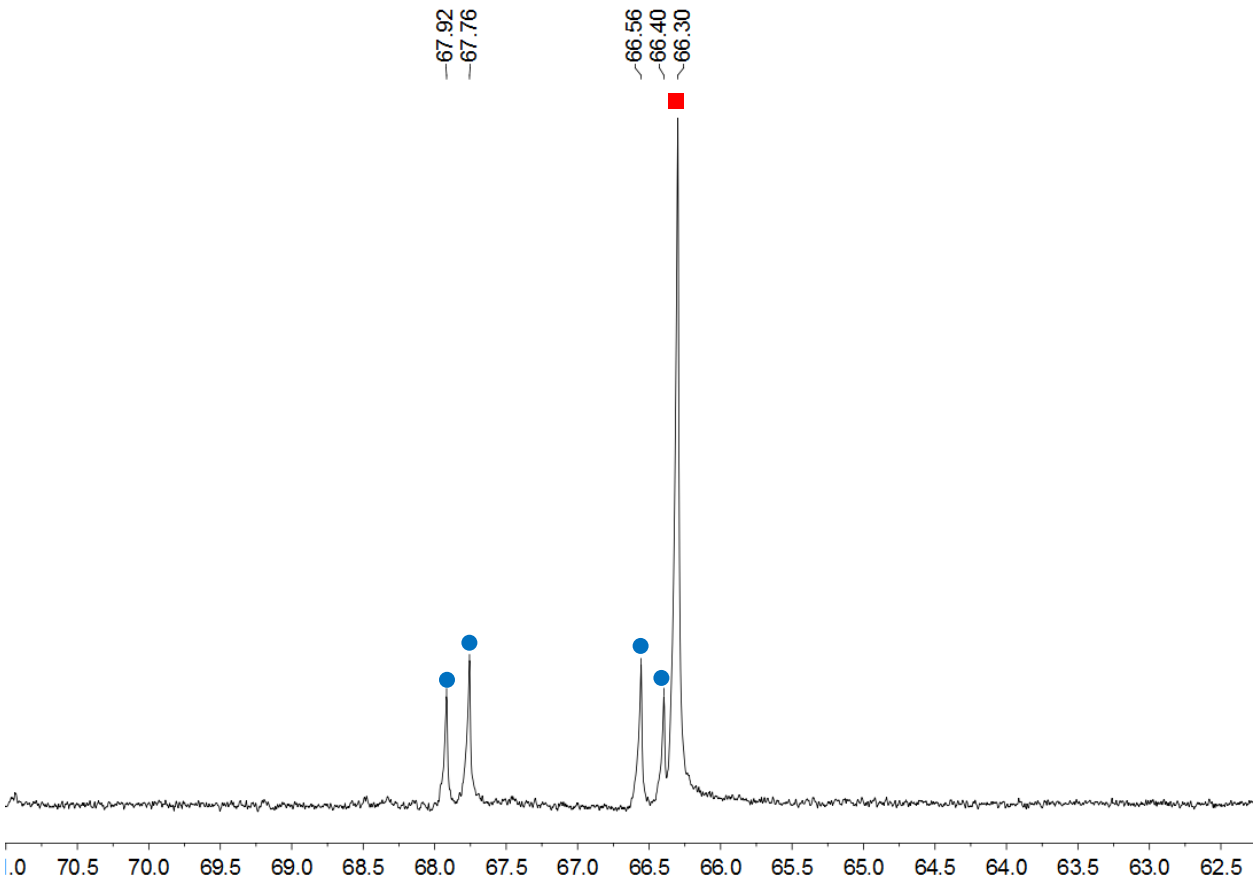


Figure 4.5. ^{31}P NMR spectrum of *cis*-CO/*trans*-CN (■) and *cis*-CO/*cis*-CN (●) isomers of **4.2** in CD_2Cl_2.

4.3 Lewis Acid Adducts of $(CO)_2(CN)_2$Fe(pdt)Ni(dxpe)

The addition of two equivalents of the Lewis acid $B(C_6F_5)_3$ (BAr^F_3) to **4.1** formed the 2:1 adduct $(CO)_2(CNBAr^F_3)_2$Fe(pdt)Ni(dppe) (**4.1**$(BAr^F_3)_2$). Upon addition of BAr^F_3, the solution lightened in color and large ν_{CN} and ν_{CO} shifts to higher energy was observed (85 and 40 cm^{-1} respectively). The IR spectrum of **4.1**$(BAr^F_3)_2$ displayed a similar pattern as **4.1**, suggesting retention of the *cis*-CO/*trans*-CN geometry. Indeed the ^{31}P and ^{19}F NMR spectra of **4.1**$(BAr^F_3)_2$ confirmed retention of the *cis*-CO/*trans*-CN arrangement. A singlet in the ^{31}P NMR spectrum at δ 56.4 indicated the phosphines of dppe are symmetry related. The ^{19}F NMR spectrum displays two inequivalent BAr^F_3 environments of equal intensity indicated the two $CNBAr^F_3{}^-$ ligands are unrelated by symmetry.

Addition of two equivalents of BAr^F_3 to **4.2** formed the 2:1 adduct $(CO)_2(CNBAr^F_3)_2$Fe(pdt)Ni(dcpe) (**4.2**$(BAr^F_3)_2$) as a mixture of the *cis*-CO/*trans*-CN and *cis*-CO/*cis*-CN isomers. As for **4.1**$(BAr^F_3)_2$, the IR spectrum of **4.2**$(BAr^F_3)_2$ shifted to higher energies compared to **4.2** ($\Delta\nu_{CN}$ = 60-90 cm^{-1}; $\Delta\nu_{CO}$ = 35-50 cm^{-1}). The use of ^{31}P

and ^{19}F NMR of **4.2**$(BAr^{F}_{3})_2$ also confirmed the geometry of the isomers. The *cis*-CO/*trans*-CN **4.2**$(BAr^{F}_{3})_2$ could be identified in the ^{31}P NMR by a singlet at δ 69.8 while the *cis*-CO/*cis*-CN isomer was identified by an AB quartet (δ 70.2, δ 69.5, $^{2}J_{PP}$ = 30 Hz). The ^{19}F NMR spectrum of **4.2**$(BAr^{F}_{3})_2$ displayed two sets of inequivalent BAr^{F}_{3} signals consistent with the presence of two different isomers with chemically inequivalent BAr^{F}_{3}'s. Overtime, the *cis*-CO/*cis*-CN isomer of **4.2**$(BAr^{F}_{3})_2$ converted to the *cis*-CO/*trans*-CN isomer.

The use of weaker Lewis acids were also probed for their ability to form adducts with **4.1**. Use of two equivalents of $BAr^{F\#}_{3}$ readily formed **4.1**$(BAr^{F\#}_{3})_2$. The IR spectrum of **4.1**$(BAr^{F\#}_{3})_2$ (ν_{CN} = 2197, 2168 cm^{-1}; ν_{CO} = 2086, 2046 cm^{-1}) is similar to that for other *cis*-CO/*trans*-CN isomers. The NMR spectra of **4.1**$(BAr^{F\#}_{3})_2$ is expected for the *cis*-CO/*trans*-CN isomer with a singlet in the ^{31}P NMR (δ 58.4) and two inequivalent $BAr^{F\#}_{3}$ environments by ^{1}H and ^{19}F NMR. The addition of the excess amounts of the weak Lewis acid BPh_3 to **4.1** was required to form the 2:1 adduct **4.1**$(BPh_3)_2$ as indicated by IR spectroscopy (ν_{CN} = 2186, 2141 cm^{-1}; ν_{CO} = 2076, 2035 cm^{-1}). Attempts to isolate **4.1**$(BPh_3)_2$ by crystallization resulted in mixtures the 2:1 adducts by and another species by IR spectroscopy (ν_{CO} = 2065, 2020 cm^{-1}) which is speculated to be the 1:1 adduct.

4.4 Structural Determination of $(CO)_2(CNBAr^{F}_{3})_2Fe(pdt)Ni(dppe)$

Crystals suitable for X-ray diffraction of *cis*-CO/*trans*-CN **4.1**$(BAr^{F}_{3})_2$ were grown from THF and pentane (Figure 4.6). The coordination of BAr^{F}_{3} had a considerable effect on the structure of **4.1**$(BAr^{F}_{3})_2$ (Table 4.1). The Ni-Fe distance of *cis*-CO/*trans*-CN **4.1**$(BAr^{F}_{3})_2$ (3.218 Å) was much longer than previously observed in **4.1** (2.809 Å).[1] This increase is attributed to the steric bulk of the BAr^{F}_{3} groups. Similarly the Ni-S-Fe angles were found to increase from 75.98° in **4.1** to 86.60° in **4.1**$(BAr^{F}_{3})_2$. This increase in Ni-Fe distance and Ni-S-Fe angle resulted in the loss of the close Ni···μ-CN interaction present in **4.1**. The presence of the BAr^{F}_{3} groups slightly affected the diatomic ligands. The Fe-CO bonds of **4.1**$(BAr^{F}_{3})_2$ were slightly elongated (Δ_{avg} = 0.03 Å) consistent with a decrease in electron density on the Fe center. Additionally, slightly shorter Fe-CN bonds (Δ_{avg} = –0.03 Å) were also observed as expected for an increase of the π-accepting ability of $CNBAr^{F}_{3}{}^{-}$ ligands. The bulk of BAr^{F}_{3} distorted the Fe-C-N angle of the semi-bridging Fe-$CNBAr^{F}_{3}$ (166.37 °). Negligible differences were observed for Ni-P, C≡O, and C≡N distances (Δ ≈ 0.01 Å).

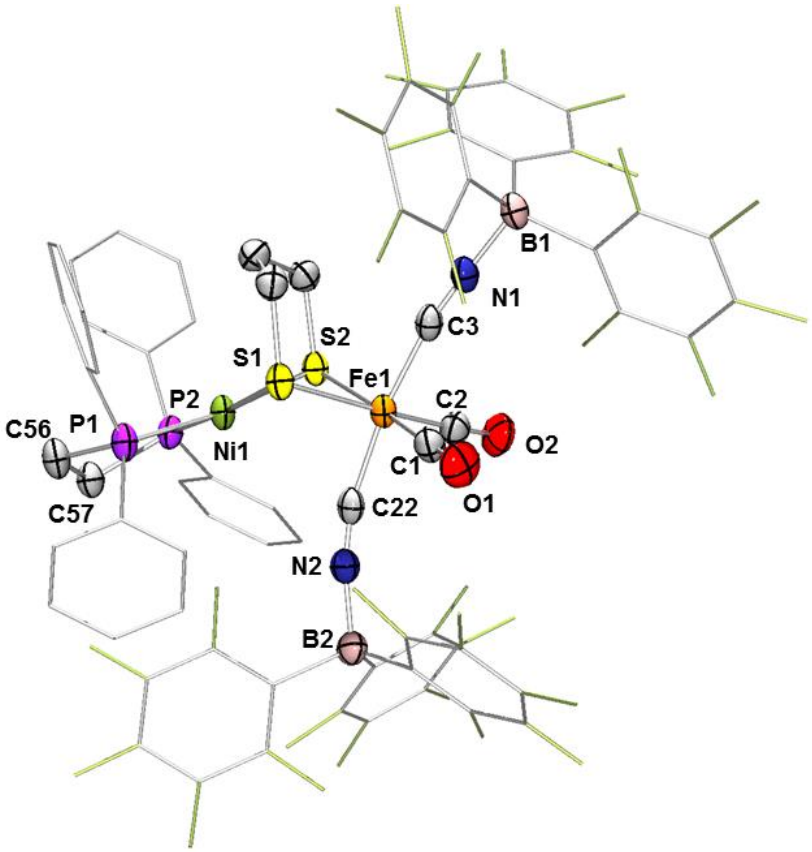


Figure 4.6. Thermal ellipsoid of *cis*-CO/*trans*-CN **4.1**$(BAr^F_3)_2$ at 50% probability. Phenyl rings and perfluoroaryl rings have been deemphasized for clarity. H atoms have been omitted for clarity.

Table 4.1. Selected distances (Å) and angles (°) of **4.1** and **4.1**$(BAr^F_3)_2$.

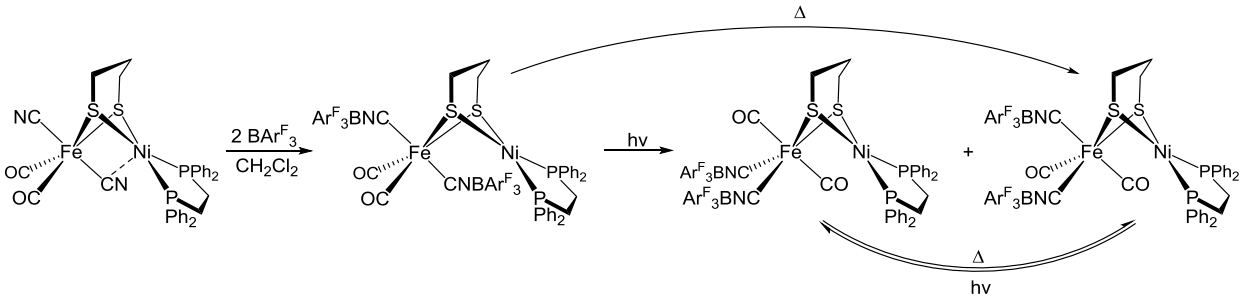
	4.1	**4.1$(BAr^F_3)_2$**
Fe···Ni	2.809	3.218
Ni···μ-CN	2.421	3.040
Fe–CO_{avg}	1.788	1.820
Fe–CN_{apical}	1.920	1.897
Fe–μ-CN_{apical}	1.968	1.924
C≡O_{avg}	1.134	1.129
C≡N_{avg}	1.151	1.156
Fe-S_{avg}	2.341	2.328
Ni-S_{avg}	2.220	2.234
Ni–P_{avg}	2.189	2.182
Fe–S–Ni_{avg}	75.98	86.60

4.5 Isomerization of $(CO)_2(CNBR_3)_2Fe(pdt)Ni(dxpe)$

The coordination of Lewis acids to **4.1** and **4.2** were found to stabilize the complexes. While irradiation of **4.1** or **4.2** resulted in decomposition, the Lewis acid adducts isomerized upon heating or irradiation with light.

$(CO)_2(CNBAr^F{}_3)_2Fe(pdt)Ni(dppe)$. Samples of *cis*-CO/*trans*-CN **4.1**$(BAr^F{}_3)_2$ isomerized to both the *trans*-CO/*cis*-CN isomer and the *cis*-CO/*cis*-CN isomer in a 4:1 ratio upon irradiation of UV light (Scheme 4.3). Upon standing in the absence of light for several days, the *trans*-CO/*cis*-CN isomer converted to the *cis*-CO/*cis*-CN isomer. The isomers can be readily identified from the ^{31}P and ^{19}F NMR spectra (Figure 4.7, 4.8). The *trans*-CO/*cis*-CN isomer of **4.1**$(BAr^F{}_3)_2$ was identified by a singlet in the ^{31}P NMR (δ 58.7) and a single set of $BAr^F{}_3$ signals by ^{19}F NMR (δ –135.2, δ –160.6, δ –166.5). The asymmetry of *cis*-CO/*cis*-CN **4.1**$(BAr^F{}_3)_2$ is apparent by an AB quartet in ^{31}P NMR (δ 58.9, δ 58.5, $^2J_{PP}$ = 37 Hz) and two inequivalent $BAr^F{}_3$ environments by ^{19}F NMR. The isomerization of **4.1**$(BAr^F{}_3)_2$ can also be monitored by IR spectroscopy (Figure 4.9). The IR spectrum of *trans*-CO/*cis*-CN **4.1**$(BAr^F{}_3)_2$ has two ν_{CN} bands (2215, 2201 cm^{-1}) with one weak ν_{CO} band at 2087 cm^{-1} and one strong ν_{CO} band at 2030 cm^{-1}. The IR spectrum of *cis*-CO/*cis*-CN **4.1**$(BAr^F{}_3)_2$ is identified by two ν_{CN} bands at 2214 and 2202 cm^{-1} and two ν_{CO} bands at 2070 and 2020 cm^{-1}.

Scheme 4.3. Formation and isomerization of **4.1**$(BAr^F{}_3)_2$.



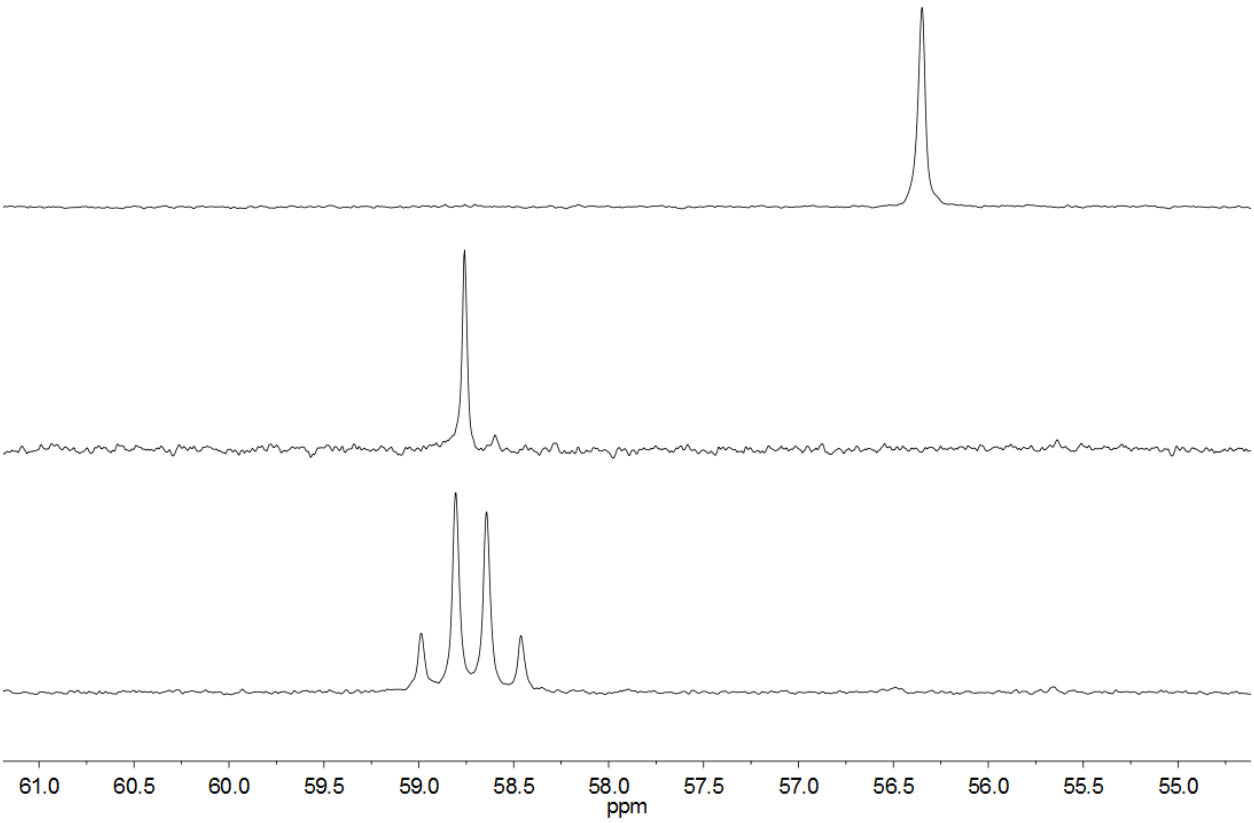


Figure 4.7. ^{31}P NMR of *cis*-CO/*trans*-CN **4.1**(BAr^F_3)$_2$ (top), *trans*-CO/*cis*-CN **4.1**(BAr^F_3)$_2$ (middle), and *cis*-CO/*cis*-CN **4.1**(BAr^F_3)$_2$ (bottom) in CD_2Cl_2.

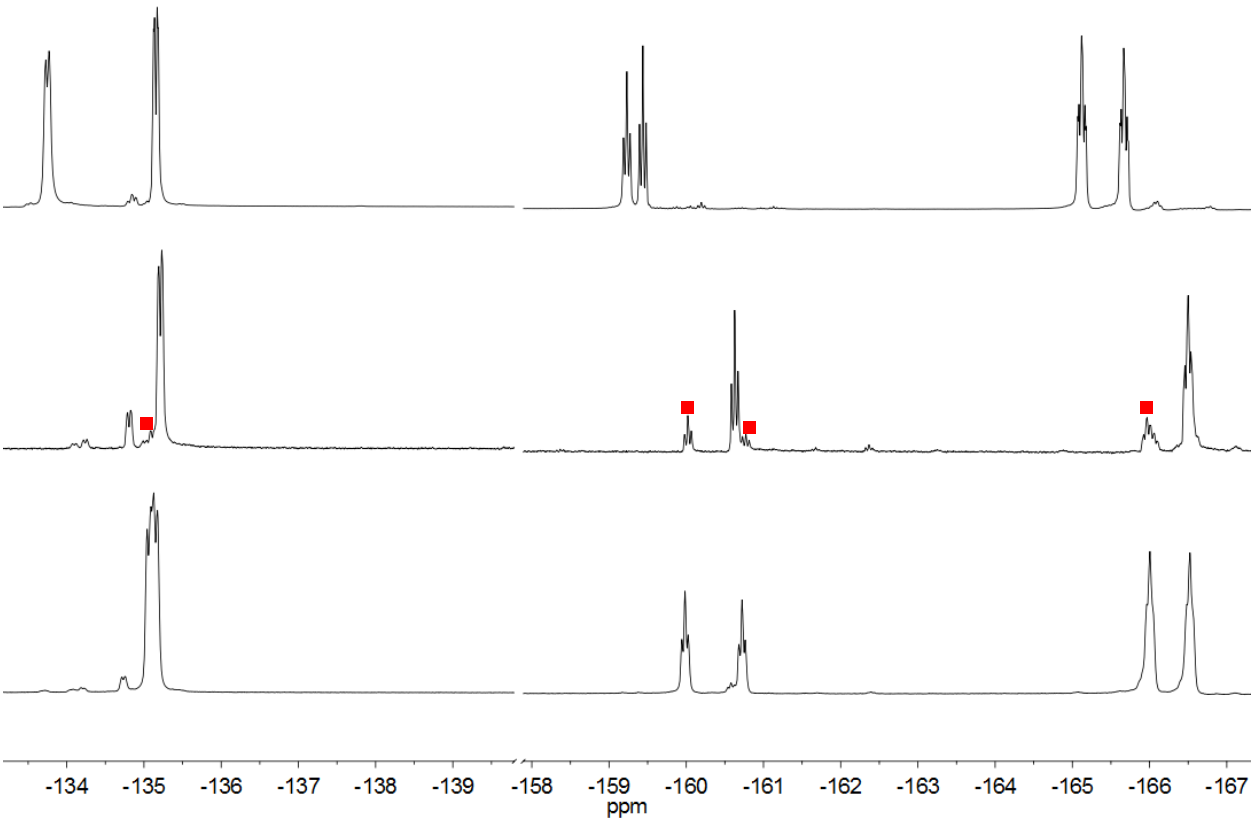


Figure 4.8. ^{19}F NMR of *cis*-CO/*trans*-CN **4.1**$(BAr^F{}_3)_2$ (top), *trans*-CO/*cis*-CN **4.1**$(BAr^F{}_3)_2$ (middle), and *cis*-CO/*cis*-CN **4.1**$(BAr^F{}_3)_2$ (bottom) in CD_2Cl_2. Trace amounts of *cis*-CO/*cis*-CN **4.1**$(BAr^F{}_3)_2$ (■).

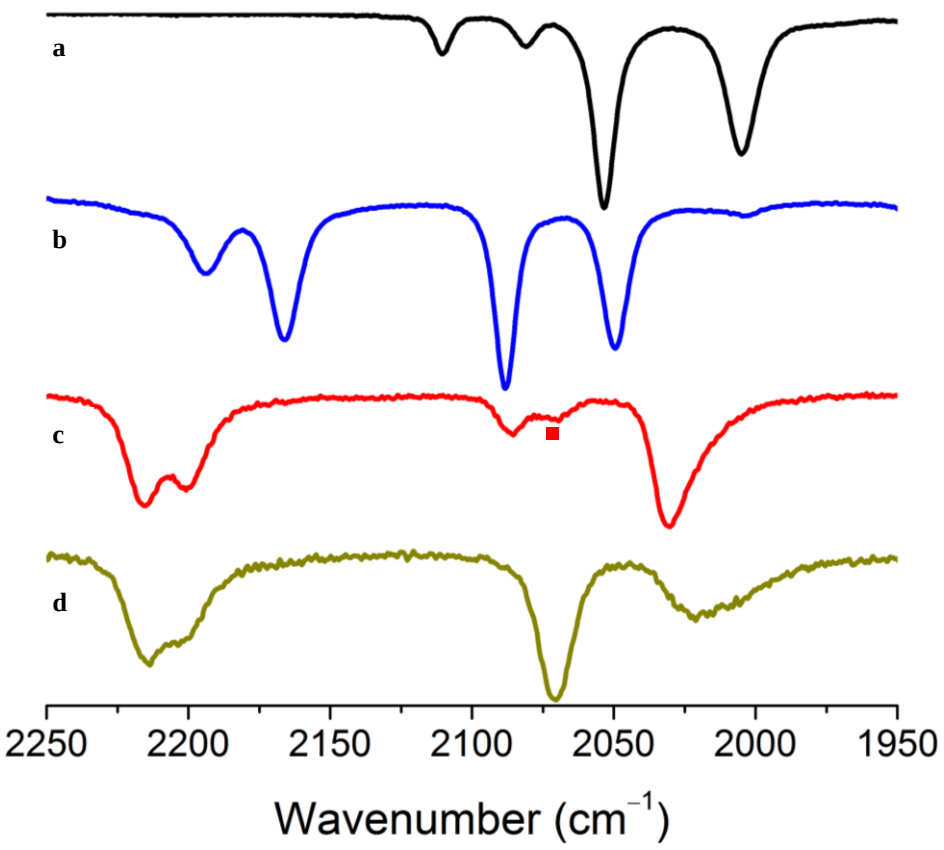


Figure 4.9. IR spectra of a) *cis*-CO/*trans*-CN **4.1**, b) *cis*-CO/*trans*-CN **4.1**$(BAr^F{}_3)_2$, c) *trans*-CO/*cis*-CN **4.1**$(BAr^F{}_3)_2$, d) and *cis*-CO/*cis*-CN **4.1**$(BAr^F{}_3)_2$. Trace amounts of *cis*-CO/*cis*-CN **4.1**$(BAr^F{}_3)_2$ (■).

Irradiation of samples of *cis*-CO/*cis*-CN **4.1**$(BAr^F{}_3)_2$ regenerated the *trans*-CO/*cis*-CN isomer. The *cis*-CO/*cis*-CN isomer also formed under thermal conditions. Heating of THF solutions of *cis*-CO/*trans*-CN **4.1**$(BAr^F{}_3)_2$ at 60 °C for 7 days in the absence of light resulted in the formation of *cis*-CO/*cis*-CN **4.1**$(BAr^F{}_3)_2$ without observation of the *trans*-CO/*cis*-CN isomer.

The isomerization mechanism upon irradiation was examined with ^{13}CO. A sample of *cis*-CO/*trans*-CN **4.1**$(BAr^F{}_3)_2$ irradiated under a ^{13}CO atmosphere resulted in complete incorporation of ^{13}CO while isomerizing to the *trans*-CO/*cis*-CN isomer (calculated ν_{CO} = 2041, 1985 cm^{-1}; experimental ν_{CO} = 2037, 1986 cm^{-1}) (Figure 4.10). An additional ν_{CO} signal at 2024 cm^{-1} was assigned to a small amount of ^{13}CO incorporated *cis*-CO/*trans*-CN **4.1**$(BAr^F{}_3)_2$ (calculated ν_{CO} = 2024 cm^{-1}). Additionally, the rate for the loss of *cis*-CO/*trans*-CN **4.1**$(BAr^F{}_3)_2$ when irradiated was slightly inhibited under CO versus Ar. Both of these results are consistent with isomerization occurring by a ligand dissociative pathway.

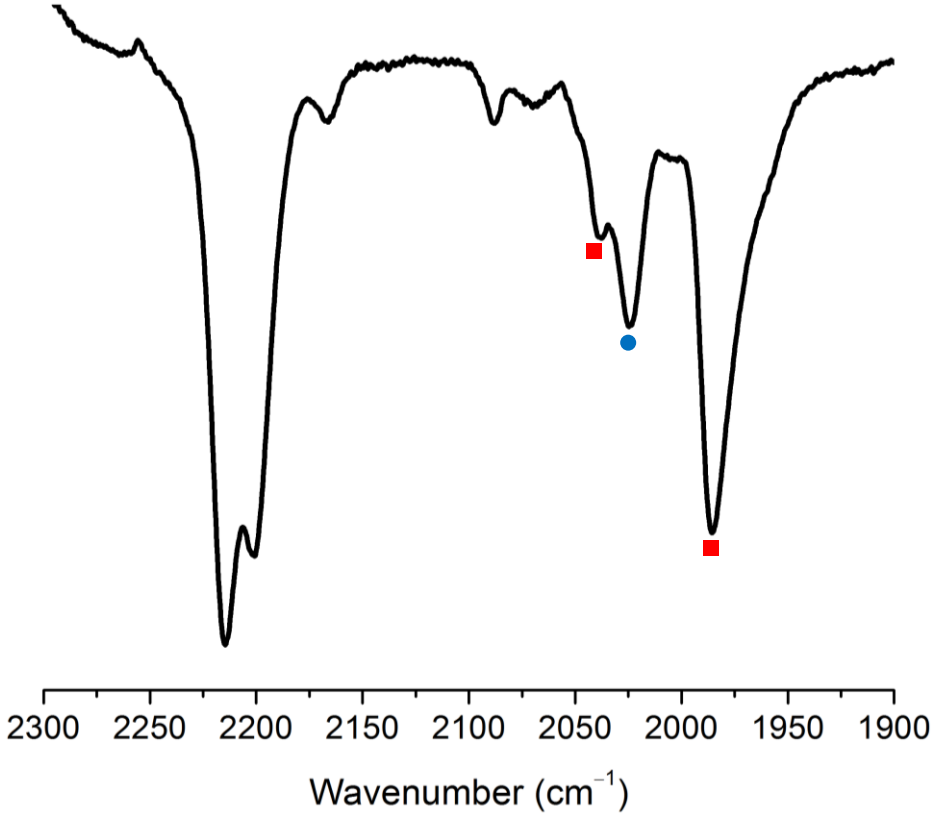


Figure 4.10. IR spectrum of irradiation of **4.1**(BAr^{F}_{3})$_2$ under ^{13}CO in CH_2Cl_2. (■) *trans*-^{13}CO/*cis*-CN **4.1**(BAr^{F}_{3})$_2$, (●) *cis*-^{13}CO/*cis*-CN **4.1**(BAr^{F}_{3})$_2$.

(CO)$_2$(CNBAr$^{F\#}_{3}$)$_2$Fe(pdt)Ni(dppe). Samples of the *cis*-CO/*trans*-CN isomer of **4.1**($BAr^{F\#}_{3}$)$_2$ isomerized to a mixture of the *trans*-CO/*cis*-CN and *cis*-CO/*cis*-CN isomers in a 4:1 ratio upon irradiation with UV light (Scheme 4.4). The *trans*-CO/*cis*-CN isomer of **4.1**($BAr^{F\#}_{3}$)$_2$ was identified by a singlet in the ^{31}P NMR spectrum (δ 57.5) and a single $CNBAr^{F\#}_{3}{}^{-}$ environment by ^{1}H and ^{19}F NMR. Upon sitting for several days in the absence of light, the *trans*-CO/*cis*-CN isomer converts to the *cis*-CO/*cis*-CN isomer. The asymmetry of the *cis*-CO/*cis*-CN isomer was identified by an AB quartet in the ^{31}P NMR (58.2, 56.9 ($^{2}J_{PP}$ = 36 Hz)) and two sets of $CNBAr^{F\#}_{3}{}^{-}$ signals in the ^{1}H and ^{19}F NMR. The IR spectra of the isomers of **4.1**($BAr^{F\#}_{3}$)$_2$ displayed similar patterns to the IR spectra of **4.1**(BAr^{F}_{3})$_2$ isomers (Figure 4.11). Care was necessary for irradiation of **4.1**($BAr^{F\#}_{3}$)$_2$ as excessive irradiation of the sample of resulted in the formation of an unidentified decomposition product observed by ^{31}P NMR at δ 65.2 ppm.

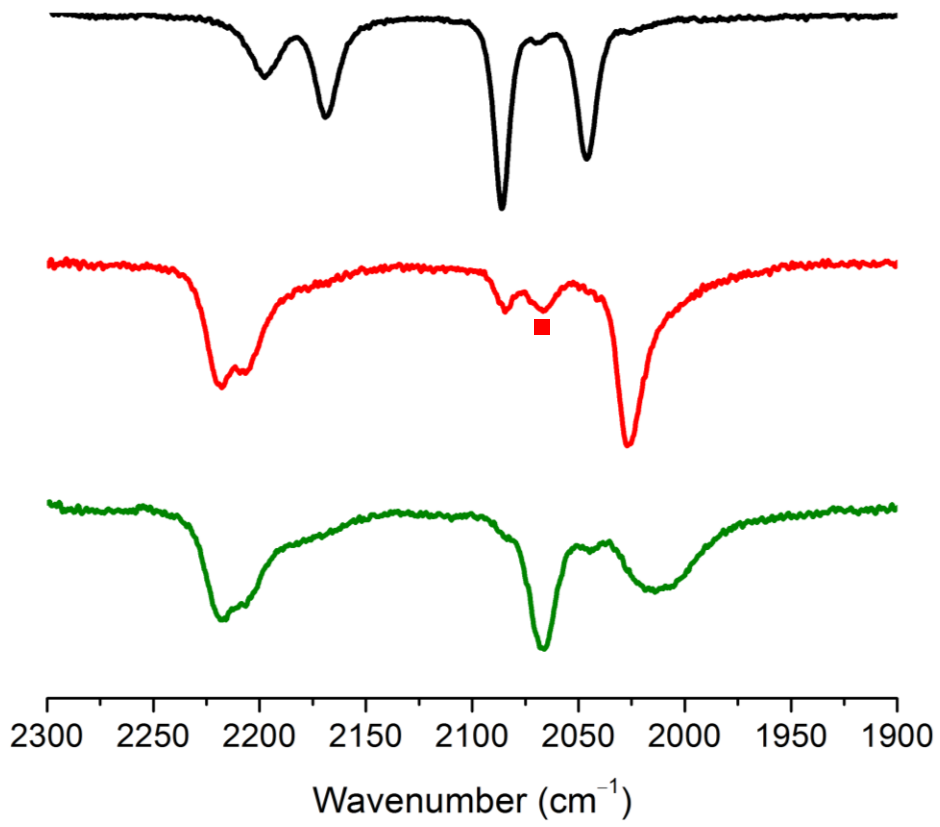
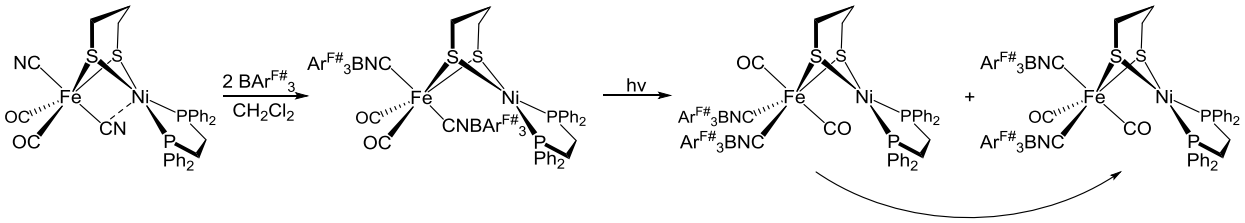


Figure 4.11. IR spectra of *cis*-CO/*trans*-CN **4.1**($BAr^{F\#}{}_3$)$_2$ (top), *trans*-CO/*cis*-CN **4.1**($BAr^{F\#}{}_3$)$_2$ (middle), and *cis*-CO/*cis*-CN **4.1**($BAr^{F\#}{}_3$)$_2$ (bottom). Trace amounts of *cis*-CO/*cis*-CN **4.1**($BAr^{F\#}{}_3$)$_2$ (■).

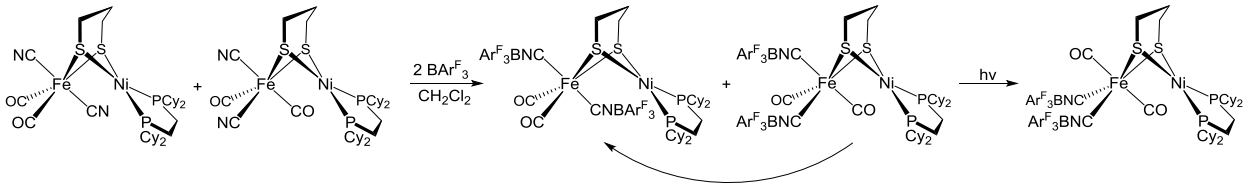
Scheme 4.4. Formation and isomerization of **4.1**($BAr^{F\#}{}_3$)$_2$.



(CO)$_2$(CNBAr$^F{}_3$)$_2$Fe(pdt)Ni(dcpe). Freshly prepared samples of **4.2**($BAr^F{}_3$)$_2$ consists of a mixture of *cis*-CO/*trans*-CN and *cis*-CO/*cis*-CN isomers. Over a period of a few hours, all of the *cis*-CO/*cis*-CN isomer converted to the *cis*-CO/*trans*-CN isomer (Scheme 4.5). Irradiation of the *cis*-CO/*trans*-CN isomer of **4.2**($BAr^F{}_3$)$_2$ converted fully to the *trans*-CO/*cis*-CN isomer as confirmed by a singlet in the ^{31}P NMR spectrum (δ 75.1) and a single set of $BAr^F{}_3$ signals in the ^{19}F NMR spectrum (δ –135.0, δ –160.4, δ –166.2). The IR spectrum of *trans*-CO/*cis*-CN **4.2**($BAr^F{}_3$)$_2$ was similar to that for other *trans*-CN/*cis*-CO isomers (Table 4.2). Samples of

trans-CO/*cis*-CN **4.2**$(BAr^F_3)_2$ were found not to convert back to either of the previously observed *cis*-CO/*trans*-CN or *cis*-CO/*cis*-CN isomers.

Scheme 4.5. Formation and isomerization of **4.2**$(BAr^F_3)_2$.



4.6 Discussion

An alternative route to $(CO)_2(CN)_2$Fe(pdt)Ni(dxpe) was developed avoiding unstable reagents. The variation of the diphosphine ligand resulted in a different mixture of isomers. The *cis*-CO/*cis*-CN isomer of $[Fe(pdt)(CO)_2(CN)_2]^{2-}$ is the major isomer in a MeOH solution (ν_{CN} = 2107, 2090 cm^{-1}; ν_{CO} = 2025, 1973 cm^{-1}) while the *cis*-CO/*trans*-CN isomer is the major isomer in the solid state (ν_{CN} = 2106, 2088 cm^{-1}; ν_{CO} = 2001, 1942 cm^{-1}).[1,2] Thought both isomers of $[Fe(pdt)(CO)_2(CN)_2]^{2-}$ are observed in solution, only one isomer of **4.1** is observed. The presence of a single isomer of **4.1** is likely due to the strong interaction between Ni and the semi-bridging CN ligand (2.421 Å).[1] This is in contrast to **4.2** for which both the *cis*-CO/*trans*-CN and *cis*-CO/*cis*-CN isomers are observed in solution. The presence of this additional isomer is thought to occur from the increased electron density on Ni by replacement of dppe with dcpe.[9] The increased electron density on Ni weakens the Ni···CN interaction as seen for **4.1**, allowing for the additional isomer of **4.2** to be present. The related compound $[(CO)_2(CN)_2Fe(SEt)_2Ni(dppe)]_6$ lacks an intramolecular Ni···μ-CN interaction and the ligands are in an *cis*-CO/*cis*-CN arrangement at the Fe center.[1]

Both **4.1** and **4.2** coordinate boranes at the Lewis basic site of the cyanide ligands. The ν_{CO} of **4.1**$(BR_3)_2$ correlated with the relative Lewis acidities of the triarylboranes ($BAr^F_3 > BAr^{F\#}_3 > BPh_3$).[10-13] Similarly, variation of the basicity of the diphosphine ligand can be observed by the IR spectra as the more electron rich **4.2** has lower ν_{CO} signals than **4.1**.[9] Only the strongly Lewis acidic boranes BAr^F_3 and $BAr^{F\#}_3$ form stable 2:1 adducts with $(CO)_2(CN)_2$Fe(pdt)Ni(dxpe). The use of excess amounts of BPh_3 was required to form **4.1**$(BPh_3)_2$ in solution, but dissociation of BPh_3 occurs when isolated samples were redissolved. In contrast the coordination of boranes to

$[Fe_2(pdt)(CO)_4(CN)_2]^{2-}$ in Chapter 2 and $[HFe(CO)_3(CN)_2]^-$ in Chapter 3 occur with a range Lewis acidity strengths. The increased Lewis basicity of $[Fe_2(pdt)(CO)_4(CN)_2]^{2-}$ and $[HFe(CO)_3(CN)_2]^-$ compared to $(CO)_2(CN)_2Fe(pdt)Ni(dxpe)$ may be attributed to the net anionic charge of the compounds.

The coordination of strongly Lewis acidic boranes to $(CO)_2(CN)_2Fe(pdt)Ni(dxpe)$ was also found to have a noticeable effect on the stability of the adducts towards irradiation. While **4.1** and **4.2** decompose upon irradiation, the Lewis acid adducts **4.1**$(BAr^F_3)_2$ and **4.2**$(BAr^F_3)_2$ isomerize when irradiated with UV light. One method for increasing the stability of the compounds is by the coordination of boranes to $(CO)_2(CN)_2Fe(pdt)Ni(dxpe)$, blocking Fe-C*N* from coordination to another metal sites. The bidentate coordination of CN^- has been observed in the related compound $[(CO)_2(CN)_2Fe(SEt)_2Ni(dppe)]_6$ exists as a hexamer in which CN^- will bridge end-on with Fe and Ni between separate NiFe units. The formation of a precipitate by the irradiation of **4.1** is likely to occur by the formation of Fe-CN-M linkages. The coordination of triarylboranes to **4.2** stabilized the compound from decomposition to Ni(pdt)(dcpe). The electron withdrawling properties of the boranes may stabilize the complex by decreasing the electron density of the Fe center, strengthening the Fe-S bond.

A driving force for the photoisomerization of the *cis*-CO/*trans*-CN isomer of $(CO)_2(CNBR_3)_2Fe(pdt)Ni(dxpe)$ may be due to the steric bulk of the $CNBR_3^-$ ligand in the semi-bridging position. The crystal structure of *cis*-CO/*trans*-CN **4.1**$(BAr^F_3)_2$ shows a highly distorted Fe-C-N bond of 166.4° for the semi-bridging Fe-$CNBAr^F_3$. A space filling plot of the structure of cis-CO/trans-CN **4.1**$(BAr^F_3)_2$ showed steric interaction between dppe and the semi-bridging $CNBAr^F_3{}^-$ ligand (Figure 4.12).

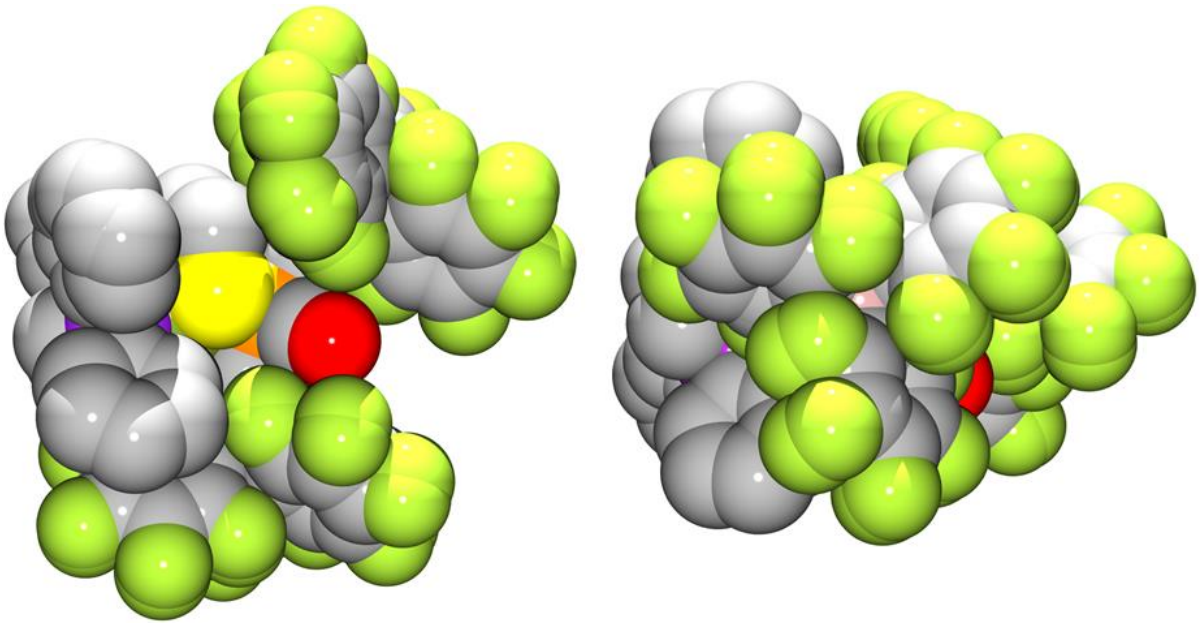


Figure 4.12. Space filling model of *cis*-CO/*trans*-CN **4.1**$(BAr^F_3)_2$ from a side on view (left) and bottom view (right).

While non-bond breaking isomerization mechanisms of octahedral complexes are known,[14,15] the photoisomerization of *cis*-CO/*trans*-CN **4.1**$(BAr^F_3)_2$ occurs by ligand dissociation as observed by incorporation of ^{13}CO and slight inhibition on the rate of isomerization under CO compared to Ar. The crystal structure of **4.1**$(BAr^F_3)_2$ offers evidence that isomerization occurs because of weaker Fe-ligand bonds. The Fe-CO bonds in **4.1**$(BAr^F_3)_2$ are slightly longer than in **4.1** suggesting that the coordination of borane weakens the Fe-CO bond. Weaker Fe-CO bonds suggest that ligand dissociation may result from decarbonylation. Other structural features of *cis*-CO/*trans*-CN **4.1**$(BAr^F_3)_2$ suggest dissociation of CO. The lengths of Fe-S bonds are unchanged upon coordination of Lewis acid to **4.1** and the Fe-CN bonds of **4.1**$(BAr^F_3)_2$ are shorter than in **4.1**. It is less likely isomerization occurs by dissociation of Fe-S or Fe-CN bonds.

The isomerization mechanism to the *cis*-CO/*cis*-CN isomer is not clear. The photoisomerization of *cis*-CO/*trans*-CN under ^{13}CO formed some ^{13}CO-incorperated *cis*-CO/*cis*-CN isomer. Incorporation of ^{13}CO may have occurred by two different routes. The formation of *cis*-^{13}CO/*cis*-CN isomer could occur directly from the *cis*-CO/*trans*-CN by decarbonylation. Another pathway for ^{13}CO incorporation in the *cis*-CO/*cis*-CN isomer could occur by isomerization from the *trans*-^{13}CO/*cis*-CN isomer though isomerization could occur by either ligand dissociation or a non-bond breaking mechanism.

The variation of diphosphine of $(CO)_2(CNBR_3)_2Fe(pdt)Ni(dxpe)$ had a noticeable effect on the geometry of the thermally stable isomer. The thermal isomer of **4.1**$(BR_3)_2$ was *cis*-CO/*cis*-CN. In contrast, the *cis*-CO/*cis*-CN isomer of **4.2**$(BAr^F{}_3)_2$ isomerized to the *cis*-CO/*trans*-CN isomer at room temperature. The isomerization to the *cis*-CO/*trans*-CN isomer of **4.2**$(BAr^F{}_3)_2$ was unexpected as the increased steric bulk of dcpe compared to dppe is expected to make the *cis*-CO/*trans*-CN isomer of **4.2**$(BAr^F{}_3)_2$ unstable.[16] This result suggests that the electronic effects may have a larger impact on the stability of an isomer than the steric effects.

4.7 Conclusions

The 2:1 Lewis acid adducts of **4.1** and **4.2** were readily formed when the stronger Lewis acids $BAr^F{}_3$ and $BAr^{F\#}{}_3$ were used. In contrast to the uncapped compounds, the resulting adducts were stable to irradiation and readily isomerized under thermal or photochemical conditions. Isomerization of **4.1**$(BAr^F{}_3)_2$ occurred without decomposition. The mechanism for photochemical isomerization occurred by ligand dissociation forming which may form by the loss of a CO ligand. The labile nature of a CO ligand in the Lewis acid adducts suggests that a CO ligand may be removed to form a coordinatively unsaturated species. The resulting unsaturated species would resemble the Ni-SI_a state of [NiFe]-H_2ase. The treatment of unsaturated species with hydride sources may form a Ni-R state model containing a more biomimetic coordination sphere at the Fe.

4.8 Experimental Procedures

All procedures were carried out in a nitrogen-filled MBraun glovebox or using standard Schlenk techniques. All solvents were degassed by sparging with nitrogen and dried by passage through activated alumina. IR spectra were recorded on a Perkin-Elmer Spectrum 100. NMR spectra were recorded on a Varian Unity 500 MHz NMR spectrometer. Signals for ^{19}F and ^{31}P NMR spectra were referenced using external standards of 1% $CFCl_3$ in $CDCl_3$ and 85% H_3PO_4, respectively. ^1H NMR spectra were referenced to internal solvent signals. CD_2Cl_2 (Cambridge Isotope Laboratories) was dried over CaH_2 before being vacuum distilled onto activated 4 Å molecular sieves. $BAr^F{}_3$ (Boulder Scientific) was sublimed under vacuum at 90 °C. Literature routes were followed for $BAr^{F\#}{}_3$,[17] $NiCl_2(dppe)$,[18] $NiCl_2(dcpe)$,[19] $Et_4N[Fe(CO)_4(CN)]$,[20] K_2pdt,[2] and $Et_4N[FeBr(CO)_3(CN)_2]$.[8] BPh_3 was synthesized by the pyrolysis of $HNMe_3BPh_4$ followed by sublimation under vacuum at 90 °C.[21]

Revised Synthesis of $(CO)_2(CN)_2Fe(pdt)Ni(dppe)$, 4.1. A solution of $Et_4N[FeBr(CO)_3(CN)_2]$ (0.900 g, 2.22 mmol) in MeOH (100 mL) was treated with a solution of K_2pdt (0.410 g, 2.22 mmol) in MeOH (50 mL). The mixture was allowed to stir for 3 hours at which time the solvent was removed under vacuum. $NiCl_2(dppe)$ (1.17 g, 2.22 mmol) was added along with 100 mL of MeCN, and the mixture was stirred for 15 min. The mixture was filtered, and the solvent was removed from the filtrate under vacuum. The crude product was extracted into THF, and the crude product was precipitated from the filtered extract upon the addition of pentane. The crude product was dissolved in MeCN and loaded onto a neutral alumina column (Brockmann Level I). A faint red band was washed off the column with MeCN. The product eluted with MeOH as a red band. The solution was evaporated under vacuum, and the residue was extracted into THF. This solution was filtered through Celite, and product was precipitated from the filtrate with pentane. The product was collected by filtration and dried under vacuum. Yield: 0.958 g (59%). IR and ^{31}P NMR spectra matched literature values.

$(CO)_2(CN)_2Fe(pdt)Ni(dcpe)$, 4.2. A solution of $Et_4N[FeBr(CO)_3(CN)_2]$ (0.500 g, 1.23 mmol) in MeOH (20 mL) was treated with a solution of K_2pdt (0.228 g, 1.23 mmol) in MeOH (20 mL). The mixture was let to stir for 3 hours at which time the solvent was removed under vacuum. In the absence of light, the residue was extracted into 20 mL of MeCN, and the mixture was treated with a suspension of $NiCl_2(dcpe)$ (0.682 g, 1.23 mmol) in MeCN (20 mL). After being stirred for 15 min, the mixture was filtered, and the solvent was stripped from the filtrate. The crude product was extracted into 20 mL of THF, the mixture was filtered, and the product was precipitated from the filtrate upon the addition of pentane. Unlike **4.1**, **4.2** did not require further purification by column chromatography. Yield: 0.423 g (45%). Anal. Calc. for $C_{33}H_{54}FeN_2NiO_2P_2S_2$ (Found): C, 52.75 (52.34); H, 7.24 (7.59); N, 3.73 (3.99).

Data for *cis*-CO/*trans*-CN Isomer. IR(CH_2Cl_2, cm^{-1}): ν_{CN} = 2113, 2090; ν_{CO} = 2045, 1995. ^{31}P NMR (CD_2Cl_2): δ 66.3 (s).

Data for *cis*-CO/*cis*-CN Isomer. IR (CH_2Cl_2, cm^{-1}): ν_{CN} = 2120; ν_{CO} = 2033, 1982. ^{31}P NMR (CD_2Cl_2): δ 67.8, 66.5 (AB quartet, $^2J_{PP}$ = 33 Hz).

$(CO)_2(CNBAr^F{}_3)_2Fe(pdt)Ni(dppe)$, 4.1$(BAr^F{}_3)_2$. A solution of $(CO)_2(CN)_2Fe(pdt)Ni(dppe)$ (290 mg, 0.4 mmol) in 10 mL of CH_2Cl_2 was treated with a solution of $BAr^F{}_3$ (410 mg, 0.8 mmol) in 30 mL of CH_2Cl_2 dropwise. The reaction caused a change in color from a red to an orange solution. The reaction solution was concentrated to 20 mL and layered with 100 mL of pentane followed by cooling to −30 °C. Yield: 570 mg (82%). Crystals suitable

for X-ray diffraction were grown from a concentrated THF solution of **4.1**(BAr^F_3)$_2$ layered with pentane and cooled at −30 °C. IR (CH_2Cl_2, cm^{-1}): ν_{CN} = 2194, 2166; ν_{CO} = 2088, 2050. ^{31}P NMR (CD_2Cl_2): δ 56.4 (s). ^{19}F NMR (CD_2Cl_2): δ −133.7 (d, *o*-F); −135.1 (d, *o*-F); −159.2 (t, *p*-F); −159.4 (t, *p*-F); −165.0 (dt, *m*-F); −165.6 (dt, *m*-F). Anal. Calc. for $C_{69}HBF_{30}FeN_2NiO_2P_2S_2$ (Found): C, 47.32 (47.24); H, 1.73 (1.64); N, 1.60 (1.52).

(CO)$_2$(CNBAr$^{F\#}_3$)$_2$Fe(pdt)Ni(dppe), 4.1(BAr$^{F\#}_3$)$_2$. Prepared by similar methods as **4.1**(BAr^F_3)$_2$. Yield 21 mg (76%). IR (CH_2Cl_2, cm^{-1}): ν_{CN} = 2197, 2168, ν_{CO} = 2086, 2046. ^{1}H NMR (CD_2Cl_2): δ 6.40 (t, B($C_6F_3H_2$)$_3$); 6.30 (t, B($C_6F_3H_2$)$_3$). ^{31}P NMR (CD_2Cl_2): δ 58.4 (s). ^{19}F NMR (CD_2Cl_2): δ −99.5 (s, *o*-F); −101.1 (s, *o*-F); −115.4 (s, *p*-F); −115.8 (s, *p*-F).

(CO)$_2$(CNBAr$^F_3$)$_2$Fe(pdt)Ni(dcpe), 4.2(BAr$^F_3$)$_2$. Analogously to the preparation of **4.1**(BAr^F_3)$_2$, a solution of **4.2** (0.144 g, 0.0192 mmol) in CH_2Cl_2 (5 mL) was treated with a solution of BAr^F_3 (0.196 g, 0.0383mmol), resulting in a color change from red or orange. The solvent was removed under vacuum, redissolved in THF, and crystallized by the addition of pentane followed by cooling to −30 °C. Yield: 0.253 g (74%).

Data for *cis*-CO/*trans*-CN Isomer. IR (CH_2Cl_2, cm^{-1}): ν_{CN} = 2190, 2149; ν_{CO} = 2085, 2046. ^{31}P NMR (CD_2Cl_2): δ 69.8 (s). ^{19}F NMR (CD_2Cl_2): δ −133.8 (d, *o*-F); −134.2 (d, *o*-F); −159.4 (t, *p*-F); −160.6 (t, *p*-F); −165.3 (t, *m*-F); −166.4 (t, *m*-F).

Data for *cis*-CO/*cis*-CN Isomer. IR (CH_2Cl_2, cm^{-1}): ν_{CN} = 2210; ν_{CO} = 2068, 2030. ^{31}P NMR (CD_2Cl_2): δ 70.2, δ 69.5 (AB quartet, $^2J_{PP}$ = 30 Hz). ^{19}F NMR (CD_2Cl_2): δ −133.1 (d, *o*-F); −134.9 (*o*-F); −158.7 (t, *p*-F); −159.3 (t, *p*-F); −165.0 (t, *m*-F); −165.5 (t, *m*-F).

Isomerization of 4.1(BAr$^F_3$)$_2$. A solution of the *cis*-CO/*trans*-CN isomer of **4.1**(BAr^F_3)$_2$ (10 mg, 0.006 mmol) in CD_2Cl_2 (1 mL) was loaded into an NMR tube fitted with a J Young valve and irradiated by a 365 nm LED array for 3 hours. ^{19}F and ^{31}P NMR measurements showed conversion of the initial isomer to a 3:1 ratio of the *trans*-CO/*cis*-CN and *cis*-CO/*cis*-CN isomers. Upon sitting in the absence of light for 5 days, the mixture shifted to a 1:25 ratio of the *trans*-CO/*cis*-CN and *cis*-CO/*trans*-CN isomers.

Data for *trans-CO/cis-CN:* IR(CH_2Cl_2, cm^{-1}): ν_{CN} = 2215, 2201; ν_{CO} = 2087(w), 2030. ^{31}P NMR (CD_2Cl_2): δ 58.7 (s). ^{19}F NMR (CD_2Cl_2): δ –135.2 (d, *o*-F); –160.6 (t, *p*-F); –166.5 (t, *m*-F).

Data for *cis-CO/cis-CN:* IR(CH_2Cl_2, cm^{-1}): ν_{CN} = 2214, 2202; ν_{CO} = 2070, 2020 cm^{-1}. ^{31}P NMR (CD_2Cl_2): δ 58.9, 58.5 (AB quartet, $^2J_{PP}$ = 37 Hz). ^{19}F NMR (CD_2Cl_2): δ –135.0 (d, *o*-F); –135.1 (d, *o*-F); –160.0 (t, *p*-F); –160.7 (t, *p*-F); –166.0 (t, *m*-F); –166.5 (t, *m*-F).

Isomerization of 4.1(BAr$^{F\#}{}_3$)$_2$. A solution of the *cis*-CO/*trans*-CN isomer of **4.1**(BAr$^{F\#}{}_3$)$_2$ (10 mg, 0.0065 mmol) in CD_2Cl_2 (1 mL) was loaded into an NMR tube fitted with a J Young valve and irradiated by a 365 nm LED array for 2 hours. ^{1}H, ^{19}F, and ^{31}P NMR showed conversion of the initial isomer to the *trans*-CO/*cis*-CN isomer. Upon sitting in the absence of light for 2 days, the mixture shifted to the *cis*-CO/*trans*-CN isomer.

Data for *trans*-CO/*cis*-CN: IR(CH_2Cl_2, cm^{-1}): ν_{CN} = 2218, 2207; ν_{CO} = 2084(w), 2027. ^{1}H NMR (CD_2Cl_2): δ 6.19 (t, B($C_6F_3H_2$)$_3$). ^{31}P NMR (CD_2Cl_2): δ 58.4 (s). ^{19}F NMR (CD_2Cl_2): δ –100.2 (s, *o*-F); –116.0 (s, *p*-F).

Data for *cis*-CO/*cis*-CN: IR(CH_2Cl_2, cm^{-1}): ν_{CN} = 2216, 2207; ν_{CO} = 2066, 2013. ^{31}P NMR (CD_2Cl_2): δ 58.2, 56.9 (AB quartet, $^2J_{PP}$ = 36 Hz).

Isomerization of 4.2(BAr$^F{}_3$)$_2$. A solution of the *cis*-CO/*trans*-CN isomer of **4.2**(BAr$^F{}_3$)$_2$ (10 mg, 0.006 mmol) in CD_2Cl_2 (1 mL) was loaded into an NMR tube fitted with a J Young valve and irradiated by a 365 nm LED array for 2 h. ^{19}F and ^{31}P NMR showed conversion to the *trans*-CO/*cis*-CN isomer of **4.2**(BAr$^F{}_3$)$_2$. No further isomerization was observed upon standing in the absence of light. IR(CH_2Cl_2, cm^{-1}): ν_{CN} = 2214, 2200; ν_{CO} = 2084(w), 2027. ^{31}P NMR (CD_2Cl_2): δ 75.1 (s). ^{19}F NMR (CD_2Cl_2): δ –135.0 (d, *o*-F); –160.4 (t, *p*-F); –166.2 (t, *m*-F).

Ph$_4$PBAr^{F24}. A solution of Ph_4PCl (0.127 g, 0.34 mmol) in 3 mL of CH_2Cl_2 was added to a suspension of NaBAr^{F24} (0.300 g, 0.34 mmol) in 10 mL CH_2Cl_2. The mixture was allowed to stir for 10 min and the solvent was removed under vacuum. The resulting residue was extracted into Et_2O and the solution was filtered through Celite. The solution was dried under vacuum, resulting in an off-white solid. Yield 0.368g (90%). ^{31}P NMR (CD_2Cl_2): δ 23.9 (s).

Isomerization Kinetics of 4.1(BAr$^F{}_3$)$_2$. A solution of *cis*-CO/*trans*-CN **4.1**(BAr$^F{}_3$)$_2$ (40 mg, 0.0023 mmol) and Ph$_4$PBAr^{F24} (55mg, 0.0046 mmol) as internal standard was prepared by dissolving in 2 mL of CD_2Cl_2. The solution was evenly divided into two J Young NMR tubes. One sample was frozen, the head space above the sample removed under vacuum, and the sample was placed under 7 psi of CO. Both samples were irradiated by a 365 nm LED array and the loss of the *cis*-CO/*trans*-CN isomer was monitored by ^{31}P NMR. The rate was determined by a linear fit of the ln of the concentration of *cis*-CO/*trans*-CN isomer verse time (Figure 4.13).

N_2: $k = 1.3 \times 10^{-3}$; $R^2 = 0.992$

CO: $k = 1.0 \times 10^{-3}$; $R^2 = 0.991$

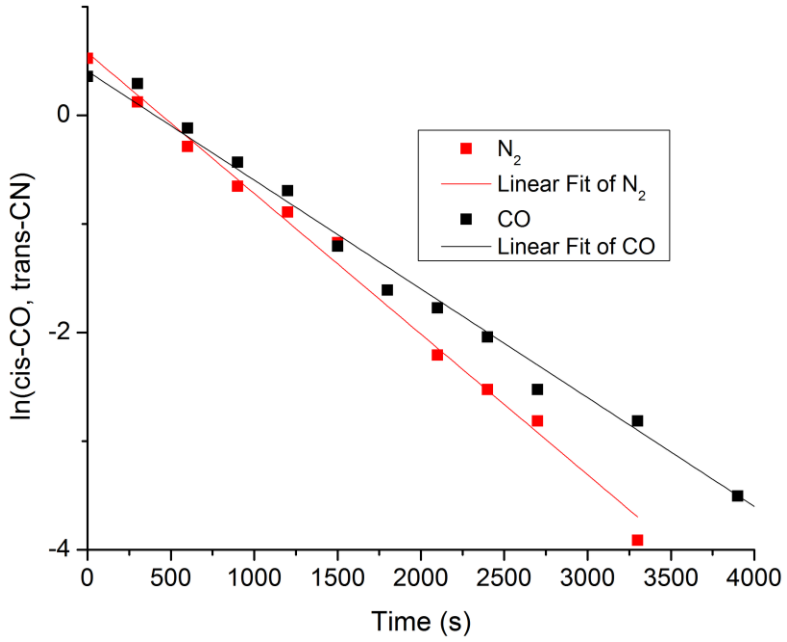


Figure 4.13. Plot of ln[*cis*-CO/*trans*-CN **4.1**$(BAr^F{}_3)_2$] versus time under CO and N_2 for the isomerization of **4.1**$(BAr^F{}_3)_2$.

Table 4.2. IR frequencies and ^{31}P NMR signals of isomers of **4.1**, **4.2**, and borane adducts.

Compound	ν_{CN} (cm^{-1})	ν_{CO} (cm^{-1})	^{31}P NMR (ppm)
cis-CO/*trans*-CN **4.1**	2110, 2081	2053, 2005	56.9
cis-CO/*trans*-CN **4.2**	2113, 2090	2045, 1995	66.3
cis-CO/*cis*-CN **4.2**	2120	2033, 1982	67.8, 66.5 ($^2J_{PP}$ = 33 Hz)
cis-CO/*trans*-CN **4.1**$(BAr^F{}_3)_2$	2194, 2166	2088, 2050	56.4
trans-CO/*cis*-CN **4.1**$(BAr^F{}_3)_2$	2215, 2201	2087 (w), 2030	58.7
cis-CO/*cis*-CN **4.1**$(BAr^F{}_3)_2$	2214, 2202	2070, 2020	58.9, 58.5 ($^2J_{PP}$ = 37 Hz)
cis-CO/*trans*-CN **4.1**$(BAr^{F\#}{}_3)_2$	2197, 2168	2086, 2046	58.4
trans-CO/*cis*-CN **4.1**$(BAr^{F\#}{}_3)_2$	2218, 2207	2084 (w), 2027	57.5
cis-CO/*cis*-CN **4.1**$(BAr^{F\#}{}_3)_2$	2216, 2207	2066, 2013	58.2, 56.9 ($^2J_{PP}$ = 36 Hz)
cis-CO/*trans*-CN **4.2**$(BAr^F{}_3)_2$	2190, 2149	2085, 2046	69.8
trans-CO/*cis*-CN **4.2**$(BAr^F{}_3)_2$	2214, 2200	2084 (w), 2027	75.1
cis-CO/*cis*-CN **4.2**$(BAr^F{}_3)_2$	2210	2068, 2030	70.2, 69.5 ($^2J_{PP}$ = 30 Hz)

4.9 References

(1) Jiang, J.; Maruani, M.; Solaimanzadeh, J.; Lo, W.; Koch, S. A.; Millar, M. "Synthesis and Structure of Analogues for the Ni-Fe Site in Hydrogenase Enzymes" *Inorg. Chem.* **2009**, *48*, 6359.

(2) Li, Z. L.; Ohki, Y.; Tatsumi, K. "Dithlolato-Bridged Dinuclear Iron-Nickel complexes $[Fe(CO)_2(CN)_2(\mu\text{-}SCH_2CH_2CH_2S)Ni(S_2CNR_2)]^-$ - Modeling the Active Site of [NiFe]- Hydrogenase" *J. Am. Chem. Soc.* **2005**, *127*, 8950.

(3) Ogata, H.; Mizoguchi, Y.; Mizuno, N.; Miki, K.; Adachi, S.; Yasuoka, N.; Yagi, T.; Yamauchi, O.; Hirota, S.; Higuchi, Y. "Structural Studies of the Carbon Monoxide Complex of [NiFe] Hydrogenase from *Desulfovibrio vulgaris* Miyazaki F: Suggestion for the Initial Activation Site for Dihydrogen" *J. Am. Chem. Soc.* **2002**, *124*, 11628.

(4) Volbeda, A.; Martin, L.; Cavazza, C.; Matho, M.; Faber, B. W.; Roseboom, W.; Albracht, S. P. J.; Garcin, E.; Rousset, M.; Fontecilla-Camps, J. C. "Structural Differences Between the Ready and Unready Oxidized States of [NiFe]-Hydrogenases" *J. Biol. Inorg. Chem.* **2005**, *10*, 239.

(5) DeLacey, A. L.; Fernandez, V. M.; Rousset, M.; Cavazza, C.; Hatchikian, E. C. "Spectroscopic and Kinetic Characterization of Active Site Mutants of *Desulfovibrio fructosovorans* [NiFe]-Hydrogenase" *J. Biol. Inorg. Chem.* **2003**, *8*, 129.

(6) Manor, B. C.; Ringenberg, M. R.; Rauchfuss, T. B. "Borane-Protected Cyanides as Surrogates of H-Bonded Cyanides in [FeFe]-Hydrogenase Active Site Models" *Inorg. Chem.* **2014**, *53*, 7241.

(7) Jiang, J.; Lo, W.; Muller, P.; Fine, N. D.; Maruani, M.; Raytman, A. "Synthesis, Structure and Stability of *fac*-$[Fe^{II}(CO)_3X_3]^{1-}$ (X=Br, I)" *Inorg. Chem. Commun.* **2009**, *12*, 527.

(8) Chen, C. H.; Liaw, W. F. "Iron-Cyanocarbonyl Complexes $PPN[Fe(CO)_4(CN)]$ and $PPN[FeBr(CO)_3(CN)_2]$" *Inorg. Synth.* **2010**, *35*, 129.

(9) Sowa, J. R.; Zanotti, V.; Facchin, G.; Angelici, R. J. "Calorimetric Studies of the Heats of Protonation of the Metal in $Fe(CO)_3$(Bidentate Phosphine, Arsine) Complexes - Effects of Chelate Ligands on Metal Basicity" *J. Am. Chem. Soc.* **1992**, *114*, 160.

(10) Britovsek, G. J. P.; Ugolotti, J.; White, A. J. P. "From $B(C_6F_5)_3$ to $B(OC_6F_5)_3$: Synthesis of $(C_6F_5)_2BOC_6F_5$ and $C_6F_5B(OC_6F_5)_2$ and Their Relative Lewis Acidity" *Organometallics* **2005**, *24*, 1685.

(11) Morrison, D. J.; Piers, W. E. "Weaker Lewis Acid, Better Catalytic Activity: Dual Mechanisms in Perfluoroarylborane-Catalyzed Allylstannation Reactions" *Org. Lett.* **2003**, *5*, 2857.

(12) Welch, G. C.; Cabrera, L.; Chase, P. A.; Hollink, E.; Masuda, J. D.; Wei, P. R.; Stephan, D. W. ″Tuning Lewis Acidity Using the Reactivity of "Frustrated Lewis Pairs": Facile Formation of Phosphine-Boranes and Cationic Phosphonium-Boranes″ *Dalton Trans.* **2007**, 3407.

(13) Nicasio, J. A.; Steinberg, S.; Inés, B.; Alcarazo, M. ″Tuning the Lewis Acidity of Boranes in Frustrated Lewis Pair Chemistry: Implications for the Hydrogenation of Electron-Poor Alkenes″ *Chem. Eur. J.* **2013**, 11016.

(14) Bailar, J. C. ″Some Problems in the Stereochemistry of Coordination Compounds - Introductory Lecture″ *J. Inorg. Nucl. Chem.* **1958**, *8*, 165.

(15) Springer, C. S.; Sievers, R. E. ″Intramolecular Isomerization of Octahedral Complexes by Mechanisms Not Involving Bond Rupture″ *Inorg. Chem.* **1967**, *6*, 852.

(16) Tolman, C. A. ″Steric Effects of Phosphosurs Ligands in Organometallic Chemistry and Homogeneous Catalysis″ *Chem. Rev.* **1977**, *77*, 313.

(17) Chakraborty, D.; Rodriguez, A.; Chen, E. Y. X. ″Catalytic Ring-Opening Polymerization of Propylene Oxide by Organoborane and Aluminum Lewis Acids″ *Macromolecules* **2003**, *36*, 5470.

(18) Barton, B. E.; Whaley, C. M.; Rauchfuss, T. B.; Gray, D. L. ″Nickel-Iron Dithiolato Hydrides Relevant to the [NiFe]-Hydrogenase Active Site″ *J. Am. Chem. Soc.* **2009**, *131*, 6942.

(19) Carroll, M. E.; Barton, B. E.; Gray, D. L.; Mack, A. E.; Rauchfuss, T. B. ″Active-Site Models for the Nickel-Iron Hydrogenases: Effects of Ligands on Reactivity and Catalytic Properties″ *Inorg. Chem.* **2011**, *50*, 9554.

(20) Ruff, J. K. ″Chemistry of Dinuclear Carbonyl Anions .IV. Thiocyanate- and Cyanide-Bridged Complexes″ *Inorg. Chem.* **1969**, *8*, 86.

(21) Reynard, K. E.; Sherman, R. E.; Smith, H. D.; Hohnstedt, L. F.; Gassenheimer, G.; Wartik, T. ″Trimethylammonium Tetraphenylborate: (A Ready Source of Triphenylborane)″ *Inorg. Synth.* **2007**, 52.

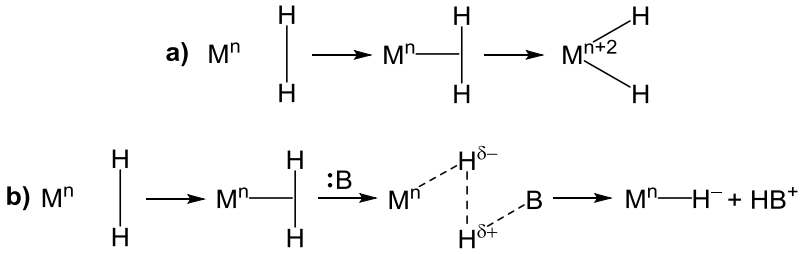
Chapter 5

Formation of Biomimetic [NiFe]-Hydrogenase Models from H_2

5.1 Introduction

Metal hydrides occur as intermediates in the catalytic cycles of [FeFe]- and [NiFe]-H_2ase. Metal hydrides can be formed by a number of different sources,[1,2] though the most biologically relevant of which is by protonation or by heterolytic cleavage of H_2. Protonation of a metal center results in a net two electron oxidation of the metal center and is the most common method for forming metal hydrides in H_2ase models.[3] The formation of metal hydrides from H_2 can occur by two different mechanisms: homolytic or heterolytic cleavage (Scheme 5.1). Homolytic cleavage results in the electrons of the H-H bond being split equally to each atom, resulting in two equivalents of H·.[4] This cleavage can occur on a single, low valent metal site by oxidative addition, resulting in a net two electron oxidation of the metal center. Heterolytic cleavage of H_2 occurs by asymmetrical splitting of H_2 into H^- and H^+.[5] The metal center binds H^- with no change in oxidation state and H^+ binds to a proton acceptor. Heterolytic cleavage of H_2 has been reported occur in the metal-free systems utilizing sterically bulky Lewis acid and bases known as frustrated Lewis base pairs (FLPs).[6,7]

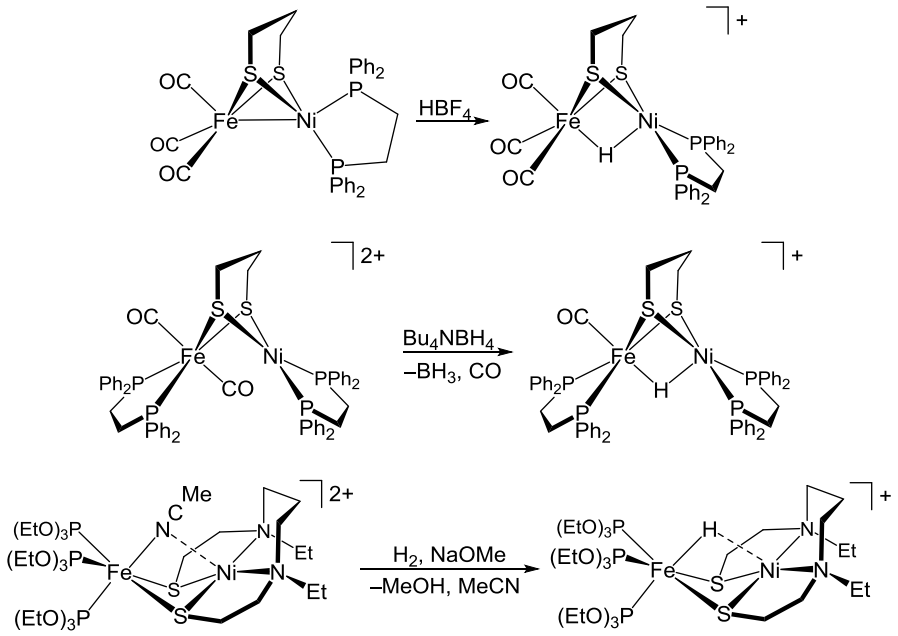
Scheme 5.1. Formation of metal hydrides from H_2 by a) homolytic cleavage via oxidative addition and b) heterolytic cleavage in the presence of base.



Models of [NiFe]-H_2ase with hydride ligands have been formed by a number of different methods (Scheme 5.2). The first report of a hydride in a model for [NiFe]-H_2ase was the protonation of $(CO)_3$Fe(pdt)Ni(dppe) with HBF_4 to form $[(CO)_3Fe(H)(pdt)Ni(dppe)]^+$.[8] A few reports describe the formation of hydride-containing H_2ase models by hydride transfer from BH_4^-.[9] Addition of Bu_4NBH_4 to the coordinatively saturated complex $[(dppe)(CO)_2Fe(pdt)Ni(dppe)]^{2+}$ formed the hydride $[(dppe)(CO)Fe(H)(pdt)Ni(dppe)]^+$ among several other hydride-containing products.[8] Although the heterolytic splitting of H_2 is key to the catalytic cycle of H_2ase, there is few reports H_2 activation by H_2ase models.[10-13] Placing a solution of the [NiFe]-H_2ase model

$[(P(OEt)_3)_3Fe(NCMe)Ni(S_2N_2')]^{2+}$ under high pressure of H_2 (0.1 – 0.8 MPa) in the presence of NaOMe formed the terminal hydride $[(P(OEt)_3)_3Fe(H)Ni(S_2N_2')]^+$.[14]

Scheme 5.2. Formation of hydrides in [NiFe]-H_2ase models by protonation (top) hydride transfer from main group hydrides (middle) and from heterolytic splitting of H_2 (bottom).



As demonstrated in Chapter 4, triarylboranes coordinate to $(CO)_2(CN)_2Fe(pdt)Ni(dxpe)$ (dxpe = dppe, dcpe) to afford the 2:1 adducts $(CO)_2(CNBAr^F{}_3)_2Fe(pdt)Ni(dppe)$ (**4.1**$(BAr^F{}_3)_2$) and $(CO)_2(CNBAr^F{}_3)_2Fe(pdt)Ni(dcpe)$ (**4.2**$(BAr^F{}_3)_2$). These products were more stable to decarbonylation than the parent complexes **4.1** and **4.2**. The greater stability towards decarbonylation suggests that the Lewis acid adducts may form an unsaturated complex, which upon treatment with a hydride donor is proposed to result in a NiFe hydride.

5.2 Formation of Hydrides from Borohydride

The formation of NiFe hydrides from the adducts $(CO)_2(CNBAr^F{}_3)_2Fe(pdt)Ni(dxpe)$ was first explored using BH_4^- as a hydride source. Combining Et_4NBH_4 with **4.1**$(BAr^F{}_3)_2$ gave rise to a mixture exhibiting three high field triplets in the ^1H NMR spectrum, consistent with three hydride species (Figure 5.1). The coupling constants of the hydride signals resemble those previously reported for $[(CO)_2(L)Fe(H)(pdt)(dppe)]^+$ ($^2J_{HP}$ = 6 Hz) and arise from coupling between the diphosphine on Ni and the hydride that bridges Fe and Ni.

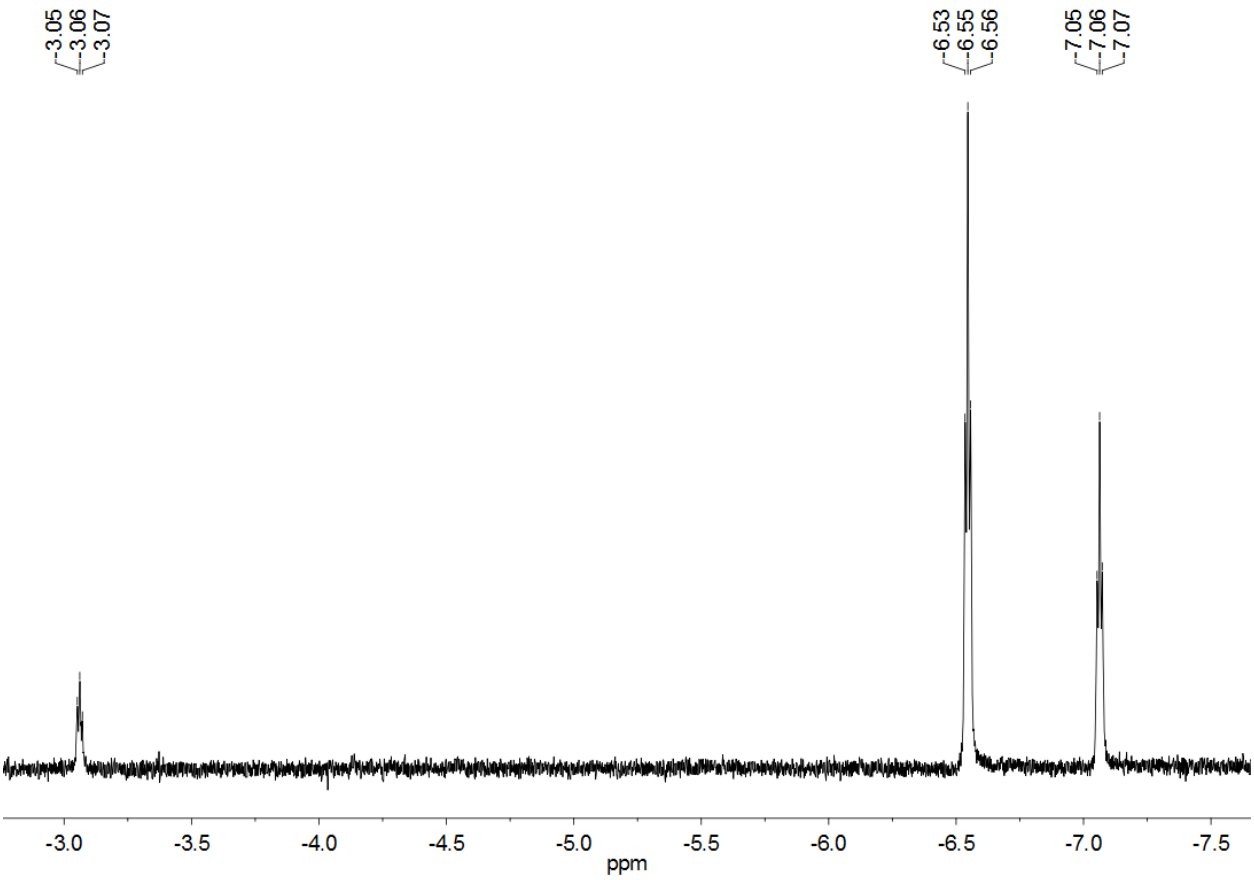
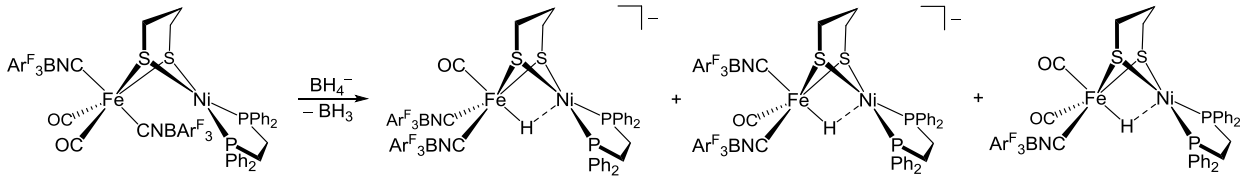


Figure 5.1. High-field portion of the ^{1}H NMR spectrum for the products of the reaction of **4.1**$(BAr^{F}{}_{3})_{2}$ with Et_4NBH_4 in CD_2Cl_2.

After purification of the mixture, the signals at δ –3.06, –7.06 ($^{2}J_{HP}$ = 5.2 Hz) were assigned to the isomers of the dicyanide hydride $[(CO)(CNBAr^{F}{}_{3})_{2}Fe(H)(pdt)Ni(dppe)]^{-}$ ([H**5.1**$(BAr^{F}{}_{3})_{2}]^{-}$). The compound associated with the ^{1}H NMR signal at δ –6.55 ($^{2}J_{HP}$ = 5.5 Hz) was not isolated, but is proposed to be the neutral mono-cyanide hydride $(CO)_{2}(CNBAr^{F}{}_{3})Fe(H)(pdt)Ni(dppe)$ based on the similar ^{1}H NMR chemical shift and $^{2}J_{HP}$ coupling constant as observed for previous compounds $(CO)_{2}(CNBPh_3)Fe(H)(pdt)Ni(dppe)$ reported in Chapter 3 (Scheme 5.3).

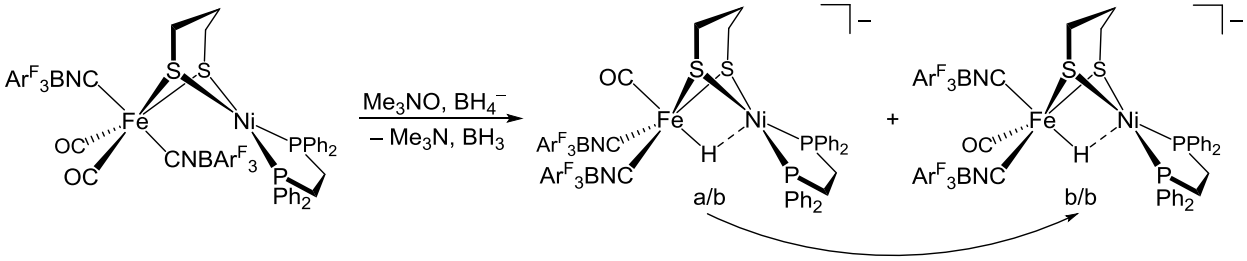
Scheme 5.3. Formation of two isomers of [H**5.1**$(BAr^{F}{}_{3})_{2}]^{-}$ and $(CO)_{2}(CNBArF_3)Fe(H)(pdt)Ni(dppe)$ by the reaction of **4.1**$(BAr^{F}{}_{3})$ with BH_4^{-}.



The addition of a decarbonylating agent greatly improved the selectivity towards formation of the *di*cyanide hydride. Treatment of a CH_2Cl_2 solution of **4.1**$(BAr^{F}{}_{3})_{2}$ with Me_3NO followed by Et_4NBH_4 formed Et_4N[H**5.1**$(BAr^{F}{}_{3})_{2}$] as

the only hydride species. Initially the signals at δ –3.06 and –7.06 were in a 1:9.5 ratio, though over time the signal at δ –3.06 decreased in intensity while the signal at δ –7.06 increased. Based on ^{19}F and ^{31}P NMR spectroscopy as well as X-ray crystallography (*vide infra*), we assign the signal at δ –7.06 to the isomer with the $CNBAr^{F}_{3}$ ligands in an apical/basal (a/b) arrangement. The signal at δ –3.06 was assigned to the basal/basal (b/b) isomer (Scheme 5.4).

Scheme 5.4. Formation and isomerization of the a/b and b/b isomers of $[H\mathbf{5.1}(BAr^{F}_{3})_2]^-$ by the treatment of $\mathbf{4.1}(BAr^{F}_{3})_2$ with Me_3NO and BH_4^-.



Variation of the decarbonylating agent had a noticeable effect on the ratio of the $[H\mathbf{5.1}(BAr^{F}_{3})_2]^-$ isomers. The use of N-methylmorpholine-N-oxide (NMO) in place of Me_3NO favored the b/b isomer with an initial b/b:a/b ratio of 2.5:1 (Figure 5.2).

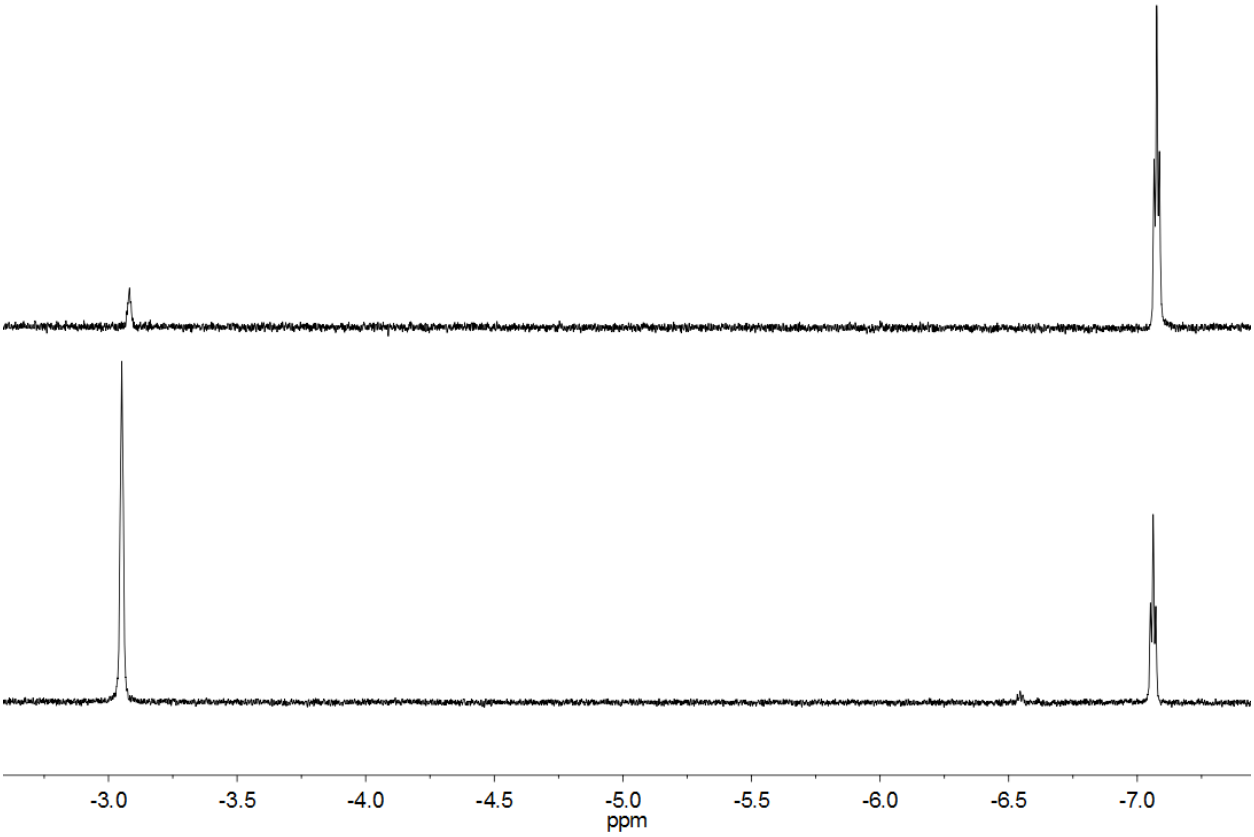


Figure 5.2. High field regions of the ^{1}H NMR spectra in CD_2Cl_2 of [H**5.1**$(BAr^{F}_{3})_2]^-$ formed from **4.1**$(BAr^{F}_{3})_2$ and BH_4^- with Me_3NO (top) or NMO (bottom).

To determine the cause of the varying ratio of hydride isomers, the decarbonylated intermediates of **4.1**$(BAr^{F}_{3})_2$ were studied by IR spectroscopy (Figure 5.3). Treatment of **4.1**$(BAr^{F}_{3})_2$ with Me_3NO resulted in the formation of an intermediate with two ν_{CN} signals (2182, 2155 cm^{-1}) and one ν_{CO} signal (1990 cm^{-1}). Treatment of the decarbonylated intermediate with Bu_4NBH_4 formed [H**5.1**$(BAr^{F}_{3})_2]^-$ as confirmed by ^{1}H NMR and IR spectroscopy. The two ν_{CN} bands of different intensities are consistent with an a/b arrangement of the $CNBAr^{F}_{3}{}^-$ ligands in the major isomer. Treatment of **4.1**$(BAr^{F}_{3})_2$ with NMO produce a different IR spectrum with two ν_{CN} signals (2189, 2167 cm^{-1}) and one ν_{CO} signal (1995 cm^{-1}). The two ν_{CN} stretches of the intermediate formed by NMO were of the same intensities, consistent with a b/b arrangement of the $CNBAr^{F}_{3}{}^-$ ligands in the major isomer. It is proposed that different decarbonylating agents give a different ratio of the isomers of the decarbonylated intermediate, resulting in varying ratios of the isomers of [H**5.1**$(BAr^{F}_{3})_2]^-$. The decarbonylated intermediates are unstable, decomposing over 30 min with the IR spectrum of the decomposed products displaying one major ν_{CN} band at 2198 cm^{-1} and two ν_{CO} bands at 2070 and 2029 cm^{-1} regardless of decarbonlyating agent.

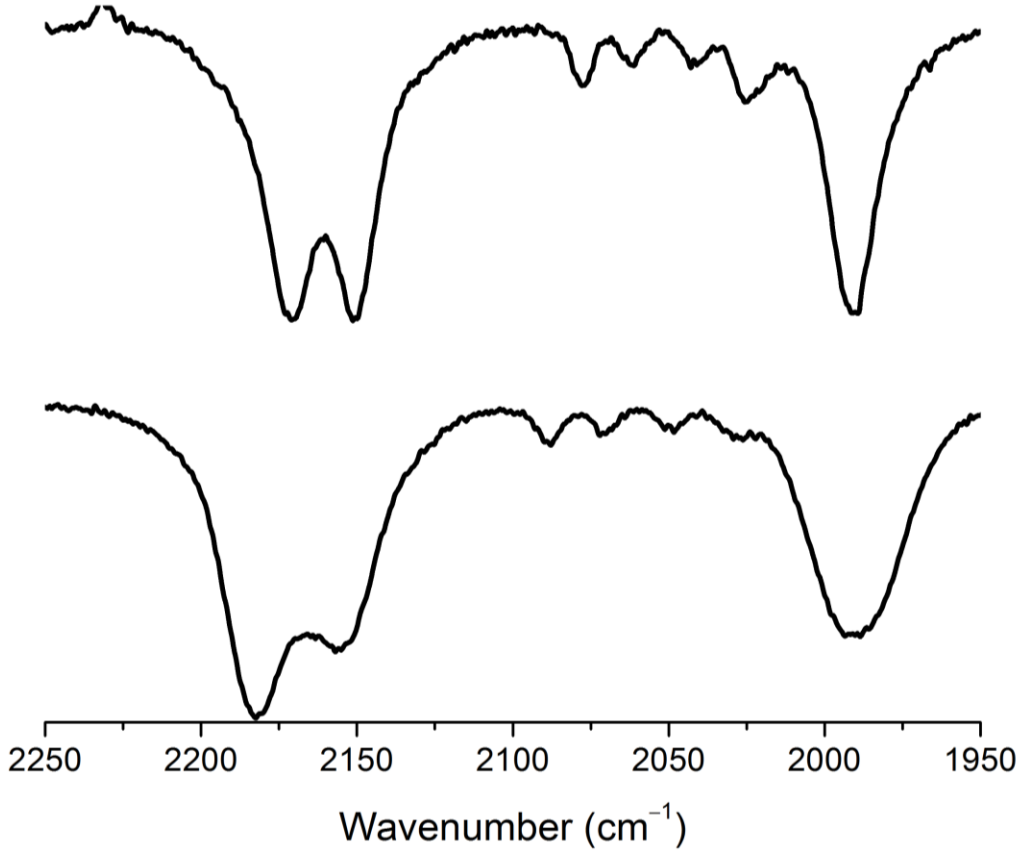


Figure 5.3. IR spectra of **4.1**$(BAr^F_3)_2$ treated with NMO (top) and Me_3NO (bottom) in CH_2Cl_2.

The reaction of **4.2**$(BAr^F_3)_2$ with BH_4^- was found to be more problematic than for **4.1**$(BAr^F_3)_2$. While treatment of **4.2**$(BAr^F_3)_2$ with Bu_4NBH_4 resulted in a change in the IR spectrum, no hydride products were identified by ^{1}H NMR spectroscopy. The use of a decarbonylating agent produced more favorable results. The reaction of Me_3NO and **4.2**$(BAr^F_3)_2$ quickly followed by treatment with Et_4NBH_4 formed three hydride-containing species by ^{1}H NMR spectroscopy as identified by three high field triplets at δ –2.68, –6.11, and –6.56 ($^2J_{HP}$ = 3 Hz). After purification, the signal at δ –6.56 was assigned to the a/b isomer of $[(CO)(CNBAr^F_3)_2Fe(H)(pdt)Ni(dppe)]^-$ ($[H$**5.2**$(BAr^F_3)_2]^-$). Though not isolated, signals at δ –2.68 and –6.11 are proposed to be the mono-cyanide product $(CO)_2(CNBAr^F_3)Fe(H)(pdt)Ni(dcpe)$ given the similar $^2J_{HP}$ coupling constant observed for $(CO)_2(CNBPh_3)Fe(H)(pdt)Ni(dcpe)$ in Chapter 3. The use of NMO or pyridine-N-oxide as decarbonylating agents did not improve the ratio of $[H$**5.2**$(BAr^F_3)_2]^-$ to $(CO)_2(CNBAr^F_3)Fe(H)(pdt)Ni(dcpe)$. The b/b isomer of $[H$**5.2**$(BAr^F_3)_2]^-$ was not observed.

The IR spectrum of $Et_4N[H$**5.1**$(BAr^F_3)_2]$ displays two ν_{CN} bands at 2162 and 2137 cm^{-1} and one ν_{CO} band at 1963 cm^{-1}, consistent with one CO and two $CNBAr^F_3{}^-$ ligands on Fe. The ^{19}F NMR spectrum showed two

inequivalent BAr^{F}_{3} groups, consistent with an a/b arrangement of the $CNBAr^{F}_{3}^{-}$ ligands (Figure 5.4). A singlet in the ^{31}P NMR was observed at δ 66.6.

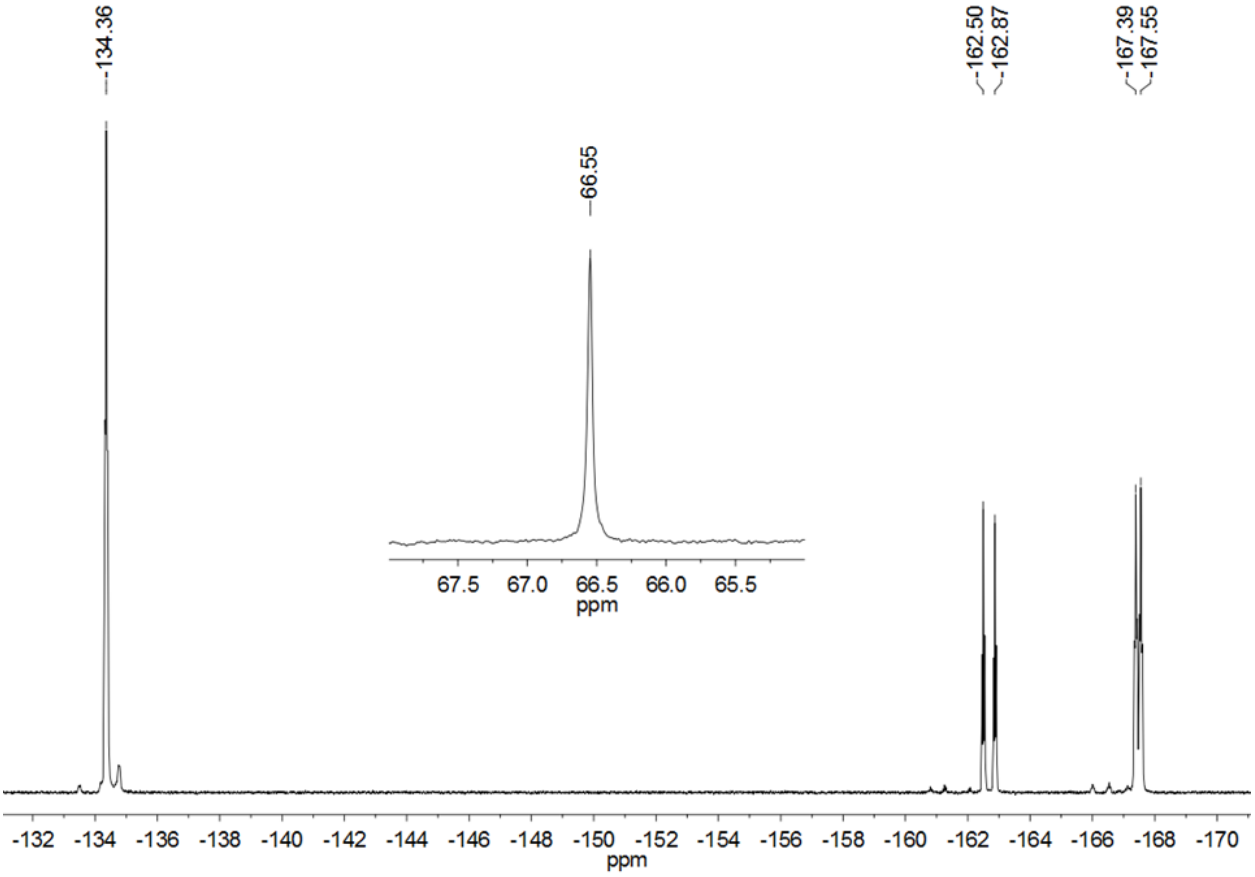


Figure 5.4. ^{19}F NMR spectrum of $Et_4N[H\mathbf{5.1}(BAr^{F}_{3})_2]$ in CD_2Cl_2 displaying two sets of inequivalent *p*-F and *m*-F signals of $CNBAr^{F}_{3}^{-}$. Inset: ^{31}P NMR spectrum of $Et_4N[H\mathbf{5.1}(BAr^{F}_{3})_2]$ in CD_2Cl_2.

The IR spectrum of $Et_4N[H\mathbf{5.2}(BAr^{F}_{3})_2]$ was similar to that of $Et_4N[H\mathbf{5.1}(BAr^{F}_{3})_2]$ (ν_{CN} = 2158, 2131 cm^{-1}; ν_{CO} = 1952 cm^{-1}) supporting the presence of two $CNBAr^{F}_{3}^{-}$ and one CO ligand (Figure 5.5). As with $Et_4N[H\mathbf{5.1}(BAr^{F}_{3})_2]$, the arrangement of the $CNBAr^{F}_{3}^{-}$ ligands on the Fe of $Et_4N[H\mathbf{5.2}(BAr^{F}_{3})_2]$ are assigned to the a/b arrangement as indicated by two inequivalent BAr^{F}_{3} environments in the ^{19}F NMR spectrum. The ^{31}P NMR spectrum of $Et_4N[H\mathbf{5.2}(BAr^{F}_{3})_2]$ displayed a singlet at δ 85.1 (Figure 5.6).

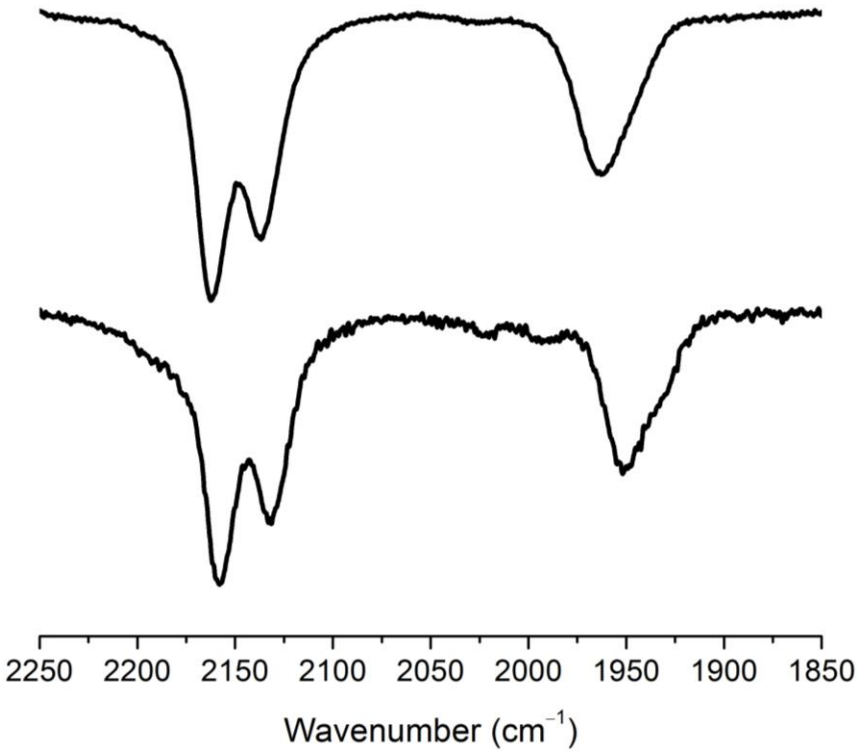


Figure 5.5. IR spectra of [H**5.1**(BAr^F_3)$_2$]$^-$ (top) and [H**5.2**(BAr^F_3)$_2$]$^-$ (bottom) in CH_2Cl_2.

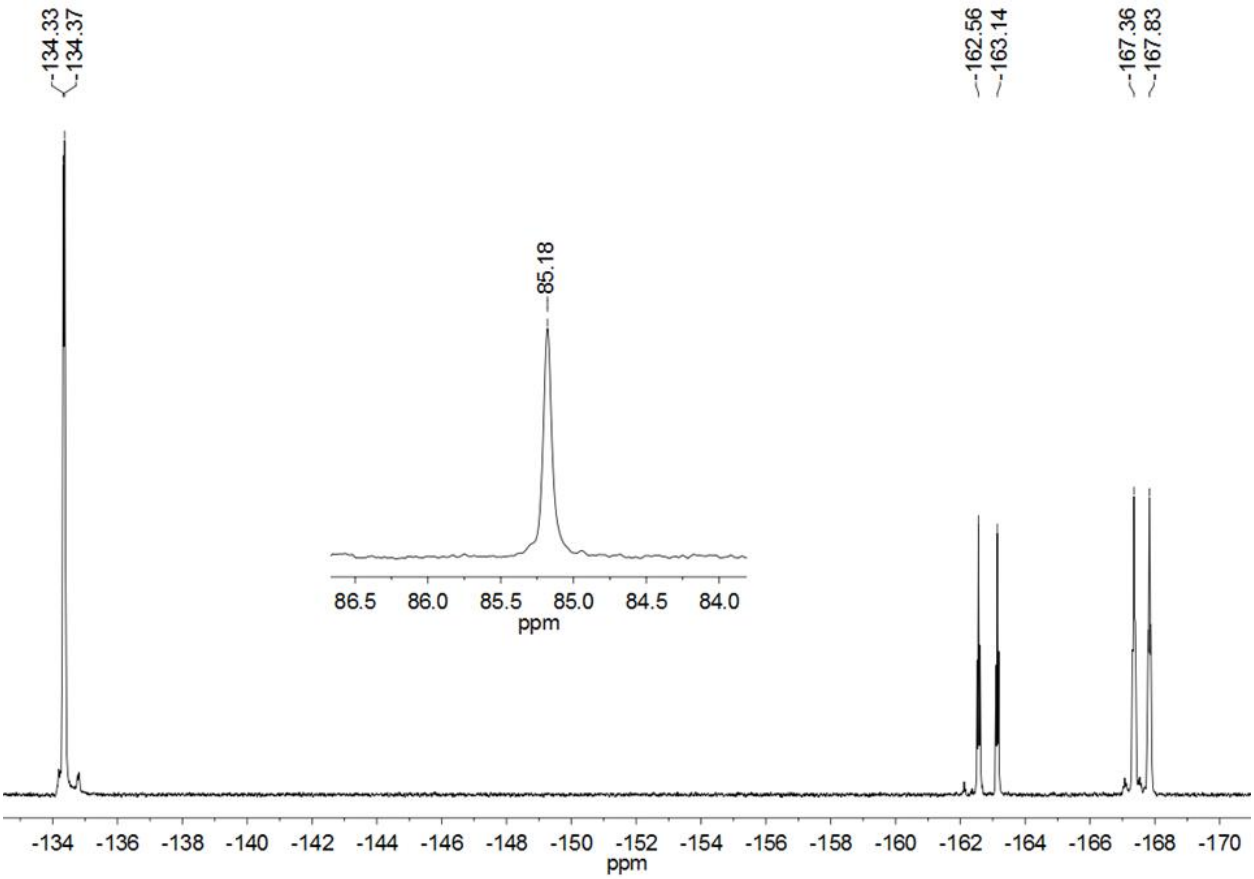


Figure 5.6. ^{19}F NMR spectrum of $Et_4N[H$**5.2**$(BAr^F{}_3)_2]$ in CD_2Cl_2 displaying two sets of inequivalent *p*-F and *m*-F signals of $CNBAr^F{}_3{}^-$. Inset: ^{31}P NMR spectrum of $Et_4N[H$**5.2**$(BAr^F{}_3)_2]$ in CD_2Cl_2.

Although the $CNBAr^F{}_3{}^-$ ligands on Fe are in an a/b arrangement thus making the compound asymmetric, the ^{31}P NMR spectra of $Et_4N[H$**5.1**$(BAr^F{}_3)_2]$ and $Et_4N[H$**5.2**$(BAr^F{}_3)_2]$ display singlets. The ^{31}P NMR singlets arise from rapid rotation of the diphosphine on the Ni centers. Lowering the temperature of samples of $Et_4N[H$**5.1**$(BAr^F{}_3)_2]$ and $Et_4N[H$**5.2**$(BAr^F{}_3)_2]$ is expected to slow the rotation of the diphosphine, resulting in the ^{31}P NMR spectra displaying two signals from the inequivalent phosphine centers. The ^{31}P NMR spectrum of CD_2Cl_2 solutions of $Et_4N[H$**5.1**$(BAr^F{}_3)_2]$ at –90 °C displayed two broad signals at δ 73 and δ 64 (Figure 5.7).

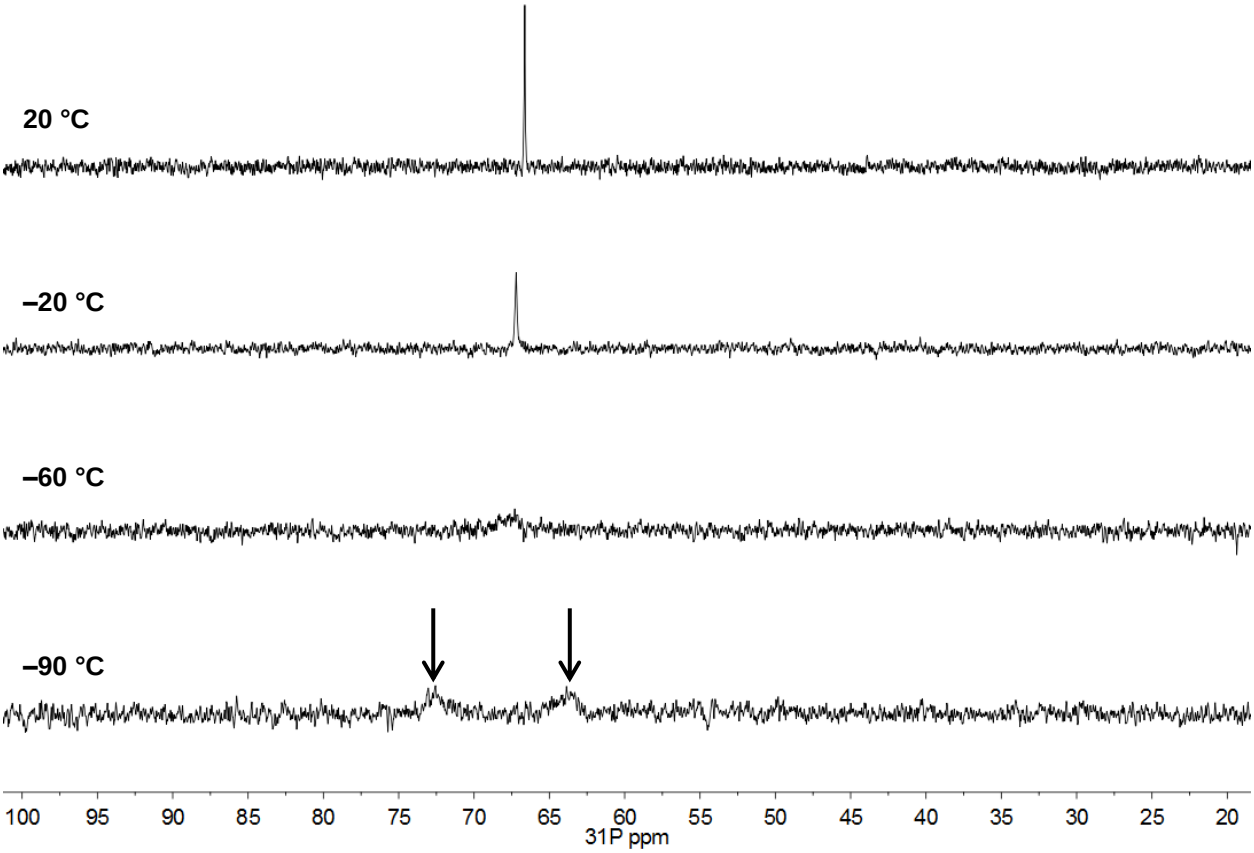


Figure 5.7. Variable temperature ^{31}P NMR of Et_4N[H**5.1**(BAr^F_3)$_2$] in CD_2Cl_2.

5.3 Structure of Et_4N[(CO)($CNBAr^F_3$)$_2$Fe(H)(pdt)Ni(dppe)]

Crystals of Et_4N[H**5.1**(BAr^F_3)$_2$] suitable for X-ray crystallography were grown from CH_2Cl_2 and hexanes. The crystallographic analysis supports the assignment of the $CNBAr^F_3{}^-$ ligands in an a/b arrangement on Fe (Figure 5.8). The hydride was located on the difference map and refined isotropically. The Fe-H distance of 1.51(3) Å was noticeably shorter than the Ni-H distance of 1.71(3) Å. The asymmetric metal hydride distances are known for NiFe hydrides.[8,15,16] The Ni···Fe distance of 2.5497(5) Å matches well with the reported distances found in the Ni-C/R states of the active site (2.57, 2.59 Å).[17,18] The Fe-CN distances are similar in Et_4N[H**5.1**(BAr^F_3)$_2$] and its precursor **4.1**(BAr^F_3)$_2$. A shorter Fe-CO bond is observed in Et_4N[H**5.1**(BAr^F_3)$_2$] (1.758(3) Å) than in **4.1**(BAr^F_3)$_2$ (1.819(2) Å, 1.821(3) Å). The Ni-P distances of Et_4N[H**5.1**(BAr^F_3)$_2$] are noticeably short (2.1382(8) Å, 2.1591(8) Å), similar to Ni-P distances reported for low valent Ni complexes.[19] However, similar Ni-P distances have been reported in the related Ni(II)Fe(II) complexes $(CO)_2(CN)_2$Fe(pdt)Ni(dppe) (2.196(1) Å, 2.181(1) Å) and **4.1**(BAr^F_3)$_2$ (2.179(1)

Å, 2.185(1) Å).[20,21] The NiS_2P_2 center adopts is in a distorted square planar geometry, reminiscent of the active site in [NiFe]-H_2ase. The NiP_2 plane has a 34.53° twist angle with respect to the NiS_2 plane.

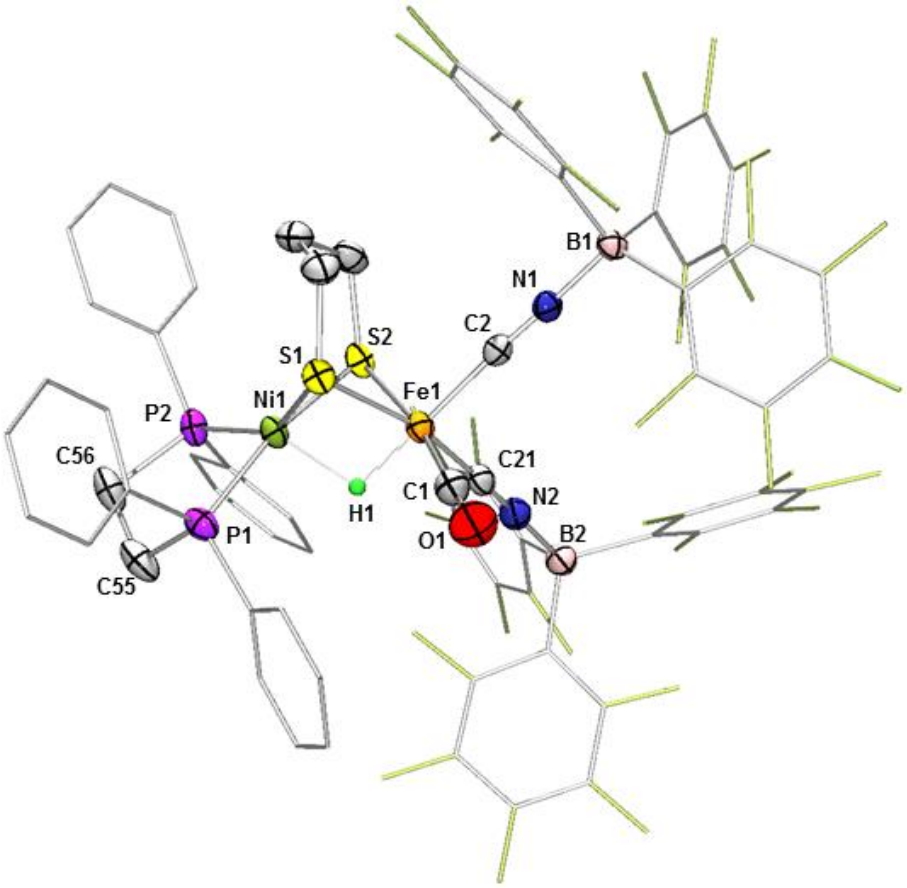


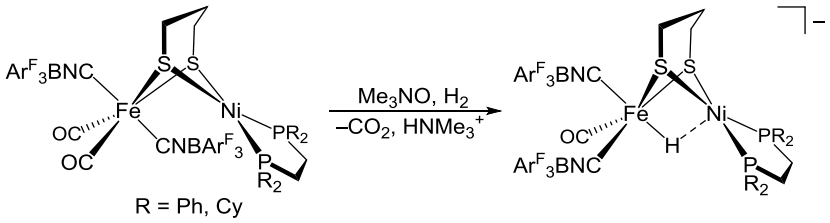
Figure 5.8. X-ray crystal structure of [H**5.1**$(BAr^F_3)_2$]$^-$ shown at 50% probability. H atoms (except for H1) were omitted for clarity. Phenyl and perfluorophenyl rings are shown as lines for clarity.

5.4 Formation of Hydrides from H_2

Some metal hydrides that are formed by hydride transfer from BH_4^- to an unsaturated metal center can also be generated from the heterolytic splitting of H_2.[14,22] As [H**5.1**$(BAr^F_3)_2$]$^-$ and [H**5.2**$(BAr^F_3)_2$]$^-$ are generated by hydride transfer from BH_4^-, the NiFe hydrides might also form from H_2. Indeed, treatment of **4.1**$(BAr^F_3)_2$ with Me_3NO under H_2 formed [H**5.1**$(BAr^F_3)_2$]$^-$ as observed by ^{1}H NMR and IR spectroscopy (Scheme 5.5). The anionic hydride complex was isolated at the Et_4N^+ salt after cation exchange with Et_4NCl. The yields of Et_4N[H**5.1**$(BAr^F_3)_2$] were similar for both the Me_3NO/Et_4NBH_4 and Me_3NO/H_2 routes. The use of D_2 gas gave the corresponding deuteride [D**5.1**$(BAr^F_3)_2$]$^-$ (^{2}H NMR: δ –7.34), confirming that H_2 is the source of the H^- ligand. The heterolytic splitting of H_2 suggests that the Me_3N present after decarbonylation serves as the proton acceptor. The formation of

[H**5.2**(BAr^F_3)$_2$]$^-$ also occurred by the decarbonylation of **4.2**(BAr^F_3)$_2$ in the presence of H_2. The use of H_2 instead of BH_4^- as a hydride source selectively gave [H**5.2**(BAr^F_3)$_2$]$^-$ as the only hydride product.

Scheme 5.5. Formation of [(CO)($CNBAr^F_3$)$_2$Fe(H)(pdt)Ni(dxpe)]$^-$ from H_2.



5.5 Reactivity Studies of Et_4N[(CO)($CNBAr^F_3$)$_2$Fe(H)(pdt)Ni(dxpe)] with Acid

Unlike previous cationic NiFe hydrides [$(CO)_{3-n}(L)_n$Fe(H)(pdt)Ni(dxpe)]$^+$ which have pK_a^{MeCN} around 14,[16] Et_4N[H**5.1**(BAr^F_3)$_2$] did not deprotonate, even in the presence of excess DBU (1,8-diazabicycloundec 7-ene, pK_a^{MeCN} = 24.34).[23] Furthermore, Et_4N[H**5.1**(BAr^F_3)$_2$] did not undergo H^+/D^+ exchange with D_2O as established by ^{1}H NMR spectroscopy.

Treatment of Et_4N[H**5.1**(BAr^F_3)$_2$] and Et_4N[H**5.2**(BAr^F_3)$_2$] with strong acids were found to release H_2. The reaction of Et_4N[H**5.1**(BAr^F_3)$_2$] with $PhNH_3BAr^{F24}$ (pK_a^{MeCN} = 10.62)[23] afforded quantitative yield of H_2 by gas chromatography (Figure 5.9). Treatment of Et_4N[H**5.2**(BAr^F_3)$_2$] with Ph_3NHBAr^{F24} also produced H_2 but only in a 50% yield.

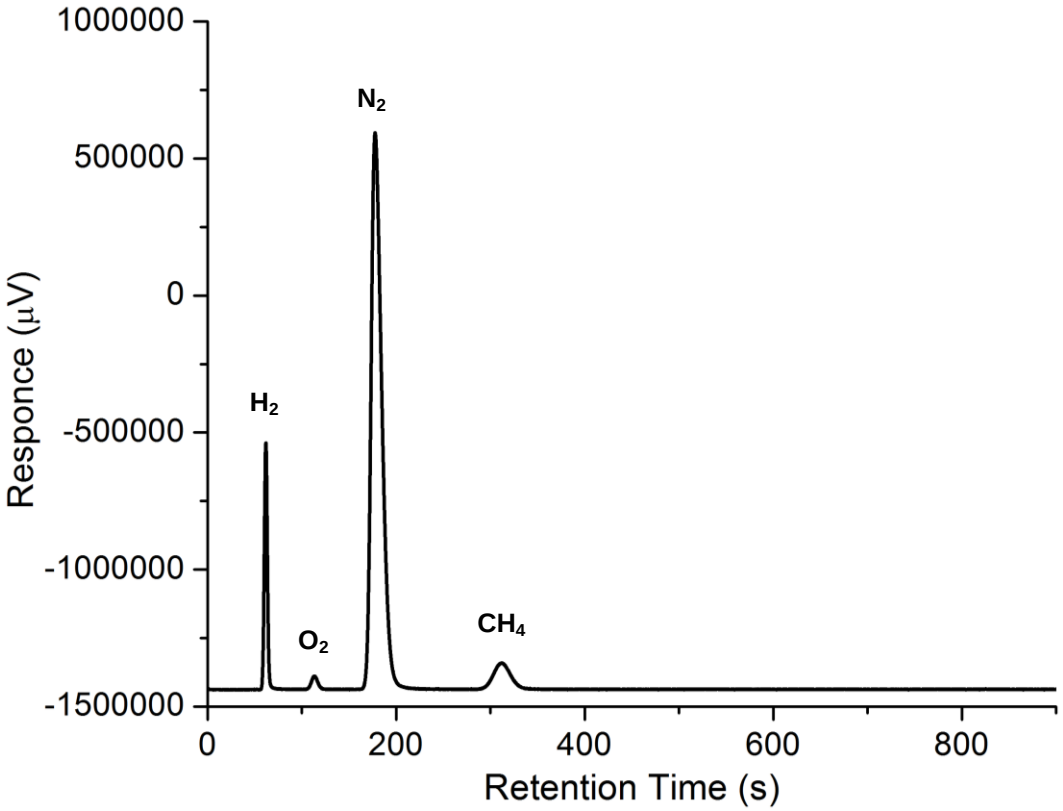
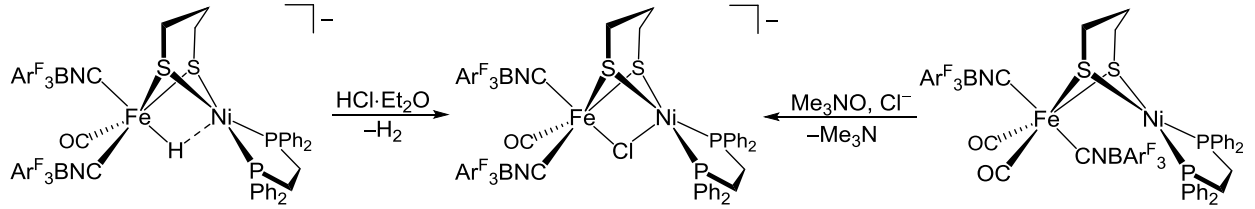


Figure 5.9. Gas chromatography trace from the headspace of the reaction of $Et_4N[H\mathbf{5.1}.(BAr^F{}_3)_2]$ with Ph_3NHBAr^{F24} in CH_2Cl_2 with added CH_4 as internal standard.

In order to trap the NiFe species formed upon release of H_2, HCl was used as a proton source as the chloride is expected to bind to the coordinatively unsaturated product. Indeed treatment of a solution of $Et_4N[H\mathbf{5.1}(BAr^F{}_3)_2]$ with HCl·Et_2O (pK_a^{MeCN} = 10.30),[24] gave H_2 and the complex $Et_4N[(CO)(CNBAr^F{}_3)_2Fe(Cl)(pdt)Ni(dppe)]$, $Et_4N[Cl\mathbf{5.1}(BAr^F{}_3)_2]$ (Scheme 5.6). The salt $Et_4N[Cl\mathbf{5.1}(BAr^F{}_3)_2]$ was prepared independently by treatment of $\mathbf{4.1}(BAr^F{}_3)_2$ with Me_3NO in the presence of Et_4NCl. The IR spectrum displayed two ν_{CN} bands at 2181 and 2149 cm^{-1} along with a single ν_{CO} band at 1996 cm^{-1}. Much like the hydrides, $Et_4N[Cl\mathbf{5.1}(BAr^F{}_3)_2]$ formed as the a/b isomer with inequivalent $CNBAr^F{}_3$ ligands according to ^{19}F NMR analysis. Unlike the hydrides $Et_4N[H\mathbf{5.1}(BAr^F{}_3)_2]$ or $Et_4N[H\mathbf{5.2}(BAr^F{}_3)_2]$ which display a singlet in the ^{31}P NMR, the ^{31}P NMR spectrum of the chloride $Et_4N[Cl\mathbf{5.1}(BAr^F{}_3)_2]$ displayed an AB quartet (δ –51.5, –48.6, $^2J_{PP}$ = 29 Hz) indicative of slow rotation of the diphosphine on Ni on the NMR time scale (Figure 5.10). The increased basicity of Cl^- compared to H^- forms a strong Ni-Cl bond, hindering rotation of the diphosphine on Ni.

Scheme 5.6. Formation of [Cl**5.1**(BAr^F_3)$_2$]$^-$ via protonation of [H**5.1**(BAr^F_3)$_2$]$^-$ with HCl·Et_2O and decarbonylation of **4.1** in the presence of Cl^-.



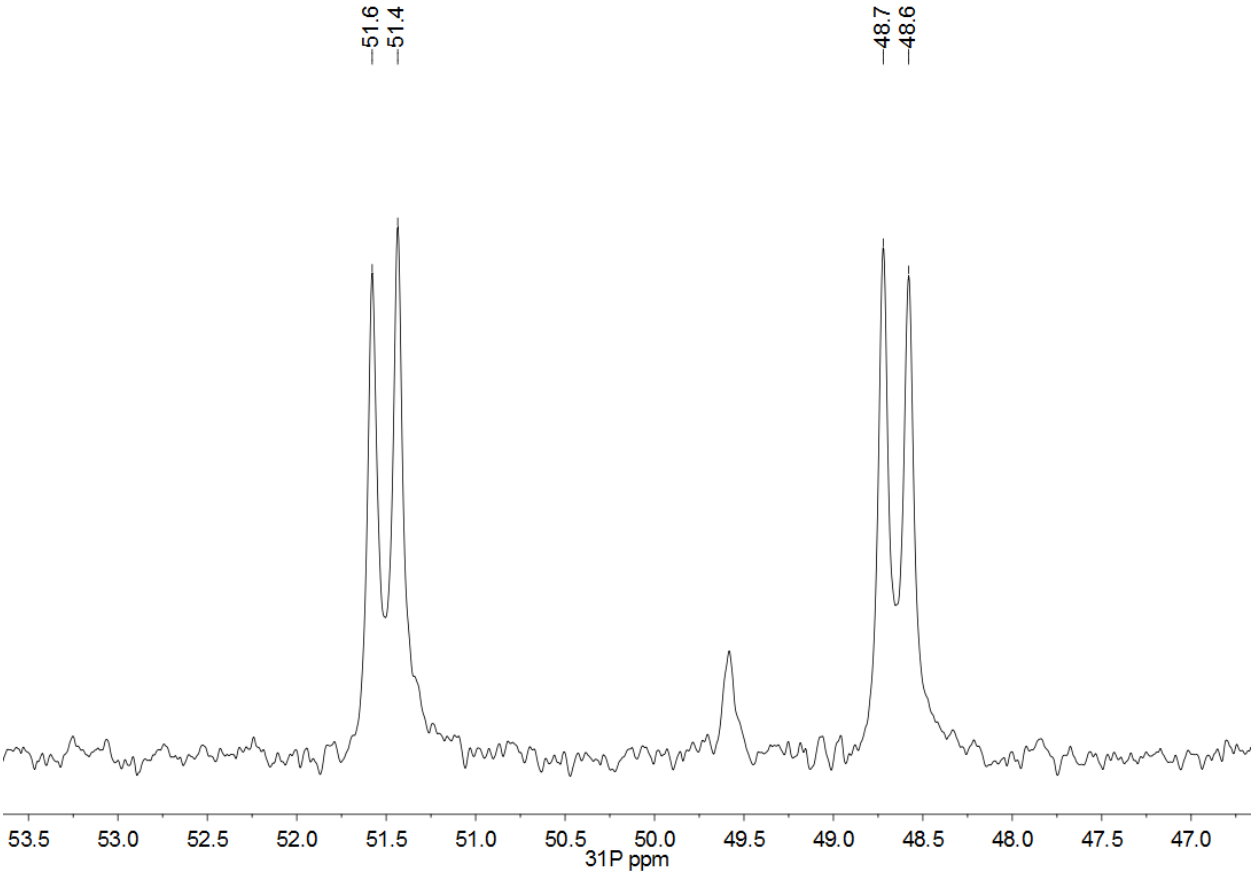


Figure 5.10. ^{31}P NMR spectrum of Et_4N[Cl**5.1**(BAr^F_3)$_2$] in CD_2Cl_2. An unknown byproduct is present at δ 49.5.

The hydride ^1H chemical shifts of [H**5.1**(BAr^F_3)$_2$]$^-$ and [H**5.2**(BAr^F_3)$_2$]$^-$ were sensitive to the counter ion. The initial hydride signals of [H**5.1**(BAr^F_3)$_2$]$^-$ and [H**5.2**(BAr^F_3)$_2$]$^-$ when formed from the Me_3NO/H_2 route were broad and shifted to slightly higher fields than when formed from Me_3NO/BH_4^- route. Cation exchange of the reaction mixture by the Me_3NO/H_2 route with Et_4NCl returned the hydride signals to the previously observed chemical shifts for Et_4N[H**5.1**(BAr^F_3)$_2$] and Et_4N[H**5.2**(BAr^F_3)$_2$] (Figure 5.11).

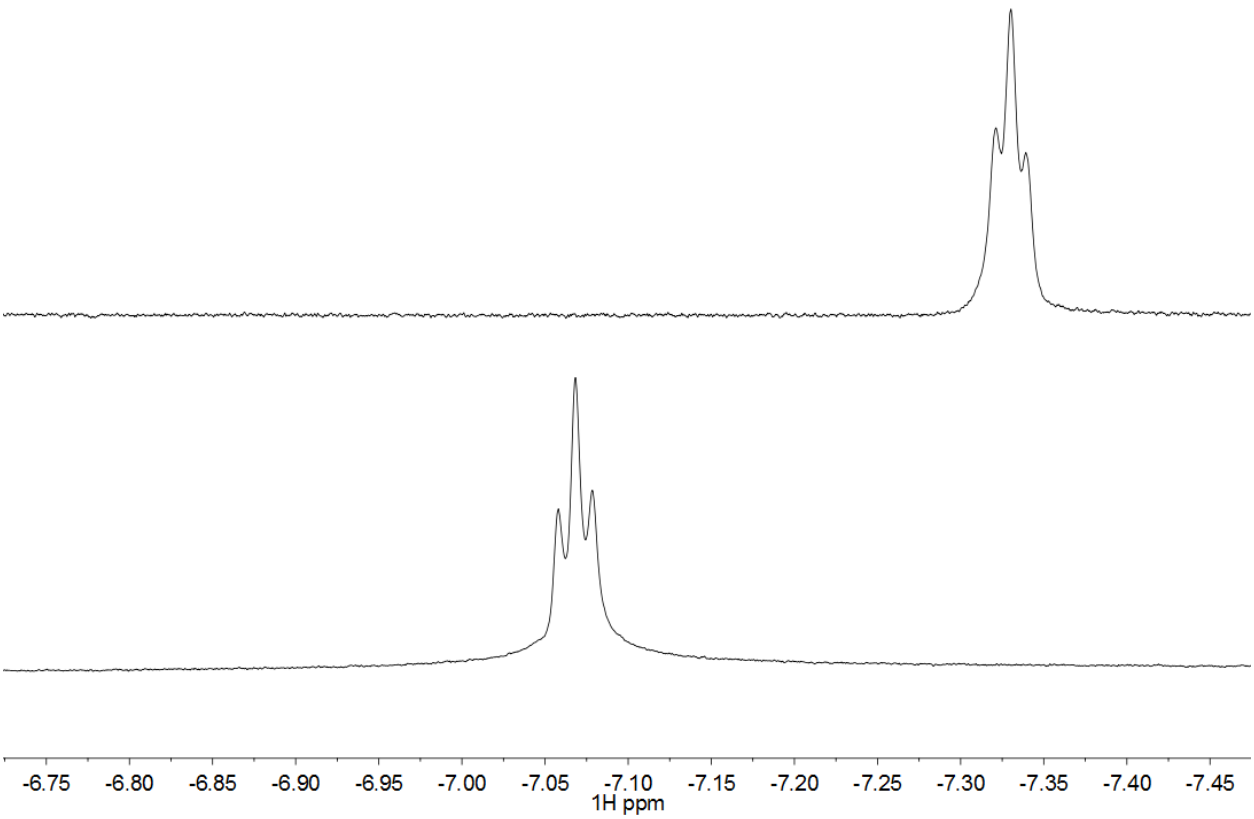
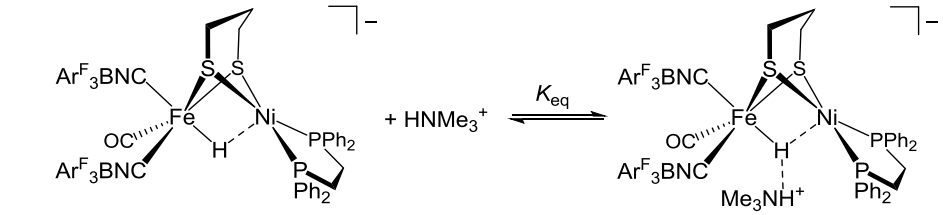


Figure 5.11. High field region of the ^{1}H NMR spectra of a crude sample in CD_2Cl_2 of [H**5.1**$(BAr^F{}_3)_2]^-$ generated from H_2 before (top) and after (bottom) ion exchange with Et_4NCl.

The shift of the hydride signal observed upon ion exchange suggested an interaction between the hydride and Me_3NH^+, a proposed byproduct from the heterolyic cleavage of H_2. Indeed, treatment of a CD_2Cl_2 solution of Et_4N[H**5.1**$(BAr^F{}_3)_2$] with Me_3NHBAr^{F24} (pK_a^{MeCN} = 17.61)[25] induced a shift of the hydride signal up field (Figure 5.12). Additional equivalents of acid caused further shifting before plateauing around δ –9. This observation is indicative of the formation of a dihydrogen bond, the interaction between a proton and a hydride, an intermediate in the formation and heterolytic cleavage of H_2. The shift of the hydride signal is related to the equilibrium constant for the formation of the dihydrogen bond (Scheme 5.7). The equilibrium constant was calculated by plotting change in the hydride signal of Et_4N[H**5.1**$(BAr^F{}_3)_2$] versus amount of added Me_3NHBAr^{F24} and fit to eq. 5.1.[26]

Scheme 5.7. Equilibrium of dihydrogen bond formation between [H**5.1**($BAr^F{}_3$)$_2$]$^-$ and $HNMe_3^+$



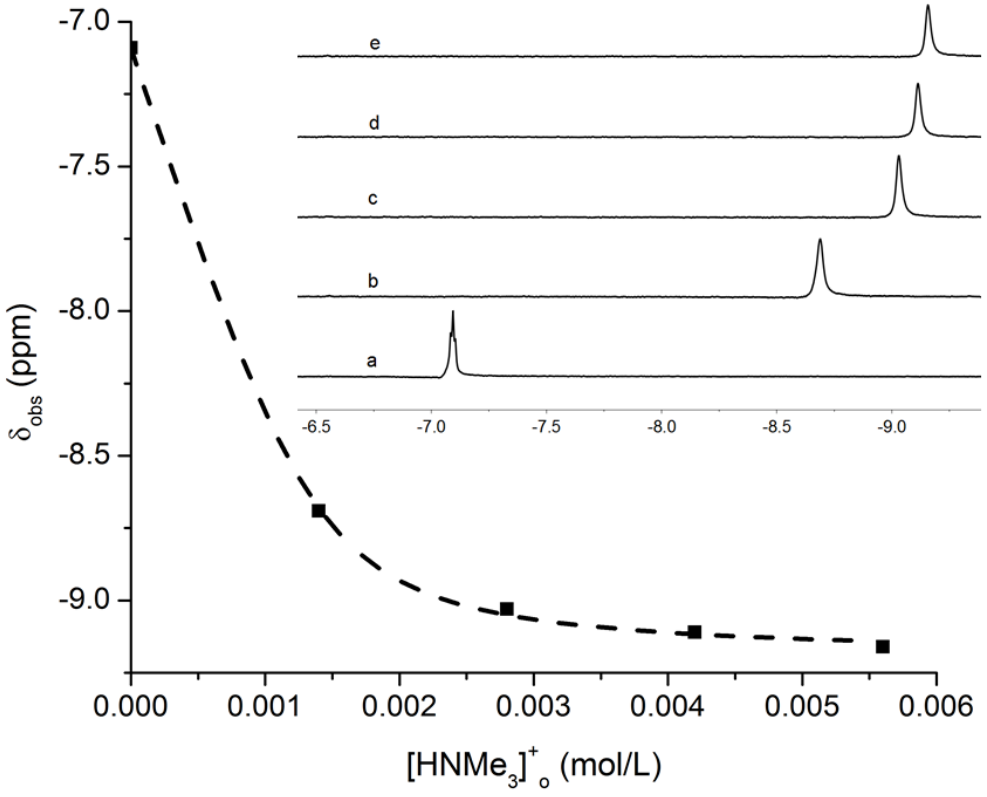


Figure 5.12. Plot of the observed hydride chemical shift (δ_{obs}) of Et_4N[H**5.1**($BAr^F{}_3$)$_2$] versus concentration of Me_3NHBAr^{F24} in CD_2Cl_2. Inset: ^{1}H NMR spectra of Et_4N[H**5.1**($BAr^F{}_3$)$_2$] after the addition of a) 0 equivalent b) 1 equivalent, c) 2 equivalents, d) 3 equivalent, e) 4 equivalent of Me_3NHBAr^{F24}.

$$\delta_{obs} = \delta_{MH} + \frac{1}{2[MH]_o}(\delta_{MHHN} - \delta_{MH})$$
$$\left[([MH]_o + [HN]_o + {}^1/_K) - \sqrt{([MH]_o + [HN]_o + {}^1/_K)^2 - 4[MH]_o[HN]_o}\right] \quad (5.1)$$

δ_{obs} = Observed hydride chemical shift of in the presence of $HNMe_3^+$
δ_{MH} = Hydride chemical shift of [H**5.1**$(BAr^F{}_3)_2]^-$ in the absence of $HNMe_3^+$
δ_{MHHN} = Hydride chemical shift of [H**5.1**$(BAr^F{}_3)_2]^-$ in the presence of excess $HNMe_3^+$
$[MH]_o$: Initial concentration of [H**5.1**$(BAr^F{}_3)_2]^-$
$[HN]_o$: Initial concentration of $HNMe_3^+$
K = Equilibrium constant for formation of a dihydrogen bond between [H**5.1**$(BAr^F{}_3)_2]^-$ and $HNMe_3^+$

From the fit, the equilibrium constant was calculated to be (9.0 ± 1.0) × 10^3 L/mol (20 °C). Treatment of Et_4N[H**5.2**$(BAr^F{}_3)_2$] with Me_3NHBAr^{F24} shifted and broadened the hydride signal further with fewer equivalents than observed for Et_4N[**5.1(**$BAr^F{}_3)_2$]. The use of the weaker acid [pyrrolidinium]BAr^{F24} (pK_a^{MeCN} = 19.56)[23] shifted the hydride signal of Et_4N[**5.2(**$BAr^F{}_3)_2$] to a lesser extent. The addition of D_2 to a mixture of Et_4N[H**5.1**$(BAr^F{}_3)_2$] and Me_3NHBAr^{F24} generated H_2 and small amounts of HD over a period of several hours.

5.6 Electrochemical Studies

The electrochemical properties of Et_4N[H**5.1**$(BAr^F{}_3)_2$] and Et_4N[H**5.2**$(BAr^F{}_3)_2$] were explored by cyclic voltammetry. A reversible reduction of Et_4N[H**5.1**$(BAr^F{}_3)_2$] occurred at –1.99 V vs $Fc^{0/+}$, at least 0.5 - 0.7 V more reducing that previously reported cationic NiFe hydrides (Figure 5.13).[16] No reduction event was observed for Et_4N[H**5.2**$(BAr^F{}_3)_2$] within the potential window of CH_2Cl_2 (> –2.5 V vs $Fc^{0/+}$).[27] As a change on the ligand of Ni resulted in a large shift in reduction potential, the reduction is assigned as the Ni(II)Fe(II)/Ni(I)Fe(II) couple.

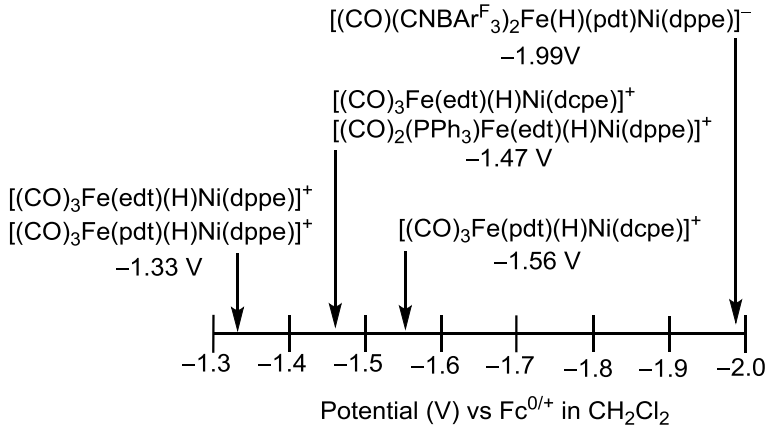


Figure 5.13. Reduction potentials of cationic NiFe hydrides and Et_4N[H**5.1**$(BAr^F{}_3)_2$].

As the catalytic cycle of [NiFe]-H_2ase involves oxidation of Ni(II)-H-Fe(II) (Ni-R state) to Ni(III)-H-Fe(II) (Ni-C state), the oxidation of the anionic hydrides was also studied. Oxidation of these compounds occurred at mild potentials as determined by cyclic voltammetry. A quasi-reversible oxidation of $Et_4N[H\mathbf{5.1}(BAr^F{}_3)_2]$ occurred at –0.08 V vs $Fc^{0/+}$ (i_{pc}/i_{pa} = 0.43, v = 0.1 V/s) while a quasi-reversible oxidation of $Et_4N[H\mathbf{5.2}(BAr^F{}_3)_2]$ occurred at –0.10 V vs $Fc^{0/+}$ (i_{pc}/i_{pa} = 0.69, v = 0.1 V/s) (Figure 5.14). The small change in oxidation potential between the compounds suggests that oxidation is Fe centered (i.e. Ni(II)Fe(II)/Ni(II)Fe(III)).

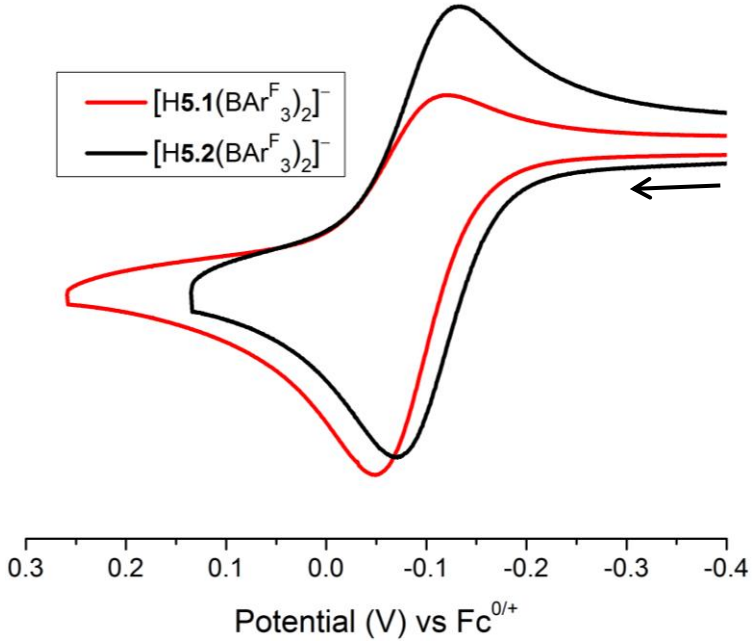


Figure 5.14. Cyclic voltammograms of the oxidation of $Et_4N[H\mathbf{5.1}(BAr^F{}_3)_2]$ (red) and $Et_4N[H\mathbf{5.2}(BAr^F{}_3)_2]$ (black) in CH_2Cl_2 with Bu_4NPF_6 (100 mM) at 0.1 V/s scan rate (25 °C).

Though oxidation of the hydrides is Fe centered, $Et_4N[H\mathbf{5.1}(BAr^F{}_3)_2]$ was still examined for use as an electrocatalyst for H_2 oxidation. The addition of the base DBU to a solution of $Et_4N[H\mathbf{5.1}(BAr^F{}_3)_2]$ under 1 atm of H_2 increased the current height of the oxidation wave at –0.08 V vs $Fc^{0/+}$ (Figure 5.15). This result is consistent with the regeneration of $Et_4N[H\mathbf{5.1}(BAr^F{}_3)_2]$ as an active species in the electrocatalytic activation of H_2. The rate was determined by use of eq. 5.2 upon plateauing of the current peak with a k_{obs} of 0.98 s^{-1}.[22]

$$\frac{i_{cat}}{i_p} = \frac{n}{0.4463}\sqrt{\frac{RTk_{obs}}{Fv}} \quad (5.2)$$

i_{cat} = catalytic current measured in the presence of base and H_2
i_p = peak current for the oxidation of $Et_4N[H\mathbf{5.1}(BAr^F{}_3)_2]$
n = number of electrons
R = ideal gas constant (J/mol K)
T = temperature (K)
k_{obs} = catalytic rate, turnover frequency (1/s)
F = Faraday constant (C/mol)
v = scan rate (V/s)

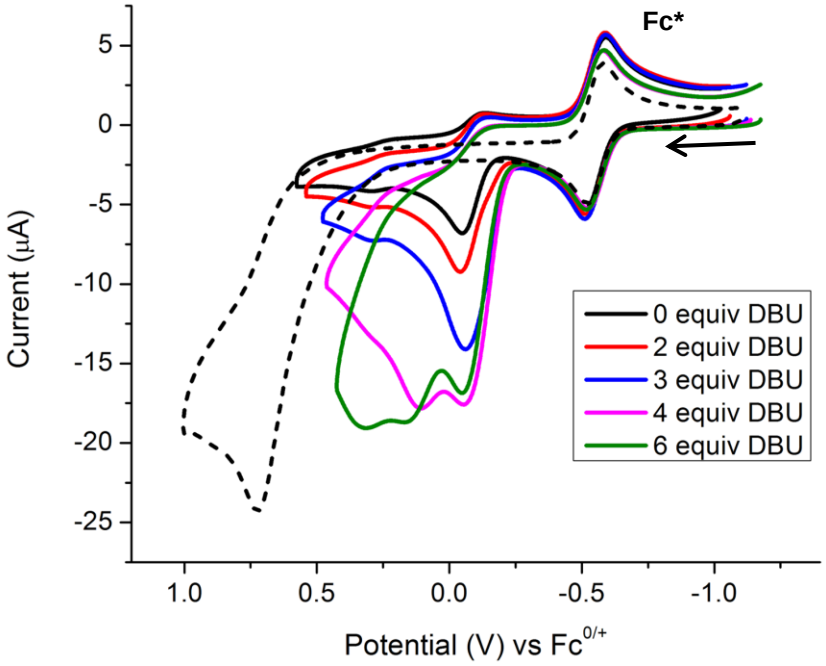


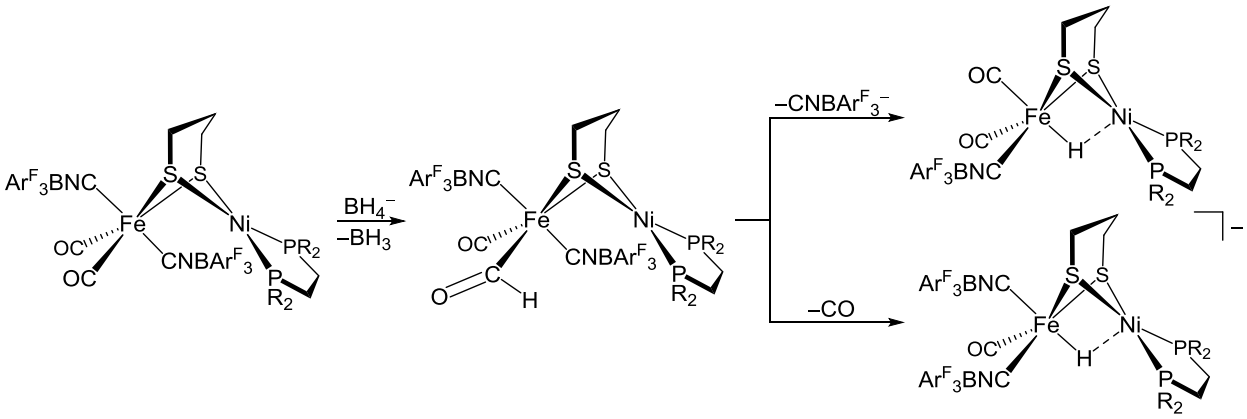
Figure 5.15. Cyclic voltammogram of the oxidation of $Et_4N[H\mathbf{5.1}(BAr^F{}_3)_2]$ in CH_2Cl_2 with increasing amounts of DBU under 1 atm of H_2 at a scan rate of 0.05 V/s (25°C). Decamethylferrocene (Fc*) was used as an internal reference (–0.55 V vs $Fc^{0/+}$). 6 equiv. of DBU under 1 atm of H_2 in the absence of catalyst is shown as a dashed black line.

5.7 Discussion

The formation of hydrides from $(CO)_2(CNBAr^F{}_3)_2Fe(pdt)Ni(dxpe)$ occurred from either hydride transfer from BH_4^- or by heterolytic cleavage of H_2 after treating **4.1**$(BAr^F{}_3)_2$ or **4.2**$(BAr^F{}_3)_2$ with a decarbonylating agent. Addition of only BH_4^- to **4.1**$(BAr^F{}_3)_2$ produced $[H\mathbf{5.1}(BAr^F{}_3)_2]^-$ along with other hydride containing products thought to be the monocyanide product $(CO)_2(CNBAr^F{}_3)Fe(H)(pdt)Ni(dppe)$. The addition of main group hydrides to metal carbonyl compounds generates metal formyl complexes.[28] Migration of the hydride from the formyl to the metal center displaces a ligand, forming a metal hydride.[29] As shown in Chapter 3, the $CNBAr^F{}_3^-$ ligand can be

prone to ligand displacement. Displacement of $CNBAr^F{}_3^-$ upon migration of the hydride from formyl would result in the generation of $(CO)_2(CNBAr^F{}_3)Fe(H)(pdt)Ni(dppe)$ (Scheme 5.8).

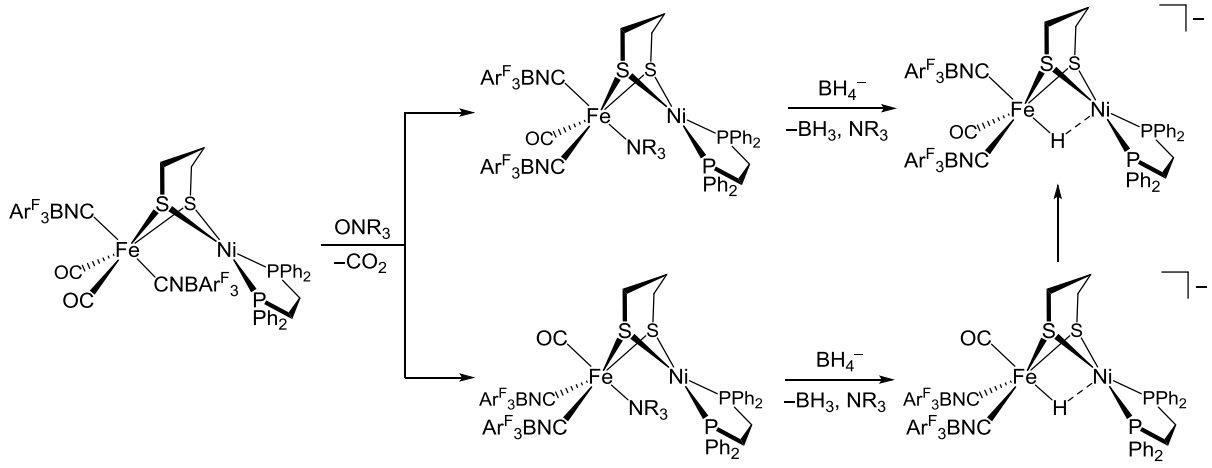
Scheme 5.8. Proposed mechanism for the formation of $[H\mathbf{5.1}(BAr^F{}_3)_2]^-$ and $(CO)_2(CNBAr^F{}_3)Fe(H)(pdt)Ni(dppe)$ from the reaction of $\mathbf{4.1}(BAr^F{}_3)_2$ upon treatment with BH_4^- via a formyl intermediate.



The use of a decarbonylating agent improved the selectivity towards forming $[H\mathbf{5.1}(BAr^F{}_3)_2]^-$ by generating a dicyanide intermediate which may be have a coordination site that is vacant or coordinated by a labile amine. The presence of a vacant coordination site on the metal allows for direct transfer of a single hydride from BH_4^- to the Fe center without forming a formyl intermediate.

The ratio of the a/b and b/b isomers of $[H\mathbf{5.1}(BAr^F{}_3)_2]^-$ generated from R_3NO/BH_4^- was sensitive to the decarbonylating agent. The use of Me_3NO formed a/b as the major isomer of $[H\mathbf{5.1}(BAr^F{}_3)_2]^-$ while the use of NMO formed b/b as the major isomer of $[H\mathbf{5.1}(BAr^F{}_3)_2]^-$. IR spectroscopy studies of the decarbonylated intermediates suggest that Me_3NO results in the major isomer has an a/b arrangement of the $CNBAr^F{}_3^-$ ligands while NMO results in the major isomer of the decarbonylated intermediate with the $CNBAr^F{}_3^-$ ligands in a b/b arrangement (Scheme 5.9). As treatment of the decarbonylated intermediates with BH_4^- forms both the a/b and b/b isomers of $[H\mathbf{5.1}(BAr^F{}_3)_2]^-$ it is likely that both an a/b and b/b isomer of the decarbonylated intermediate is present in solution. As the different major isomers of the decarbonylated agents are unlikely to be due to steric effects as Me_3N and N-methylmorpholine are of similar size, the difference may result from the difference in the basicity of the amines with Me_3N as a stronger base than N-methylmorpholine.[30] By trans-influence, also known as the structural trans-effect, stronger σ-donors would be thermodynamically preferred to be *trans* to stronger π-acceptor ligands.[31] The preference for a stronger donor ligand to be *trans* to an acceptor ligand implies that $CNBAr^F{}_3^-$ may be a better π-acceptor ligand than CO. This is further supported by the thermodynamically preferred isomer of $[H\mathbf{5.1.}(BAr^F{}_3)_2]^-$ being the a/b isomer in which the hydride is *trans* to $CNBAr^F{}_3^-$.

Scheme 5.9. Proposed mechanism for the formation of $[H\mathbf{5.1}(BAr^F{}_3)_2]^-$ by the reaction of $\mathbf{4.1}(BAr^F{}_3)_2$ from amine oxide and BH_4^-.



The hydrides were also found to form by biologically relevant methods by the heterolytic cleavage of H_2 at moderate pressures at room temperature. The use of H_2 as a hydride source was milder and more selective for the generation of $[H\mathbf{5.2}(BAr^F{}_3)_2]^-$ from $\mathbf{4.2}(BAr^F{}_3)_2$ without the formation of the mono-cyanide hydride $(CO)_2(CNBAr^F{}_3)Fe(H)(pdt)Ni(dcpe)$. The reaction of $\mathbf{4.2}(BAr^F{}_3)_2$ with decarbonylating agents is by comparison to $\mathbf{4.1}(BAr^F{}_3)_2$ slow and gives a mixture of products as indicated by IR spectroscopy. This mixture of decarbonyled intermediates with BH_4^- to form a mixture of hydride complexes. The selectivity of H_2 over BH_4^- for the formation of $[H\mathbf{5.2}(BAr^F{}_3)_2]^-$ as the only hydride complex likely arises from H_2 being a weaker hydride donor than BH_4^- and reacts only with a dicyanide intermediate to form $[H\mathbf{5.2}(BAr^F{}_3)_2]^-$.[32,33]

The hydrides $Et_4N[H\mathbf{5.1}(BAr^F{}_3)_2]$ and $Et_4N[H\mathbf{5.2}(BAr^F{}_3)_2]$ are the most biomimetic models of [NiFe]-H_2ase to date in terms of structure and reactivity. The ν_{CO} stretches of $Et_4N[H\mathbf{5.1}(BAr^F{}_3)_2]$ and $Et_4N[H\mathbf{5.2}(BAr^F{}_3)_2]$ occur at similar frequencies as the ν_{CO} stretches found in the Ni-R state of [NiFe]-H_2ase (Table 5.1).[34] The ν_{CO} of $Et_4N[H\mathbf{5.1}(BAr^F{}_3)_2]$ is 5 cm^{-1} higher than observed for the N-R state in *D. vulgaris*. The similar ν_{CO} frequencies suggests that the electron density on the Fe center in $Et_4N[H\mathbf{5.1}(BAr^F{}_3)_2]$ and $Et_4N[H\mathbf{5.2}(BAr^F{}_3)_2]$ closely matches the electron density on the Fe center in [NiFe]-H_2ase.

Table 5.1. IR Frequencies of the Ni-R state of [NiFe]-H_2ase and Model Compounds.

Compound	ν_{CN} (cm^{-1})	ν_{CO} (cm^{-1})
Ni-R state, *A. vinosum*	2072, 2059	1936
Ni-R state, *D. gigas*	2073, 2060	1940
Ni-R state, *D. fructosovorans*	2074, 2060	1938
Ni-R state, *D. vulgaris*	2074, 2061	1948
Et_4N[H**5.1**$(BAr^F_3)_2$]	2162, 2137	1963
Et_4N[H**5.2**$(BAr^F_3)_2$]	2158, 2132	1952

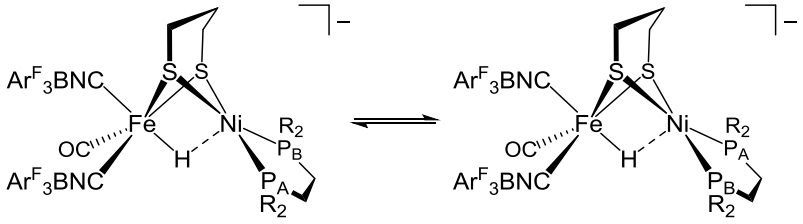
The structure of [H**5.1**$(BAr^F_3)_2]^-$ greatly resembled the X-ray structures of the active sites of [NiFe]-H_2ase in the reduced states (Table. 5.2).[17,18] The Ni···Fe distance of [H**5.1**$(BAr^F_3)_2]^-$ is very similar to the distance in the active site. The Fe center is bound by one CO ligands and two CN^- ligands as found in the enzyme, however the location of the CO and one $CNBAr^F_3{}^-$ ligand are interchanged compared to the enzyme. Furthermore the NiS_2P_2 twist in [H**5.1**$(BAr^F_3)_2]^-$ is reminiscent of the distorted NiS_4 environment of the native enzyme. A shorter Fe-H bond than Ni-H is observed in the structure of [H**5.1**$(BAr^F_3)_2]^-$. The asymmetrical M-H bonds in [H**5.1**$(BAr^F_3)_2]^-$ have been previously reported in other NiFe hydrides.[8,15,16]

Table 5.2. Key Distances (Å) and Angles (º) of [H**5.1**$(BAr^F_3)_2]^-$ and the Active Site of *D. vulgaris* Miyazaki F in the Reduced State(s).

	[H5.1$(BAr^F_3)_2]^-$	***D. vulgaris* Miyazaki F Ni-C/R (PDB: 1H2R)**	***D. vulgaris* Miyazaki F Ni-C/R (PDB: 1WUL)**
Fe···Ni	2.5497(5)	2.59	2.57
Fe-H	1.51(3)	N/A	N/A
Ni-H	1.71(3)	N/A	N/A
Fe-C_{apical}	1.889(3) ($CNBAr^F_3{}^-$)	1.84 (CO)	1.80 (CO)
Fe-C_{basal}	1.758(3) (CO), 1.866(2) ($CNBAr^F_3{}^-$)	1.86 (CO), 2.21 (SO)	1.99 (CN^-), 2.03 (CO)
Fe-S	2.3246(6), 2.2977(8)	2.29, 2.36	2.26, 2.32
Ni-S	2.1952(8), 2.3046(8)	2.43, 2.33	2.23, 2.52
Ni-term-L	2.1382(8), 2.1591(8) ($L = PR_3$)	2.32, 2.24 ($L = SR^-$)	2.13, 2.21 ($L = SR^-$)
C_{basal}-Fe-C_{basal}	94.0(1)	89	93
C_{basal}-Fe-C_{apical}	90.6(1), 96.0(1)	90, 98	90, 95

The NMR spectra of $Et_4N[H\mathbf{5.1}(BAr^F{}_3)_2]$ and $Et_4N[H\mathbf{5.2}(BAr^F{}_3)_2]$ reveal interesting details of the dynamics of these compounds in solution. Both compounds have an a/b arrangement of the $CNBAr^F{}_3{}^-$ ligands as indicated by two $BAr^F{}_3$ environments in ^{19}F NMR spectra but display singlets in the ^{31}P NMR spectra. The inequivalent $BAr^F{}_3$ signals indicate no rotation of ligands on the Fe center on the NMR time scale. The equivalence of the phosphine sites indicates that the Ni(diphosphine) center is nonridgid and undergoes rapid rotation on the NMR time scale (Scheme 5.10). Similar dynamics have been reported in related cationic NiFe hydrides.[15] This rotation suggests a weak Ni-H interaction. Strong interaction between Ni and a bridging ligand would slow rotation of the diphosphine, causing the disphosphine to display two signals in the ^{31}P NMR spectrum instead of a singlet. Such a situation is observed for $Et_4N[Cl\mathbf{5.1}(BAr^F{}_3)_2]$ which has inequivalent $CNBAr^F{}_3{}^-$ signals and inequivalent phosphine signals are present in the ^{19}F and ^{31}P NMR spectra respectively.

Scheme 5.10. Representation of Ni(diphosphine) dynamic processes of $[(CO)(CNBAr^F{}_3)_2Fe(H)(pdt)Ni(dxpe)]^-$.



Though previous cationic NiFe hydrides are protic,[15,16] $Et_4N[H\mathbf{5.1}(BAr^F{}_3)_2]$ and $Et_4N[H\mathbf{5.2}(BAr^F{}_3)_2]$ display hydridic character. Treatment of $Et_4N[H\mathbf{5.1}(BAr^F{}_3)_2]$ and $Et_4N[H\mathbf{5.2}(BAr^F{}_3)_2]$ with strong acids release H_2 while treatment with weak acids form a dihydrogen bond between the metal hydride and acid. Dihydrogen bonding is typically found in terminal hydrides.[35,36] The X-ray structure of [FeFe]-H_2ase model $[HFe(Hadt)(CO)_2(dppv)_2]^{2+}$ is characterized by both a terminal hydride and ammonium center that engage in dihydrogen bonding as apparent by the close FeH···HN distance of 1.88(7) Å but does not release H_2 until reduced.[37] A similar interaction has been characterized by neutron diffraction with a FeH···HN distance of 1.489(10) Å reported for $[Cp^{C6F4N}Fe(P^{tBu2}N^{tBu2}H)(H)]^+$.[38] Dihydrogen bonding for bridging hydrides is rare, and has only occurred when the hydride bridges very electron rich metal centers.[39] The crystal structure of the cluster $[Re_3(\mu\text{-}H)_4(CO)_9(HNMe_2)]^-$ is reported to have a close $Re_2(\mu\text{-}H)$ ···HN contact of 2.24 Å between one of the bridging hydrides and the proton of the dimethylamine ligand (Figure 5.16). The bridging hydrides of [FeFe]-H_2ase models are protic and do not undergo dihydrogen bonding, even with an intramolecular ammonium in position to form a dihydrogen bond.[40]

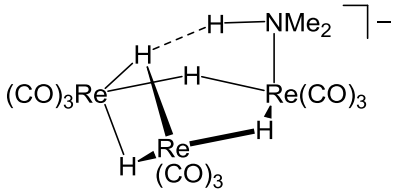
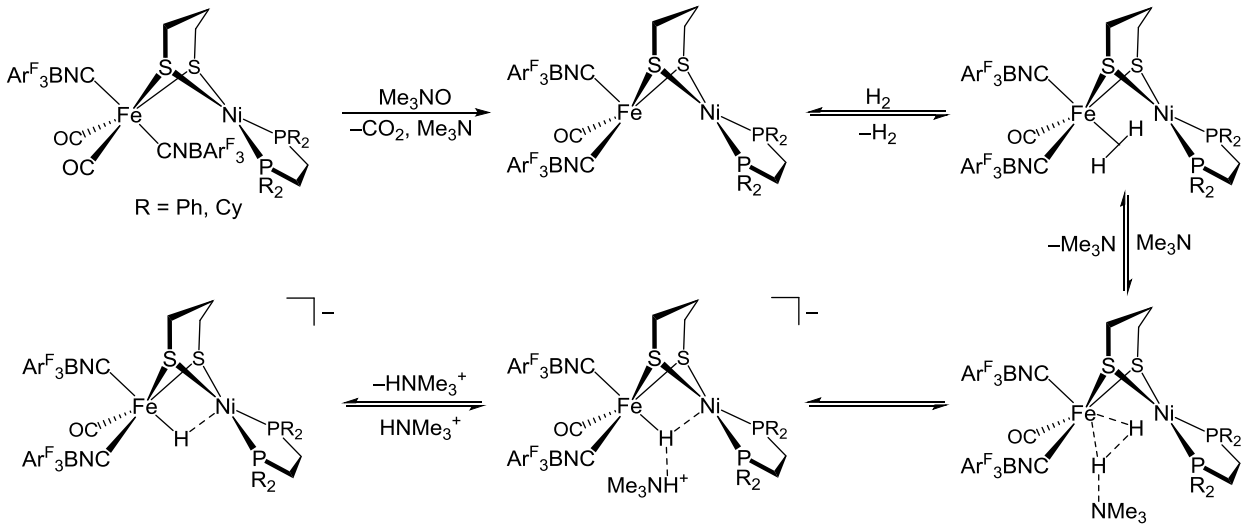


Figure 5.16. Structure of $[Re_3(\mu\text{-}H)_4(CO)_9(HNMe_2)]^-$ with dihydrogen bond between a bridging hydride and amine proton depicted.

Given the presence of dihydrogen bonding with weak acids, the hydrides $[H\mathbf{5.1}(BAr^F{}_3)_2]^-$ and $[H\mathbf{5.2}(BAr^F{}_3)_2]^-$ are best described as terminal Fe-H with a weak Ni-H interaction as opposed to a bridging hydride. As $[H\mathbf{5.1}(BAr^F{}_3)_2]^-$ and $[H\mathbf{5.2}(BAr^F{}_3)_2]^-$ resemble the Ni-R state of [NiFe]-H_2ase in both structure and reactivity, it is reasonable to conclude that the catalytic cycle of [NiFe]-H_2ase occurs by terminal hydrides similar to the catalytic cycle of [FeFe]-H_2ase.

The proposed mechanism for the activation of H_2 to form $[H\mathbf{5.1}(BAr^F{}_3)_2]^-$ and $[H\mathbf{5.2}(BAr^F{}_3)_2]^-$ is shown in Scheme 5.11. Protonation studies of $[(CO)(CNBAr^F{}_3)_2Fe(H)(pdt)Ni(dxpe)]^-$ elude to heterolytic splitting of H_2 to form the hydrides. Dihydrogen bond formation with weak acids is a known intermediate in heterolytic splitting of H_2. The treatment of the hydrides with HCl trapped the unsaturated species as the Ni(II)Fe(II) bridging chloride consistent with the metal centers maintaining 2+ oxidation state throughout H_2 activation and H_2 formation. Although homolytic splitting of H_2 at Fe followed by deprotonation of one hydride ligand would also result in Ni(II)(H)Fe(II), homolytic splitting of H_2 is unlikely as it would invoke in a seven-coordinate Fe(IV) intermediate.

Scheme 5.11. Proposed mechanism for the formation of $[H\mathbf{5.1}(BAr^F{}_3)_2]^-$ and $[H\mathbf{5.2}(BAr^F{}_3)_2]^-$ by H_2 activation.



In the catalytic cycle of [NiFe]-H_2ase, Ni undergoes redox involving Ni(II), Ni(III), and possibly Ni(I) oxidation states. The Fe maintains a 2+ oxidation state throughout the cycle. The lack of redox chemistry at Fe in [NiFe]-H_2ase may be due to the presence of both cyanide and carbonyl ligands, which enforces a low-spin Fe(II) state throughout the catalytic cycle. Maintaining of a Fe(II) state was observed for the reduction of the hydrides as a large shift in reduction potential was observed between dppe and dcpe (> 0.5 V) indicating a Ni(II)/ Ni(I) couple. It is unclear whether the reduction of the cationic NiFe hydrides $[(CO)_2(L)Fe(H)(pdt)Ni(dxpe)]^+$ is Ni- or Fe-centered.[16] The oxidation of $Et_4N[H\mathbf{5.1}(BAr^F{}_3)_2]$ and $Et_4N[H\mathbf{5.2}(BAr^F{}_3)_2]$ was found to occur at very similar potentials (ΔE_{ox} = 0.02 V). Given the small difference in oxidation potentials of the hydrides, the oxidation event is assigned to the Fe(II)/Fe(III) couple, the reverse of what is observed in Nature. Although oxidation occurs at Fe and not at Ni as observed in Nature, $Et_4N[H\mathbf{5.1}(BAr^F{}_3)_2]$ was found to serve as an electrocatalyst for the oxidation of H_2 in the presence of base, a first for [NiFe]-H_2ase models. Oxidation of H_2 was found to occur at a similar rate as previously reported Fe hydrides.[22] Catalytic oxidation of H_2 is rare for H_2ase models, and often occurs at rates too slow to observe by cyclic voltammetry.[11,14]

5.8 Conclusions

The hydrides $Et_4N[(CO)(CNBAr^F{}_3)_2Fe(H)(pdt)Ni(dxpe)]$ could be derived from coordination of Lewis acids to the nonfunctional [NiFe]-H_2ase models $(CO)_2(CN)_2Fe(pdt)Ni(dxpe)$. These hydrides exhibited similar reactivity to the Ni-R state of [NiFe]-H_2ase: formation of hydrides from heterolytic cleavage of H_2, formation of H_2 upon protonation of the hydride with acids via a dihydrogen bond, oxidation at mild potentials, and electrocatalytic oxidation of H_2 in the presence of a base. Though models of the Ni-R state are often thought of as bridging hydrides, the cationic hydrides $Et_4N[H\mathbf{5.1}(BAr^F{}_3)_2]$ and $Et_4N[H\mathbf{5.2}(BAr^F{}_3)_2]$ exhibit terminal hydride character previously unobserved in [NiFe]-H_2ase model complexes. It is then reasonable to infer that the Ni-R state of [NiFe]-H_2ase is best described as a terminal hydride and not a bridging hydride. It is currently not clear if [NiFe]-H_2ase functions by an Fe or Ni terminal hydride as the hydride could reside on either of the two metals.[41]

Although $Et_4N[H\mathbf{5.1}(BAr^F{}_3)_2]$ and $Et_4N[H\mathbf{5.2}(BAr^F{}_3)_2]$ greatly resemble the Ni-R state of [NiFe]-H_2ase, oxidation of the hydrides was found to occur at Fe and not at Ni as identified for Ni-R. Furthermore, it is reasonable to assume that oxidation in these models would occur at Fe if uncapped CN^- ligands were present in the model (i.e. $[(CO)(CN)_2Fe(H)(pdt)Ni(dxpe)]^-$). The uncapped CN^- ligands of $[(CO)(CN)_2Fe(H)(pdt)Ni(dxpe)]^-$ would make the Fe center more electron rich and therefore more prone to oxidation compared to $CNBAr^F{}_3{}^-$ ligated Fe sites of

$[(CO)(CNBAr^{F}_{3})_2Fe(H)(pdt)Ni(dxpe)]^-$. This result suggests that oxidation at Ni as seen in Nature may be favored over oxidation at Fe due to the coordination of four cysteinate ligands (two bridging, two terminal) to Ni in a SF_4 geometry. Therefore the ligand environment at Ni will need to be addressed in future model complexes in order to correctly model the catalytic cycle of [NiFe]-H_2ase.

5.9 Experimental Procedures

All procedures were carried out in a nitrogen-filled MBraun glovebox or using standard Schlenk techniques. All solvents were degassed by sparging with nitrogen and dried by passage through activated alumina. IR spectra were recorded on a Perkin-Elmer Spectrum 100. Elemental analyses were conducted at the University of Illinois, Microanalytical Laboratory. Cyclic voltammetry was performed under argon at room temperature using a CHI 630D potentiostat with glassy carbon working electrode, Pt wire counter electrode and the pseudoreference electrode Ag wire, and with Fc or Fc* as internal standard. Production of H_2 was quantified by gas chromatography on a column packed with 5 Å molecular sieves (carrier gas: Ar), using an Agilent 7820A instrument equipped with a thermal conductivity detector. The response factor for H_2/CH_4 was 3.8 under experimental conditions as established by calibration with standard H_2/CH_4 mixtures. NMR spectra were recorded on a Varian Unity 500 MHz NMR spectrometer. Signals for ^{19}F and ^{31}P NMR spectra were referenced using external standards of 1% $CFCl_3$ in $CDCl_3$ and 85% H_3PO_4, respectively. ^1H NMR spectra were referenced to internal solvent signals. CD_2Cl_2 (Cambridge Isotope Laboratories) was dried over CaH_2 before being vacuum distilled onto activated 4 Å molecular sieves.

$Et_4N[(CO)(CNBAr^{F}_{3})_2Fe(H)(pdt)Ni(dppe)]$, $Et_4N[H5.1(BAr^{F}_{3})_2]$. In a thick-walled glass pressure tube, a solution of **4.1**$(BAr^{F}_{3})_2$ (150 mg, 0.0857 mmol) in CH_2Cl_2 (10 mL) was frozen by inserting the tube into liquid nitrogen. Under a flow of Ar, a buffer layer of CH_2Cl_2 (5 mL) was frozen on top of the frozen solution of **4.1**$(BAr^{F}_{3})_2$. A solution of Me_3NO (7.7 mg, 0.103 mmol) in CH_2Cl_2 (2 mL) was frozen on top of the buffer layer. The head space was evacuated and refilled with 40 psig of H_2 followed by thawing of the frozen solution. After the mixture was stirred for 2 hours, the solvent was removed under vacuum, and the residue was extracted into Et_2O. The extract was filtered through Celite and analyzed by ^{19}F NMR spectroscopy, which showed that 60% of signals corresponded to product. A solution of this sample in 10 mL of CH_2Cl_2 was stirred with excess Et_4NCl (142 mg, 0.857 mmol). The solvent was removed under vacuum, and the product was extracted into 10 mL of THF, which was then filtered through Celite and evaporated. The solid was dissolved in a minimal amount of THF and loaded onto a column of neutral alumina (Brockmann Level IV) packed with THF. A red band eluted with THF and was

discarded. The remaining brown band was eluted off the column using CH_2Cl_2. The solution was concentrated to 5 mL, layered with 20 mL of pentane, and cooled to −30 °C yielding red crystals (44 mg, 28%). IR (CH_2Cl_2, cm^{-1}): ν_{CN} = 2162, 2137; ν_{CO} = 1963. ^{1}H NMR (CD_2Cl_2): δ −7.05 (t, $^2J_{HP}$ = 5.2 Hz). ^{31}P NMR (CD_2Cl_2): δ 66.6 (s). ^{19}F NMR (CD_2Cl_2): δ −134.4 (m, *o*-F); −162.5 (t, *p*-F); −162.9 (t, *p*-F); −167.4 (t, *m*-F); −167.6 (t, *m*-F). Anal. Calc. for $C_{76}H_{51}B_2F_{30}FeN_3NiOP_2S_2 \cdot 0.3CH_2Cl_2$ (Found): C, 48.83 (48.81); H, 2.77 (2.43); N, 2.30 (2.24).

Borohydride Route to Et_4N[H5.1(BAr^F_3)$_2$]. A solution of **4.1**(BAr^F_3)$_2$ (100 mg, 0.057 mmol) in 10 mL of CH_2Cl_2 was treated with 1.2 mL (1.2 equivalent) of a stock solution of Me_3NO in CH_2Cl_2 (0.057 M) causing the solution to darken in color. The solution was quickly treated with a suspension of Et_4NBH_4 (8.3 mg, 0.057 mmol) in 10 mL CH_2Cl_2 and stirred for 30 minutes. The solvent was removed under reduced pressure and the resulting solid was extracted into 20 mL of Et_2O and the mixture was passed through Celite. Once the solution was concentrated to approximately 3 mL, pentane (20 mL) was added, forming a brown solid which was isolated by filtration. The remaining workup is similar to that described with Me_3NO and H_2. Yield: 22 mg (21%). Crystals suitable for X-ray diffraction were grown by diffusion of pentane into a solution of Et_4N[H**3**(BAr^F_3)$_2$] in CH_2Cl_2 at 0 °C. Crystals of Et_4N[H**5.1**(BAr^F_3)$_2$] are slow to dissolve in solvents. To further purify, crystals were washed in cold Et_2O, redissolved in CH_2Cl_2 and layered with pentane at –30 °C.

Et_4N[(CO)($CNBAr^F_3$)$_2$Fe(pdt)(H)Ni(dcpe)], Et_4N[H5.2(BAr^F_3)$_2$]. In a thick-walled glass pressure tube, a solution of **4.2**(BAr^F_3)$_2$ (140 mg, 0.0789 mmol) in CH_2Cl_2 (10 mL) was treated with Me_3NO (7.1 mg, 0.0946 mmol) in CH_2Cl_2 (2 mL) and immediately frozen by inserting the tube into liquid nitrogen. The headspace was evacuated and refilled with H_2 (40 psig), and the solution was thawed. After stirring this mixture for 2 hours, solvent was removed and the residue was extracted into Et_2O. The extract was filtered through Celite and the solvent removed under vacuum. ^{19}F NMR analysis showed ~50% of signals product. The crude sample was dissolved in 10 mL of CH_2Cl_2 and treated with excess Et_4NCl (131 mg, 0.789 mmol). The solvent was removed under vacuum, and the product was extracted into 10 mL Et_2O. The mixture was filtered through Celite, and the filtrate was dried under vacuum. The solid was dissolved in a minimal amount of THF and loaded onto a column of neutral alumina (Brockmann Level IV) eluting THF. The first red band was discarded, and the remaining brown band was eluted with CH_2Cl_2. The solution was concentrated to 5 mL, layered with 20 mL of pentane, and cooled to –30 °C precipitating an oil. Upon storing under vacuum, the oil converted to a solid. The solid recrystallized from 5 mL of CH_2Cl_2, layered with 20 mL of pentane and cooled in a –30 ºC, yielding red crystals (49 mg, 33%).

IR (CH_2Cl_2, cm^{-1}): ν_{CN} = 2158, 2132; ν_{CO} = 1952. ^{1}H NMR (CD_2Cl_2): δ −6.56 (t, $^2J_{HP}$ = 3 Hz). ^{31}P NMR (CD_2Cl_2): δ 85.1 (s). ^{19}F NMR (CD_2Cl_2): δ −134.3 (d, *o*-F); −162.5 (t, *p*-F); −163.0 (t, *p*-F); −167.3 (t, *m*-F); −167.8 (t, *m*-F). Anal. Calc. for $C_{76}H_{75}B_2F_{30}FeN_3NiOP_2S_2$ (Found): C, 48.58 (48.83); H, 4.02 (4.00); N, 2.24 (2.35).

$Et_4N[(CO)(CNBAr^F{}_3)_2FeCl(pdt)Ni(dppe)]$, $Et_4N[Cl$5.1$(BAr^F{}_3)_2]$. A solution of $Et_4N[H$**5.1**$(BAr^F{}_3)_2]$ (10 mg, 0.0054 mmol) in CD_2Cl_2 (0.7 mL) was treated with HCl (2 M in Et_2O, 6 μL, 2.2 equiv, 0.012 mmol), resulting in that the solution turning slightly lighter in color. ^{1}H NMR confirmed the formation of H_2 (δ 4.60). ^{31}P NMR spectrum displayed a major species (~60%) as an AB quartet at δ 51.5 and 48.6, and ^{19}F NMR displayed signals for two inequivalent $BAr^F{}_3$ environments, both consistent with an apical/basal arrangement of $CNBAr^F{}_3^-$ ligands. Assignment of this major species as $Et_4N[Cl$**5.1**$(BAr^F{}_3)_2]$ was confirmed by independent synthesis of $Et_4N[Cl$**5.1**$(BAr^F{}_3)_2]$ from **4.1**$(BAr^F{}_3)_2$ and Et_4NCl. Thus, a solution of **4.1**$(BAr^F{}_3)_2$ (0.10 g, 0.057 mmol) in CH_2Cl_2 (10 mL) was treated with a solution of Me_3NO (5.1 mg, 0.069 mmol) in CH_2Cl_2 (1 mL) followed by Et_4NCl (9.5 mg, 0.057 mmol) in CH_2Cl_2 (5 mL). After the solution was allowed to stir for 15 min, solvent was removed under vacuum. The crude solid was dissolved in a minimal amount of THF and loaded onto a column of neutral alumina (Brockmann Level IV) eluting THF. The first red band was discarded, and the remaining brown band was eluted with CH_2Cl_2. The solution was concentrated to 5 mL, layered with 20 mL of pentane, and cooled to −30 °C depositing an oil. Upon storing under vacuum, the oil was converted to a solid (40 mg, 37%). IR (CH_2Cl_2, cm^{-1}): ν_{CN} = 2181, 2149; ν_{CO} = 1996. ESI-MS: m/z 1757 $[M - Et_4N]^-$. ^{31}P NMR (CD_2Cl_2): δ 51.5, δ 48.6 (AB quartet, $^2J_{PP}$ = 29 Hz). ^{19}F NMR (CD_2Cl_2): δ −134.1(d, *o*-F); −134.6 (d, *o*-F); −161.9 (t, *p*-F); δ −162.4 (t, *p*-F); −167.0 (t, *m*-F); −167.2 (t, *m*-F). Anal. Calc. for $C_{76}H_{50}B_2ClF_{30}FeN_3NiOP_2S_2$ (Found): C, 48.33 (48.30); H, 2.67 (2.43); N, 2.22 (2.43).

Synthesis of $HNMe_3BAr^{F24}$. $HNMe_3Cl$ (54 mg, 0.56 mmol) and $NaBAr^{F24}$ (500 mg, 0.56 mmol) were dissolved in CH_2Cl_2 (40 mL) and stirred for 10 min. The solvent was removed under vacuum forming an off-white solid. The product was extracted into Et_2O (40 mL), passed through Celite, and the solvent was removed under vacuum. The product was crystallized from CH_2Cl_2 and hexanes at 0 °C to yield $HNMe_3BAr^{F24}$ as a white solid. Yield 0.44 g (84%). ^{1}H NMR (CD_2Cl_2): δ 7.72 (s, 8H, *o*-H BAr^{F24-}); 7.57 (s, 4H, *p*-H BAr^{F24-}); 6.38 (t, 1H, $HN(CH_3)_3$, $^1J_{NH}$ = 55 Hz); 3.05 (d, 9H, $HN(CH_3)_3$).

Synthesis of Pyrrolidinium BAr^{F24} ($Pyr•HBAr^{F24}$). Pyrrolidine (64 mg, 9.0 mmol) was dissolved in CH_2Cl_2 (10 mL) and treated with $HBF_4•Et_2O$ (1.3 mL, 9.0 mmol) and stirred for 30 minutes. The solvent was removed under vacuum producing a white powder. The solid was washed with pentane (20 mL) and Et_2O (20 mL) and dried under vacuum. Yield 1.32 g (92%) of [Pyrrolidinium]BF_4.

[Pyrrolidinium]BF_4 (36 mg, 0.226 mmol) and $NaBAr^{F24}$ (200 mg, 0.226 mmol) were combined and dissolved in CH_2Cl_2 (40 mL) and let stir for 1 hour. The solvent was removed under vacuum, producing an oil. An ether extract of this oil (10 mL) was passed through Celite, and the solvent was removed under vacuum. The resulting oil was triturated with pentane producing an off-white solid. The solid was dissolved in CH_2Cl_2 (5 mL), layered with pentane (20 mL) and cooled to 0 °C yielding white crystals (0.19 g, 90%). ^{1}H NMR (CD_2Cl_2): δ 7.72 (s, 8H, *o*-H BAr^{F24-}); 7.57 (s, 4H, *p*-H BAr^{F24-}); 6.14 (t, 2H, H_2N, $^1J_{NH}$ = 53 Hz); 3.58 (s, 4H, $N(CH_2)_2(CH_2)_2$); 2.20 (s, 4H, $N(CH_2)_2(CH_2)_2$).

Synthesis of $[PhNH_3]BAr^{F24}·2Et_2O$. $[PhNH_3]BF_4$ (41 mg, 0.226 mmol) was dissolved in MeCN (5 mL) and this solution was treated with a solution of $NaBAr^{F24}$ (200 mg, 0.226 mmol) in MeCN (5 mL). The mixture was stirred for 10 min, followed by removal of the solvent. The product was extracted into Et_2O (10 mL) and passed through Celite, and the filtrated was dried under vacuum. The resulting off-white solid was dissolved in CH_2Cl_2, layered with pentane, and cooled to –30 °C, yielding white crystals (210 mg, 83%). Two molecules of Et_2O were identified in the ^{1}H NMR spectrum. Drying the sample under vacuum for 24 hours was not found to remove the Et_2O. ^{1}H NMR (CD_2Cl_2): δ 8.69 (br, 3H, H_3NPh); 7.72 (s, 8H, *o*-H BAr^{F24-}); 7.63-7.61 (m, 3H, H_3NPh); 7.56 (s, 4H, *p*-H BAr^{F24-}); 7.35-7.33 (m, 2H, H_3NPh); 3.57 (m, 8H, $(CH_3CH_2)_2O$); 1.17 (m, 12H, $(CH_3CH_2)_2O$).

Titration of $Et_4N[H5.1(BAr^F{}_3)_2]$ with $HNMe_3BAr^{F24}$. A sample of $Et_4N[H\mathbf{5.1}(BAr^F{}_3)_2]$ (2.6 mg, 0.0014 mmol) was dissolved in 1 mL of CD_2Cl_2. A 0.14 M solution of $HNMe_3BAr^{F24}$ was prepared by dissolving 130 mg of $HNMe_3BAr^{F24}$ (0.14 mmol) in CD_2Cl_2 (1 mL). A ^{1}H NMR spectrum was collected before addition of $HNMe_3BAr^{F24}$ and after each addition. The sample was frozen in liquid nitrogen between acquisitions to minimize decomposition. The samples were warmed to room temperature immediately prior to recording each ^{1}H NMR spectrum.

Table 5.3. ^{1}H NMR Signals for the Titration of $Et_4N[H\mathbf{5.1}(BAr^F{}_3)_2]$ with $HNMe_3BAr^{F24}$

mol $HNMe_3^+$	[$HNMe_3^+$] (M)	δ (ppm)
0	0	–7.09
1.4×10^{-6}	1.4×10^{-3}	–8.69
2.8×10^{-6}	2.8×10^{-3}	–9.03
4.2×10^{-6}	4.2×10^{-3}	–9.11
5.6×10^{-6}	5.6×10^{-3}	–9.16

The unknown values of δ_{MHHN} and K were determined by a nonlinear fit of experimental values using the Leven-Marquardt algorithm (eq 5.1).

Titration of $Et_4N[H\mathbf{5.2}(BAr^F{}_3)_2]$ with Pyr•$HBAr^{F24}$. A sample of $Et_4N[H\mathbf{5.2}(BAr^F{}_3)_2]$ (2.5 mg, 0.0013 mmol) was placed in a J Young NMR tube and dissolved in 0.9 mL of CD_2Cl_2. A 0.067 M solution of Pyr•$HBAr^{F24}$ was prepared by dissolving 62 mg of Pyr•$HBAr^{F24}$ (0.067 mmol) in CD_2Cl_2 (1 mL). A ^{1}H NMR spectrum was collected before addition of Pyr•$HBAr^{F24}$ and after each addition. The sample was frozen in liquid nitrogen between acquisitions to minimize decomposition. The samples were warmed to room temperature immediately prior to recording each ^{1}H NMR spectrum.

Production of H_2 by Protonation of $Et_4N[H\mathbf{5.1}(BAr^F{}_3)_2]$ with $PhNH_3BAr^{F24}\cdot 2Et_2O$. Three vials were loaded with a known amount of $Et_4N[H\mathbf{5.1}(BAr^F{}_3)_2]$ (~3 mg) and 0.5 mL of CH_2Cl_2 and sealed with a rubber septum. A stock solution of acid was prepared from $PhNH_3BAr^{F24}\cdot 2Et_2O$ (60 mg, 0.0054 mmol) in 1.75 mL of CH_2Cl_2. An aliquot of 0.5 mL of stock solution of acid was injected through the septum, resulting in a color change of the solution from brown to orange. An internal standard of 100 μL of CH_4 was injected through the septum into the headspace of the vial. Each vial was allowed to stir for at least 30 minutes before the headspace was analyzed by gas chromatography.

Table 5.4. H_2 Production from $Et_4N[H\mathbf{5.1}(BAr^F{}_3)_2]$ and $PhNH_3BAr^{F24}\cdot 2Et_2O$.

Run	Mass of $Et_4N[H\mathbf{5.1}(BAr^F{}_3)_2]$ (mg)	μmol $Et_4N[H\mathbf{5.1}(BAr^F{}_3)_2]$	μmol of H_2 detected	mol% H_2
1	3.0	1.62	1.69	104%
2	3.0	1.62	1.51	93%
3	3.3	1.78	1.91	107%

Calculated mol% of H_2 = 101±7%

Derivation of Equation 5.2

NMR signals:

$$\delta_{obs} = \chi_{MH}\delta_{MH} + \chi_{MHHN}\delta_{MHHN}$$

$$\delta_{obs} = \frac{[MH]}{[MH]+[MHHN]}\delta_{MH} + \frac{[MHHN]}{[MH]+[MHHN]}\delta_{MHHN}$$

$$\delta_{obs} = \frac{[MH]_o - [MHHN]}{[MH]_o - [MHHN] + [MHHN]}\delta_{MH} + \frac{[MHHN]}{[MH]_o - [MHHN] + [MHHN]}\delta_{MHHN}$$

$$\delta_{obs} = \frac{[MH]_o - [MHHN]}{[MH]_o}\delta_{MH} + \frac{[MHHN]}{[MH]_o}\delta_{MHHN}$$

$$\delta_{obs} = \delta_{MH} + \frac{[MHHN]}{[MH]_o}(\delta_{MHHN} - \delta_{MH})$$

$$[MHHN] = \frac{[MH]_o(\delta_{obs} - \delta_{MH})}{\delta_{MHHN} - \delta_{MH}}$$

Equilibrium Constant: MH + HN ↔ MHHN

$$K = \frac{[MHHN]}{[MH][HN]}$$

$$K = \frac{[MHHN]}{\{[MH]_o - [MHHN]\}\{[HN]_o - [MHHN]}$$

$$[MHHN] = K[MH]_o[HN]_o - K[MH]_o[MHHN] - K[HN]_o[MHHN] + K[MHHN]^2$$

$$0 = K[MH]_o[HN]_o + (-K[MH]_o[MHHN] - K[HN]_o[MHHN] - [MHHN]) + K[MHHN]^2$$

$$0 = K[MH]_o[HN]_o - K[MHHN]\left([MH]_o + [HN]_o + \frac{1}{K}\right) + K[MHHN]^2$$

Quadratic equation where x = [MHHN], a = K, b = – K([MH]$_o$ + [HN]$_o$ + 1/K), c = K[MH]$_o$[HN]$_o$

$$x = \frac{-b \pm \sqrt{b^2 - 4ac}}{2a}$$

$$[MHHN] = \frac{K\left([MH]_o + [HN]_o + {}^1/_K\right) \pm \sqrt{K^2\left([MH]_o + [HN]_o + {}^1/_K\right)^2 - 4K^2[MH]_o[HN]_o}}{2K}$$

$$[MHHN] = \frac{1}{2}\left[\left([MH]_o + [HN]_o + {}^1/_K\right) \pm \sqrt{\left([MH]_o + [HN]_o + {}^1/_K\right)^2 - 4[MH]_o[HN]_o}\right]$$

Let: $$x = \left[\left([MH]_o + [HN]_o + {}^1/_K\right) \pm \sqrt{\left([MH]_o + [HN]_o + {}^1/_K\right)^2 - 4[MH]_o[HN]_o}\right]$$

Combine both equations

$$\frac{[MH]_o(\delta_{obs} - \delta_{MH})}{\delta_{MHHN} - \delta_{MH}} = \frac{x}{2}$$

$$[MH]_o(\delta_{obs} - \delta_{MH}) = \frac{x}{2}(\delta_{MHHN} - \delta_{MH})$$

$$\delta_{obs} - \delta_{MH} = \frac{x}{2[MH]_o}(\delta_{MHHN} - \delta_{MH})$$

$$\delta_{obs} = \delta_{MH} + \frac{1}{2[MH]_o}(\delta_{MHHN} - \delta_{MH})x$$

$$\delta_{obs} = \delta_{MH} + \frac{1}{2[MH]_o}(\delta_{MHHN} - \delta_{MH})\left[\left([MH]_o + [HN]_o + {}^1/_K\right) - \sqrt{\left([MH]_o + [HN]_o + {}^1/_K\right)^2 - 4[MH]_o[HN]_o}\right]$$

5.10 References

(1) Hartwig, J. *Organotransition Metal Chemistry: From Bonding to Catalysis*; University Science Books: Sausalito, California, 2010.

(2) Kaesz, H. D.; Saillant, R. B. "Hydride Complexes of Transition-Metals" *Chem. Rev.* **1972**, *72*, 231.

(3) Tschierlei, S.; Ott, S.; Lomoth, R. "Spectroscopically Characterized Intermediates of Catalytic H_2 Formation by [FeFe] Hydrogenase Models" *Energ. Environ. Sci.* **2011**, *4*, 2340.

(4) Hoff, C. D. "Thermodynamic and Kinetic Studies of Stable Low Valent Transition Metal Radical Complexes" *Coord. Chem. Rev.* **2000**, *206*, 451.

(5) Kubas, G. J. In *Advances in Inorganic Chemistry*; VanEldik, R., Ed. 2004; Vol. 56, p 127.

(6) Stephan, D. W. "Frustrated Lewis Pairs: A New Strategy to Small Molecule Activation and Hydrogenation Catalysis" *Dalton Trans.* **2009**, 3129.

(7) Stephan, D. W.; Erker, G. "Frustrated Lewis Pairs: Metal-free Hydrogen Activation and More" *Angew. Chem. Int. Ed.* **2010**, *49*, 46.

(8) Barton, B. E.; Whaley, C. M.; Rauchfuss, T. B.; Gray, D. L. "Nickel-Iron Dithiolato Hydrides Relevant to the [NiFe]-Hydrogenase Active Site" *J. Am. Chem. Soc.* **2009**, *131*, 6942.

(9) van der Vlugt, J. I.; Rauchfuss, T. B.; Whaley, C. M.; Wilson, S. R. ″Characterization of a Diferrous Terminal Hydride Mechanistically Relevant to the Fe-Only Hydrogenases″ *J. Am. Chem. Soc.* **2005**, *127*, 16012.

(10) Camara, J. M.; Rauchfuss, T. B. ″Mild Redox Complementation Enables H_2 Activation by [FeFe]-Hydrogenase Models″ *J. Am. Chem. Soc.* **2011**, *133*, 8098.

(11) Camara, J. M.; Rauchfuss, T. B. ″Combining Acid-Base, Redox and Substrate Binding Functionalities to Give a Complete Model for the [FeFe]-Hydrogenase″ *Nat. Chem.* **2012**, *4*, 26.

(12) Olsen, M. T.; Barton, B. E.; Rauchfuss, T. B. ″Hydrogen Activation by Biomimetic Diiron Dithiolates″ *Inorg. Chem.* **2009**, *48*, 7507.

(13) Ogo, S.; Kabe, R.; Uehara, K.; Kure, B.; Nishimura, T.; Menon, S. C.; Harada, R.; Fukuzumi, S.; Higuchi, Y.; Ohhara, T.; Tamada, T.; Kuroki, R. ″A Dinuclear Ni(μ-H)Ru Complex Derived from H_2″ *Science* **2007**, *316*, 585.

(14) Ogo, S.; Ichikawa, K.; Kishima, T.; Matsumoto, T.; Nakai, H.; Kusaka, K.; Ohhara, T. ″A Functional [NiFe]-Hydrogenase Mimic That Catalyzes Electron and Hydride Transfer from H_2″ *Science* **2013**, *339*, 682.

(15) Barton, B. E.; Rauchfuss, T. B. ″Hydride-Containing Models for the Active Site of the Nickel-Iron Hydrogenases″ *J. Am. Chem. Soc.* **2010**, *132*, 14877.

(16) Carroll, M. E.; Barton, B. E.; Gray, D. L.; Mack, A. E.; Rauchfuss, T. B. ″Active-Site Models for the Nickel-Iron Hydrogenases: Effects of Ligands on Reactivity and Catalytic Properties″ *Inorg. Chem.* **2011**, *50*, 9554.

(17) Ogata, H.; Hirota, S.; Nakahara, A.; Komori, H.; Shibata, N.; Kato, T.; Kano, K.; Higuchi, Y. ″Activation Process of [NiFe] Hydrogenase Elucidated by High-Resolution X-Ray Analyses: Conversion of the Ready to the Unready State″ *Structure* **2005**, *13*, 1635.

(18) Higuchi, Y.; Ogata, H.; Miki, K.; Yasuoka, N.; Yagi, T. ″Removal of the Bridging Ligand Atom at the Ni-Fe Active Site of [NiFe] Hydrogenase Upon Reduction with H_2, as Revealed by X-Ray Structure Analysis at 1.4 Angstrom Resolution″ *Struct. Fold. Des.* **1999**, *7*, 549.

(19) Chambers, G. M.; Angamuthu, R.; Gray, D. L.; Rauchfuss, T. B. ″Organo Ruthenium-Nickel Dithiolates with Redox-Responsive Nickel Sites″ *Organometallics* **2013**, *32*, 6324.

(20) Jiang, J.; Maruani, M.; Solaimanzadeh, J.; Lo, W.; Koch, S. A.; Millar, M. ″Synthesis and Structure of Analogues for the Ni-Fe Site in Hydrogenase Enzymes″ *Inorg. Chem.* **2009**, *48*, 6359.

(21) Manor, B. C.; Rauchfuss, T. B. "Hydrogen Activation by Biomimetic [NiFe]-Hydrogenase Model Containing Protected Cyanide Cofactors" *J. Am. Chem. Soc.* **2013**, *135*, 11895.

(22) Liu, T. B.; DuBois, D. L.; Bullock, R. M. "An Iron Complex with Pendent Amines as a Molecular Electrocatalyst for Oxidation of Hydrogen" *Nat. Chem.* **2013**, *5*, 228.

(23) Kutt, A.; Leito, I.; Kaljurand, I.; Soovali, L.; Vlasov, V. M.; Yagupolskii, L. M.; Koppel, I. A. "A Comprehensive Self-Consistent Spectrophotometric Acidity Scale of Neutral Bronsted Acids in Acetonitrile" *J. Org. Chem.* **2006**, *71*, 2829.

(24) Kutt, A.; Rodima, T.; Saame, J.; Raamat, E.; Maemets, V.; Kaljurand, I.; Koppel, I. A.; Garlyauskayte, R. Y.; Yagupolskii, Y. L.; Yagupolskii, L. M.; Bernhardt, E.; Willner, H.; Leito, I. "Equilibrium Acidities of Superacids" *J. Org. Chem.* **2011**, *76*, 391.

(25) Coetzee, J. F.; Padmanab.Gr "Properties of Bases in Acetonitrile as Solvent .4. Proton Acceptor Power and Homoconjugation of Mono- and Diamines" *J. Am. Chem. Soc.* **1965**, *87*, 5005.

(26) Donghi, D.; Beringhelli, T.; D'Alfonso, G.; Mondini, M. "NMR Investigation of the Dihydrogen-Bonding and Proton-Transfer Equilibria Between the Hydrido Carbonyl Anion $[HRe_2(CO)_9]^-$ and Fluorinated Alcohols" *Chem. Eur. J.* **2006**, *12*, 1016.

(27) Izutsu, K. In *Electrochemistry in Nonaqueous Solutions*; Wiley-VCH: 2009, p 89.

(28) Ellis, W. W.; Miedaner, A.; Curtis, C. J.; Gibson, D. H.; DuBois, D. L. "Hydride Donor Abilities and Bond Dissociation Free Energies of Transition Metal Formyl Complexes" *J. Am. Chem. Soc.* **2002**, *124*, 1926.

(29) Whaley, C. M.; Rauchfuss, T. B.; Wilson, S. R. "Coordination Chemistry of $[HFe(CN)_2(CO)_3]^-$ and Its Derivatives: Toward a Model for the Iron Subsite of the [NiFe]-Hydrogenases" *Inorg. Chem.* **2009**, *48*, 4462.

(30) Hall, H. K. "Correlation of the Base Strengths of Amines" *J. Am. Chem. Soc.* **1957**, *79*, 5441.

(31) Coe, B. J.; Glenwright, S. J. "Trans-Effects in Octahedral Transition Metal Complexes" *Coord. Chem. Rev.* **2000**, *203*, 5.

(32) DuBois, M. R.; DuBois, D. L. "The Roles of the First and Second Coordination Spheres in the Design of Molecular Catalysts for H_2 Production and Oxidation" *Chem. Soc. Rev.* **2009**, *38*, 62.

(33) Mock, M. T.; Potter, R. G.; Camaioni, D. M.; Li, J.; Dougherty, W. G.; Kassel, W. S.; Twamley, B.; DuBois, D. L. "Thermodynamic Studies and Hydride Transfer Reactions from a Rhodium Complex to BX_3 Compounds" *J. Am. Chem. Soc.* **2009**, *131*, 14454.

(34) De Lacey, A. L.; Fernandez, V. M.; Rousset, M.; Cammack, R. "Activation and Inactivation of Hydrogenase Function and the Catalytic Cycle: Spectroelectrochemical Studies" *Chem. Rev.* **2007**, *107*, 4304.

(35) Crabtree, R. H. "Recent Advances in Hydrogen Bonding Studies Involving Metal Hydrides" *J. Organomet. Chem.* **1998**, *557*, 111.

(36) Epstein, L. M.; Shubina, E. S. "New Types of Hydrogen Bonding in Organometallic Chemistry" *Coord. Chem. Rev.* **2002**, *231*, 165.

(37) Carroll, M. E.; Barton, B. E.; Rauchfuss, T. B.; Carroll, P. J. "Synthetic Models for the Active Site of the [FeFe]-Hydrogenase: Catalytic Proton Reduction and the Structure of the Doubly Protonated Intermediate" *J. Am. Chem. Soc.* **2012**, *134*, 18843.

(38) Liu, T. B.; Wang, X. P.; Hoffmann, C.; DuBois, D. L.; Bullock, R. M. "Heterolytic Cleavage of Hydrogen by an Iron Hydrogenase Model: An Fe-H···H-N Dihydrogen Bond Characterized by Neutron Diffraction" *Angew. Chem. Int. Ed.* **2014**, *53*, 5300.

(39) Beringhelli, T.; D'Alfonso, G.; Panigati, M.; Mercandelli, P.; Sironi, A. "An Intramolecular N-H···(μ-H)Re_2 Dihydrogen Hond and a novel μ_3-η_2 Coordination Mode of the Pyrazolate Anion on a Triangular Cluster Face" *Chem. Eur. J.* **2002**, *8*, 5340.

(40) Wang, N.; Wang, M.; Zhang, T. T.; Li, P.; Liu, J. H.; Sun, L. C. "A Proton-Hydride Diiron Complex with a Base-Containing Diphosphine Ligand Relevant to the [FeFe]-Hydrogenase Active Site" *Chem. Commun.* **2008**, 5800.

(41) Simmons, T. R.; Artero, V. "Catalytic Hydrogen Oxidation: Dawn of a New Iron Age" *Angew. Chem. Int. Ed.* **2013**, *52*, 6143.